BRITISH COLUMBIA | Ministry of Energy and Mines

GEOCHEMICAL EXPLORATION PATHFINDERS TO DRIFT COVERED COPPER-GOLD SULPHIDE MINERALIZATION IN CENTRAL BRITISH COLUMBIA

Open File 2010-09

Ray Lett

BRITISH COLUMBIA GEOLOGICAL SURVEY

GEOLOGICAL SURVEY OF CANADA COMMISSION GÉOLOGIQUE DU CANADA

KEYWORDS: Geochemistry, soils, British Columbia, porphyry, copper, gold.

Executive Summary

Open File 2010-9 describes soil geochemical orientation surveys over the Mouse Mountain and Shiko Lake porphyry Cu-Au mineral occurrences and two other areas near Soda Creek and Alexandria. Bedrock in this part of British Columbia between Williams Lake and Quesnel is mainly glacial drift-covered and consists of Mesozoic-age rocks overlain by younger plateau basalts. The primary aim of the soil sampling was to examine the soil geochemical expression of porphyry Cu-Au and related sulphide mineralization in drift and barren bedrock covered areas. Another aim of the soil sampling was to improve geochemical exploration methods in parts of British Columbia that have been impacted by the Mountain Pine Beetle. In each survey area samples from F-H, B and C soil horizons were analysed for multi-elements by a range of techniques including instrumental neutron activation (INAA), aqua regia-inductively coupled mass spectrometry (aqua regia-ICPMS), Mobile Metal Ion leach (MMI) ^{TM}, Enzyme Leach^{SM}, BioLeach^{SM} and Soil Gas Hydrocarbons ^{SM} (SGH) and for soil pH and loss on ignition (LOI). Gold and other mineral grains were also identified and counted in the heavy mineral concentrate of C soil horizon samples.

Gold, Cu, Mo and V soil anomalies outlined by soil sampling over the Mouse Mountain and Shiko Lake mineral properties are most likely caused by minerals entrained in a till deposited down-ice from bedrock hosted sulphide mineralization. At Soda Creek and Alexandria where there is no obvious economic mineralization the elevated Ni and V in soil are probably a geochemical expression of a till derived for non-mineralized bedrock. Copper, Au, Ni and V by aqua regia-ICPMS show greatest anomaly contrast in the C soil horizon compared to the B and F-H horizons whereas Ag and Mo are more elevated in the F-H organic horizon. Anomaly size and contrast for selected elements by MMI^{TM}, BioLeach^{SM} and Enzyme Leach ^{SM} in the B soil is generally similar to the contrast for elements by a more rigorous aqua regia digestion, but the different partial leaches display a preference for enhancing certain metals. For example MMI^{TM} enhances Au anomaly contrast compared to that of Cu whereas BioLeach^{SM} enhances Co and Cu contrast compared to Au. Anomaly contrast by a partial leach also reflects the soil horizon sampled. For example, MMI^{TM}, BioLeach^{SM} and Enzyme Leach^{SM} contrast for Cu, Mo, Pb, Ni and Zn is smaller in Upper B horizon samples compared to that in lower B horizon samples stressing the need for consistency when maintaining the soil sampling in the same horizon.

The number and relative shape of Au grains in the C soil sample heavy mineral concentrates complements the soil geochemistry in locating a buried bedrock source for the minerals. Comparison of SGH, multi element and pH patterns in the soil at Mouse Mountain and Shiko Lake suggest that the geochemistry may have been modified by a reduced chimney induced by oxidizing sulphides in bedrock. A model developed by interpreting all of the geochemical data displays the most likely relationship between the bedrock, drainage and soil geochemistry in areas where bedrock is concealed beneath a till veneer.

Table of Contents Page

Mouse Mountain Geochemistry

Soil geochemistry

3.2 Soda Creek

Soda Creek Geochemistry

Soil geochemistry

Anomaly Definition

3.3 Alexandria

Alexandria Geochemistry

1. Introduction

Ideally, any geochemical survey should start with a planning and design stage, followed by sample collection, sample preparation and analysis, scrutiny of data for reliability, results display and data interpretation and, finally, recommendations for the next exploration phase if one is warranted. Survey design should try to utilize all of the available existing bedrock geological, surficial geological, geophysical, geochemical and logistical data for an area so that the optimum combination of sample type, collection method, preparation and analytical technique can be selected to most reliably identify a source of mineralization from the data. A common error when planning a geochemical survey is to assume that, because there is existing background geosciences information (e.g. bedrock geology, surficial geology, and previous stream sediment and soil survey geochemical data) for a particular area, an orientation geochemical survey is unnecessary. The orientation survey is a much safer design strategy for a survey because a geochemical expression varies from area to area depending on geology, surficial environment and the style of mineralization. A common criticism levelled at undertaking an orientation survey is that it increases the cost of an exploration program and delays the start of exploration. In fact, a small number of soil or sediment samples collected nearby or over a mineral occurrence can provide valuable data to pathfinder elements and geochemical backgrounds. Even observing obvious environment features such as the presence of wetland that would explain highly anomalous (but misleading) Cu values in the soil could provide sufficient information to avoid a costly survey failure.

Orientation studies, therefore, seek to find the optimum survey parameters for most reliably distinguishing a geochemical anomaly from background “noise” and then attributing the anomaly to a mineralized bedrock source. Clearly, a threshold value is needed for defining an anomaly and so orientation survey data can be analysed statistically to determine geochemical backgrounds for each element measured. Geochemical backgrounds and thresholds can be refined from historical survey data provided that sampling and analytical methods are similar to those intended for the proposed survey. Orientation survey results also indicate the expected anomaly contrast (peak value to background ratio) for each element determined based on variables such as the density of sampling, type of sample collected, sample grain size, analytical digestion technique and element detection method. Selective leaches are commonly used to improve stream sediment and soil geochemical anomaly contrast by releasing an element bound to a specific phase of a sample. Hall, (1998), describes many of the contemporary partial and selective leach methods and critically evaluates analytical precision for elements detected by each method.

Cameron *et al,* (2004), classify leaches for discriminating between the endogenic component of soil (i.e. primary minerals inherited by weathering from bedrock) and the exogenic component of soil (i.e. secondary minerals developed through a soil forming process) into selective leaches as opposed to those that are precursor leaches. Selective leaches ideally dissolve specific secondary minerals (e.g. manganese oxides) to release bound metals from an exogenic source whereas precursor leaches remove more labile, exogenic elements before incorporation into a secondary mineral matrix. Typical of selective leaches is ammonium acetate to dissolve carbonates and secondary Fe oxides and of the precursor leach class, water is a good example. Cameron *et al*, (2004), have compared the responses commercial selective and precursor leaches in a soil survey over the Cross Lake, Ontario Achaean-age volcanic massive sulphide (VMS) deposit where the Zn-Ag sulphide mineralization is covered by up to 50 metres of glacial clay and sand. Commercial selective and precursor leaches such as Enzyme Leach^{SM} and Mobile Metal Ion (MMI^{TM}) revealed apical (i.e. a peak directly over the surface projection of mineralization) and twin peak (i.e. flanking peaks, distal to the surface projection of mineralization) geochemical anomalies compared to more subdued Zn contrast developed from the results of analysis with an aqua regia digestion. Zinc and Cd were found to be elements with the strongest signal because not only are they major components of the mineralization, but also because they can be very mobile in the near-surface environment.

Among the conclusions Cameron *et al*, (2004) make from their survey data is an important point that the geochemical response and patterns obtained with the various leaches (e.g. Ammonium acetate, Enzyme Leach^{SM,} MMI^{TM}) vary in size and shape depending on the soil horizon sampled. The configuration of the geochemical patterns is believed to reflect near-surface redistribution of labile elements above a reducing vertical column-shaped zone induced by the sulphide mineral body beneath water-saturated glacial sediment. Varying, oxidation-reduction potential, soil pH and carbonate content of soil across this zone demonstrate apical and twin peak (“rabbit ear”) patterns. Hamilton, (2007), proposed a reduced chimney model in glacial clay to explain geochemical patterns over volcanogenic massive suphide mineralization and kimberlite bodies in Ontario.

Much of the present mineral exploration in British Columbia has focused on the Quesnel terrane because of geology favourable for hosting porphyry Cu-Au deposits (e.g. Mount Polley). The release of new Geoscience BC region stream and lake sediment data for the QUEST project area by Jackaman, (2008) and the published results of mineral deposits studies and mapping carried out by Logan *et al.* (2010) are further evidence for the area’s prospectivity. However, geochemical exploration for new deposits within the British Columbia interior has had to contend with the problem of bedrock largely concealed by glacial and volcanic deposits, and a paucity of information about viable exploration methods. An orientation survey by Cook and Dunn, (2006), near Vanderhoof, BC, revealed that partial extraction of trace elements from soil samples with Enzyme Leach^{SM} and MMI^{TM} improved geochemical contrast over the Tommy and Ted epithermal Au mineralized vein compared to contrast by a strong acid digestion. Also, the response for elements identified as mineralization pathfinders were enhanced by the partial extraction analysis.

While the geochemical studies by Cook and Dunn (2006) significantly advanced the understanding of element dispersion in soil developed on shallow, transported overburden covering Au-bearing veins, the geochemical expression is likely to be different over other styles of mineralization (e.g. Cu-Au Porphyry) and in areas where the glacial deposits are thicker. For example, Heberlein and Samson (2010) describe the analysis of soil samples from several horizons along traverses crossing the northern BC Kwanika porphyry Cu-Au deposit with aqua regia, MMI^{TM}, Enzyme Leach^{SM}, BioLeach^{SM}, Ionic Leach^{SM}. The Cu-Au mineralization at Kwanika is concealed beneath up to 40 metres of Quaternary-age sand, gravel and conglomerate. Heberlein and Samson, (2010), found that analysis of the B-horizon soils using aqua regia and commercial selective leaches failed to reliably detect ore indicator and pathfinder elements (e.g. Cu, Au, Mo, Ag, As, Sb, Se, U, W, Cd, Ca). Analysis of Ah (humus) horizon samples, however, produced significant apical W anomalies over the surface projection of the Cu-Au mineralization. Soil gas hydrocarbon (SGH), soil conductivity and pH, expressed as Inverse Difference Hydrogen (IDH) detected the presence of a reduced vertical column above the sulphides.

In a subsequent soil geochemical survey over the Mount Milligan porphyry Cu-Au deposit in central BC, Heberlein, (2010), found that analysis of B-soil horizon samples for elements with an aqua regia digestion was the most effective geochemical tool for detecting the Cu-Au sulphide mineralization through 25 metres of glacial sediment, although there were also MMI^{TM}, Enzyme Leach^{SM}, BioLeach^{SM} anomalies in the upper B soil horizon. Despite disturbance of soil profiles from previous exploration the SGH soil analysis and soil pH patterns suggested the existence of a reduced "chimney" above the mineralization similar to that found above the Kwanika deposit. The Ah horizon geochemistry revealed twin peak anomalies spatially related to the Cu-Au mineralization although the patterns were less continuous because of the surface disturbance.

Cameron *et al*, (2004), and Heberlein, (2010), clearly show that soil horizon and the method of geochemical analysis for trace elements are key factors for enhancing anomaly contrast. Overburden type and thickness also influence the geochemical expression of mineralized bedrock in the overlying soil. For example, Cameron *et al*, (2004), and Heberlein, (2010), attribute the soil geochemical expression of the buried mineralization to complex physico chemical dispersion mechanisms active in glacial sediments deposited mainly by fluvial processes (e.g. lacustrine sediment, glacial fluvial sediment). Much of the bedrock in British Columbia is covered by a combination of lacustrine deposits, glacio fluvial and fluvial sediment; gravity and ice-transported debris ranging from colluvium to till. Hence, the geochemistry of soil formed on the glacial sediment can reflect physical dispersal of mineralized bedrock resulting from gravity or ice flow transport. In addition, geochemical patterns may be superimposed on the sediment by electrochemical dispersion processes induced by the buried mineral sulphides. Interpreting soil geochemical data in glaciated areas where buried mineralization can be refined if these processes are identified. Identifying the different mineralization-related geochemical dispersion processes in glacial sediment was a primary reason for undertaking the orientation surveys in the British Columbia interior. BC Geological Survey Open File 2010-09 reports on detailed soil sampling at four sites in a mainly drift covered area underlain by Mesozoic-age rocks and more recent plateau basalts between Williams Lake and Quesnel. Two of the areas, Mouse Mountain and Shiko Lake, have well-developed Cu and Au mineralization. At the other two sites there are stream sediment geochemical anomalies, but no visible sulphide mineralization. The surveys were carried out to:

- Examine the geochemical expression of porphyry Cu-Au-Mo mineralization in soil where the mineralized bedrock is covered by till and/or recent plateau basalt.
- Improve geochemical exploration methods in areas that have been economically impacted by the Mountain Pine beetle infestation.
- Complement geological, geophysical and geochemical data that has been generated in the QUEST project area (Logan *et al.* 2010).
- Explain regional stream sediment geochemical anomalies.

Locations of the areas are shown on Figure 1.1.

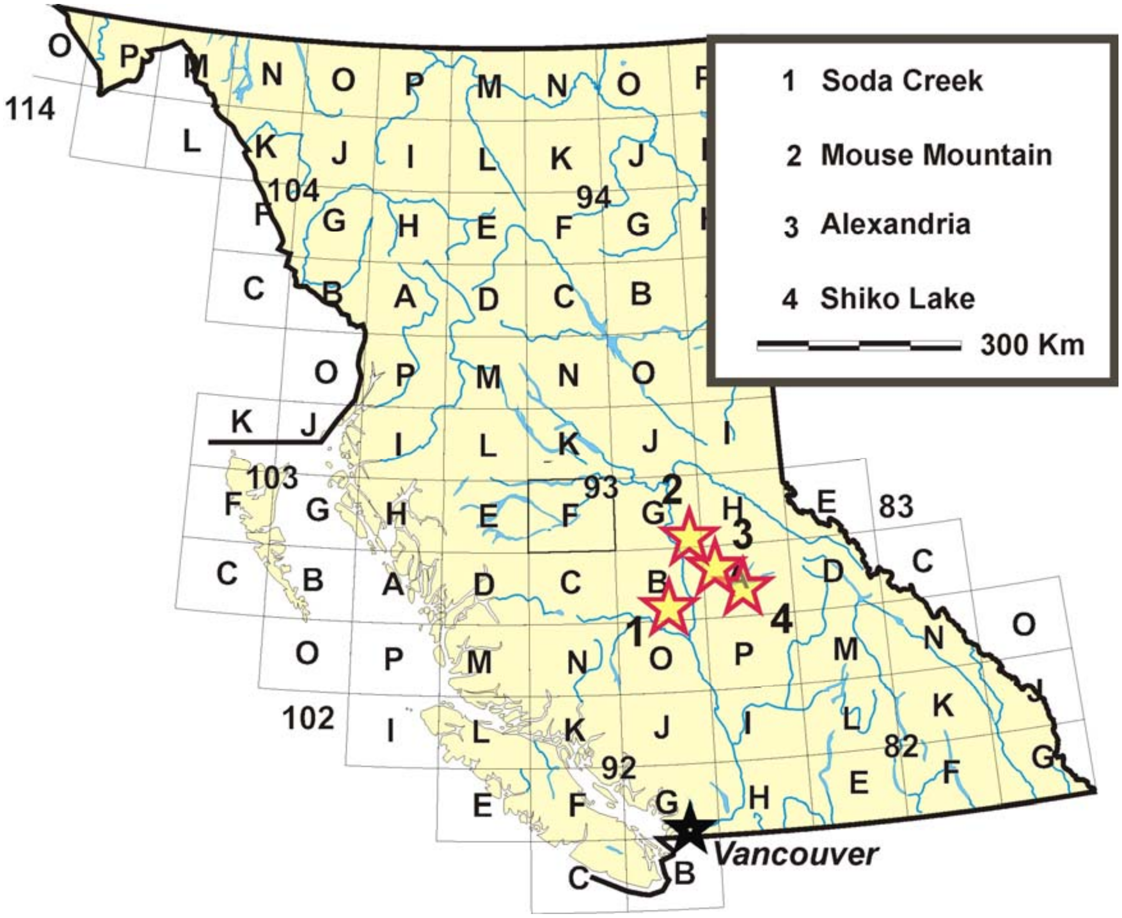

Figure 1.1. Location of the Mouse Mountain, Shiko Lake, Soda Creek and Alexandria survey areas

2. Survey Techniques

2.1 Field Sampling

Samples from the different soil horizons were taken at intervals down vertical profiles in the areas surveyed. The profiles were located at stations along road and bush traverses that were generally orientated to cross the regional ice-flow direction. Ideally, several traverses up-ice and down-ice from a mineralized zone (where known) were sampled although it was often not practical to carry out an extensive sampling pattern. Where possible, the following samples were taken from:

- The decomposed humus (F-H) horizon just beneath the surface litter of recently deposited vegetation,
- the upper B-soil horizon just under the eluviated (Ae) horizon (where visible)
- the lower B-soil horizon sample close to the transition from the B to C soil horizons

- a sample at 20-25 cm depth independent of horizon for MMI analysis and;
- a sample of the C soil-horizon glacial sediment (typically till).

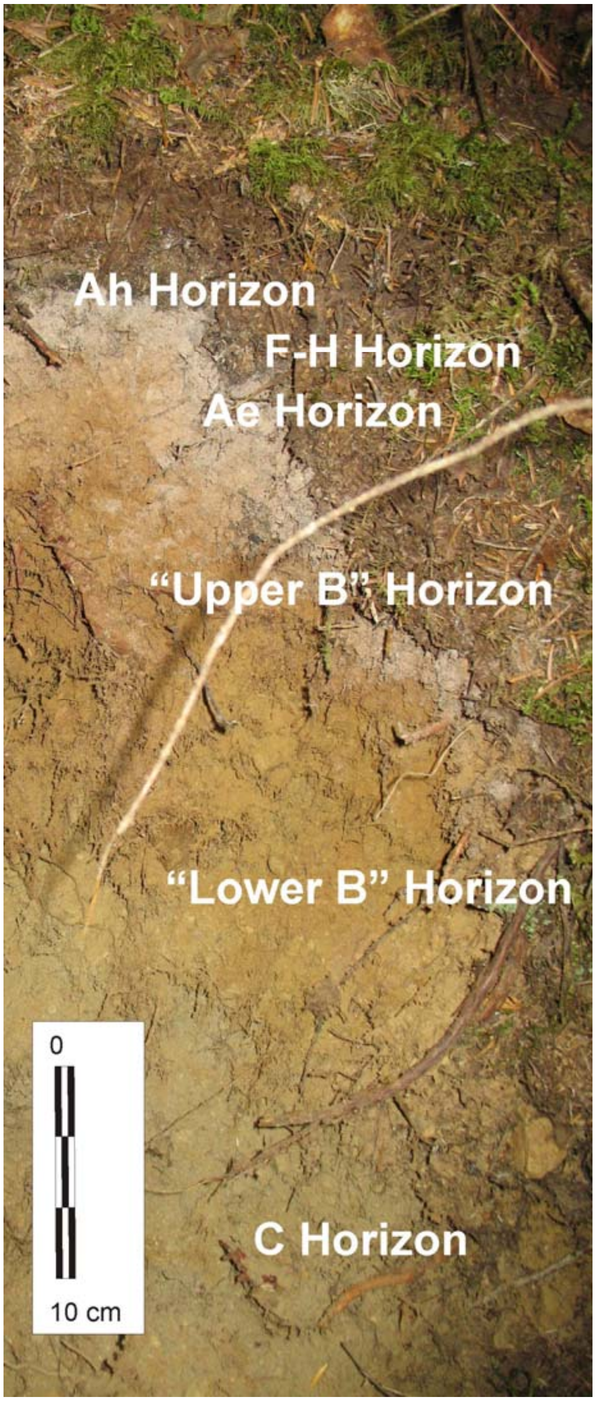

Figure 2.1. A typical soil profile from Mouse Mountain with the key horizons identified.

Horizons were identified in the field using the Canadian Soil Classification System, (1998), nomenclature. The samples were collected from hand-dug pits or from trenches excavated in road cuts. Duplicate samples were taken a frequency of 1 duplicate per 20 routine samples. The depth, soil texture, soil colour (Munsell Classification) and structure were recorded for each sample with details of the percentage, size and shape of rock clasts and presence (or absence) or clast striations. Still digital photographs were taken of each profile and a short video made to record details of the area surrounding the station. At the end of each day the B soil horizon pH was measured on a 1:1v/v soil to distilled water slurry with an Extech P110 pH meter calibrated daily with pH 4 and 7 buffers. Multiple samples were collected from each horizon for different analyses. For example, B-horizon soil and litter samples for aqua regia-ICPMS analysis were collected in a Hubco^{TM} polyester weave bag and the C soil horizon (glacial sediment) were collected in a large PVC bag. Samples intended for Enzyme Leach^{SM}, SGH^{SM}, BioLeach^{SM} and MMI^{TM} analysis were collected and doubled bagged in sealed PVC Ziplock^{TM} bags. A number of sediment samples were also collected from streams draining the areas surveys and were stored in Hubco^{TM} bags. Figure 2.1 shows a typical soil profile from the Mouse Mountain area.

2.2 Sample Preparation

The F-H soil horizon, B soil horizon and C soil horizon samples were oven dried at 35 to 40^{o}C and prepared in the Geological Survey laboratory, Victoria, BC, before analysis. Part of the B-soil horizon sample and stream sediment samples were disaggregated and sieved to – 80 mesh (<0.18 mm) whereas C-soil horizon (glacial sediment) samples were sieved to – 230 mesh (0.063 mm). The + 2mm size fraction of the glacial sediment was archived for later identification of clast lithology. The F-H horizon samples were milled. Sieved or milled duplicate samples (generally from one of the field replicate) and standard reference materials were inserted into each batch of 20 samples before analysis. No preparation was carried out before the soil samples were sent for Enzyme Leach^{SM}, SGH^{SM}, BioLeach^{SM} and MMI^{TM} analysis.

2.3 Sample Analysis

The methods used to study the soil geochemistry, previously described by Lett and Sandwith, (2008), are:

- Aqua regia digestion followed by inductively coupled plasma mass spectroscopy (AR-ICPMS) analysis of the <0.18 mm B horizon soil sample fraction and < 0.063 mm C-horizon soil sample fraction for 37 elements including Au and Cu at Acme Analytical Laboratories, Vancouver. F-H horizon samples were milled before AR-ICPMS analysis.
- Instrumental neutron activation analysis (INAA) of the <0.18 mm B horizon soil sample fraction and < 0.063 mm C horizon sample fraction for 33 elements including Au at Activation Laboratories Limited, Ancaster, Ontario.
- Enzyme Leach^{SM} and BioLeach^{SM} analysis of the <0.18 mm B horizon soil fraction for elements including Br & I. BioLeach^{SM} is a proprietary selective extraction developed by Activation Laboratories Limited that utilizes bacterial decomposition of mineral sulphides. The bacteria cell membranes rupture when

organisms die leaving a diagnostic organic and inorganic geochemical signature. BioLeach^{SM} dissolves the dead bacterial remnants in the surface soils and detects the geochemical signature of the sulphide minerals (E.Hoffman, *pers. com*).

- Soil Gas Hydrocarbon analysis^{SM} (SGH) for C5 - C17 organic compounds that have been absorbed on B-horizon soil samples (Activation Laboratories Limited). The underlying theory of SGH analysis has been documented by Sutherland and Hoffman (2008), and its application for detected buried VMS and porphyry Cu-Au sulphide mineralization is described by Cameron *et al*, (2004), by and Heberlein, (2010). Briefly, soil gas hydrocarbon analysis using a proprietary selective extraction applied to soil followed by high resolution mass spectrometer analysis of the extract detects concentrations of up to 150 aromatic and aliphatic organic compounds absorbed to soil particles. The organic compounds are believed to be the metabolites from dead chemotrophic bacteria that have formed active colonies on the surface of sulphide and sulphate minerals. Chemotrophic bacteria convert the sulphur from sulphide and sulphate into a range of sulphur compounds that are released when the bacterium dies. These compounds then diffuse into the soil where they can be detected. The method has been refined so that light aliphatic compounds are assumed to migrate more rapidly and for apical anomalies over the suphide mineralization whereas the larger, aromatic molecules for peripheral, ring shaped patterns enclosing a vertical "reduced" chimney. Concentrations of nineteen sub-classes of alkanes, alkenes, thiophenes, aromatic and polyaromatic are used to help predict the character of the sub-surface sulphides. A basis of the interpretation is a statistical analysis of the raw SGH data with a comparison of results against SGH patterns found over known types of sulphide mineralization. This enables a prediction to be made of the degree of to which the soil anomalies reflect concealed sulphide mineralization. In the case of buried Cu-Au porphyry mineralization a ranking of 6 (high) reflects that all of that all of organic classes support the presence of Cu-Au bearing sulphides whereas a ranking of 1 (low) indicates a complete absence that none of any organic classes.
- Mobile Metal Ion (MMI^{TM}) analysis, a method described by Mann *et al.*, (1998), for the analysis of soil samples for metals including Cu, Pb, Zn, Ni, Cd, Au, Ag, Co with a proprietary selective extraction at SGS Laboratories Limited, Toronto. The MMI^{TM} multielement package used in this project is identified as MMI_M in the SGS Fee Schedule and MMI5 in SGS digital reports.
- Loss on ignition (LOI) at 500^{o}C of the <0.18 mm fraction of the B-Horizon soil samples at Acme Analytical Limited.
- Mineral grain identification, gold grain shape (reshaped, modified, pristine) and the number of Au grains in C soil horizon sample heavy mineral concentrates (> SG 3.3) at Overburden Drilling Management, Nepean, Ontario.
- Repeat laboratory analysis of the – 2 mm sieved fraction of the B soil horizon samples for pH using the method described by Heberlein (2010). The soil pH was measured on a 1:1v/v soil to distilled water slurry with an Extech P110 pH meter calibrated daily with pH 4, 7 and 10 buffers. A pH measurement was made after

mixing the slurry for 1-2 minutes and then after addition of 1 drop of 10 percent HCl to dissolved secondary carbonate minerals. A value of inverse hydrogen difference (IDH) was calculated from pH values using the method advocated by Smee, (2003 and 2010).

Table 2.1 lists detection limits for aqua-ICPMS, INAA, Enzyme Leach^{SM}, BioLeach^{SM} and Mobile Metal Ion (MMI^{TM}) analysis.

Element	AR-ICP	INAA	MMI	Enzyme	BIOL
Ag_ppb	2	5	1	0.2	0.2
Al	100	-	1	-	-
As	0.1	0.5	10	1	0.5
Au_ppb	2	2	0.1	0.05	0.05
Ba	0.5	50	10	1	1
Be	-	-	-	2	0.07
Bi	0.02	-	1	0.8	0.1
Br	-	0.5	-	5	5
Ca	100	10000	10	-	-
Cd	0.01	-	1	0.2	0.05
Ce	-	3	5	0.1	0.02
Cl	-	-	-	2	-
Co	0.1	1	5	1	0.1
Cr	0.5	5	100	20	2
Cs	-	1	-	0.1	0.01
Cu	0.01	-	10	3	0.5
Dy	-	-	1	0.1	0.01
Er	-	-	0.5	0.1	0.01
Eu	-	0.2	0.5	0.1	0.01
Fe	100	100	1	-	-
Ga	0.2	-	-	1	0.1
Gd	-	-	1	0.1	0.03
Ge	-	-	-	0.5	0.05
Hf	-	1	-	0.1	0.04
Hg_ppb	5	1	-	1	0.05
Ho	-	-	-	0.1	0.01
I	-	-	-	2	1
In	-	-	-	0.1	0.1
La	0.5	0.5	1	0.1	0.01
Li	-	-	5	2	0.2
Lu	-	-	-	0.1	0.01
Mg	100	-	1	-	-
Mn	1	-	-	1	0.1
Mo	0.01	1	5	1	2
Nb	-	-	0.5	1	0.2
Nd	-	5	1	0.1	0.03
Ni	0.1	20	5	3	0.2
Pb	0.01	-	10	1	0.1

Element	AR-ICP	INAA	MMI	Enzyme	BIOL
Pr	-	-	1	0.1	0.01
Pt	-	-	1	1	0.5
Pd	-	-	1	1	0.5
Rb	-	15	5	1	0.1
Ru	-	-	-	1	0.05
Sb	0.02	0.1	1	0.1	0.2
Sc	0.1	0.1	5	100	0.5
Se	0.1	3	-	5	1
Sm	-	0.1	1	0.1	0.03
Sn	-	200	1	0.8	-
Sr	0.5	50	10	1	0.1
Ta	-	0.5	1	0.1	0.01
Tb	-	0.5	1	0.1	0.01
Te	0.02	-	10	1	1
Th	0.1	-	0.5	0.1	0.02
Ti	10	-	3	100	-
Tl	0.02	-	0.5	0.1	0.2
Tm	-	-	-	0.1	0.01
U	0.1	0.5	1	0.1	0.01
V	2	-	-	1	1
W	0.2	1	1	1	0.01
Y	-	-	5	0.5	0.02
Yb	-	0.5	1	0.1	0.02
Zn	0.1	50	20	10	2
Zr	-	-	5	1	0.5

Table 2.1. Elements determined by aqua regia-ICPMS, INAA, Enzyme Leach^{SM}, BioLeach ^{SM} and Mobile Metal Ion (MMI^{TM}) analysis with instrumental detection limits. All detection limits for elements by Enzyme Leach^{SM}, BioLeach^{SM} and MMI^{TM} are in parts per billion (ppb); elements determined by aqua regia-ICPMS and INAA are in parts per million (ppm) or unless stated. **-** indicates that an element was not determined or that all values were below detection limit.

2.4 Data Variability – Quality Control

No interpretation of geochemical data can be made with any degree of confidence unless there is an estimate for the variability attributable to sampling and to sample analysis (precision). Sampling and analytical variability is typically determined by scrutinizing the data generated from the routine analysis of duplicate samples collected at field sites and of randomly inserted standards and prepared duplicate samples submitted with the survey samples for commercial analysis. Quality control data for this project has been generated using the National Geochemical Reconnaissance (NGR) - Regional Geochemical Survey (RGS) quality control scheme based on the analysis of data from a block of 20 samples following the protocol documented by Friske, *et al.*, (1991). Each block comprises:

- Seventeen routine soil samples,
- A field duplicate soil sample collected adjacent to one of the routine samples,
- A control reference standard containing known element concentrations.
- An analytical duplicate sample split after sample preparation from, whenever possible, one of the field duplicate samples.

A blank sample such as analytical grade silica is often included with the prepared samples before analysis although not in every batch. The random location of control reference samples within each batch are selected before sampling, whereas field duplicate sites are chosen randomly during fieldwork. Field duplicate samples are generally collected from the same sample pit but from a different face of the pit.

Estimates of sampling and analytical precision are most commonly quoted in geochemical survey quality control reports because a measure of accuracy requires that samples and standard reference materials are analysed by the same method. Since most of the element reference values quoted for standards are based on a near total determination whereas survey samples are typically analysed by partial aqua regia digestion method a measure of accuracy would be misleading. However, data produced by the INAA analysis of standards can used as a measure of accuracy because INAA produces a “near total” determination and hence a realistic comparison of the sample value to the standard quoted value for each element.

There are several ways for calculating a numerical value for accuracy and precision from quality control data. For example, relative standard deviation (standard deviation of the determinations/mean of the determinations) is one measure of precision determined from the results of repeated analysis of a standard included with the survey samples. The relative standard deviation (RSD) calculated from standards data has a limitation as precision estimate in that it is only realistic close to the concentration of the element in the standard and not over the whole concentration range. Also, precision is normally quoted at the 95th percentile level at twice the RSD. However, keeping these constraints in mind RSD can still be a valuable guide to precision. Table 2 lists % RSD values for elements determined by aqua regia–ICPMS analysis of CANMET standards TILL-1, TILL-2 and TILL-4 with the mean concentration calculated for each element in the standard. These standards were randomly inserted at a frequency of 1 standard per 20 survey soil samples. Percent RSD values for most elements in Table 2 are less than 7% i.e. the precision at the 95% confidence limit would be better than 15%. For some of the elements (e.g. Ag) the mean concentration reported for the three CANMET TILL reference standards is similar so that the precision is not realistic of values over a large concentration range. However, other elements (e.g. Cu, Pb) are reported in the CANMET TILL-1, 2 and 4 standards over a wider concentration range more typical of the soil geochemistry in a mineralized area and, hence, the precision determined from the standard analysis is a better guide to the analytical variation.

Element	Mean	CANMET Till 1(4)	Mean	CANMET Till 2 (4)	Mean	CANMET Till 4(3)
Ag_ppb_ARMS	201.750	**4.006**	221.75	**4.82**	158.33	**4.21**
Al_%_ARMS	1.708	**3.043**	2.60	**5.39**	1.90	**3.51**
As_ppm_ARMS	15.050	**1.015**	21.83	**3.21**	102.50	**1.92**
Au_ppb_ARMS	10.150	**107.589**	1.15	**36.20**	3.57	**7.06**
B_ppm_ARMS	20.000	**0.000**	20.00	**0.00**	20.00	**0.00**
Ba_ppm_ARMS	74.725	**3.417**	86.53	**6.13**	62.80	**1.77**
Bi_ppm_ARMS	1.953	**1.565**	5.16	**5.20**	45.78	**1.65**
Ca_%_ARMS	0.293	**3.419**	0.13	**7.69**	0.10	**5.59**
Cd_ppm_ARMS	0.218	**9.195**	0.35	**12.54**	0.15	**16.41**
Co_ppm_ARMS	13.325	**1.889**	14.25	**4.86**	6.50	**3.08**
Cr_ppm_ARMS	27.000	**3.229**	36.38	**8.16**	24.77	**5.13**
Cu_ppm_ARMS	44.858	**1.808**	143.33	**6.60**	238.66	**2.21**
Fe_%_ARMS	3.120	**2.002**	3.25	**5.11**	3.32	**1.96**
Ga_ppm_ARMS	5.975	**1.933**	7.50	**8.68**	6.00	**4.41**
Hg_ppb_ARMS	84.000	**1.190**	59.50	**10.13**	41.67	**36.03**
K_%_ARMS	0.048	**12.155**	0.29	**7.12**	0.27	**4.22**
La_ppm_ARMS	17.925	**5.113**	28.10	**7.46**	26.40	**5.58**
LOI_%	6.675	**1.498**	7.08	**3.56**	4.83	**5.97**
Mg_%_ARMS	0.540	**3.855**	0.68	**4.48**	0.50	**2.00**
Mn_ppm_ARMS	1090.500	**2.405**	619.25	**4.91**	268.33	**2.05**
Mo_ppm_ARMS	0.650	**2.350**	11.48	**6.51**	14.09	**2.08**
Na_%_ARMS	0.025	**8.000**	0.02	**6.71**	0.03	**11.18**
Ni_ppm_ARMS	17.025	**3.911**	30.33	**4.63**	14.33	**1.76**
P_%_ARMS	0.080	**1.443**	0.05	**3.85**	0.07	**2.83**
Pb_ppm_ARMS	14.915	**6.250**	23.51	**3.00**	40.12	**4.07**
S_%_ARMS	0.018	**32.991**	0.04	**43.30**	0.06	**28.87**
Sb_ppm_ARMS	4.675	**2.195**	0.31	**5.59**	0.55	**5.81**
Sc_ppm_ARMS	4.150	**6.064**	4.50	**14.80**	4.17	**9.70**
Se_ppm_ARMS	0.450	**12.830**	0.55	**10.50**	0.73	**20.83**
Sr_ppm_ARMS	10.100	**3.960**	12.60	**7.16**	9.33	**5.29**
Te_ppm_ARMS	0.025	**23.094**	0.03	**35.53**	0.15	**9.96**
Th_ppm_ARMS	2.325	**13.140**	9.55	**8.31**	11.50	**5.70**
Ti_ppm_ARMS	0.075	**5.333**	0.10	**6.45**	0.11	**5.23**
Tl_ppm_ARMS	0.118	**0.000**	0.36	**4.88**	0.42	**3.67**
U_ppm_ARMS	0.825	**6.998**	3.23	**8.20**	2.63	**5.80**
V_ppm_ARMS	50.750	**3.010**	38.75	**5.16**	38.00	**2.63**
W_ppm_ARMS	0.100	**0.000**	0.98	**5.92**	100.00	**0.00**
Zn_ppm_ARMS	63.925	**2.518**	110.68	**3.89**	57.93	**2.34**

Table 2.2. Relative standard deviation (%RSD) for elements by aqua regia-ICPMS calculated from repeated analysis of CANMET standard reference materials. Number of analyses in brackets e.g. (3).

Another common method for estimating precision is from results of duplicate sample analyses. Scatter graphs, constructed by plotting element values for the first sample of a duplicate pair (e.g. Cu_1_ppm) against the second value measured for the duplicate pair (e.g.

Cu_2_ppm) is a simple way for to visually demonstrating variability. In Figure 2.2 the results of 19 duplicate analyses of prepared soil samples from this project reveal a close correlation between the values for each sample in the duplicate pair.

While this method clearly displays the degree of correlation between the two measured values in the first and second of a duplicate sample pair it does not provide a numeric estimate for sampling and/or analytical precision. Thompson and Howarth (1978) and more recently (Stanley and Lawie, 2007) apply a regression model to calculating a numeric value of precision over a concentration range from the results of random duplicate sample analyses.

From a regression model the standard deviation of the determination (S_c) is expressed as a function of concentration (c) and the standard deviation at zero concentration (S_o) by the equation: $S_c = S_o + kc$ and a value of precision (P_c) can be estimated at any concentration by the equation $P_c = 2S_c/c$. Ideally, the Thompson and Howarth method for calculating precision needs the results for more than 50 duplicate sample analyses. However, there is a modified procedure for more than 10 but where there are less than 50 duplicate sample analyses. This procedure estimates precision from a control chart that is constructed from the difference between the two values for each sample duplicate pair (X1-X2) plotted as a function of the mean of the two values [(X1+x2)/2]. The median value (M_d) for the duplicate value difference is related the standard deviation (σ_c) of the difference by the equation:

$$M_d = 0.954\,\sigma_c$$

The graphs are constructed for the normal population deviates at different percentiles. For example, at the 50th percentile the normal deviate is 0.6745 and the relationship between M_d and σ_c is:

$$M_d = 0.6745 /2\ \sigma_c \ = \ 0.954\sigma_c$$

For the 90th percentile the normal deviate is 1.6449 and $M_d = 2.3262\,\sigma_c$
For the 99th percentile the normal deviate is 2.5758 and $M_d = 3.6427\,\sigma_c$

For a +/-10% , 95% confidence limit control graph at a concentration of 100 ppm σ_c is 5 ppm and the control points for the 90th and 99th percentiles respectively are 11.65ppm and 23.3 ppm. Figure 2.3 shows a MS Excel control chart with points plotted from the duplicate Cu analytical data for the project described in this report. The same data was used to create scatter plot shown in the Figure 2.2.

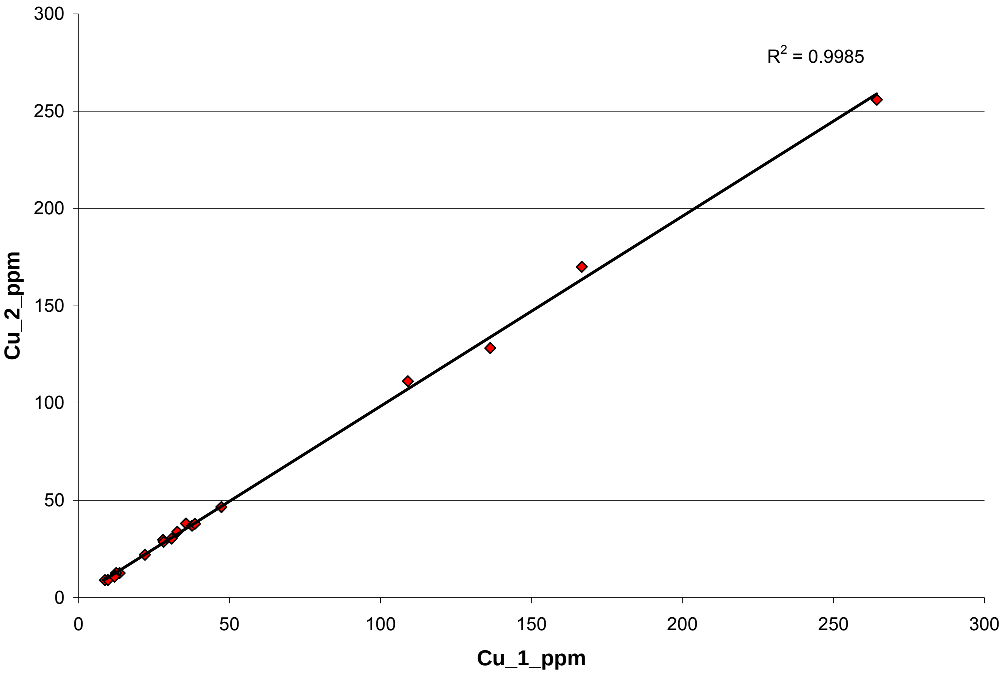

Figure 2.2. Scatter graph of Cu values for 19 duplicate soil samples.

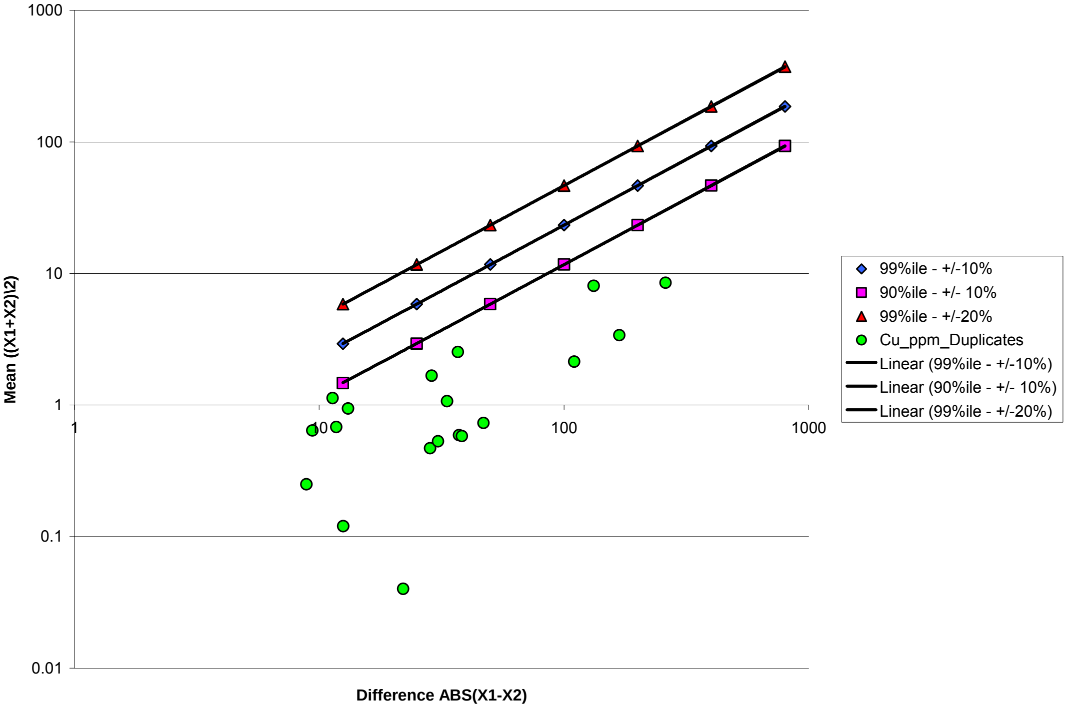

Figure 2.3: Control Chart for Cu analytical duplicates.

Control lines plotted on the graph are for a +/- 10 percent variation at the 90th and 99th percentile and for a +/- 20 percent variation at the 99 percentile. Ninety percent of the mean duplicate pair values plotted as a function of the difference between the duplicate pair values must fall below the 90th percentile line for precision to be better that +/- 10% at a 95% confidence level. Similarly, 99 % of the duplicate pair values must fall below the 99 percentile lines if variation is better than -/+ 10%. In Figure 2.3 all of the values for the analytical duplicate values are within the 90th percentile line and analytical precision is therefore better than +/- 10%. Figure 2.4 is a graph plotted from Cu values for field duplicate soil samples from the same data set. In this case the Cu variation will represent the sum of analytical and sampling variation. Two of the points on the graph are above the 99th percentile, +/- 20 percent variation control line indicating that the combined analytical-soil sampling precision exceeds +/-20 percent. Examining the identity of the points on the graph reveals that the two samples above the 99th percentile, +/- 20 percent variation control line are duplicates of upper B horizon soil. The greater variation of Cu might reflect upper B horizon samples with a larger median grain sized material compared to that of Lower B and C horizon samples. A higher content of sieved sediment with a median grain size close < 0.177 mm would decrease the combined analytical-sampling precision especially if small (e.g. 0.25 gram) samples are analysed. There is not sufficient duplicate sample data for a statistical test (t-test) to confirm if there is actually a difference between clusters of points on the graph. In Figure 2.4 three duplicate sample values are above the 90%ile 10% control line. Binomial probability tables predict 18 percent of points (3 out of 15) will fall outside of the 90th percentile +/- 10% control line by chance alone and therefore Cu sampling-analytical data variation is certainly greater than +/- 10% at the 95% confidence level.

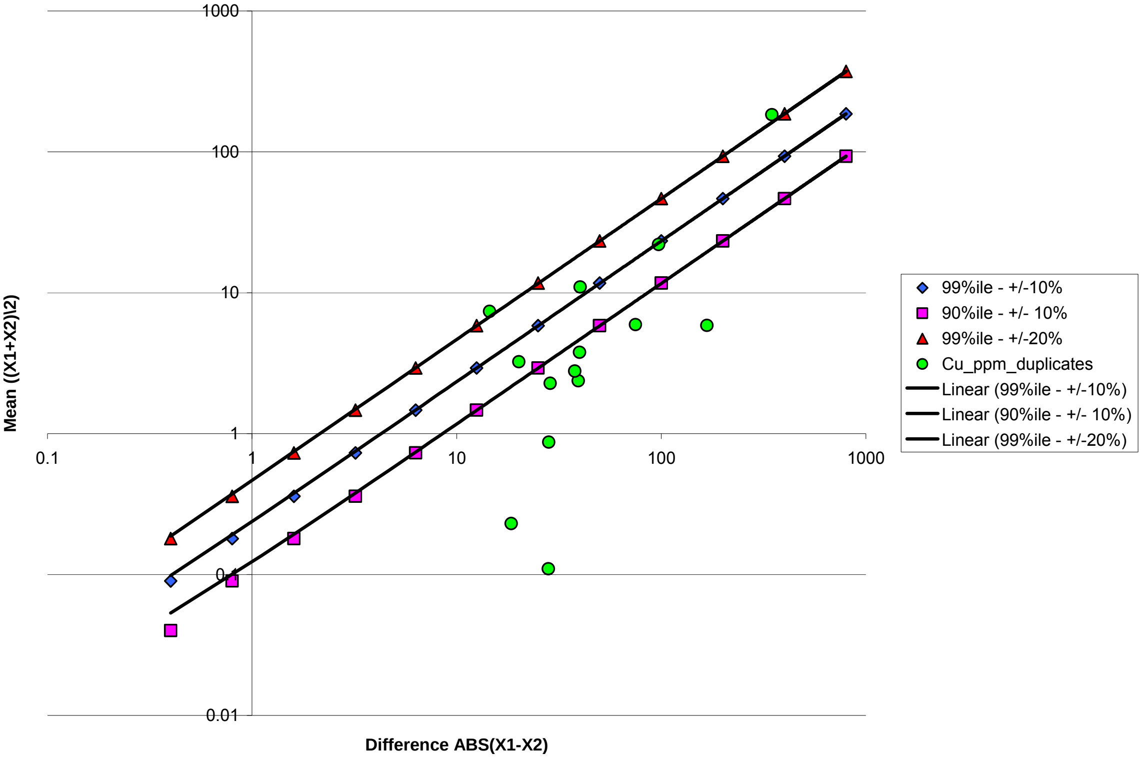

Figure 2.4: Control chart for Cu Field sampling duplicates.

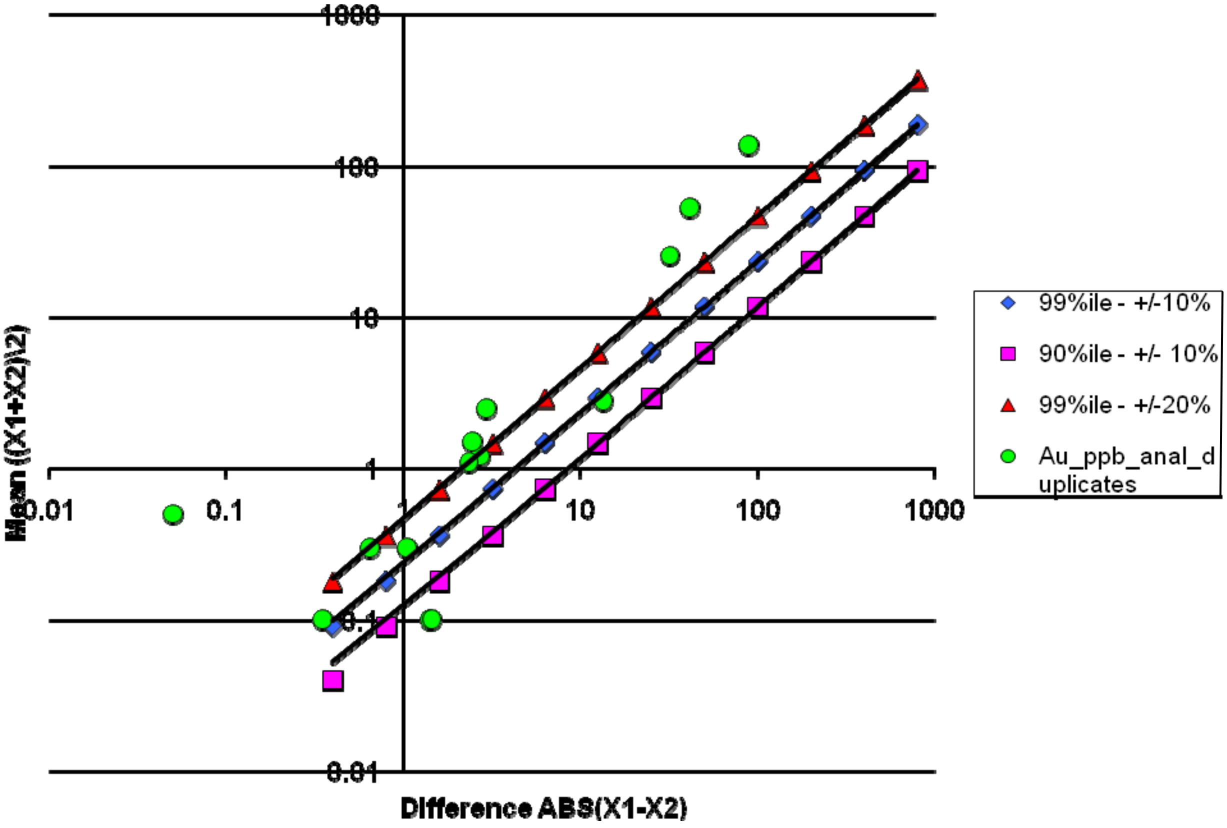

Figure 2.5: Control chart for Au in field duplicate soil samples.

Control charts have been created from analytical duplicate and field soil sample duplicate data for other elements. A reliable estimate of precision is difficult for some elements (e.g. Au) when many of the mean duplicate sample values are reported below detection limit. One option is to set values below detection limit at the detection limit or half the detection limit so that there are sufficient points to create a graph. However, this adjustment introduces a bias that makes the reliability of the precision estimate from the control graph questionable. Figure 2.5 shows field duplicate soil sample data for Au determined by aqua regia-ICPMS. While most of the values exceed the 99th percentile +/- 20 percent control line only 3 are above a mean concentration of 10 ppb suggesting that a working detection limit is higher than this concentration and that the variation in the 20 to 100 ppb range exceeds +/- 20 percent.

A similar control graph from analytical duplicates for Au by aqua regia-ICPMS in Figure 2.6 suggests that the field sampling and splitting of material to create the analytical duplicate samples contribute independently to the large Au variation in the soil. A lower detection limit for Au by aqua regia-ICPMS compared to that by instrumental neutron activation (INAA) allows a more realistic precision estimate. Only two duplicate soil samples have INAA Au values above the instrumental detection limit (2 ppb) and hence the control graph in Figure 2.7 is a misleading indication for INAA analytical variability.

Field duplicate soil sample control charts for Ag, As and Co in Figures 2.8 to 2.10 show that combined sampling-analytical precision is close to or just exceeds the +/- 20 percent for these elements. For Co the analytical technique does not appear to influence precision as shown by a comparison of the variation for the field duplicate samples analysed for Co by aqua regia-ICPMS (Figure 2.10) to those analysed for Co by INAA (Figure 2.11). Precision estimates for the majority of elements determined by aqua regia-ICPMS and by INAA based on an examination of the control graphs plotted from the field duplicate sample results are summarised in Table 2.3. For most of the elements determined by aqua regia-ICPMS and INAA the combined sampling-analytical precision lies in the +/- 10 to 20 percent range.

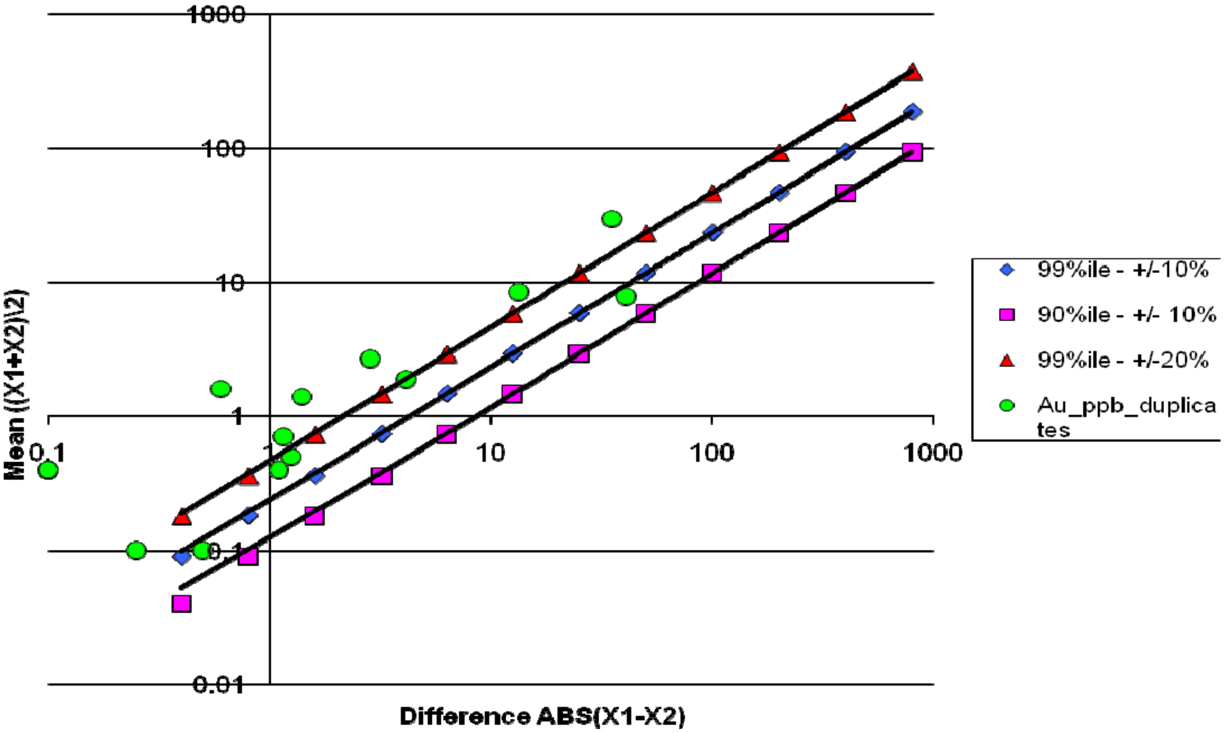

Figure 2.6. Control chart for Au by aqua regia-ICPMS in analytical duplicate samples.

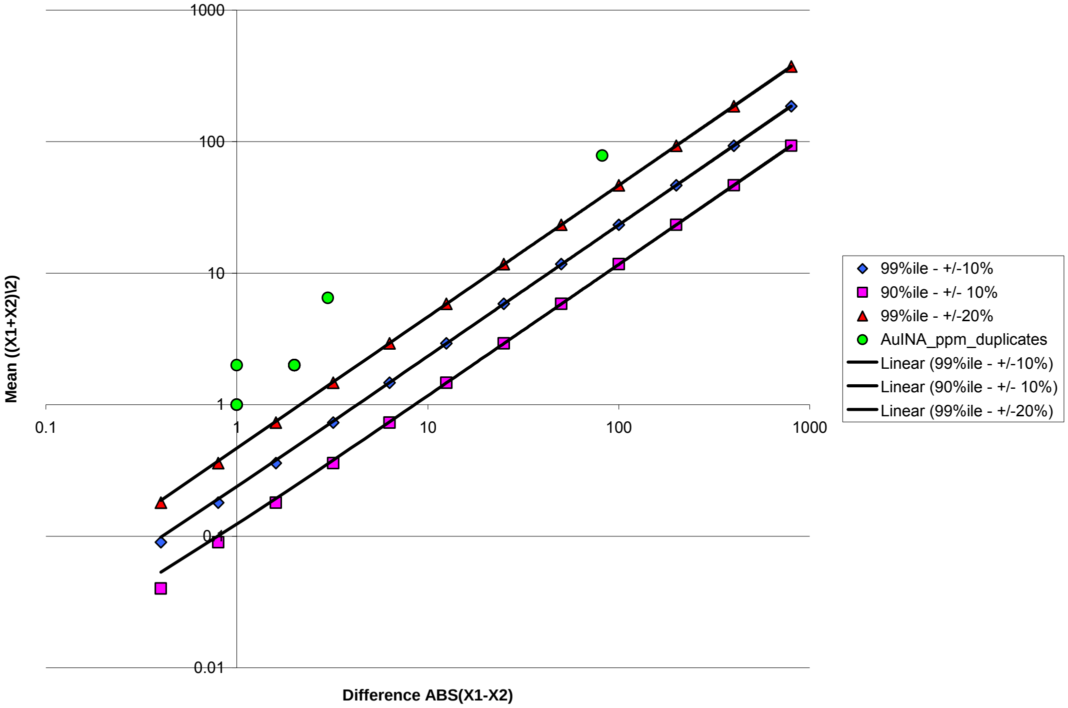

Figure 2.7: Control chart for Au by instrumental neutron activation (INAA) in analytical duplicate samples.

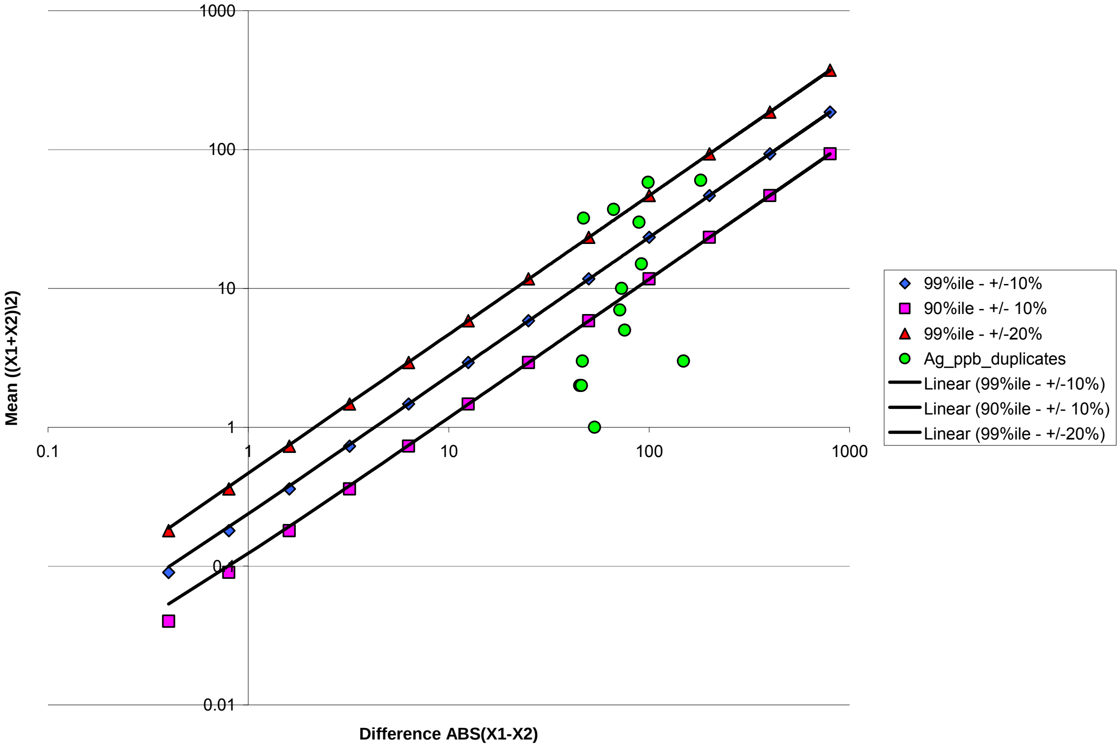

Figure 2.8: Control chart for Ag by aqua regia - ICPMS in field duplicate samples.

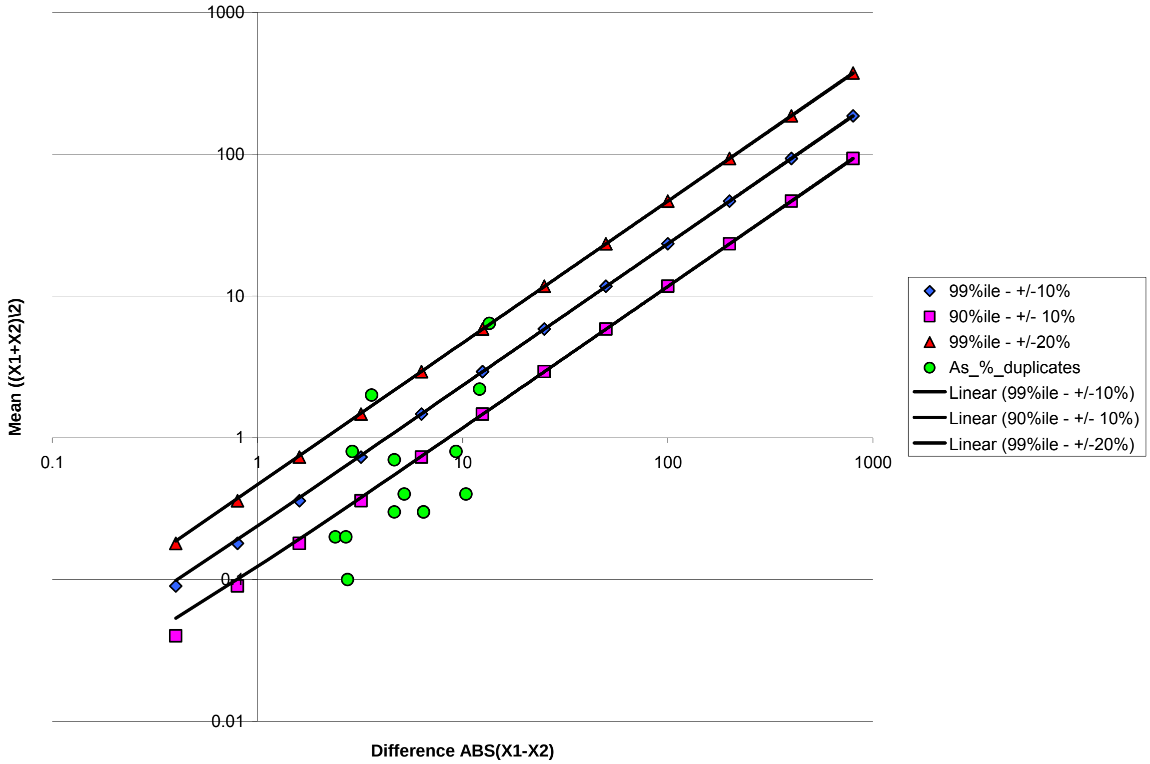

Figure 2.9: Control chart for As by aqua regia - ICPMS in field duplicate samples.

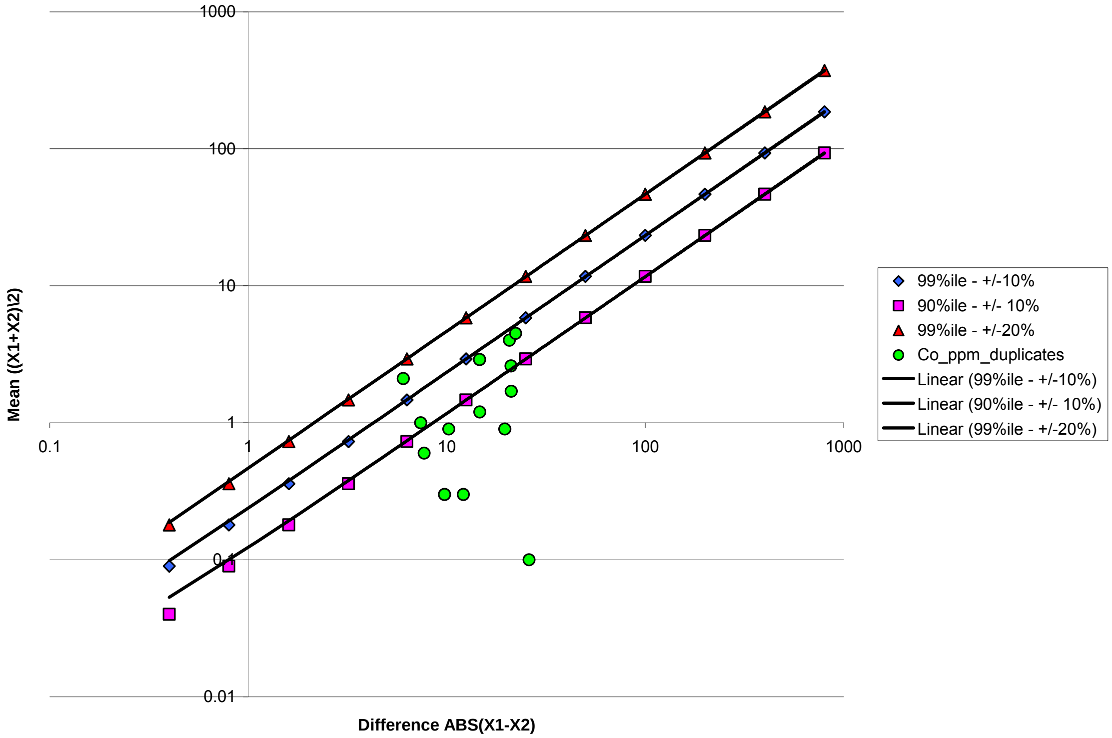

Figure 2.10: Control chart for Co by aqua regia - ICPMS in field duplicate samples.

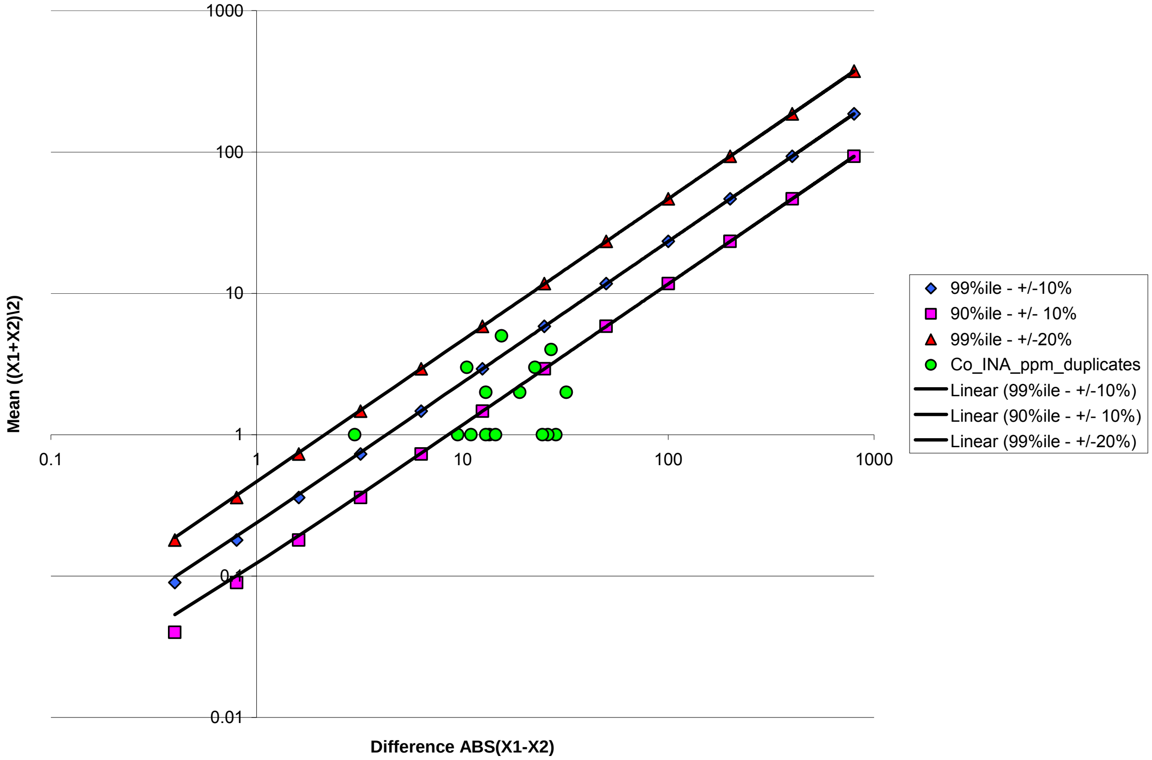

Figure 2.11: Control chart for Co by INAA in field duplicate samples.

Element	> +/- 20 %	+/- 20% to +/- 10%	< +/- 10 %
Ag_ppb_ARMS	x		
Al_%_ARMS		x	
As_ppm_ARMS		x	
As_ppm_INAA			
Au_ppb_ARMS		x	
Ba_ppm_INAA		x	
Ba_ppm_ARMS		x	
Bi_ppm_ARMS		x	
Ca_%_ARMS	x		
Ce_ppm_INA			x
Co_ppm_ARMS		x	
Cr_ppm_ARMS		x	
Cr_ppm_INAA		x	
Cu_ppm_ARMS		x	
Fe_%_ARMS		x	
Fe_%_INAA			x
Ga_ppm_ARMS			x
Hg_ppb_ARMS	x		
La_ppm_ARMS			x
LOI_%	x		
Mg_%_ARMS	x		
Mn_ppm_ARMS		x	
Mo_ppm_ARMS		x	
Ni_ppm_ARMS	x		
Pb_ppm_ARMS		x	
Sb_ppm_INA	x		
Sb_ppm_ARMS		x	
Sc_ppm_ARMS	x		
Sc_ppm_INA	x		
Sr_ppm_ARMS		x	
Te_ppm_ARMS			
Th_ppm_ARMS		x	
Ti_ppm_ARMS		x	
U_ppm_ARMS		x	
V_ppm_ARMS			x
Zn_ppm_ARMS			x
Soil pH (Field)			x

Table 2.3. Combined sampling-analytical precision ranges at the 95% confidence level for elements determined by aqua regia-ICPMS and INAA.

Field duplicates and analytical duplicates samples were included with the soil samples analysed for elements by Enzyme Leach^{SM}, BioLeach^{SM} and Mobile metal ion (MMI ^{TM}) techniques and for C5 to C17 soil organic compounds by the Soil Gas Hydrocarbon (SGH) ^{SM} method. A small number of blind field duplicates samples were analysed by these techniques compared to a larger number analysed by aqua regia-ICPMS and INAA for quality control. The analytical duplicate data used to create control graphs is from the commercial laboratory quality control results because no blind analytical duplicates were included in the samples sent for analysis. For this reason a comparison of sampling and analytical variability from control graphs for Enzyme Leach^{SM}, BioLeach^{SM} and MMI ^{TM} can be misleading. For example, the field duplicate control graph for Cu by MMI ^{TM} in Figure 2.12 has only four values for duplicate samples and shows a large sampling variability that can be attributed to two samples, one of which is highly organic. The analytical duplicate control graph in Figure 2.13 from the commercial laboratory duplicate analyses in Figure 2.13 indicates a variability in the 20 to 30 percent range since one of the points is above the 99 percentile control line. Paired sampling and analytical control graphs for Cu by Enzyme Leach^{SM} are shown in Figures 2.14 and 2.15 and for Cu by bioleach in Figures 2.16 and 2.17.

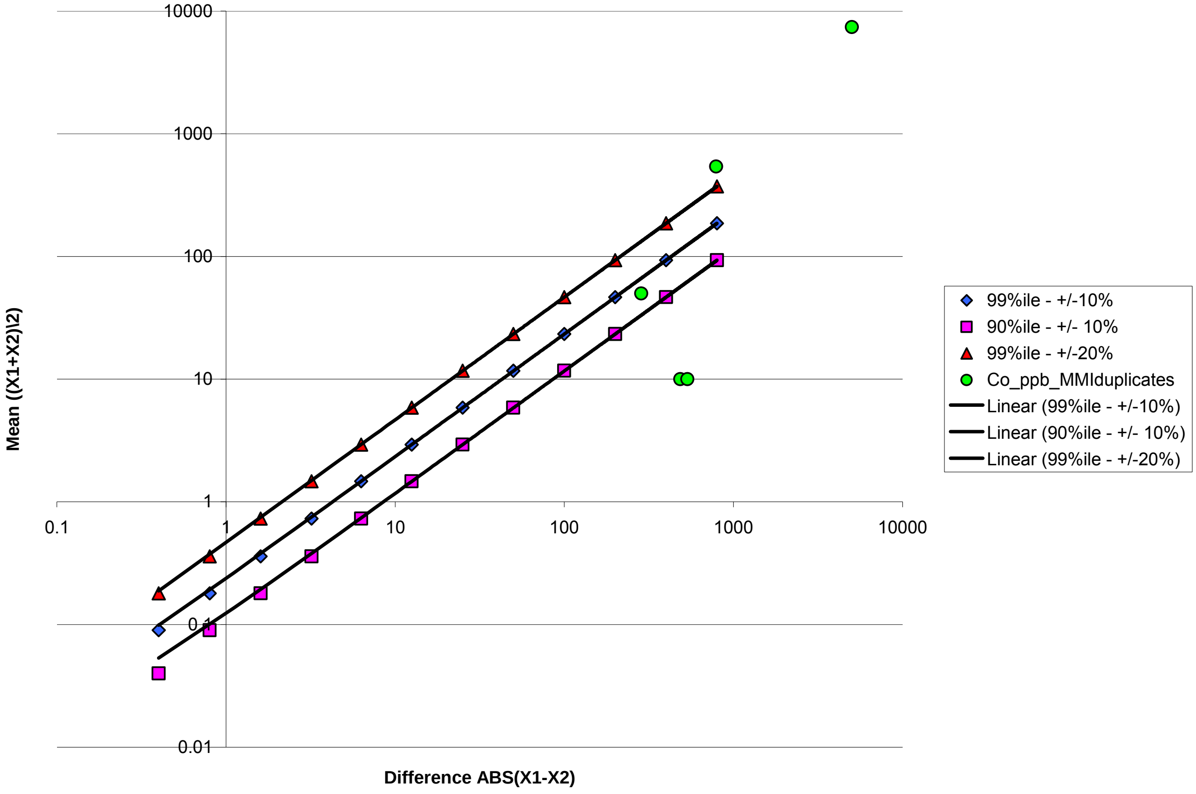

Figure 2.12. Control chart for Cu by MMI^{TM} in field duplicate samples.

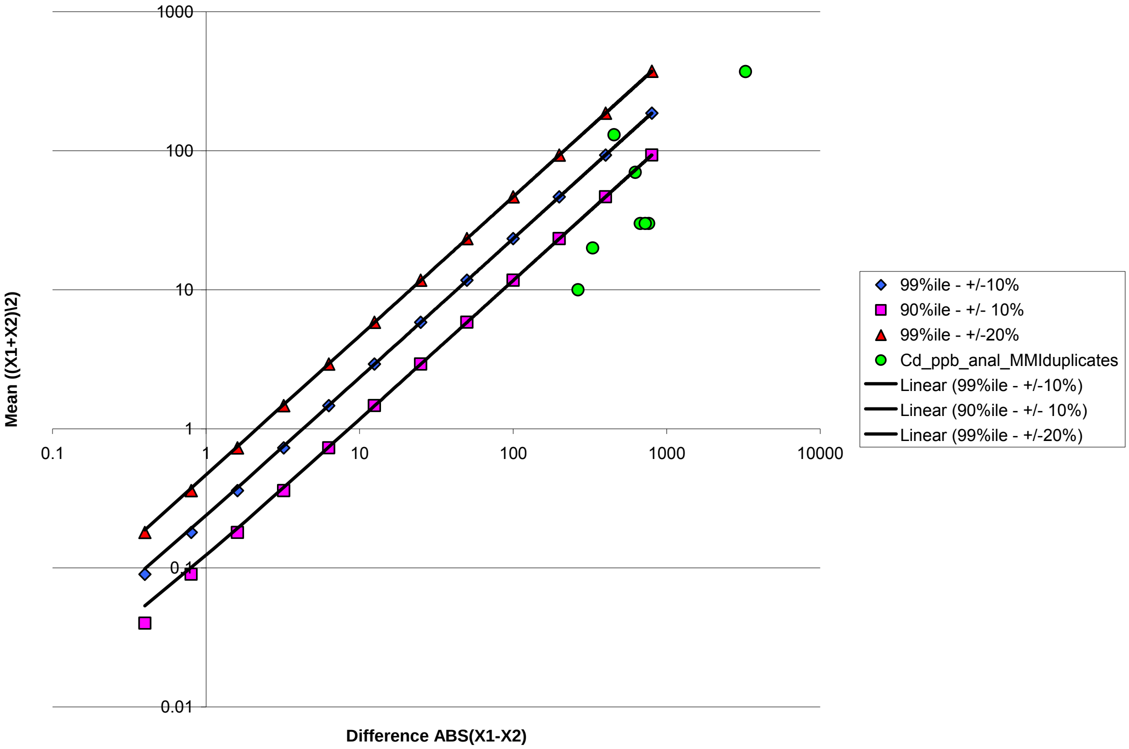

Figure 2.13. Control chart for Cu by MMI^{TM} in analytical duplicate samples.

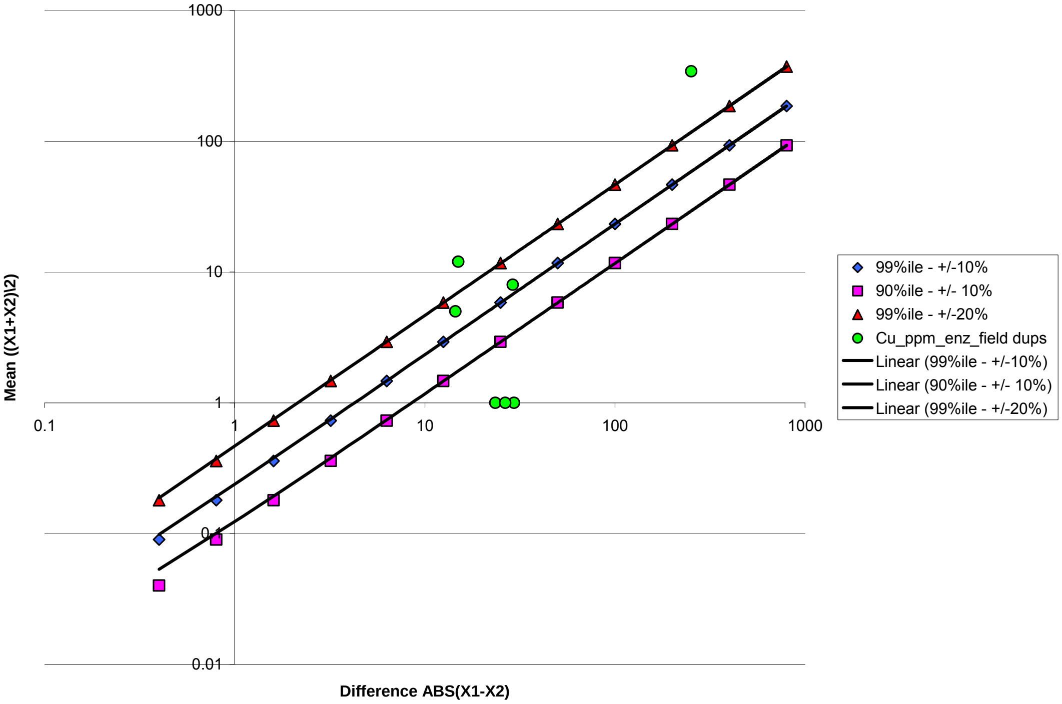

Figure 2.14. Control chart for Cu by Enzyme Leach^{SM} in field duplicate samples.

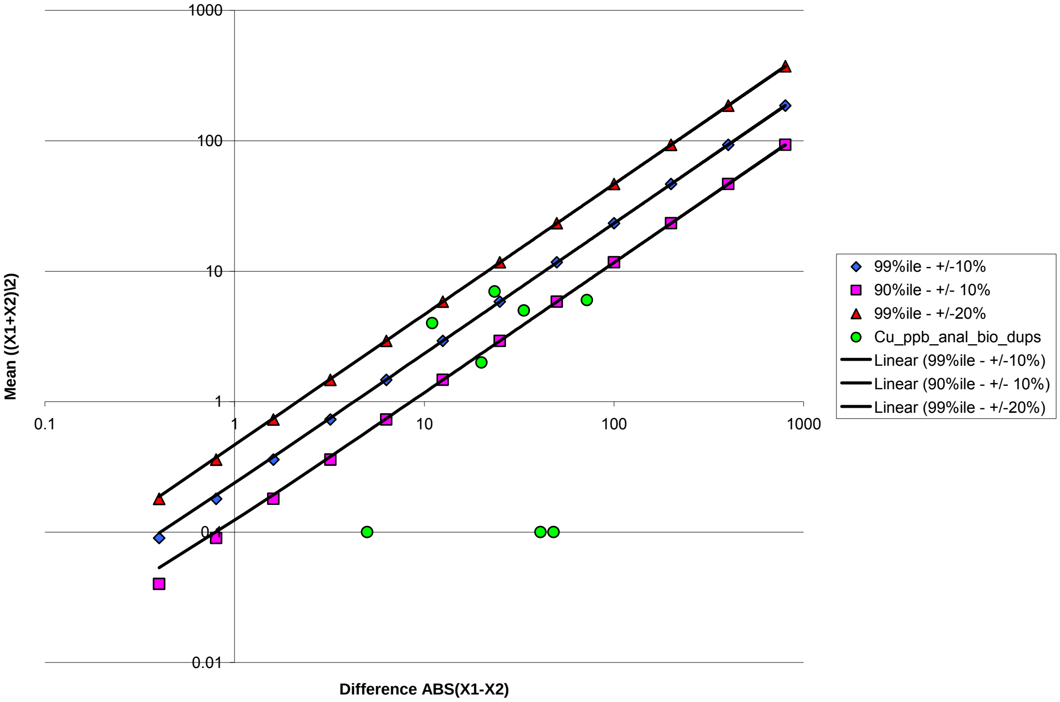

Figure 2.15. Control chart for Cu by Enzyme Leach^{SM} in analytical duplicate samples.

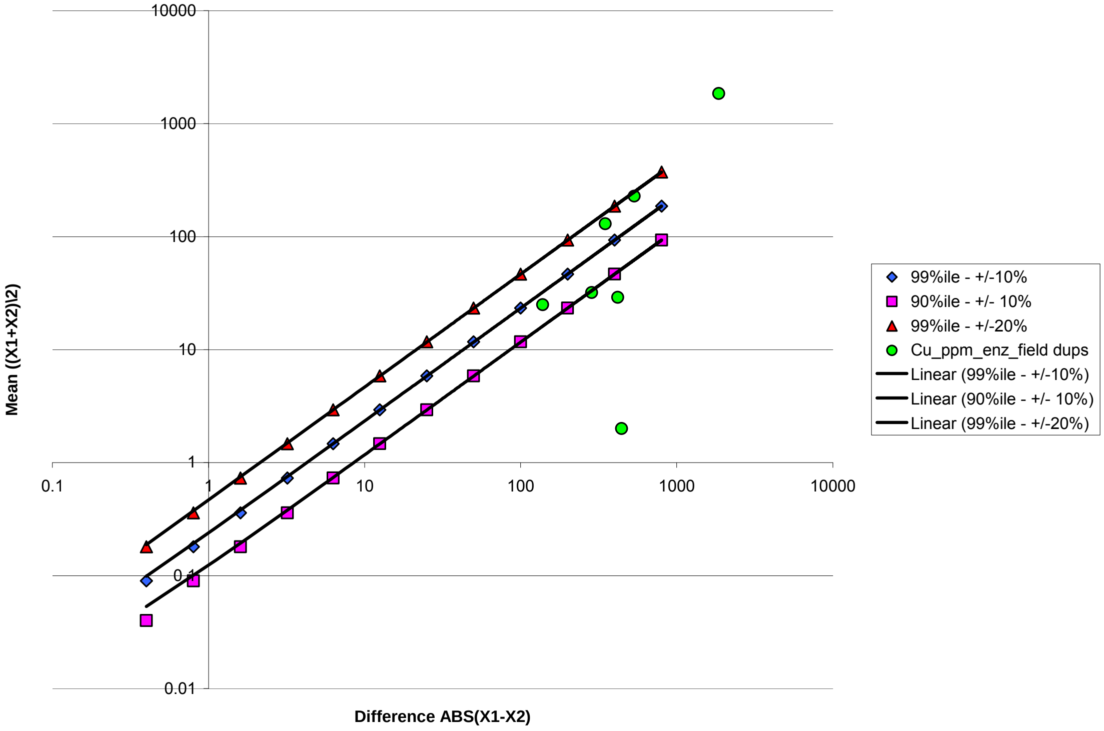

Figure 2.16. Control chart for Cu by BioLeach^{SM} in field duplicate samples.

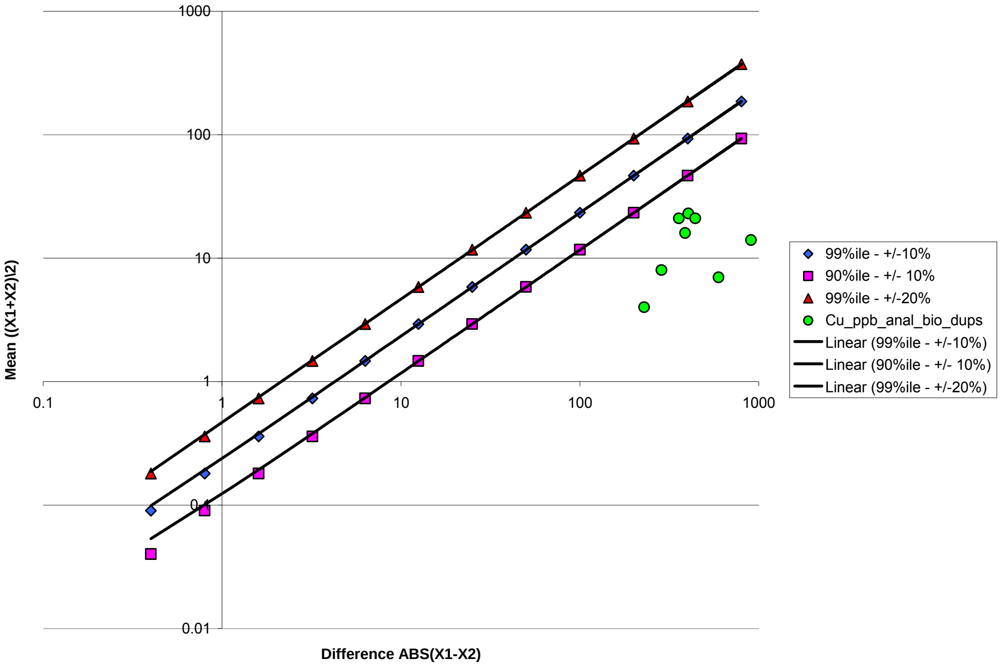

Figure 2.17. Control chart for Cu by BioLeach^{SM} in analytical duplicate samples.

Control graphs show that analytical precision for Enzyme Leach^{SM} is better than +/- 20 percent and for Bioleach^{SM} is better than +/- 10 percent. Combined analytical-sampling variability from field duplicate analyses shows a lower precision especially at higher concentrations, but, again, the precision estimate may be misleading because of the small number of field duplicate samples analysed. Also, the duplicate field sample pair with the highest detected Cu for all three methods displays the largest difference between the first and second duplicate value. This large difference may be explained by loss on ignition (LOI) values of 7.8 and 12.6 suggesting that not only has the soil an elevated organic carbon content typical of the upper B horizon but also the samples is relatively heterogeneous. If the Cu values for this duplicate field sample were excluded from the sampling-analytical control graph the precision for MMI^{TM} and Bioleach^{SM} would be better than +/- 20 percent over the 1 to 1000 ppb range. Sampling-analytical precision for many elements, especially Au, determined by the three partial extraction methods cannot be estimated from control graphs because most of the values are below detection level. Where concentrations are above detection limit analytical precision is typically better than +/- 10 percent at the 95th percentile. Iodine and Br are elements of interest because of their potential to detect buried mineralized rock. Figure 2.18 shows the control graph for Br in field duplicates by BioLeach^{SM} and in Figure 2.19 the BioLeach^{SM} each field duplicates for Iodine are plotted. For both elements the sampling-analytical precision just exceeds +/- 20 percent and, again, is mainly the results of a large difference between duplicate Br and I values for soil samples with higher LOI. Figures 2.19 and 2.20 show control graphs for Br and I in field duplicate samples by Enzyme Leach^{SM} and BioLeach^{SM} Field duplicate Br and I values have more variation than Bioleach^{SM} Br and I field duplicates samples. However, control graphs from the analytical duplicate values for Br and I by BioLeach^{SM} and by Enzyme Leach^{SM} indicate a precision better than +/-10 percent.

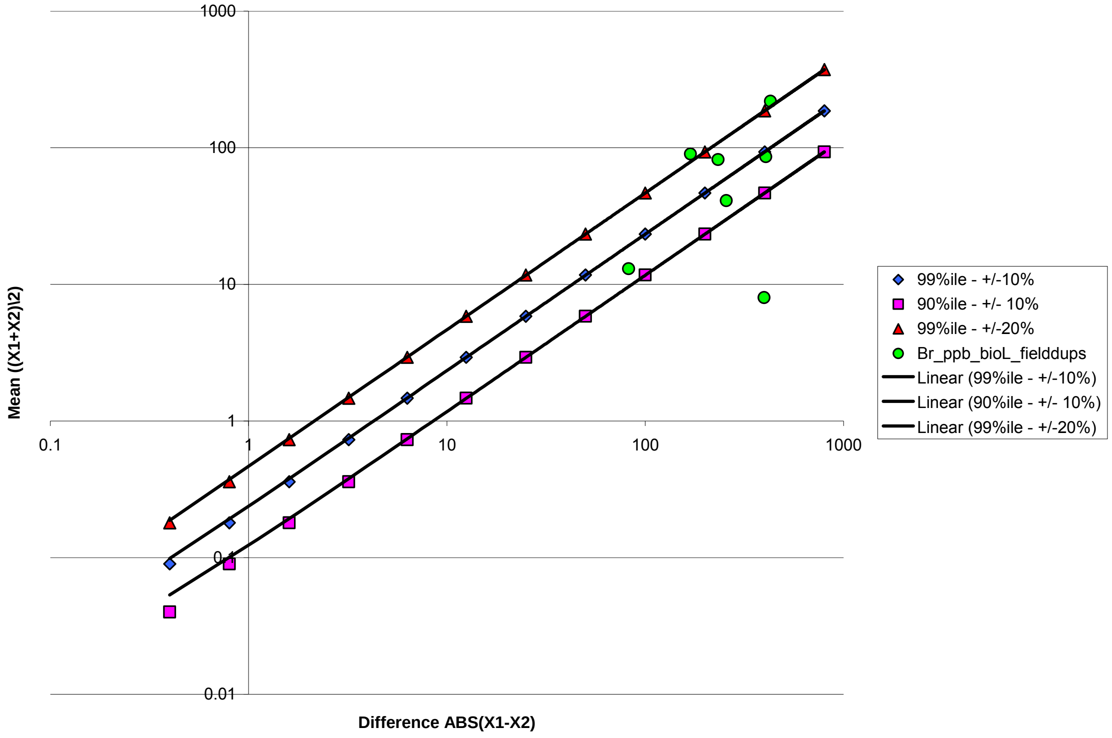

Figure 2.18. Control chart for Br by BioLeach^{SM} in field duplicate samples.

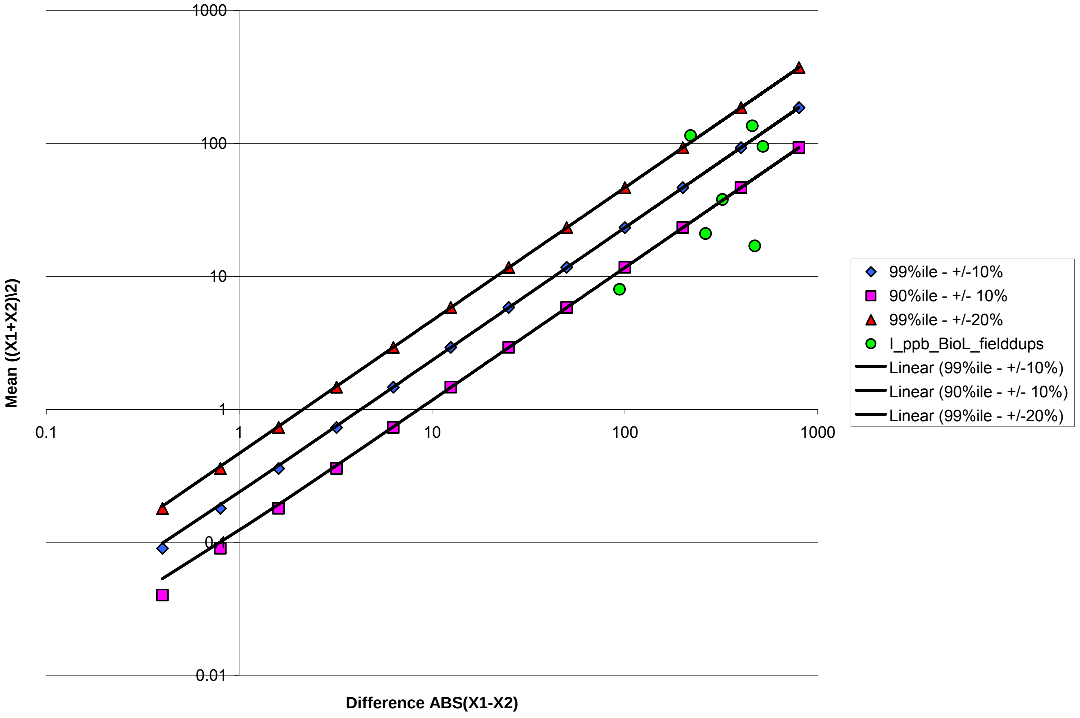

Figure 2.19. Control chart for I by BioLeach^{SM} in field duplicate samples.

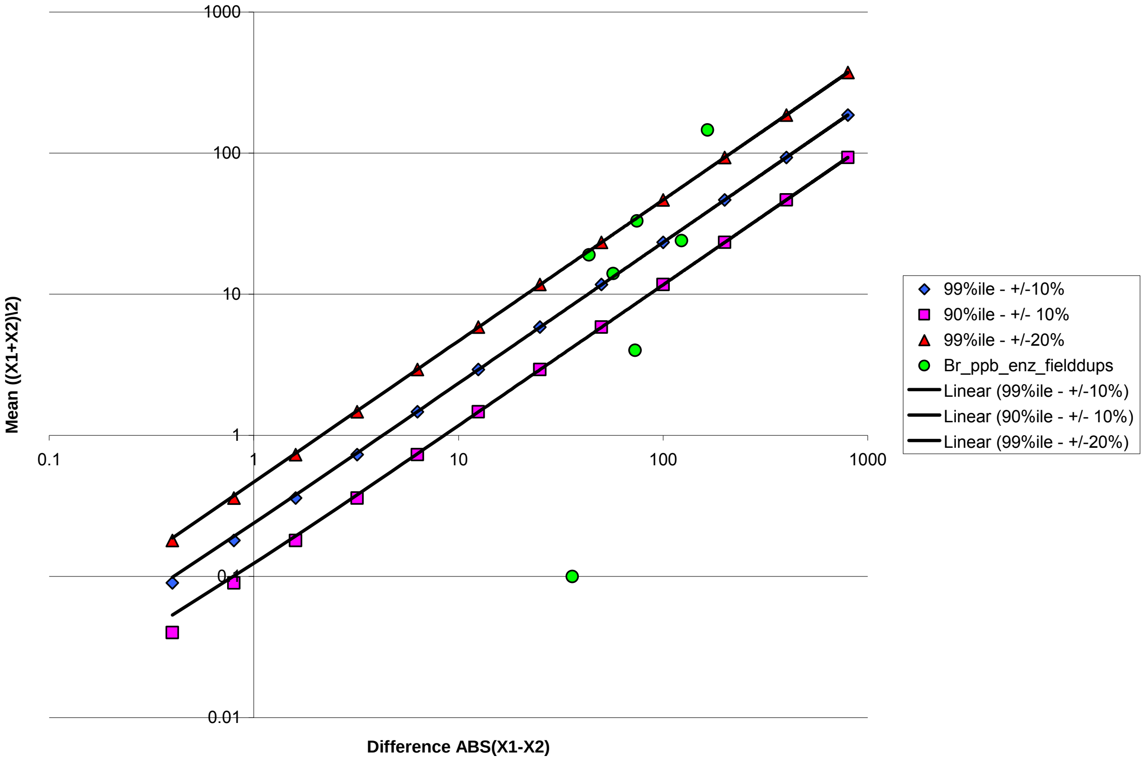

Figure 2.20. Control chart for Br by Enzyme Leach^{SM} in field duplicate samples.

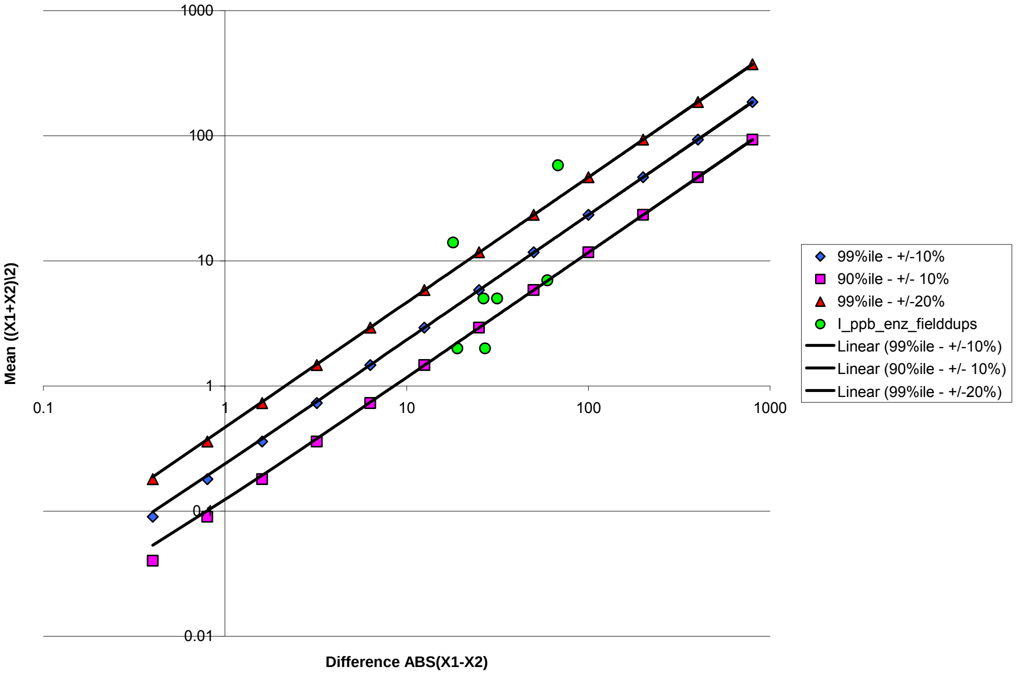

Figure 2.21. Control chart for I by Enzyme Leach^{SM} in field duplicate samples.

Figures 2.22 and 2.23 are control graphs for 002 alkyl_alkanes and 003 alkyl benzenes as an example of the variation displayed by two of the hydrocarbons measured by the by SGH^{SM} method. Control graphs for analytical duplicates indicate that the precision is less than +/- 10 percent at the 95 % confidence level whereas sampling variability is close to or more than +/- 20 percent.

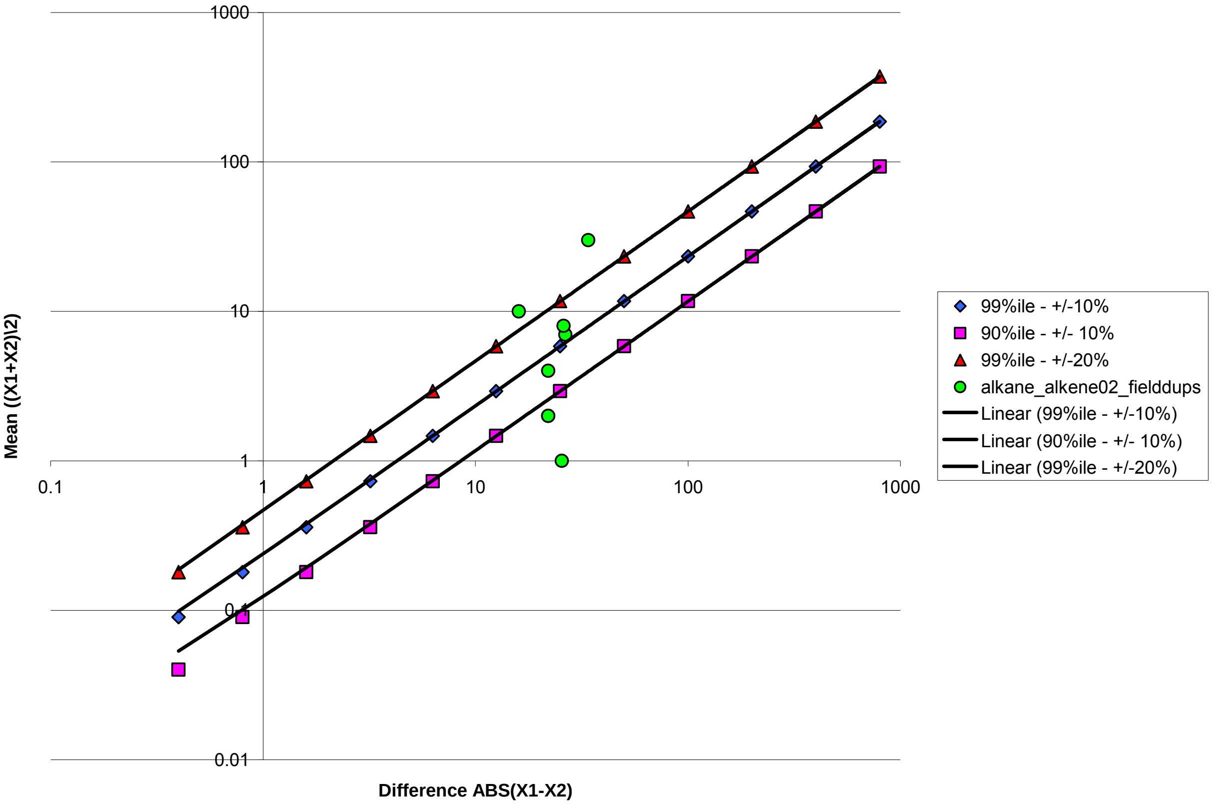

Figure 2.22. Control chart for 002alkyl_alkenes by SGH^{SM} in field duplicate samples.

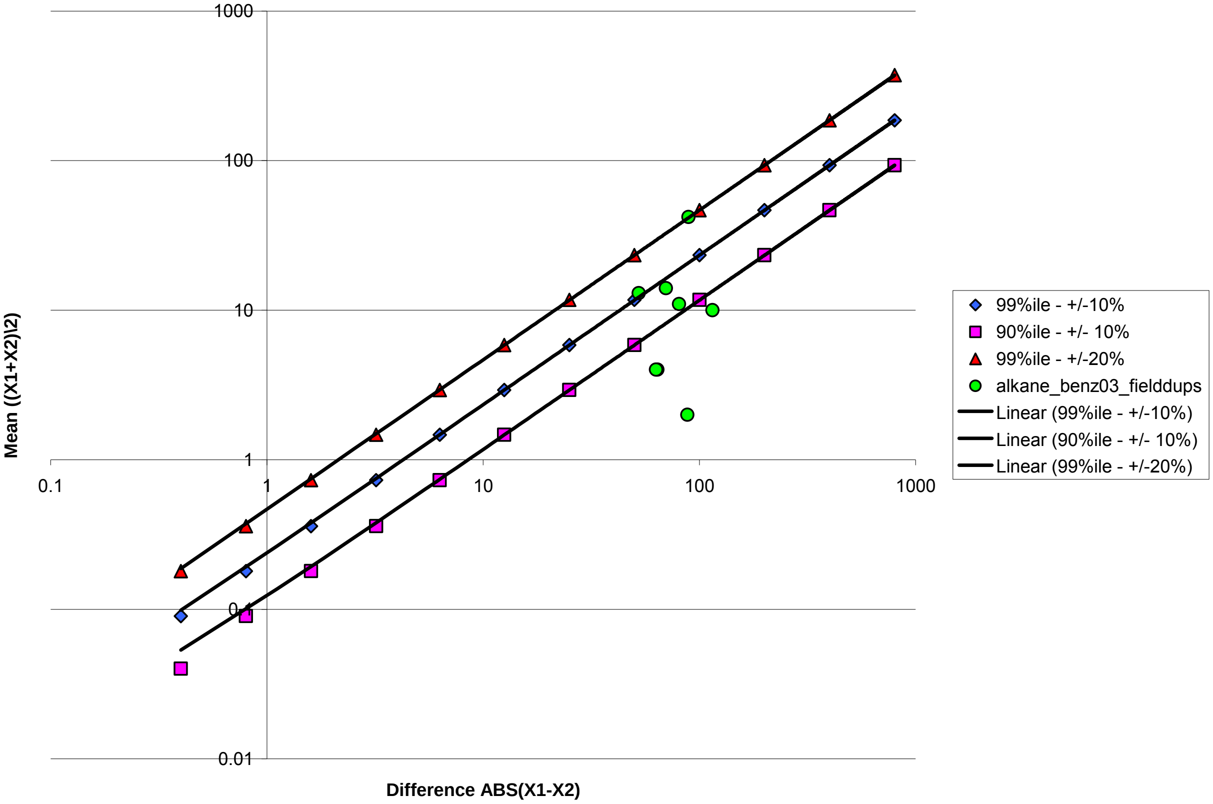

Figure 2.23. Control chart for 003 alkyl_benzenes by SGH^{SM} in field duplicate samples.

In summary, analysis of data generated from the repeated determination of blind standards and duplicate prepared inserted into batches of 20 samples before analysis reveals that the analytical precision for aqua regia-ICPMS and INAA determined elements is better than +/- 20 percent at the 95th percentile confidence level. Combined sampling – analytical precision for pathfinder elements (e.g. Cu, Co, Mo, As) these two methods estimated by control graphs created by plotting the difference between the first and second field sample duplicate value as function of the mean value is between +/- 10 and 20 although some elements such as Ag and Hg show a variation exceeding +/- 20 percent.

3 Geochemical Case Studies

A typical geochemical survey can generate a large amount of field and analytical information so that a geochemist is faced with a challenging task when attempting to interpret this volume of data. Geochemical models are one option to help deal with this problem by providing a framework of basic principles (e.g. dispersion mechanisms) upon which data for specific properties (e.g. element values, pH) can then be interpreted. Applied to mineral exploration, geochemical models can simplify the information typically found in case histories by creating visual relationships between a mineral deposit and the deposit geochemical response. All of the information describing the bedrock geology, surficial geology, and features of the local environment, alteration and style of mineralization in an area with the types of sample collected, sampling strategy and the results of the geochemical sampling must be documented concisely to develop a model. Consequently, the published background geological and surficial information with relevant supporting geochemical data (e.g. rock geochemistry, stream sediment geochemistry) for the four orientation survey areas has been compiled in a systematic format so that it can be more easily used to support a preliminary analysis and interpretation and, subsequently, the development of a geochemical model to explain the dispersion of elements from buried Cu-Au porphyry mineralization.

3.1 Mouse Mountain - *MINFILE NUMBER:* 093G 003

Location: NTS – 93G 12	LATITUDE 53°03'00"	UTM NORTH – 5618050
	LONGITUDE - 122°19'16"	UTM EAST – 573000

MINFILE Status*:* Past Producer **Commodities:** Cu, Au, Ag

Mineral Deposit Profile: Class - L03: Alkalic porphyry Cu-Au

Significant and associated minerals*:* Chalcopyrite, malachite, azurite; traces of fluorite, sphalerite, bornite, ankerite, fuchsite.

Geology*:* Soil profiles were sampled over an area surrounding the Mouse Mountain mineral property located 10 km east of Quesnel, BC, (Figure 3.1.1) and most recently developed by Richfield Ventures Corp. The Mouse Mountain property is underlain by Triassic arc-related volcanic, sedimentary and intrusive rocks mapped in the past by Panteleyev, *et al*. (1996) and by Logan *et al.* (2008). Jonnes and Logan, (2007), have described local geology, Cu-Au mineralization and alternation of the property in detail. They identified three separate pyrite, chalcopyrite, malachite and azurite, northwest trending mineralized zones (Rainbow, Valentine, High-Grade) within carbonate - potassic altered monzonite stock that intrudes Upper Triassic lapilli tuff. One traverse of profiles sampled during the BCGS project crosses the Rainbow Zone and a second traverse is located about 2 km to the south of BC Highway 26.

The poorly exposed Rainbow mineralized zone in the northwest part of the property is within fine-grained, pink – orange – yellow monzonite that has intruded a green to grey coloured, crystal-rich, lapilli volcaniclastic tuffite. Jonnes and Logan, (2007), describe the tuffite to be a heterolithic breccia or crystal lithic tuff based on, among other criteria, the presence of augite-phyric basalt clasts that may be up to 50 cm in size. This volcanic rock is mainly clast-supported and is distinguished from an unsorted, matrix supported polymictic breccia that outcrops out to the south of Mouse Mountain by the presence of better sorting, more rounded clasts and the absence of ultramafic clasts. There is only weak, pervasive sericitization of the heterolithic breccia. Thin bedded, dark grey and black siltstone, green and grey pyroxene basalt, hornblende porphyry and plagioclase porphyry have also been mapped by Jonnes and Logan, (2007), in the area around Mouse Mountain. The Cu-Au mineralization in the Valentine Zone to the east of Mouse Mountain is hosted in a variably altered, microporphyritic monzonite.

Alteration and Mineralization:

Rainbow Zone: Where visible, Cu-Au mineralization consists of disseminated and vein hosted pyrite, chalcopyrite, malachite and azurite with traces of fluorite, sphalerite and bornite within ankerite-fuchsite altered monzonite. Up to 0.25 percent Cu and 100 ppb Au have been reported in samples of bed rock. Monzonite in the Rainbow Zone shows pervasive, texturally destructive quartz-carbonate (mainly ankerite) and fuchsite-maraposite alternation.

Valentine Zone: Alkalic-porphyry-style alteration is displayed at the Valentine zone by a concentric propylitic envelope surrounding phyllic and then potassic mineral assemblages. The potassic alteration core consists of a potassium feldspar-magnetite-biotite-chlorite-diopside actinolite minerals that host disseminated and stockwork pyrite and chalcopyrite mineralization. A phyllic alteration envelope characterized by sericite, quartz and pyrite surrounds the potassic core. Surrounding the phyllic zone is a propylitic alternation halo that consists of chlorite, carbonate and epidote. Discrete, pervasive ankerite alternation zones, focused along north and north-east trending structures, overprint the propylitic-phyllic-postassic alternation and are associated with elevated As, Sb and Mo. Dolomite, pyrite, calcite, quartz and sericite are common minerals in the alternation overprint. There is supergene enrichment near the bedrock surface by hematite, malachite and azurite along fracture surfaces in outcrop.

High Grade Zone: In this zone, located 750 metres south of the Valentine Zone, Cu-Au mineralization is hosted in a mineralogically distinct phase of fine to medium textured monzonite. Alternation is similar to that displayed at the Valentine Zone and much of the monzonite matrix had been replaced by fine grained magnetite and with biotite, epidote and chlorite representing the alternation of clinopyroxene. Veins of coarser magnetite represent a later phase of potassic alternation. Chalcopyrite, malachite and azurite are the principal Cu minerals in the High Grade Zone.

Local Environment: The upland topography of the area around Mouse Mountain is typical of the Fraser River basin where most of the land surface below the 1200 m elevation is drift covered (Holland, 1964). Mouse Mountain, a prominent uneven rocky ridge rising to 1020 metres, with a steeper northwest-facing slope and more gradual southeast-facing slope, could be interpreted as a Roche moutonnée formed by regional ice flow from the southeast towards the end of the Wisconsin glaciation. Glaciers advanced into the region from both the Cariboo and Coast mountains, resulting in ice-flow events towards the north and North West respectively. These ice-flow events were followed by a later, northwest advance from the Cariboo Mountains only. Tipper, 1971, describes north-trending glacial groves as a most common surface landform in the area immediately east of Quesnel that could reflect erosion by one or more glacial advance(s) (or glaciations) across the region. The extent of the last glacial advance of ice into the Mouse Mountain area is uncertain. Glacial sediments deposited on gentler hillsides by the advancing ice from the south are typically a sandy diamicton (basal till) whereas reworked (possibly englacial) till and colluvium mantle steeper hillsides. During final stages of deglaciation, ice blocked the Fraser River, reversed the river flow, and formed a large proglacial lake that filled much of the Fraser River basin. Thick sand and clay units near Prince George are typical of sediments deposited in this lake. Near Mouse Mountain, however, an intermittent thin veneer of sand and gravel could be evidence of reworking the underlying the till by the proglacial lake water.

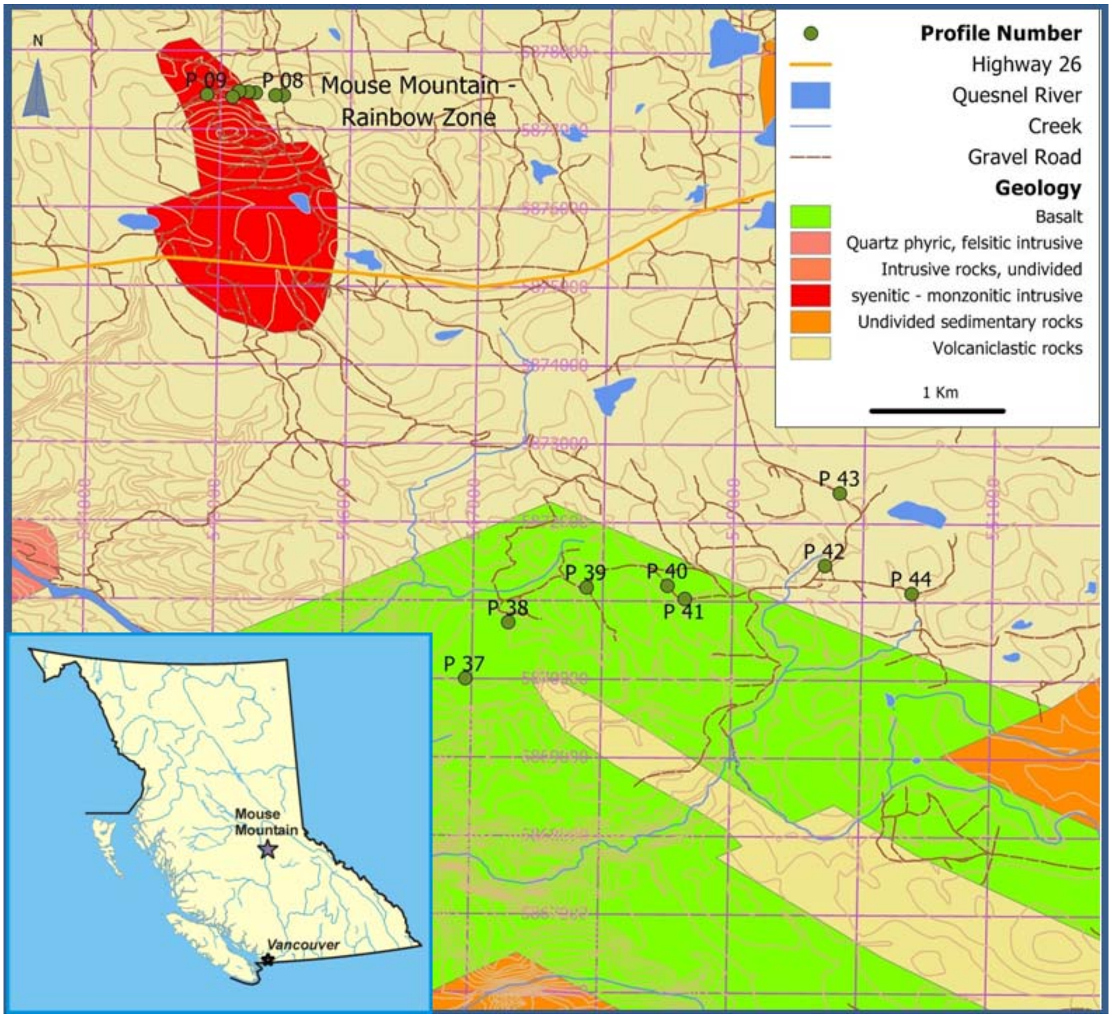

Figure 3.1. Mouse Mountain, Geology, and Traverse Locations. Geology from Massey *et al.* 2005.

On the better drained uplands the soil formed is mainly a humo ferric podzol developed from a parent glacial sediment and bedrock. Vegetation comprises a mainly Interior Douglas-Fir (*Pseudotsuga menziesii glauca),* White Spruce *(Picea glauca),* Lodgepole Pine *(Pinus contorta latifolia),* Trembling Aspen (*Populus tremuloides*) and Paper Birch (*Betula papyrifera*) canopy that is typical of the Douglas-Fir-White Spruce ecological sub-zone (Lord, 1982). Willow (*Salix*), Alder (*Alnus*) and Devils Club (*Oplopanax horridus*) are abundant understory species. Much of the area around Mouse Mountain has been logged and locally the Mountain Pine beetle has damaged the timber. Figure 3.1 shows geology and features of Mouse Mountain.

Mouse Mountain Geochemistry

Lithogeochemistry

No rock samples were collected and analysed as part of geochemical studies documented in this project. However, Jonnes and Logan, (2007), do report results of hydrofluoric-nitric-hydrochloric-perchloric acid digestion-ICPMS analysis of rock samples collected from the Valentine zone during their mapping of the Mouse Mountain property. These data reveal elevated median values for Cu (2274 ppm), V (219 ppm), Au (307 ppb) and Pd (22 ppb) in the mineralized rock. Vanadium and Cu are also among elements that are elevated in the volcanic rocks that surround the Valentine Zone (Figure 3.1.1). Figure 3.1.2 is a box plot that displays trace element statistics calculated from the geochemistry of 10 Nicola volcanic rock samples. The samples, collected by Logan, (2008), during regional mapping in the area around Mouse Mountain were analysed by hydrofluoric-nitric-hydrochloric-perchloric acid digestion-ICPMS. Vanadium Cu and Zn are elements with relatively high background in Nicola Group rocks based on 3rd quartile values.

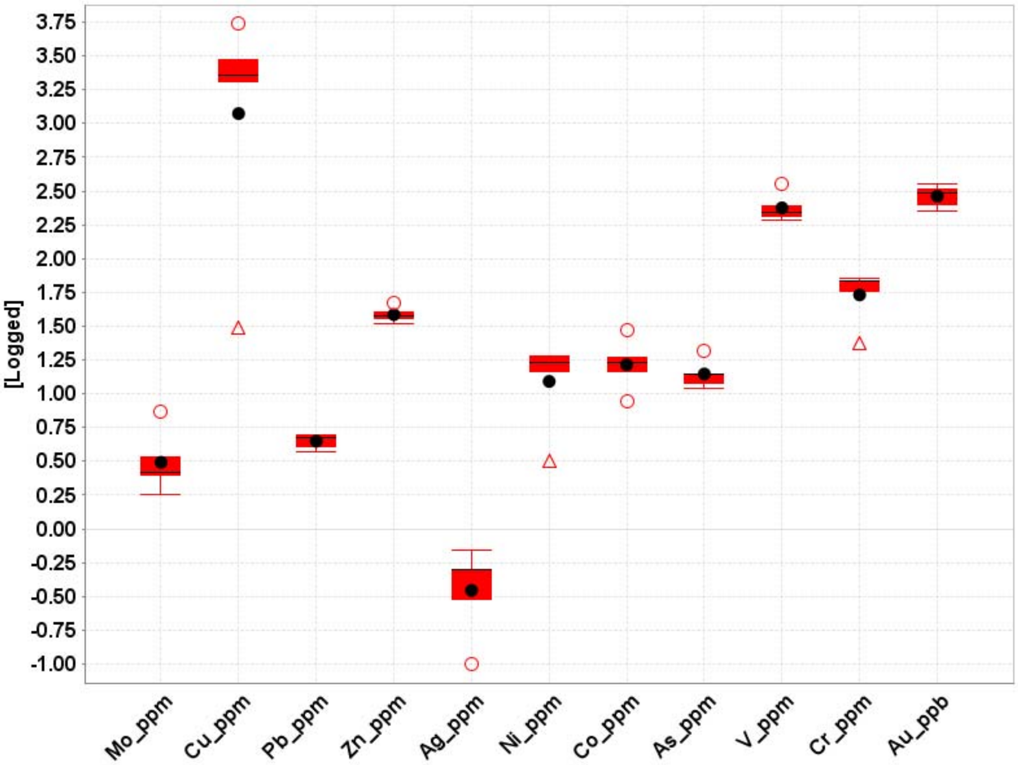

Figure: 3.1.1 A box plot showing the distribution of Au, As, Ag, Co, Cr, Cu, Mo, Ni, Pb, V and Zn in Valentine zone rock samples collected by Logan, (2008). Box plots display the median value of the distribution (┃), values in the 1st and 3rd quartile range (■), values below the 3rd quartile + interquatile distance x 1.5, (┤), values above the 1st quartile + interquartile distance x 1.5 (├) and outlier values (○▲). Element values displayed on the vertical axis have been log transformed.

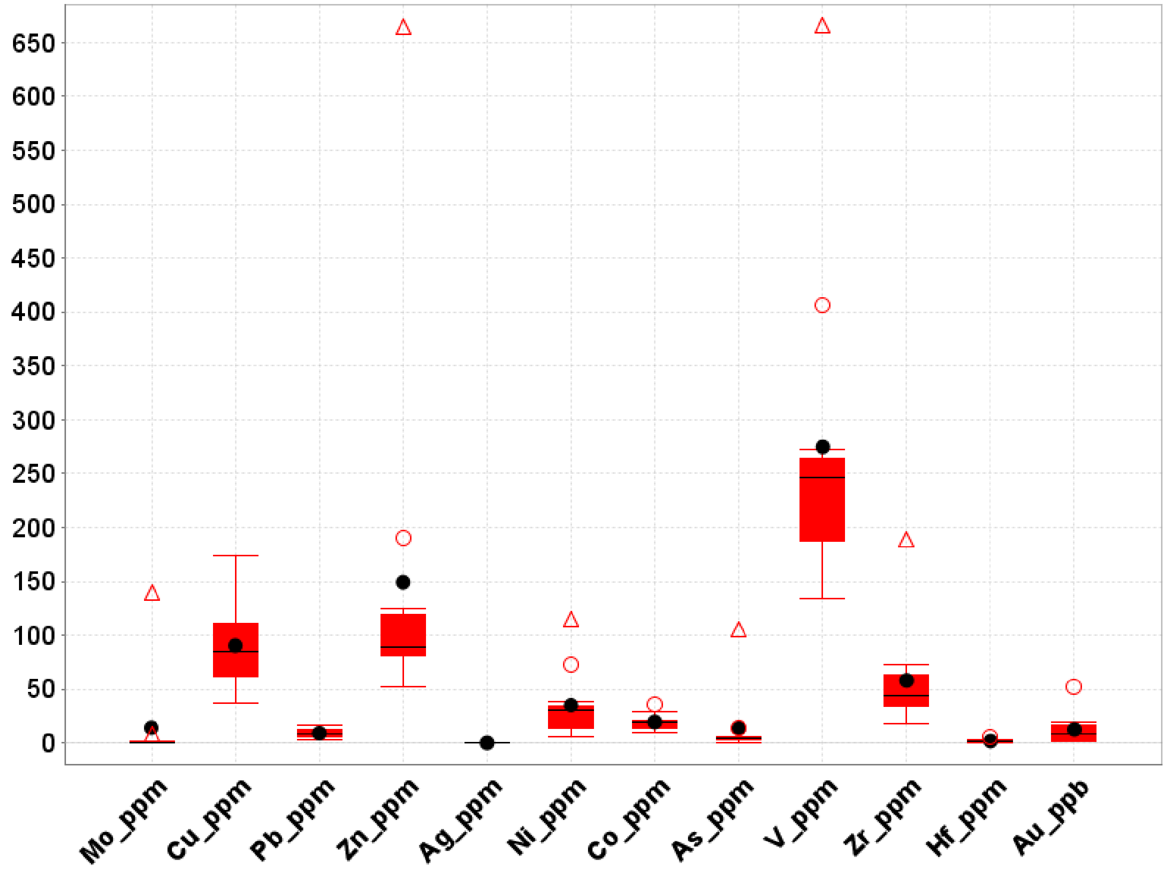

Figure: 3.1.2. A box plot showing the distribution of Au, Ag, As, Co, Cu, Hf, Mo, Ni, Pb, Zn and Zr in 10 Nicola Group rock samples collected by Logan, (2008). Non-transformation element values are displayed on the vertical axis.

Drainage geochemistry

No drainage sediment were collected and analysed as part of the studies documented in this Open File. However, Box plots created from regional geochemical data sorted by rock type are an indication of element background variations. For example, Figure 3.1.3 and 3.1.4 show elevated Ag, Hg, Cu, Mo and Zn in regional survey sediment from streams in NTS 93A draining Nicola Group basalt (Jackaman, 1999). Only As and Au are anomalous in sediment from a sample site, 93G841262, in a stream draining south from Mouse Mountain based on a 3rd Quartile threshold value.

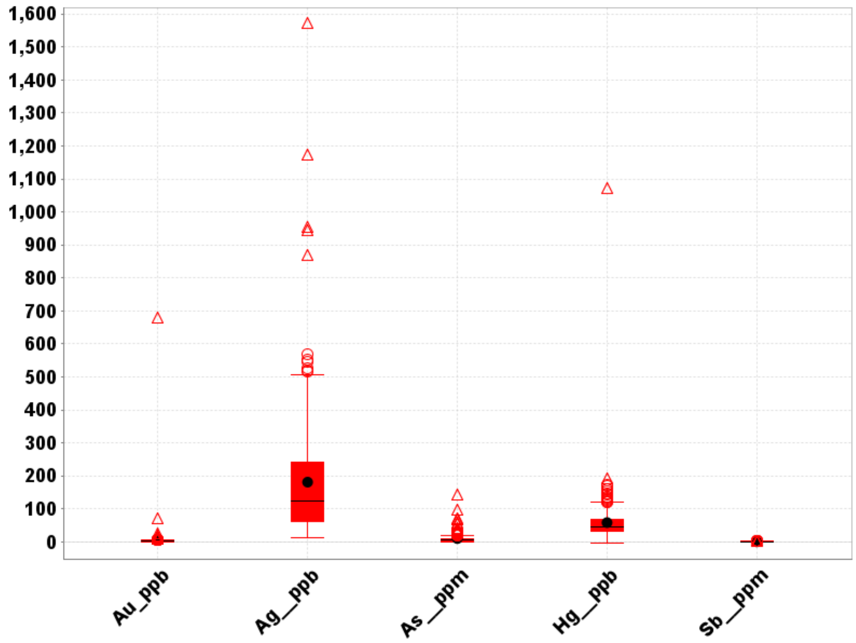

Figure 3.1.3: A box plot showing the distribution of Au, Ag, As, Hg and Sb in 255 sediment samples from streams draining Nicola Group basaltic rocks in NTS 93A (Jackaman, 2008).

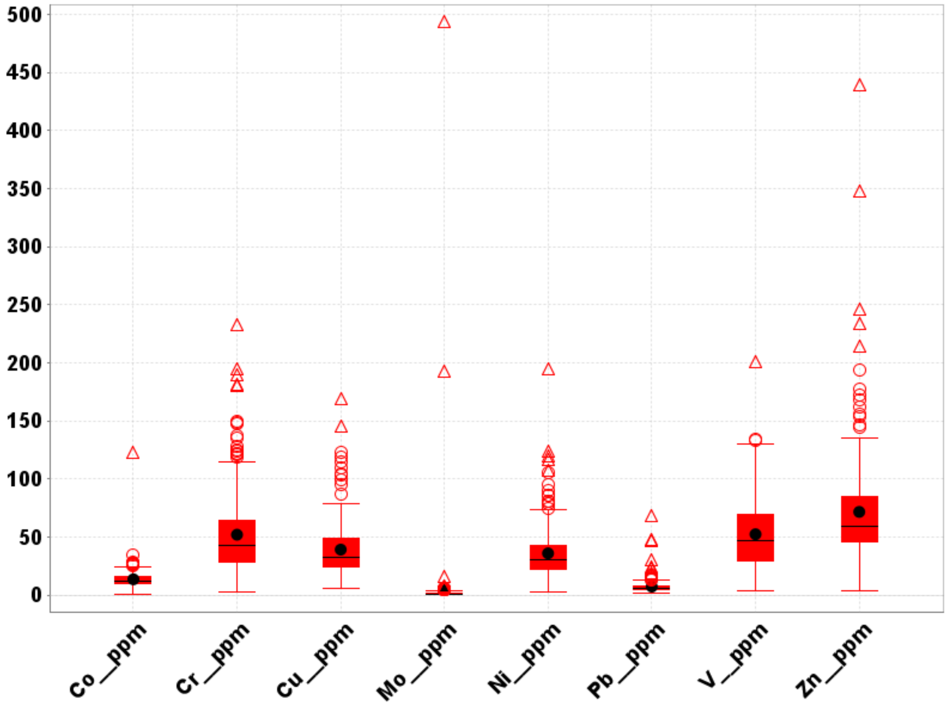

Figure 3.1.4: A box plot showing the distribution of Co, Cr, Cu, Mo, Ni, Pb, V and Zn in 255 sediment samples from streams draining Nicola Group basaltic rocks in NTS 93A.

Soil geochemistry

Ideally, is should be possible to establish a spatial link between soil and the underlying bedrock geochemistry from survey data. However, a link becomes complicated in areas where soil geochemical anomalies have been displaced from their bedrock sources by glacial dispersal. Also, the geochemical patterns in transported glacial sediments can then be modified by soil-forming processes adding to their complexity. The Mouse Mountain data will aim to simplify the complexity of the soil geochemical data through examining:

- element associations in soil horizons;
- geochemical differences and similarities within and between soil horizons;
- anomaly contrast for elements by different near total and partial leach methods ;
- influence of soil pH and loss on ignition (LOI) and;
- any relationship between C horizon geochemistry and the heavy mineral distribution.

Element Associations

Correlation coefficients are a guide to the strength of inter-element associations with a high positive or negative coefficient (> +0.8 or – 0.8) indicating a strong positive or negative relationship between two variables. However, coefficients can be misleading because they can reflect one or two high, strongly related values isolated form the main data cluster and thus give a false indication of the true relationship between variables. Consequently, correlation coefficients should be tested by plotting bivariate scatter graphs to confirm the significance of the coefficient. The following strong positive (unless indicated) inter-element associations are revealed in a correlation coefficient matrix calculated from the Mouse Mountain soil geochemical data. Each high positive or negative coefficient was compared with a scatter graph plotted from values for the element pair.

F-H: Horizon: (1) Fe-V-Co-Ni-Sc; (2) La-Ce-Th-Sm-Eu-Yb; (3) Zn-Cd
Upper B Horizon: (1) As-Sb-Mo; (2) Cr-Sc; (3) V-Fe; (4) Mo-Lu (negative); (5) Yb-Sm.
Lower B Horizon: (1) Cu-Mo-V-As-Sb; (2) Yb-Sm
C horizon: (1) Mn-Cu-Sr-V-Sc-Bi-Ba; (2) Cr-Ni; (3) As-Mo-Zn; (4) Na-Al (negative).

Element associations in the C horizon most likely reflect the chemical signature of different mineral assemblages in the silt-clay fraction of the till. Weathering and soil forming processes in the soil profile re-distribute the elements resulting in different associations. The F-H horizon has a distinct REE signature that might be caused by accumulation of these elements initially in understory vegetation and subsequently in the forest litter. There only mineral pathfinder associations detected in the F-H horizon are Cd-Zn.

Soil Horizon Geochemical Comparisons

Elevated Cu, Au, Ag, As, Sb, V and Mo could be anticipated in soil based on a published account of the Cu-Au mineralization at Mouse Mountain and the lithogeochemistry (Jonnes and Logan, 2007). All of the statistics (mean, median, maximum, variance, quartiles, percentiles) for each element in the F-H, upper B, Lower B and C soil horizons were calculated from the element analyses of the samples from the traverse crossing the Rainbow Zone combined with results from the samples collected in the area south of Mouse Mountain. The down-profile variation of Cu from the F-H into the C soil horizon in Figure 3.1.5 is typical of several other elements in Mouse Mountain soil profiles such as Cr, Ni and V. This increase with depth may reflect both higher content of elements in the - 0.063 mm fraction of the C horizon material compared to the – 0.180 mm fraction of B and A horizon samples and greater abundance of Fe-Mg Al-silicate minerals of the till fine fraction. For example, Mg (Figure 3.1.6) a major element in Fe-Mg Al-silicate mineral chemistry also increases with depth while Ca deceasing from maximum values in the F-H horizon. Several other elements such as Au, Ag and Zn follow Ca in that they decrease with depth from higher values in the F-H horizon to lower concentrations in the C horizon.

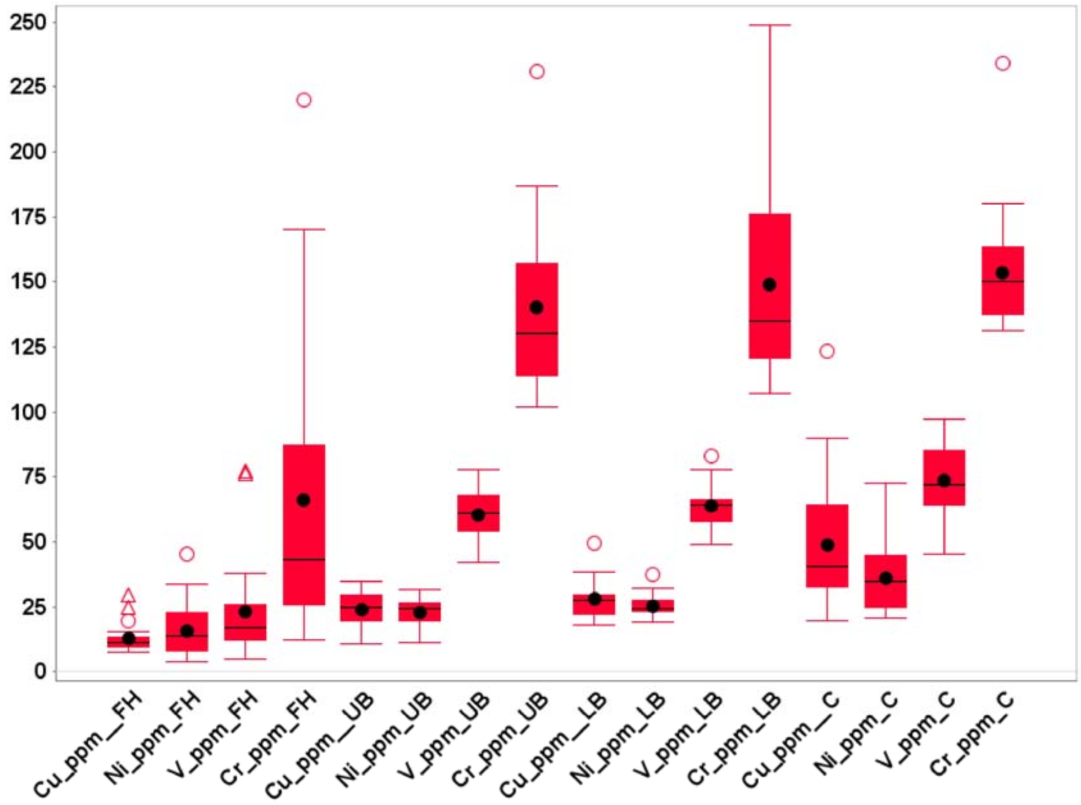

Figures: 3.1.5. A box plot showing the distribution of Cu, Ni and V by aqua regia-ICPMS and Cr by INAA in 22 soil samples from the C, lower B, Upper B and F-H horizons.

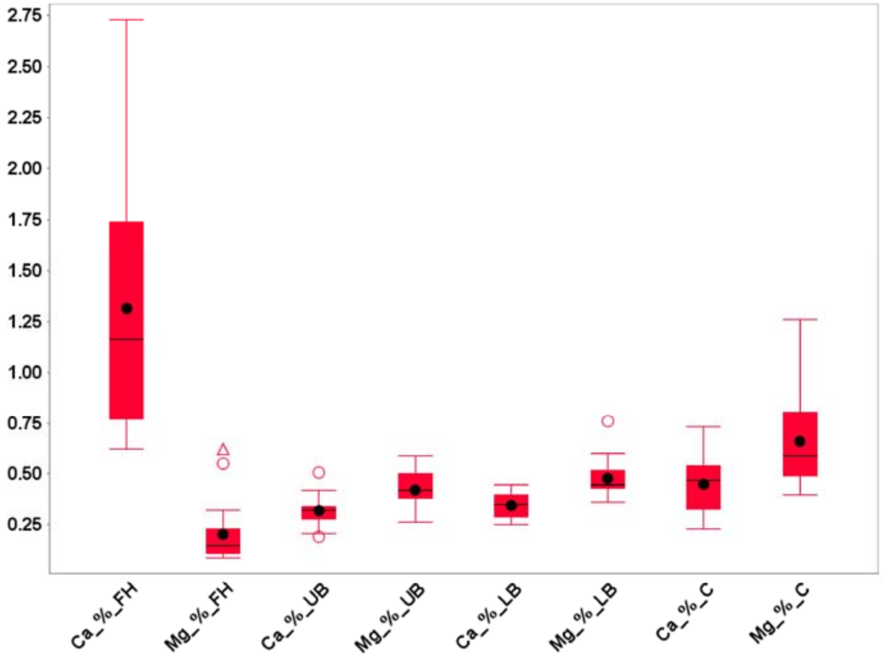

Figure: 3.1.6. Box plot showing the distribution of Ca and Mg in 22 soil samples from the C, lower B, Upper B and F-H horizons analysed by aqua regia-ICPMS. Element values displayed on the vertical axis have been log transformed.

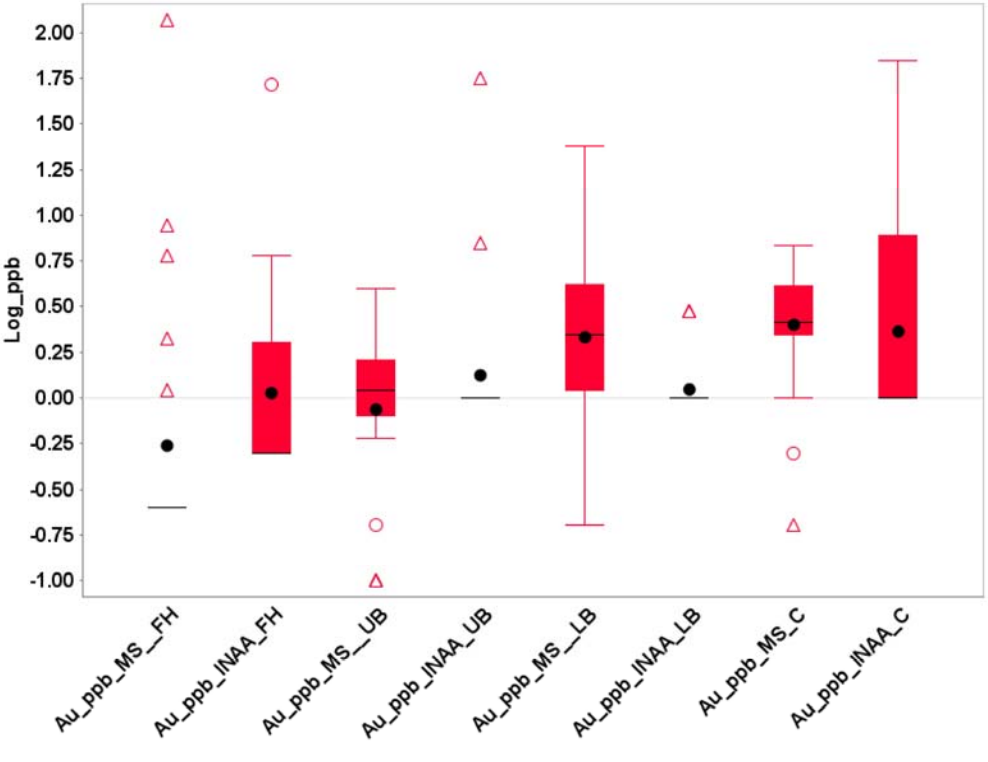

Figure: 3.1.7. Box plot showing the distribution of Au by aqua regia-ICPMS and Au by INAA in 22 soil samples from the C, lower B, Upper B and F-H horizons. Element values displayed on the vertical axis have been log transformed (Log_ppb).

Gold in Figure 3.1.7 shows a wide scatter of values in the soil horizons compared to other elements and there are different INAA and aqua regia-ICPMS concentration in the same sample. Higher Au values are present in the F-H and C horizons compared to the B horizon.   Figure 3.1.8 shows that Ag and Zn are higher in the F-H horizon compared to the levels in the B and C soil horizons. Arsenic and Sb, two common Au pathfinder elements, in Figure 3.1.9 follow the trend of Cu, Ni and V by increasing from the F-H into the B and C horizon. Figure 3.1.10 shows that Mo and Pb have trend similar to that of Ag and Zn, with decreasing values from the F-H into the C soil horizon. Lanthanum and Yb in Figure 3.1.11 have very different concentrations in soil especially in the F-H horizon.

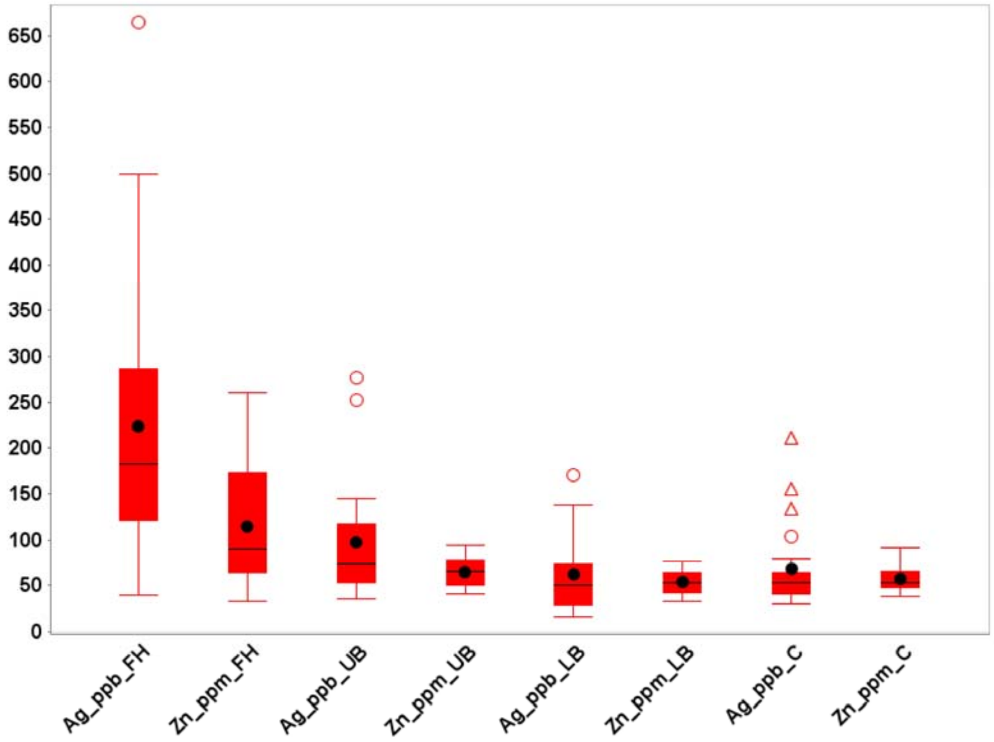

Figure: 3.1.8. Box plot showing the distribution of Ag and Zn by aqua regia-ICPMS in 22 soil samples from the C, lower B, Upper B and F-H horizons.

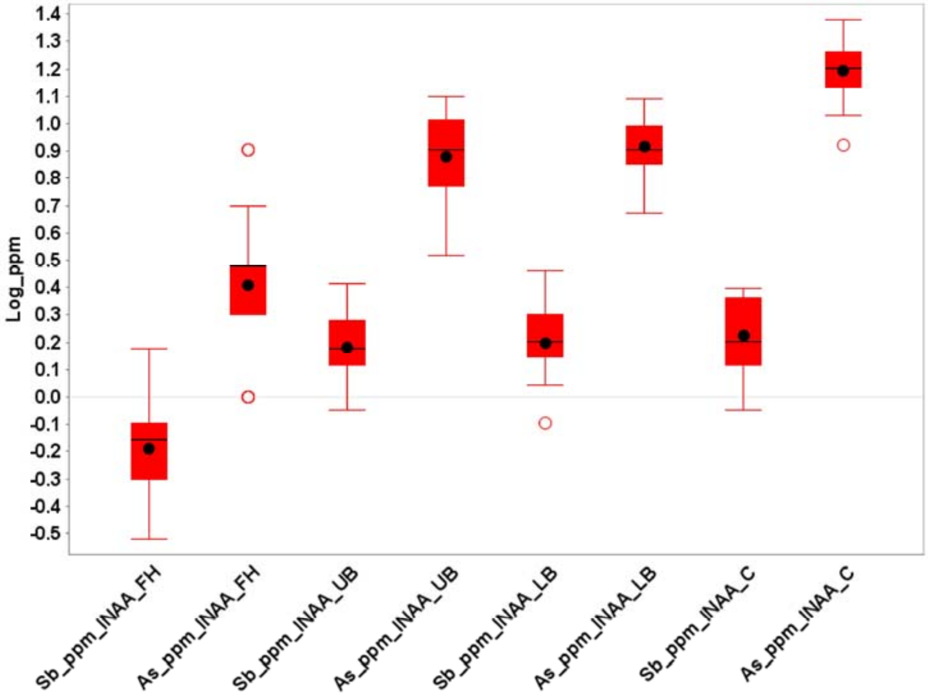

Figure: 3.1.9. Box plot showing the distribution of As and Sb by INAA in 22 soil samples from the C, lower B, Upper B and F-H horizons. Element values displayed on the vertical axis have been log transformed (log_ppm).

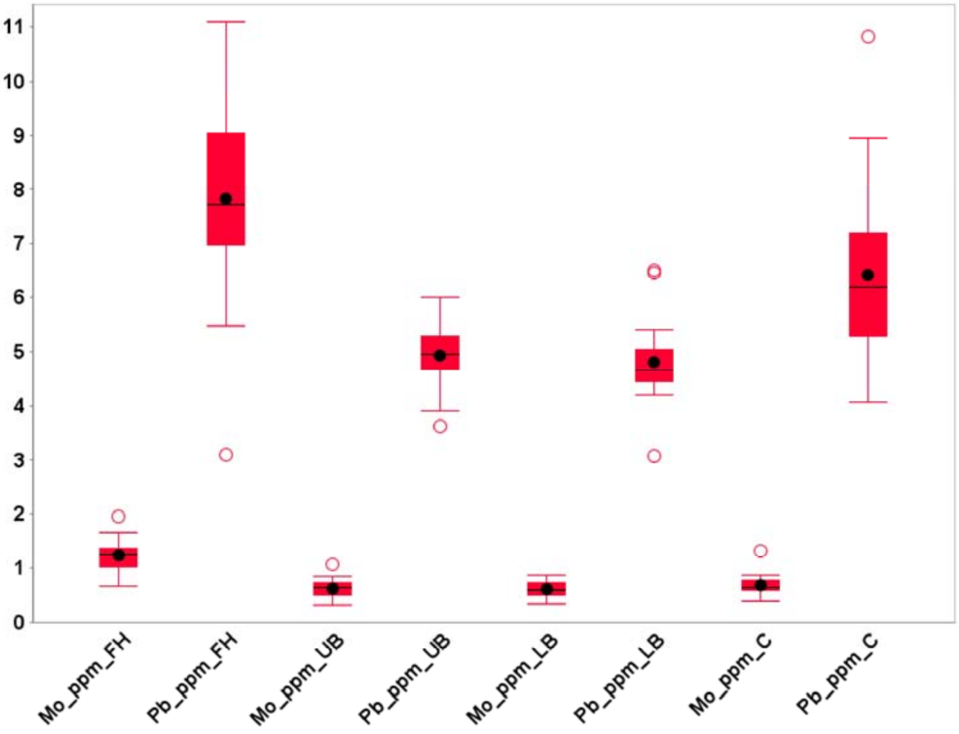

Figure: 3.1.10. Box plot showing the distribution of Mo and Pb by aqua regia-ICPMS in 22 soil samples from the C, lower B, Upper B and F-H horizons.

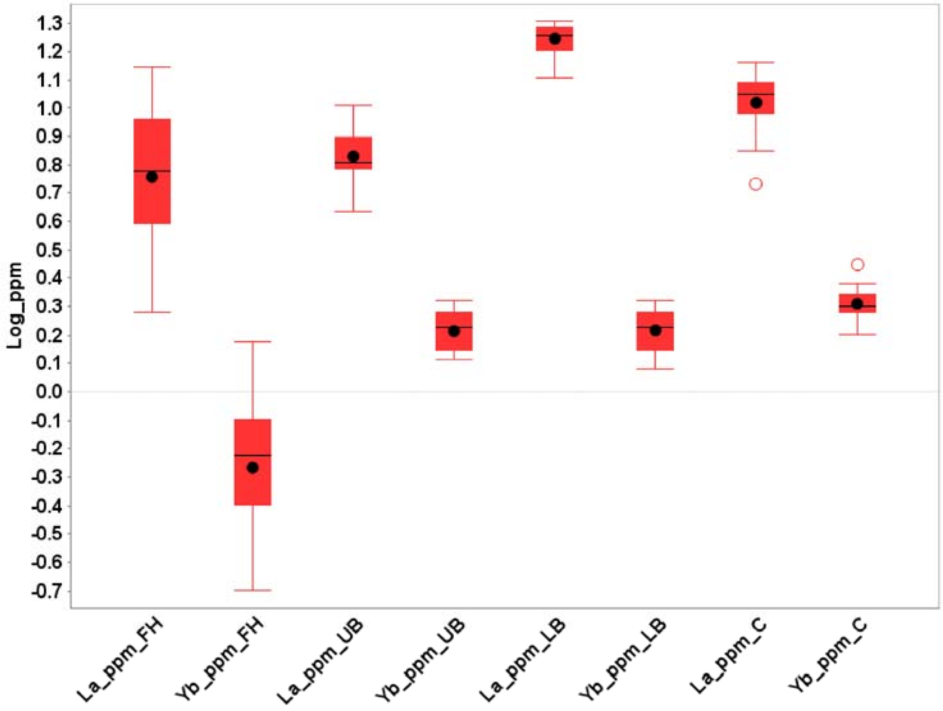

Figure: 3.1.11. Box plot showing the distribution of La and Yb by aqua regia-ICPMS in 22 soil samples from the C, lower B, Upper B and F-H horizons. Element values displayed on the vertical axis have been log transformed (log_ppm).

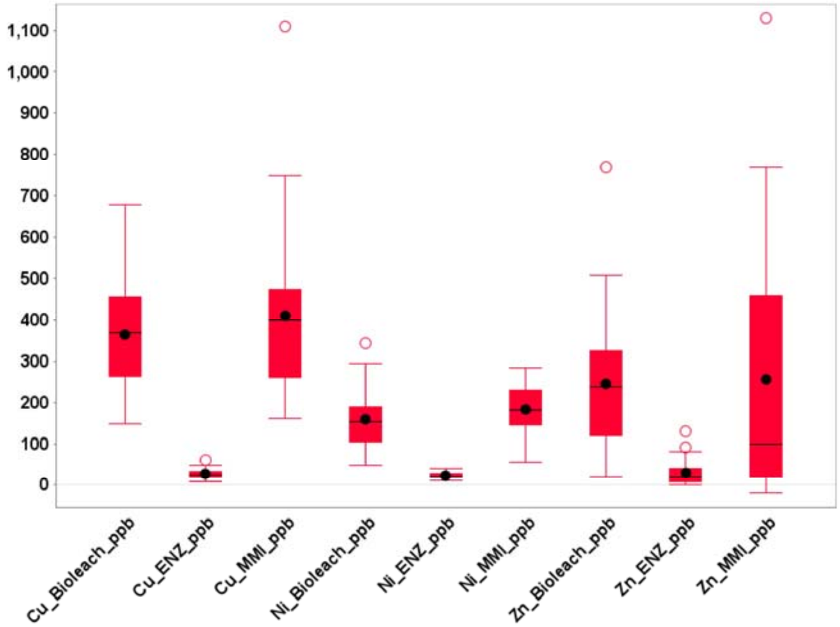

Figure 3.1.12: Box plot showing the distribution of Cu, Ni and Zn analysed by Bio Leach^{SM}, Enzyme Leach^{SM} and MMI ^{SM}.

Partial leach analysis of soil samples is intended to improve geochemical anomaly contrast and comparison of the Cu, Ni and Zn liberated from the Mouse Mountain soils with BioLeach^{SM}, Enzyme Leach^{SM} and MMI^{TM} is shown in Figure 3.2.12. Clearly MMI^{TM} extracts more Cu and Zn although the range is represented by one high, outlier value. Median values for the all three elements by BioLeach^{SM} and MMI^{TM} are similar suggesting that the extraction mechanisms operate in the same way. Figures 3.1.13 and 3.1.14 show that Ag, Au and Pb, unlike Cu, Ni and Zn, have higher median values and values cover a wider range by MMI^{SM} compared to BioLeach^{SM} and therefore MMI^{TM} analysis could improve anomaly contrast. The selectivity of the extractions is element dependant as shown in Figure 3.1.15 where much more Co and As has been liberated by BioLeach^{SM} compared to MMI^{TM}

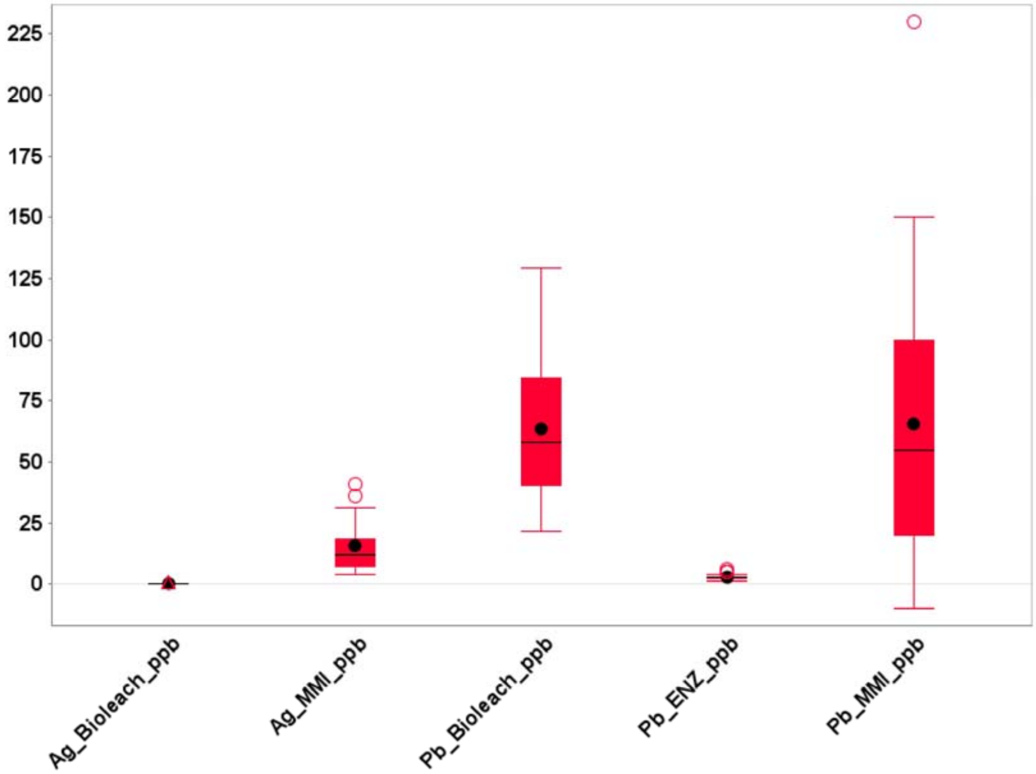

Figure 3.1.13: Box plot showing the distribution of Pb and Ag analysed by BioLeach^{SM}, Enzyme Leach^{SM} and MMI ^{SM}. Enzyme Leach^{SM} data are not displayed because most of the values are below detection limit.

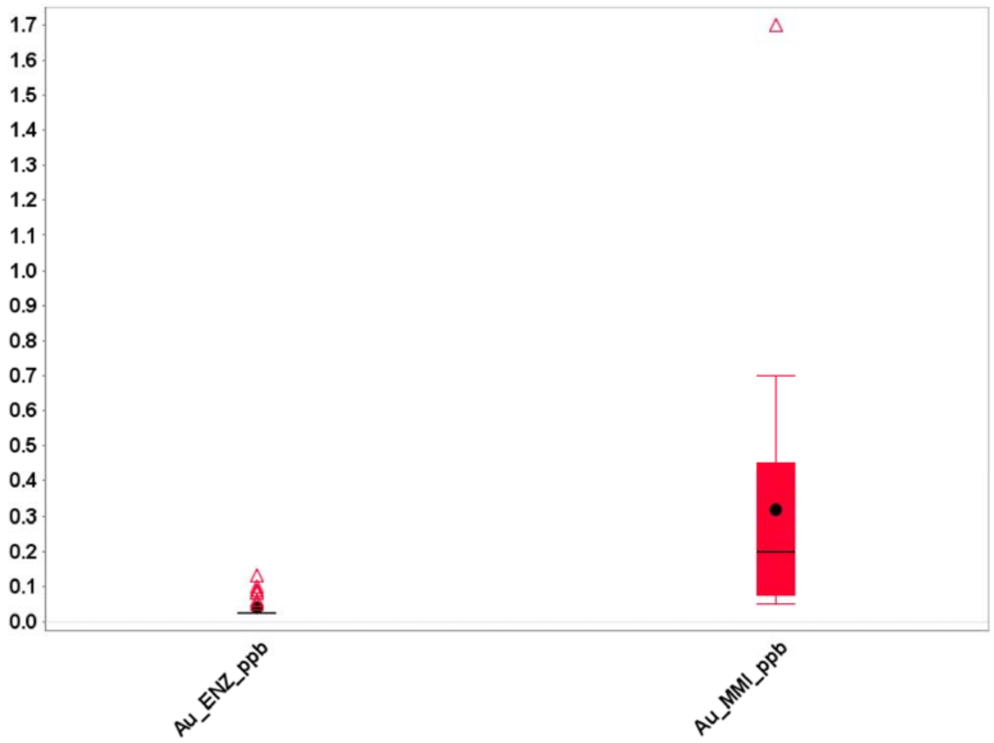

Figure 3.1.14: Box plot for Au analysed by Enzyme Leach^{SM} and MMI ^{SM}. BioLeach^{SM} Au data are not displayed because only one value is above detection limit.

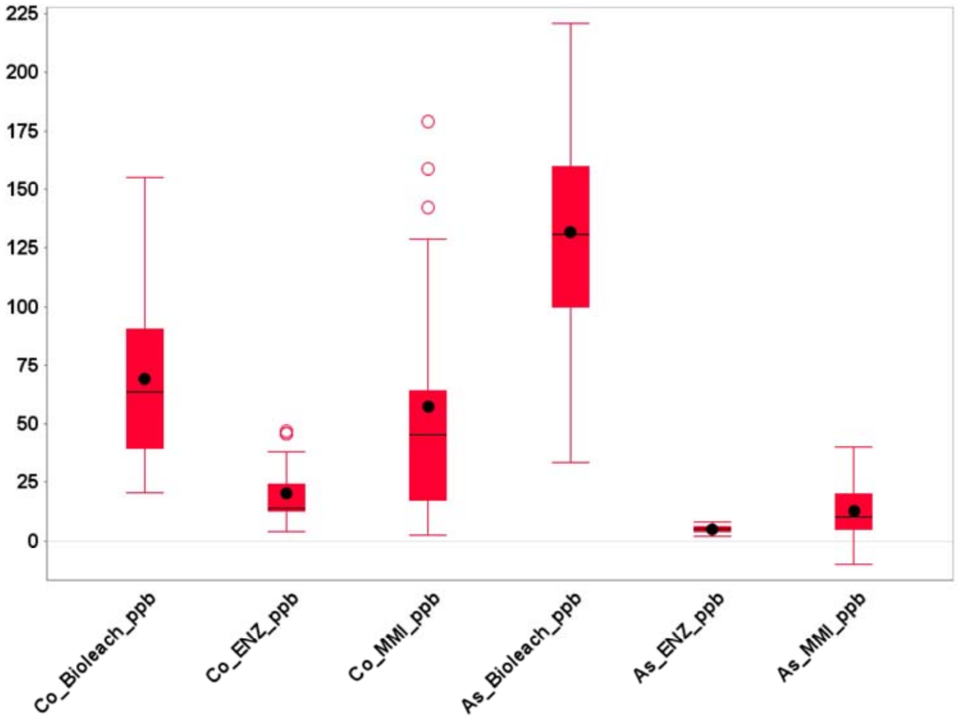

Figure 3.1.15: Box plot for As and Co analysed by Enzyme Leach^{SM} and MMI ^{SM} and BioLeach^{SM}.

Depending on an element there may be a strong correlation between geochemical patterns from soil horizon to soil horizon or an absence of a relationship. For example, Figure 3.1.16 is a scatter plot of Cu in the F-H horizon compared to Cu in the Upper B horizon that shows that there is almost no relationship between Cu in the two horizons whereas Au in Figure 3.1.17 shows much a stronger correlation although many of the determination at the detection limit. Figure 3.1.18 shows better correlation for Cu in the Upper B soil horizon compared to the lower B soil horizon although the correlation coefficient (+ 0.47) indicates that only 25 percent of the variation is due to the association between the Cu values in the two populations There is an almost random scatter of Cu in the lower B and the C soil horizon (Figures 3.1.19)

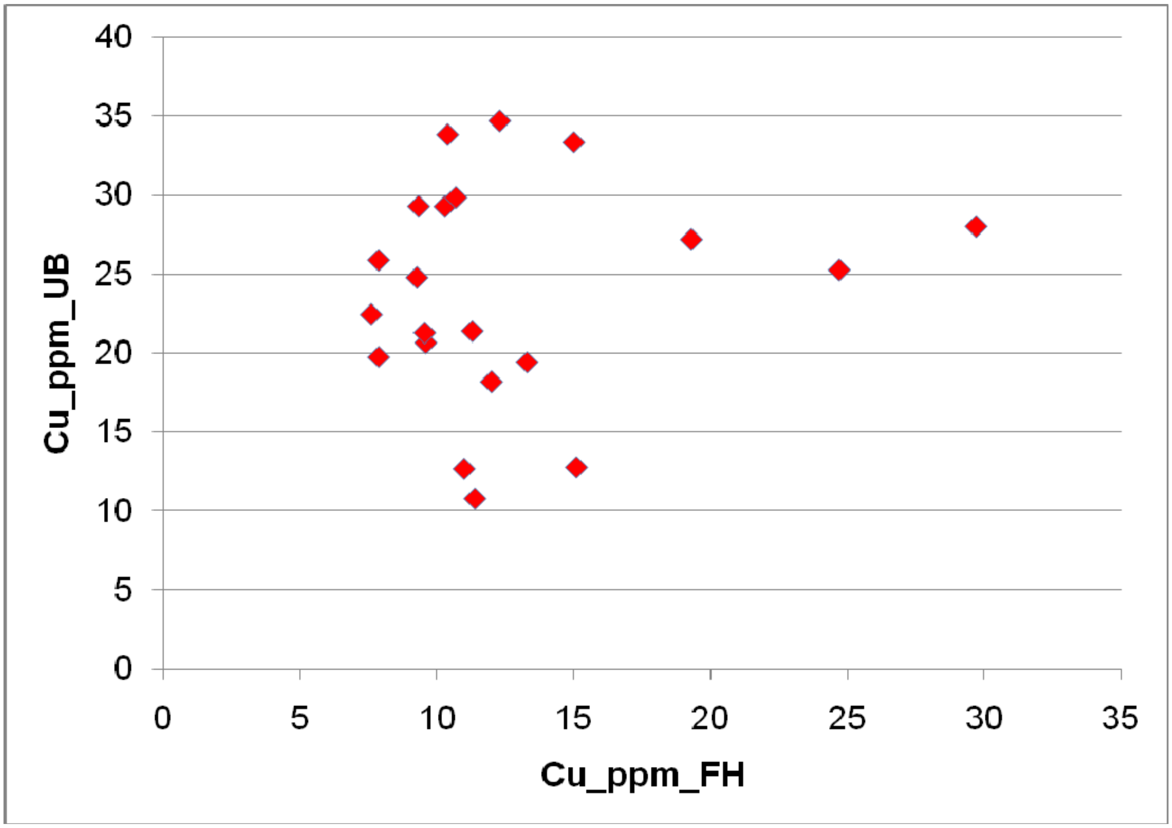

Figure 3.1.16: Scatter plot for Cu by aqua regia-ICPMS in the F-H horizon compared to Cu in the upper B horizon compared to the lower B horizon.

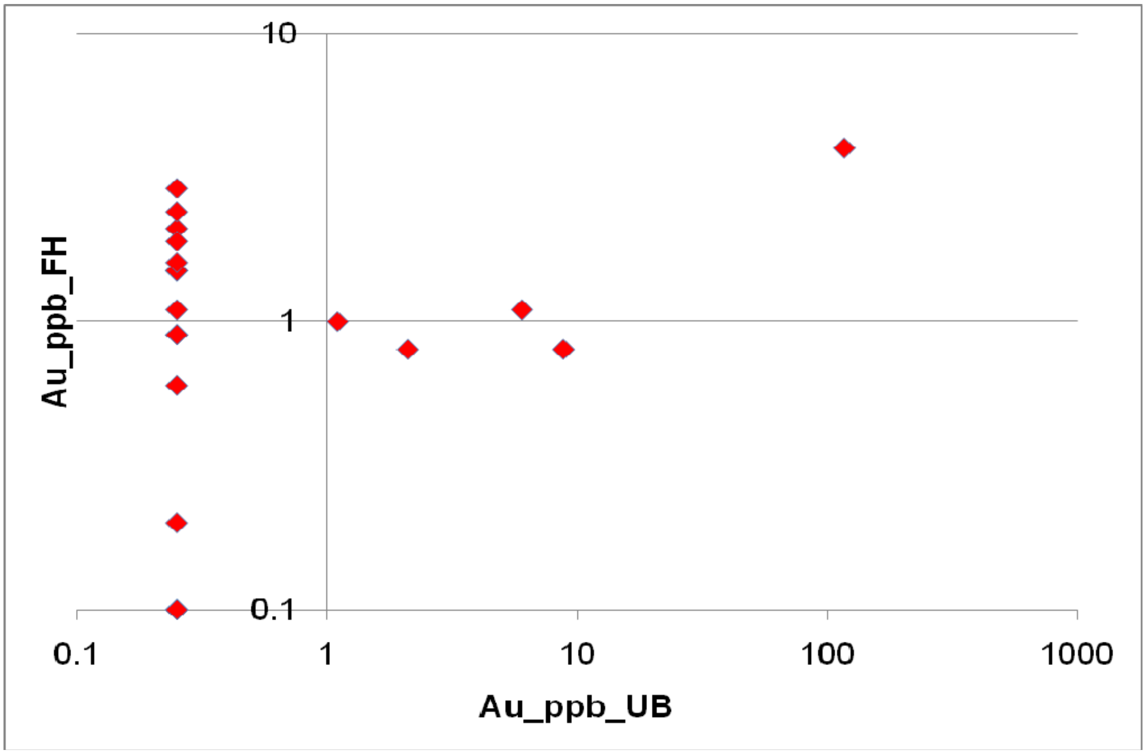

Figure 3.1.17: Scatter plot for Au by aqua regia-ICPMS in the F-H horizon compared to Au in the upper B horizon compared to the lower B horizon.

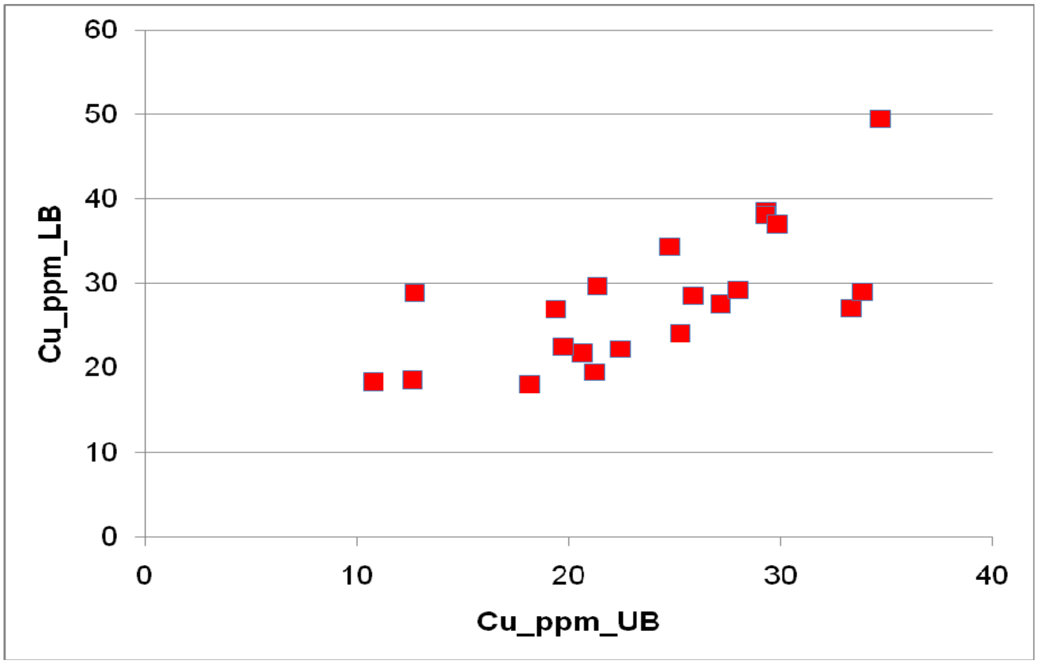

Figure 3.1.18: Scatter plot for Cu by aqua regia-ICPMS in the Upper B soil horizon compared to Cu in the Lower B horizon.

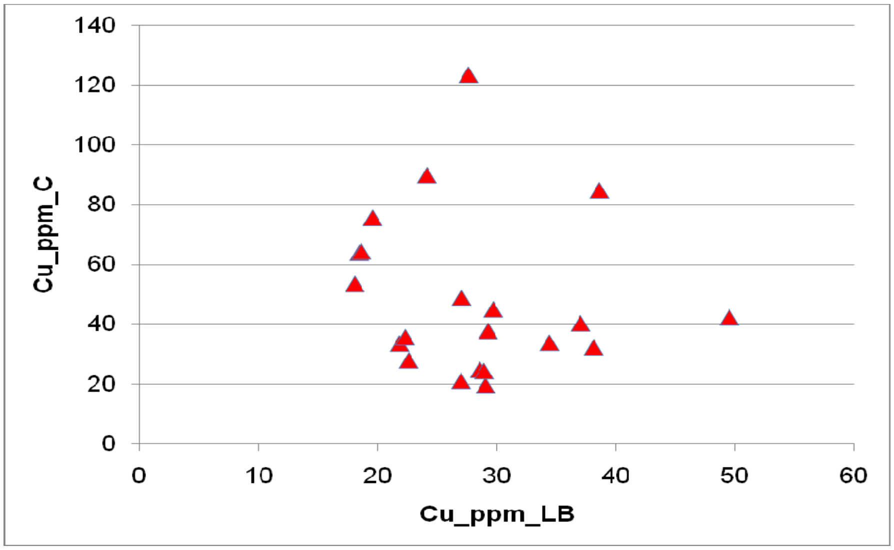

Figure 3.1.19: Scatter plot for Cu by aqua regia_ICPMS in the Lower B soil horizon compared to Cu in the C soil horizon.

Geochemical differences among soil horizons can reflect element variations introduced by sampling, sample preparation and analysis, natural variations in the soil geochemistry and element anomalies caused by the presence of mineralization. While a geochemical difference can be revealed by plotting element values for one horizon against the same element values for another horizon on scatter plot, the difference can be confirmed numerically with a Student t test statistic. Hence, a two sample t-test is applied to the Mouse Mountain soil geochemical data to establish if there is a statistical difference at the 0.05 percent significance level between population means for selected aqua regia-ICPMS and INAA measured elements representing the FH, Upper B, Lower B and C soil horizons. An analysis of variance (F-test) is applied before the t-test to determine if the data for each horizon has an equal or unequal variance. Once population variance equality or inequality is determined, the appropriate t-test is used to test the null hypothesis (H_o) that there is no significant difference between the element means of population samples representing each horizon (Davis, 1973).

ARMS & INAA

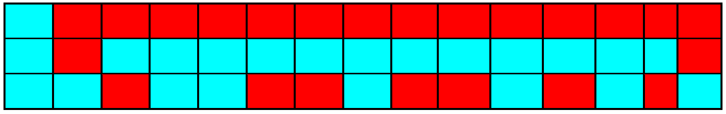

Mouse Mt	Au	Ag	As	*Br*	Co	Cu	*Cr*	Hg	*Fe*	Mn	Mo	Ni	Pb	V	Zn
LFH - Upper B	🟦	🟥	🟥	🟥	🟥	🟥	🟥	🟥	🟥	🟥	🟥	🟥	🟥	🟥	🟥
Upper B - Lower B	🟦	🟥	🟦	🟦	🟦	🟦	🟦	🟦	🟦	🟦	🟦	🟦	🟦	🟦	🟥
Lower B - C	🟦	🟦	🟥	🟦	🟦	🟥	🟥	🟦	🟥	🟥	🟦	🟥	🟦	🟥	🟦

Figure 3.1.20: Summary of a t-test applied to establish if there is a difference at the 0.05% significances level for Au, Ag, As, Br, Cu, Cr, Hg, Fe, Mn, Mo, Ni, Pb, V and Zn means in the F-H horizon compared to the upper B soil horizon, the upper B compared to lower B soil horizon and the lower B horizon compared to the C soil horizon by aqua regia_ICPMS and by INAA (INAA determined elements are in italics). A blank square indicates that there were insufficient values above detection limit for a test to be applied. A red square indicates a significant difference at the 0.05 significance level between the means. A blue square indicates no difference.

Figure 3.1.20 summarizes the results of the t-test applied to Au, Ag, As, Br, Cu, Co, Cr, Hg, Fe, Mn, Mo, Ni, Pb, V, Zn data for the F-H horizon compared to element data for the upper B soil horizon; element data for the upper B compared to element data for the lower B soil horizon and element data for the lower B horizon compared to the element data for C soil horizon. Except for Au there is a difference (at the 0.05 significance level) between population means for all elements in the F-H horizon tested against the upper B-horizon means. The significance of the Au t-test could be misleading because of the large number values that are at below or close to the instrumental detection limit and the variability of Au in the soil. Except for Ag, there is no significant difference between the means of the upper B soil horizon element populations compared to lower B soil horizon means. However, lower B soil horizon element means compared to the C-soil horizon element means reveal that As, Cu, Cr, Fe, Mn, Ni and V, are significantly different. Copper and Au scatter graphs plotted for soil horizon are evidence for the degree of similarity or difference. In Figure 3.1.21 a t-test is applied to the population means of Enzyme Leach^{SM} and BioLeach^{SM} extracted Au, As, Br, Cu, I, Mo, Mn, Pb, V and Zn from upper B horizon soils compared lower B horizon soils shows that there is no significant difference for any of the elements determined by Enzyme Leach^{SM} for the two horizons at Mouse Mountain and only a significant difference for Zn by BioLeach^{SM}. Also shown in Figure 3.2.21 are the results of the t-test for mobile MMI^{TM} extracted elements compared to BioLeach^{SM} extracted elements in lower B horizon soils. There is no significant difference in the means at the 0.05 percent level between the two methods for Co, Cu, Ni, Pb and Zn, but the means for As, Ba and Mo are significantly different.

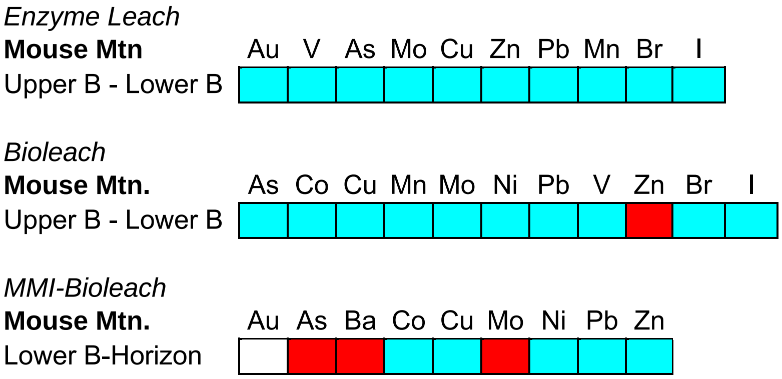

Enzyme Leach

Mouse Mtn	Au	V	As	Mo	Cu	Zn	Pb	Mn	Br	I
Upper B - Lower B	🟦	🟦	🟦	🟦	🟦	🟦	🟦	🟦	🟦	🟦

Bioleach

Mouse Mtn.	As	Co	Cu	Mn	Mo	Ni	Pb	V	Zn	Br	I
Upper B - Lower B	🟦	🟦	🟦	🟦	🟦	🟦	🟦	🟦	🟥	🟦	🟦

MMI-Bioleach

Mouse Mtn.	Au	As	Ba	Co	Cu	Mo	Ni	Pb	Zn
Lower B-Horizon	☐	🟥	🟥	🟦	🟦	🟥	🟦	🟦	🟦

Figure 3.1.21: Summary of a t-test applied to establish if there is a difference at the 0.05% significances level for elements by Enzyme Leach^{SM} and BioLeach^{SM} in the upper B horizon compared to the lower B horizon. Red square indicates a significant difference at the 0.05 significance level between the means. A blue square indicates no difference and a blank square indicates that there were insufficient values above detection limit for a test to be applied. The Figure also shows a t-test applied to compare MMI^{TM} determined elements in the lower B- soil horizon to BioLeach^{SM}-determined elements in the same horizon.

Soil Sampling Results

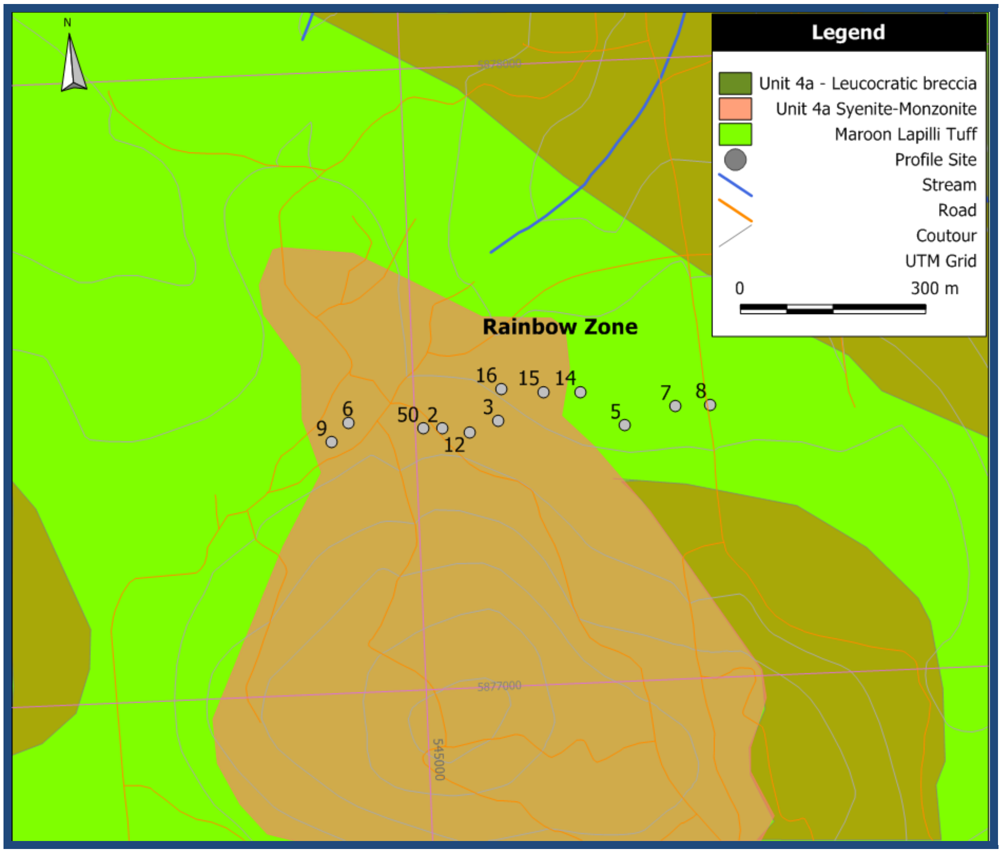

Figure 3.1.22: Soil sample profiles along a traverse crossing the Rainbow Zone, Mouse Mountain.

Rainbow Traverse:

Figure 3.1.22 shows location of soil profiles along a traverse crossing the Rainbow Zone and the variation of Cu in the soil horizons is displayed in Figure 3.2.23. Although there are gaps in the continuity of the F-H and C soil geochemistry because not all horizons at each profile were sampled there is an increase in the C soil horizon Cu along the traverse from west to east. Highest Cu occurs in the C horizon at Profile 7 and there is a corresponding, but smaller Cu values in the Lower B soil horizon of the same profile. There is a smaller C soil horizon Cu peak at Profile 15, but no corresponding Cu increase in the B and F-H horizons. A number of elements show a similar pattern to Cu across the Rainbow Zone. For example, Ni in the C horizon and, to a lesser extent the B soil horizon, increases from west to east (Figure 3.1.24). Vanadium values display a “saw tooth” pattern in the C soil horizon with the highest values in Profile 7 (Figure 3.1.25). Unlike Ni and Cu, the V content of the B and F-H horizon follows that in the C soil horizon although the size of the V peaks are smaller. A common association of Cu, Ni and V in the C soil horizon samples suggest that they could be weathered and released from Mg-Fe alumino silicate minerals forming the matrix of the glacial sediments.

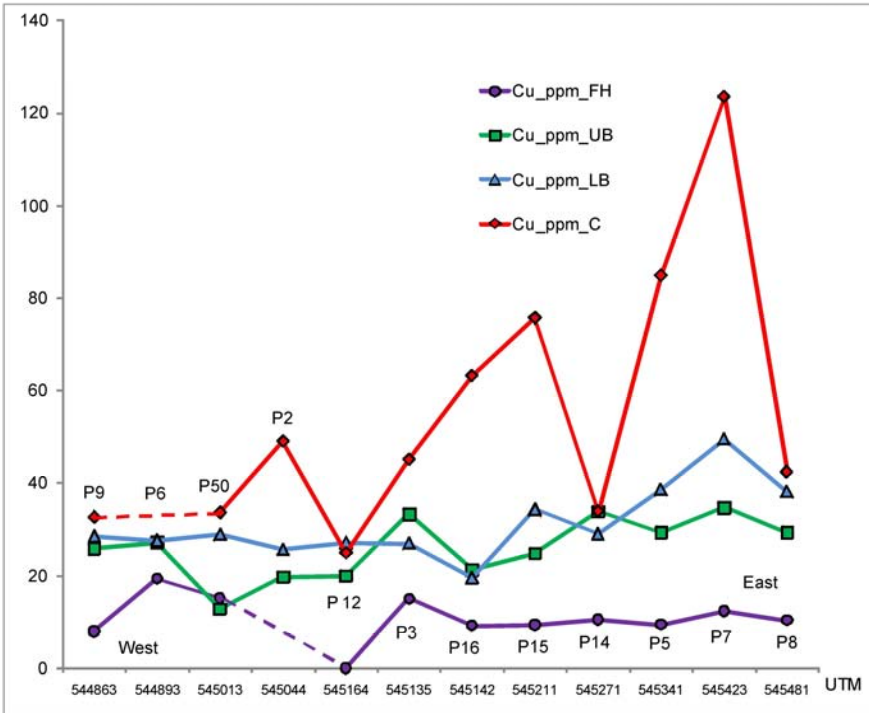

Figure 3.1.23. Copper by aqua regia-ICPMS in soil across the Rainbow zone at Mouse Mountain. FH = FH horizon (typically < 0.5 cm depth), UB = Upper B Soil Horizon typically 5-10 cm depth, LB = Lower B soil Horizon typically 20 to 30 cm depth, C = C soil horizon typically > 30 cm depth. A dashed line indicates that there was no C or FH horizon collected at the Profile site.

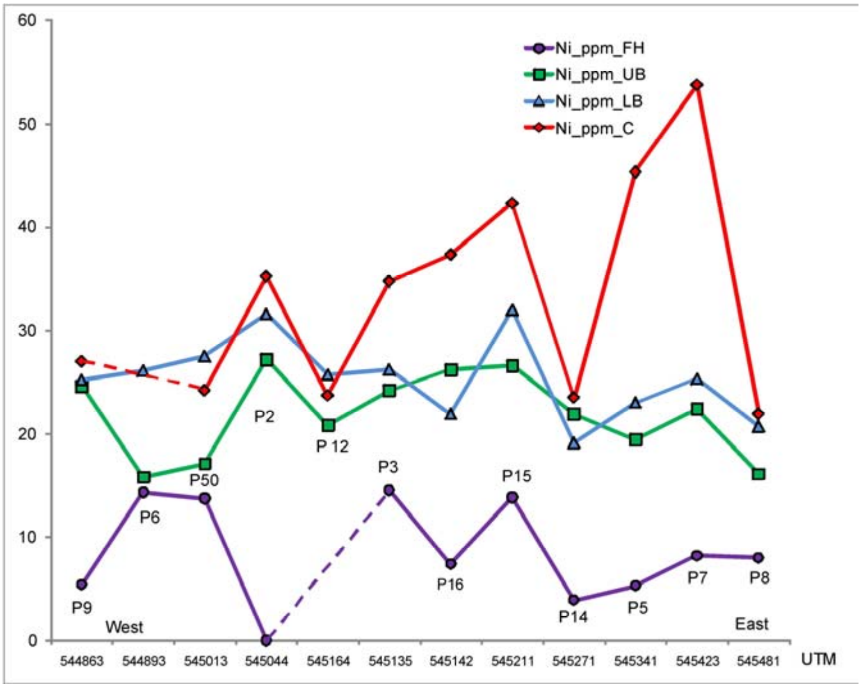

Figure 3.1.24 Nickel by aqua regia-ICPMS in the soil across the Rainbow zone at Mouse Mountain.

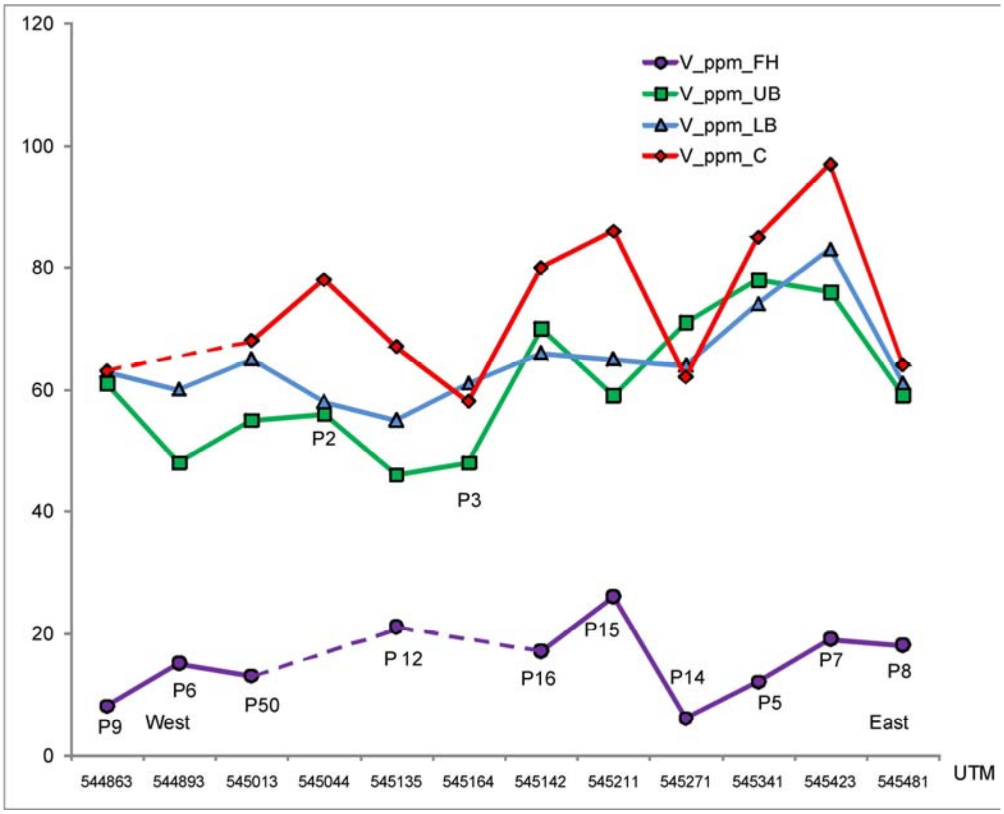

Figure 3.1.25 Vanadium by aqua regia-ICPMS in the soil across the Rainbow zone Mouse Mountain.

Major elements should show a similar pattern to minor and trace elements if their common source is weathered till. Magnesium content of the C soil horizon in Figure 3.1.26 follows a pattern similar to Cu and Ni. These elements in the C horizon decrease exponentially from east to west along the similar to the dilution profile displayed by the till geochemical signature of minerals transported by ice from a bedrock source. Klassen, (2001), suggests that an exponential decay profile is characteristic of the erosion, modification and deposition of debris transported at the base of an ice-sheet (basal till) whereas a more linear decay curve can be explained by englacial transport of debris with minimal modification (englacial till). The “saw tooth” patterns for the major and trace elements displayed in Figures 3.1.23 to 3.1.26 all have a geochemical signature of material deposited by ice transport. However, an absence of a clear, exponential decay curve suggests that the C horizon material was not deposited as a simple basal till, but is most likely as sediment with a more complex depositional history.

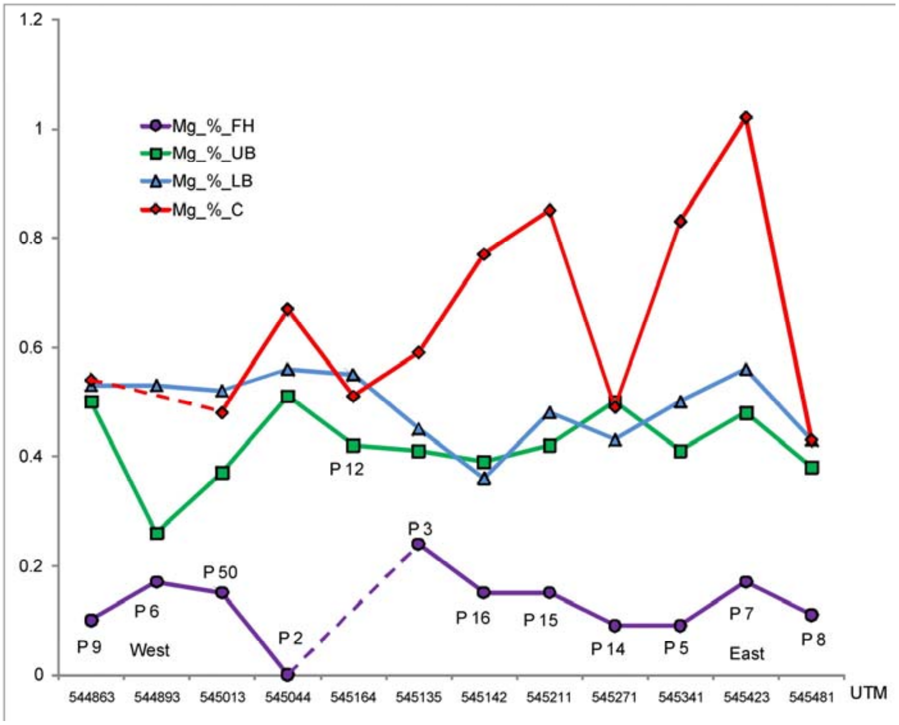

Figure 3.1.26 Magnesium by aqua regia_ICPMS in the soil across the Rainbow Zone.

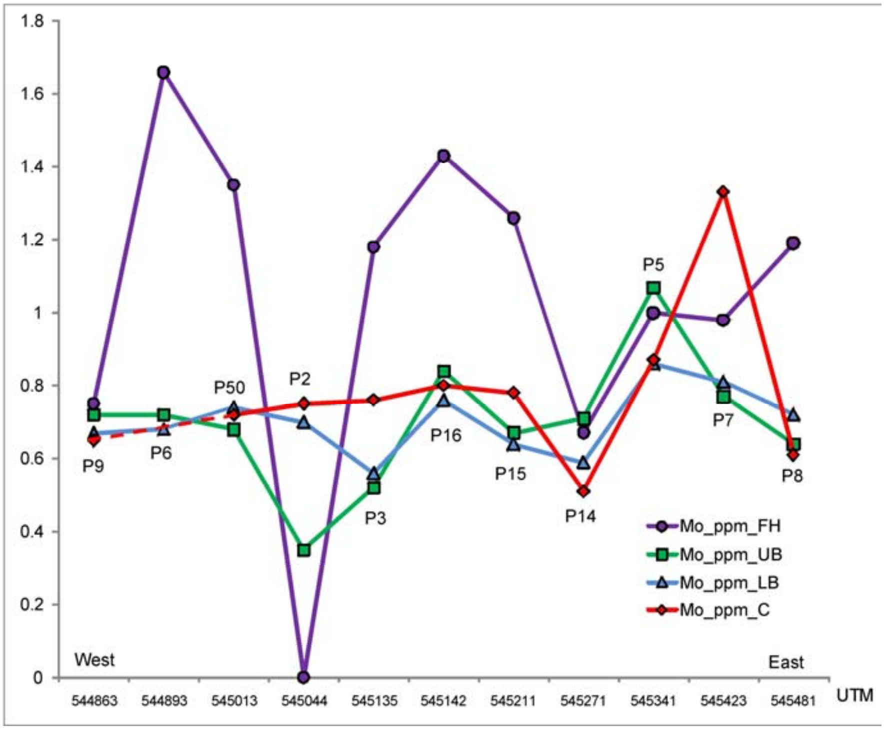

Figure 3.1.27 Molybdenum by aqua regia_ICPMS in the soil across the Rainbow Zone.

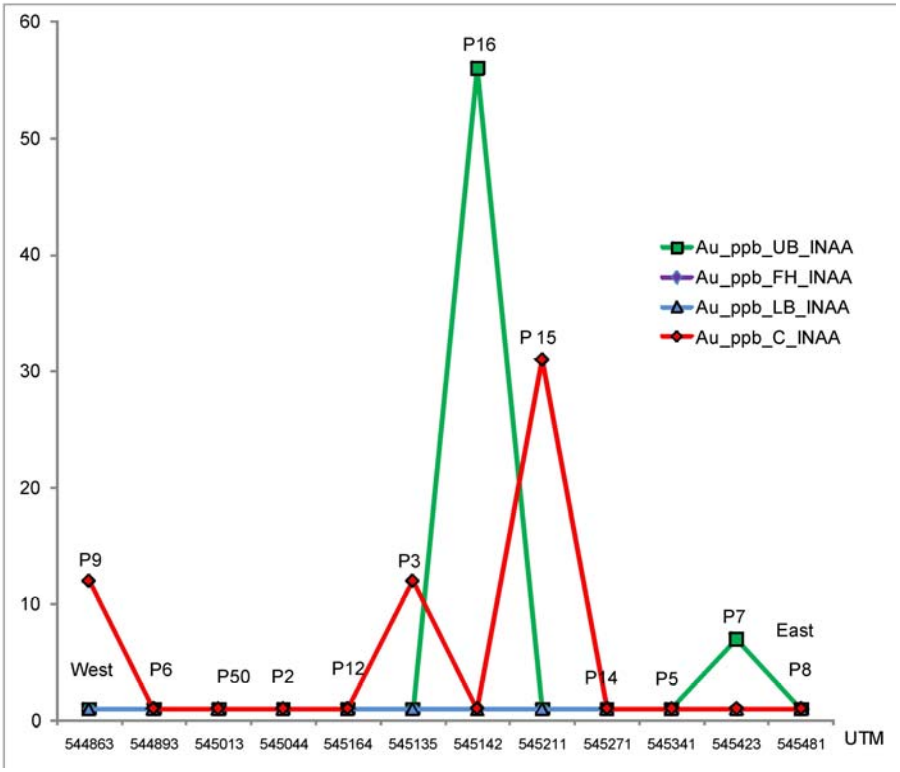

Figure 3.1.28 Gold by INAA in soil across the Rainbow Zone.

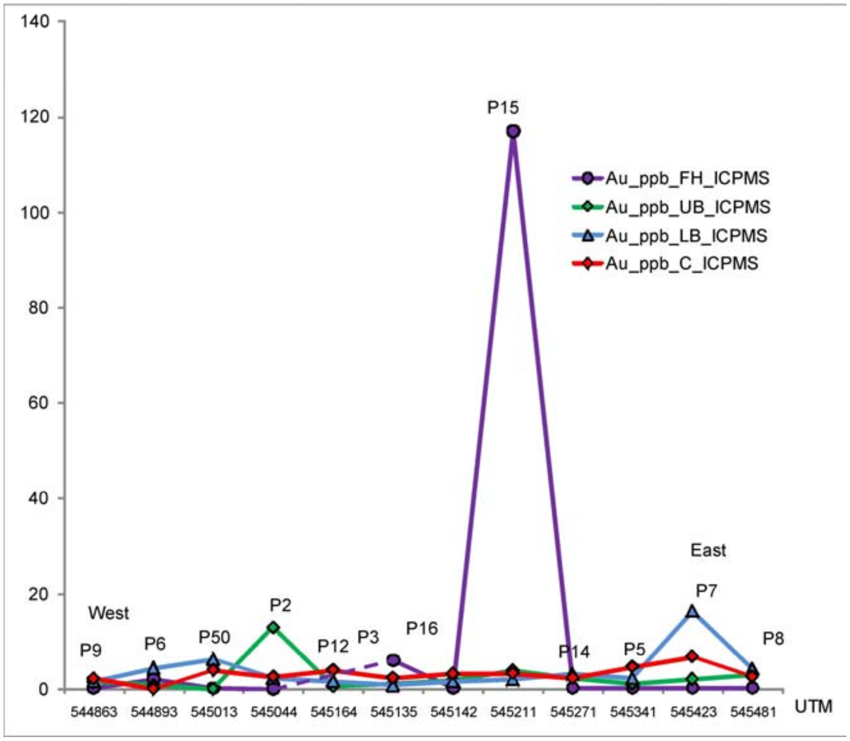

Figure 3.1.29 Gold by aqua regia-ICPMS in soil across the Rainbow Zone.

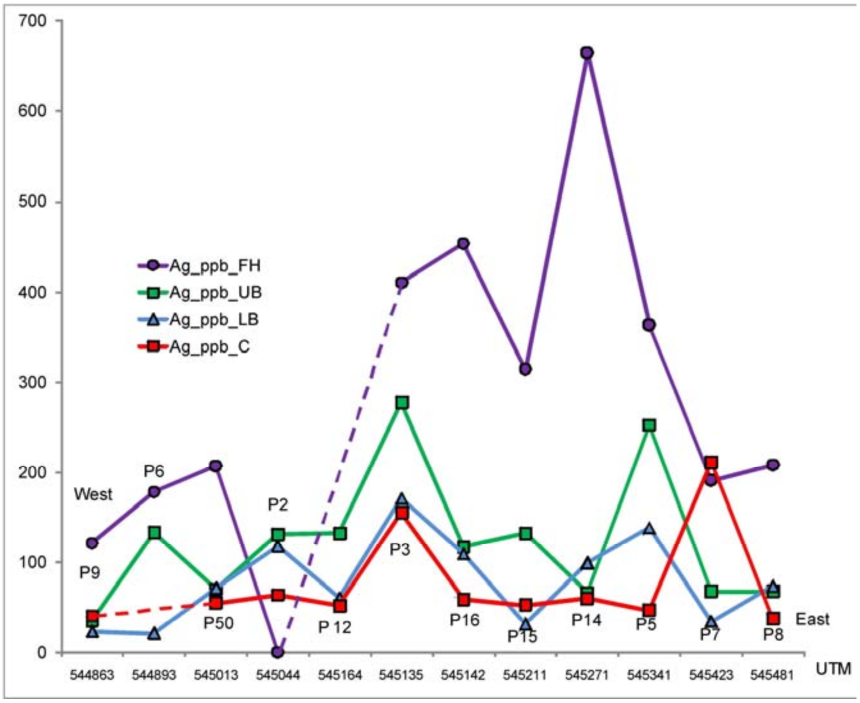

Figure 3.1.30 Silver by aqua regia_ICPMS in soil horizons the Rainbow Zone.

Gold by INAA in Figure 3.1.28 and Au by aqua regia-ICPMS in Figure 3.2.29 show sharp, single sample peaks in the soil at Profiles 15 and 16. The highest Au up to 117ppb detected in soil by aqua regia-ICPMS is in an F-H horizon sample at Profile 15 with a corresponding, but smaller anomaly in C horizon of the same profile. In the C horizon sample at Profile 15 there is 33 ppb by INAA. The is also 56 ppb Au in an Upper B horizon sample at the adjacent Profile 16 with elevated Au in the F-H horizon. Silver in Figure 3.1.30 displays a multiple F-H horizon peak at Profile 14, but levels are smaller in the mineral horizons over the interval between Profile 12 and 8. Both Mo in Figure 3.1.28 and Ag are generally higher in the F-H horizon compared to levels the B and C horizons. Arsenic, a common Au pathfinder, displays a peak in the C soil at Profile 16 where there is elevated Au the Upper B soil horizon (Figures 3.1.31). Figure 3.2.32 shows that Hg in the C soil horizon increases to a sharp peak at Profile 7 and increases along the Traverse from west to east. This pattern is similar to variation of Cu, V, Ni and Mg. Mercury contrast is more subdued in the lower B soil and almost absent in the Upper B soil. The Hg distribution in soil could be explained by Hg degassing from sulphide minerals entrained in the glacial sediment or of vapour transport into the soil from a concealed a fault.

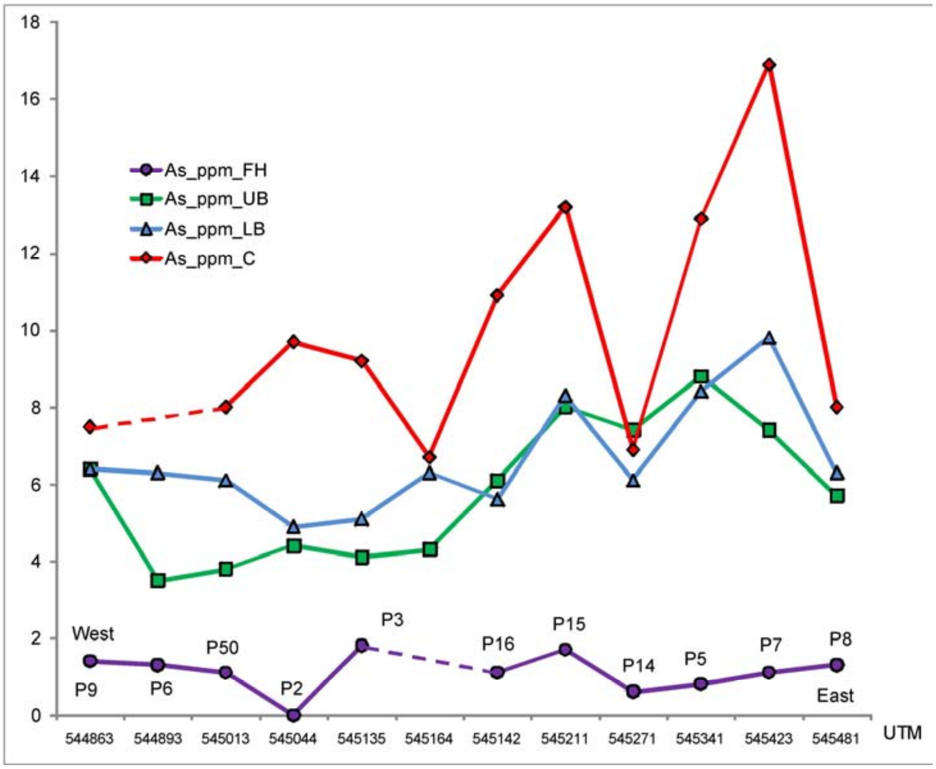

Figure 3.1.31 Arsenic by aqua regia_ICPMS in soil across the Rainbow zone.

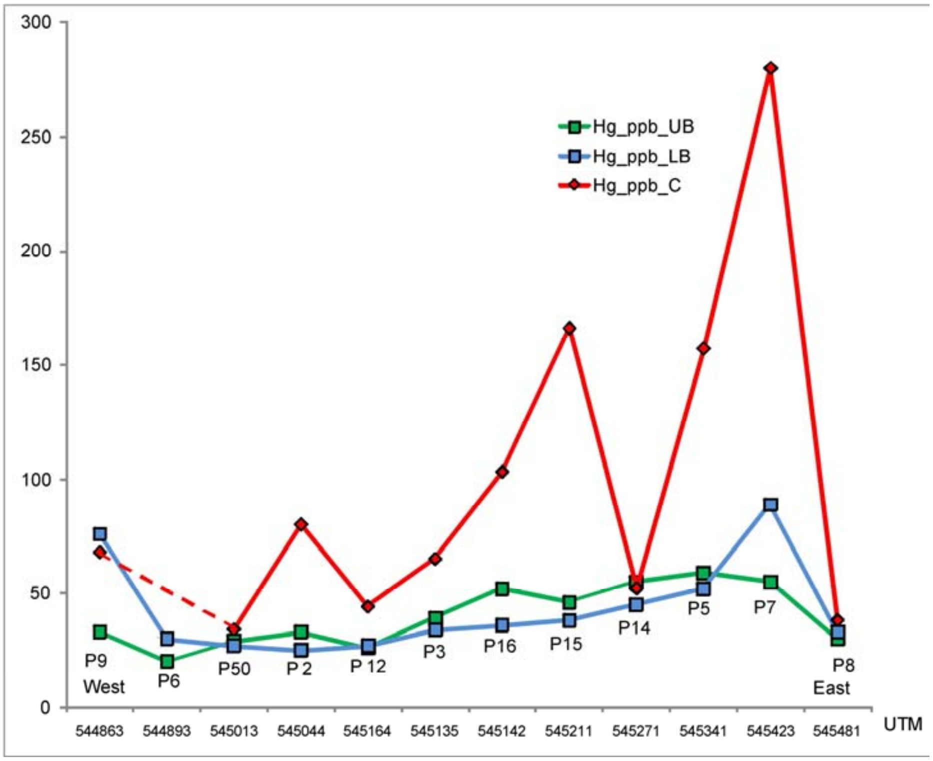

Figure 3.1.32 Mercury by aqua regia_ICPMS in soil across the Rainbow zone.

Element variation across the Rainbow Zone in Figure 3.1.23 to 3.1.32 reflects analyses from soil samples by near total (INAA) or strong mineral acid digestion (aqua regia-ICPMS) methods. Partial leaches such as Mobile metal ion (MMI)^{TM}, Enzyme Leach^{SM} and BioLeach^{SM} selectively dissolve different soil forming minerals or remove metals absorbed or complexed to mineral surfaces. The selective ability of these reagents increases geochemical anomaly contrast so that, ideally, a leach can better detect the most mobile phase of an element dispersed by ground water from a mineralized source. Variation of MMI^{TM} Cu, Enzyme Leach^{SM} Cu, BioLeach^{SM} Cu and aqua regia-ICPMS Cu in the lower B (or at a uniform 20-25 cm depth below the Ah-B horizon boundary in the case of MMI^{TM}) along the Mouse Mountain Rainbow Traverse is shown in Figure 3.1.33. In the Figure the MMI^{TM} and Bioleach values have been divided by 10 so that the Cu variation by the three methods can be more easily compared. While the partial leach graphs are not continuous because not all of the soil samples from the profiles were analysed, there are sharp MMI^{TM}, Enzyme Leach^{SM} and BioLeach^{SM} peaks at Profiles 3 and 14. However, many of the aqua regia-ICPMS determined elements including Cu form a peak at Profile 7 roughly 300 metres to the south east where partial leach Cu values are low. Figure 3.1.33 shows that aqua regia-ICPMS and partial leach Cu patterns in soil are generally similar and that contrast is improved by MMI^{TM} and BioLeach^{SM}.

Most soil samples have only trace amounts or non-detectable amounts of Au determined Enzyme Leach^{SM} and BioLeach^{SM}. However, there is a steady increase in Au extracted by MMI^{TM} from west to east along the Rainbow Traverse and there is a sharp Au peak at Profile 3. Figure 3.1.34 compares Au by MMI^{TM} with Au by aqua regia-ICPMS and with the number of

Au grains isolated from the heavy mineral fraction of C soil horizon samples. Two Au grains of which one was described as being "pristine" where found at Profile 7 and of the 6 Au grains found in the C soil horizon at Profile 8 of which were described as being "pristine" suggesting that the native Au grains did not under go any appreciable abrasion during their displacement from bedrock. Figure 3.1.35 compares Ag extracted by MMI^{TM}, BioLeach^{SM}, Enzyme Leach^{SM} and aqua regia-ICMS determined values. Very little of the Ag is liberated from the lower B soil with BioLeach^{SM} and Enzyme Leach^{SM}, but there is appreciable metal extracted by MMI^{TM} and the MMI^{TM} pattern across the Rainbow Zone is very similar to that of aqua regia-ICPMS in the lower B horizon.

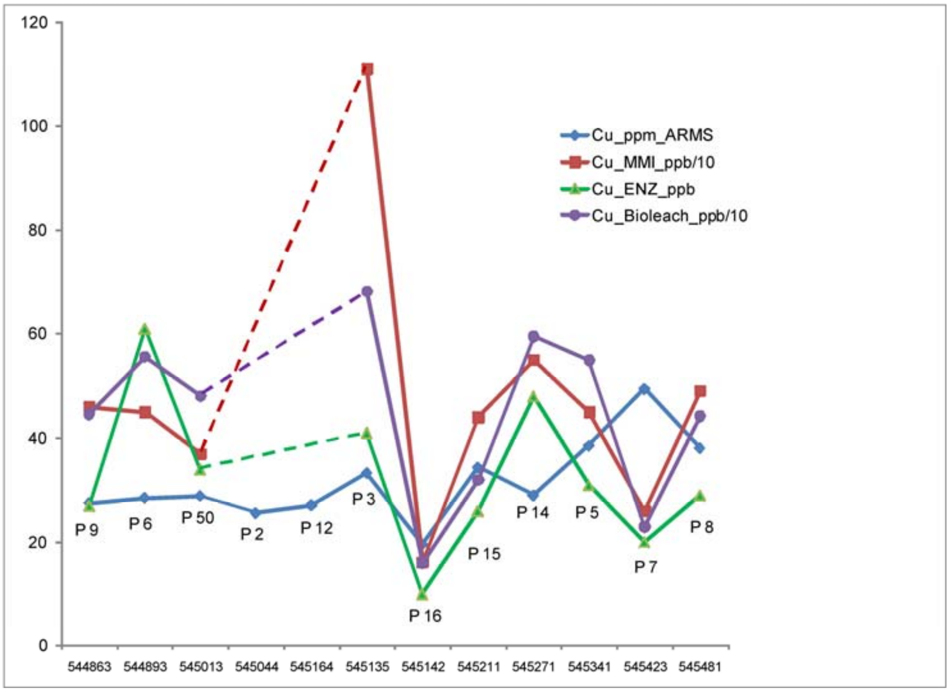

Figure 3.1.33 Aqua regia_ICPMS, MMI^{TM}, Enzyme Leach^{SM} and BioLeach^{SM} Cu in lower B soil - Rainbow Zone.

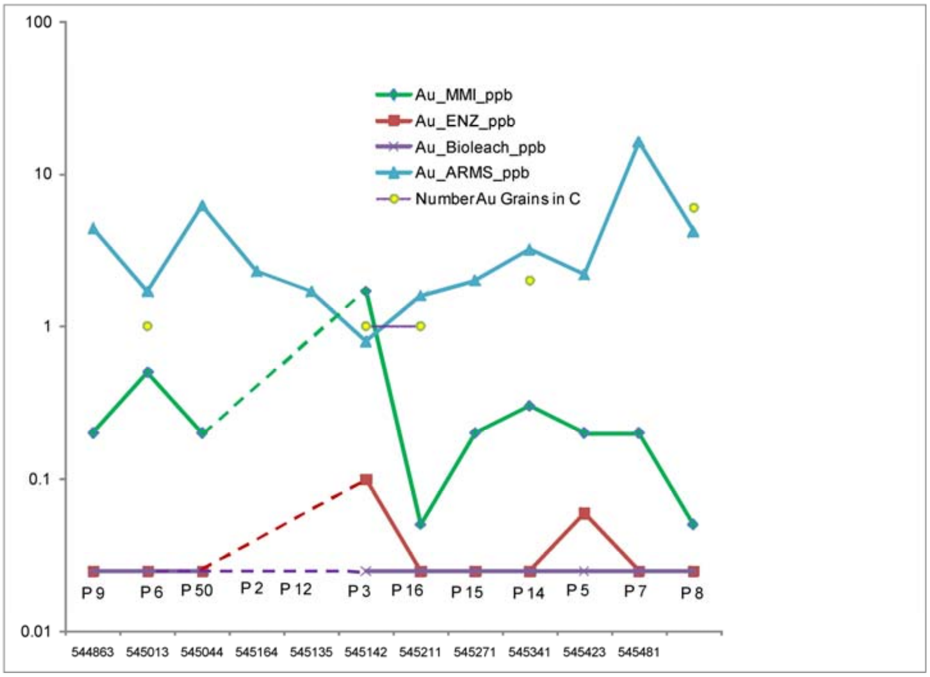

Figure 3.1.34 Aqua regia_ICPMS Au, MMI^{TM} Au, Enzyme Leach^{SM} Au and BioLeach^{SM} Au in lower B soil - Rainbow Zone.

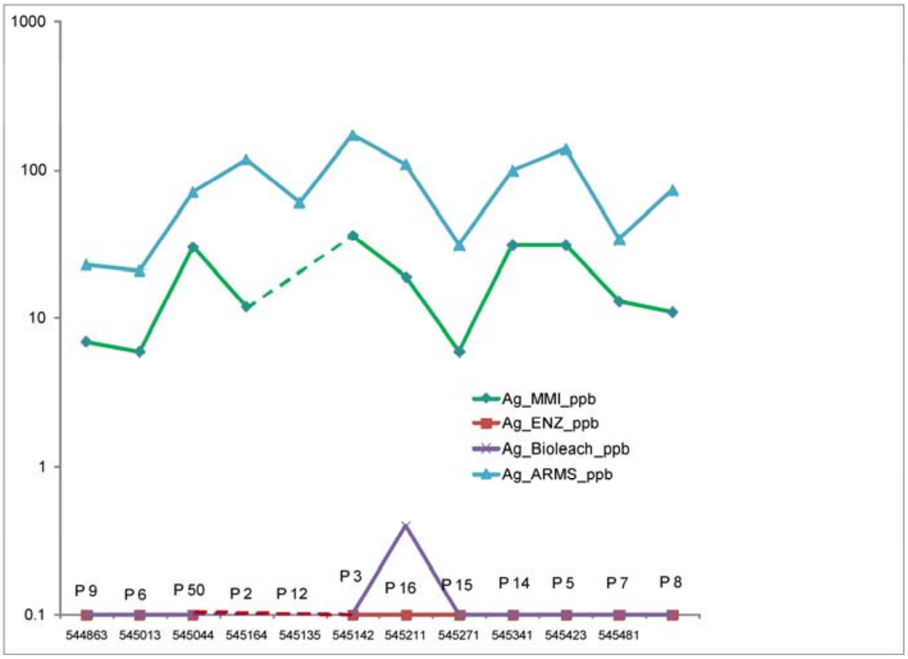

Figure 3.1.35: MMI, Enzyme Leach, Bioleach and aqua regia-ICPMS Ag in lower B soil - Rainbow Zone.

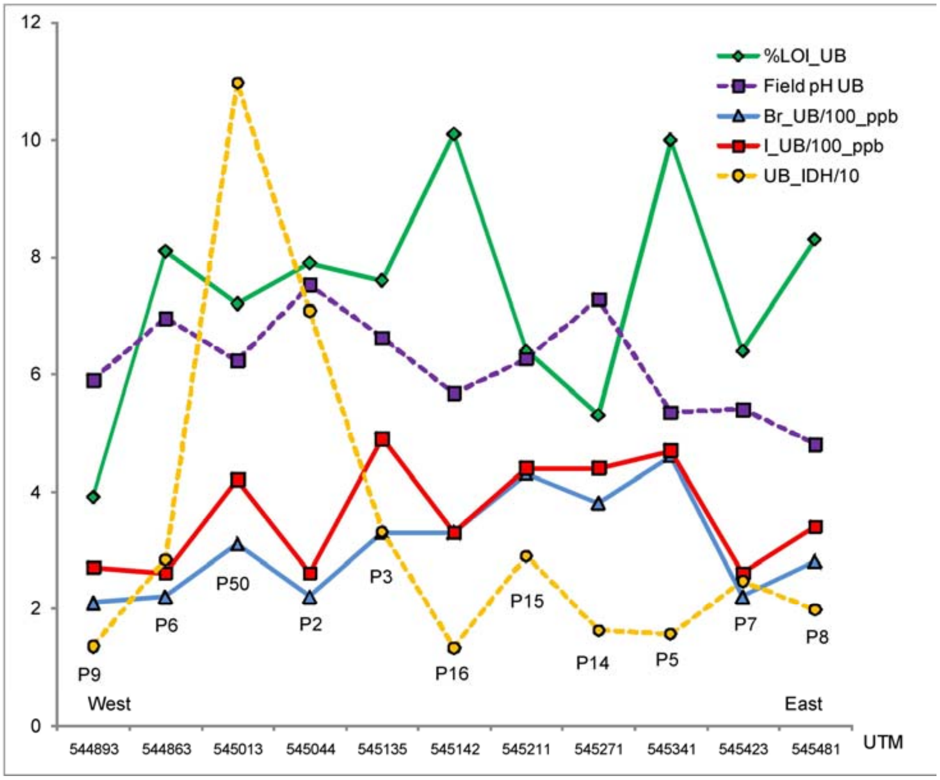

Figure 3.1.36: Bioleach Br and I, Field pH, IDH (pH) and LOI in Upper B soil - Rainbow Zone.

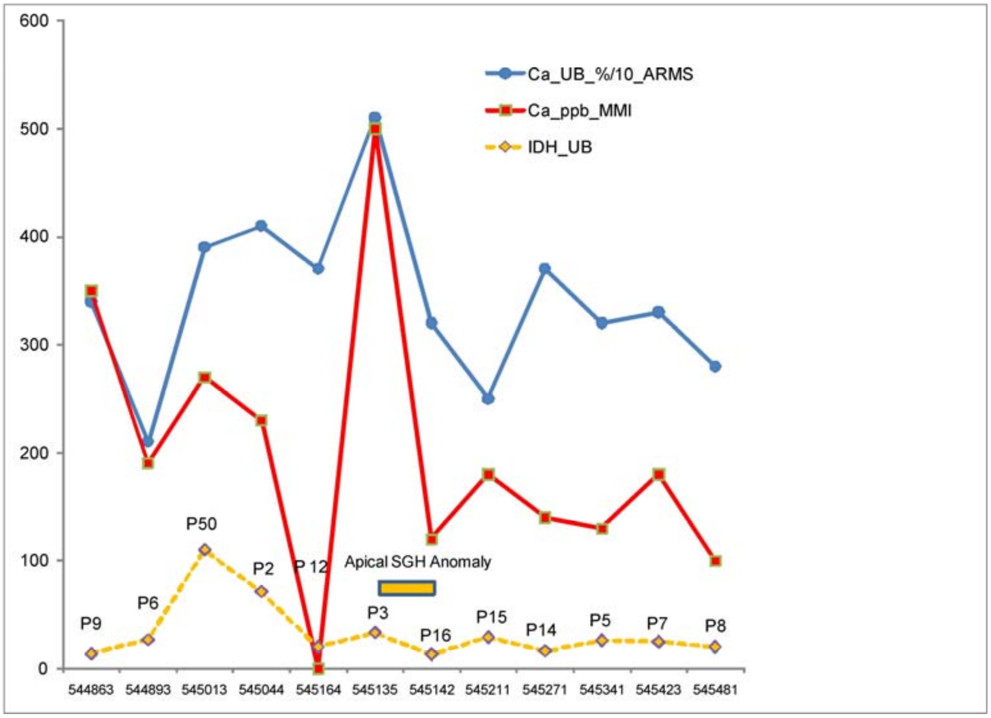

Figure 3.1.37: Calcium by MMI^{TM} and aqua regia-ICPMS and IDH (pH) in Lower B soil - Rainbow Zone.

Figure 3.1.36 shows the variation of BioLeach^{SM} Br, BioLeach^{SM} I, LOI (loss on ignition), field measured pH and Inverse difference hydrogen ion (IDH) in the Upper B horizon along the Rainbow traverse. BioLeach^{SM} Br and BioLeach^{SM} I variation are very similar, but the patterns do not appear to reflect changes in soil pH and soil LOI (organic matter). Most acid Upper B soil is at the east end of the traverse at Profiles P7 and P8 and there is a marked IDH peak at Profile 50. It is tempting to interpret BioLeach^{SM} Br and BioLeach^{SM} I patterns as an expression of volatile halogen release from deeply buried base-precious metal mineralization. However, it is difficult to interpret the BioLeach^{SM} Br and BioLeach^{SM} I results because the patterns appear to have no spatial relationship with increasing of metal content of soil towards the east end of the traverse. BioLeach^{SM} Br and BioLeach^{SM} I are interpreted as components released from ruptured cell membranes of soil bacteria colonies killed by the presence of sulphide minerals. The BioLeach^{SM} Br and BioLeach^{SM} I extracted and detected with propriety leach (Hoffman, *pers comm.).*

Figure 3.1.37 compares aqua regia-ICPMS Ca, MMI^{TM} Ca and pH expressed as IDH across the Rainbow Zone. There is a reasonable correlation of aqua regia and MMI^{TM} Ca except that the sharp zero MMI^{SM} Ca zero value at Profile 12 reflects no analysis. The general decrease of IDH and Ca from west to east could be explained by higher content of remobilized Ca in the soil caused by the near-surface effect of a sulphide induced reducing column between Profile 3 and 16. Location of this reduced “chimney” is based on the position of an apical SGH^{SM} anomaly flanked by two “lows” interpreted by Sutherland and Hoffman, (2008) from Rainbow Zone Upper B soil horizon (SGH) data. Moreover, the authors rank the anomaly strength as 4 on a scale of 1 to 6 indicating that most organic classes that are characteristic of Cu-Au sulphide bearing mineralization are present beneath the soil. However, Sutherland and Hoffman, (2008), caution that the number of soil samples from the Rainbow Zone analysed for SGH compounds would be insufficient to reliably outline an exploration target.

Sample Traverse South of BC Highway 26

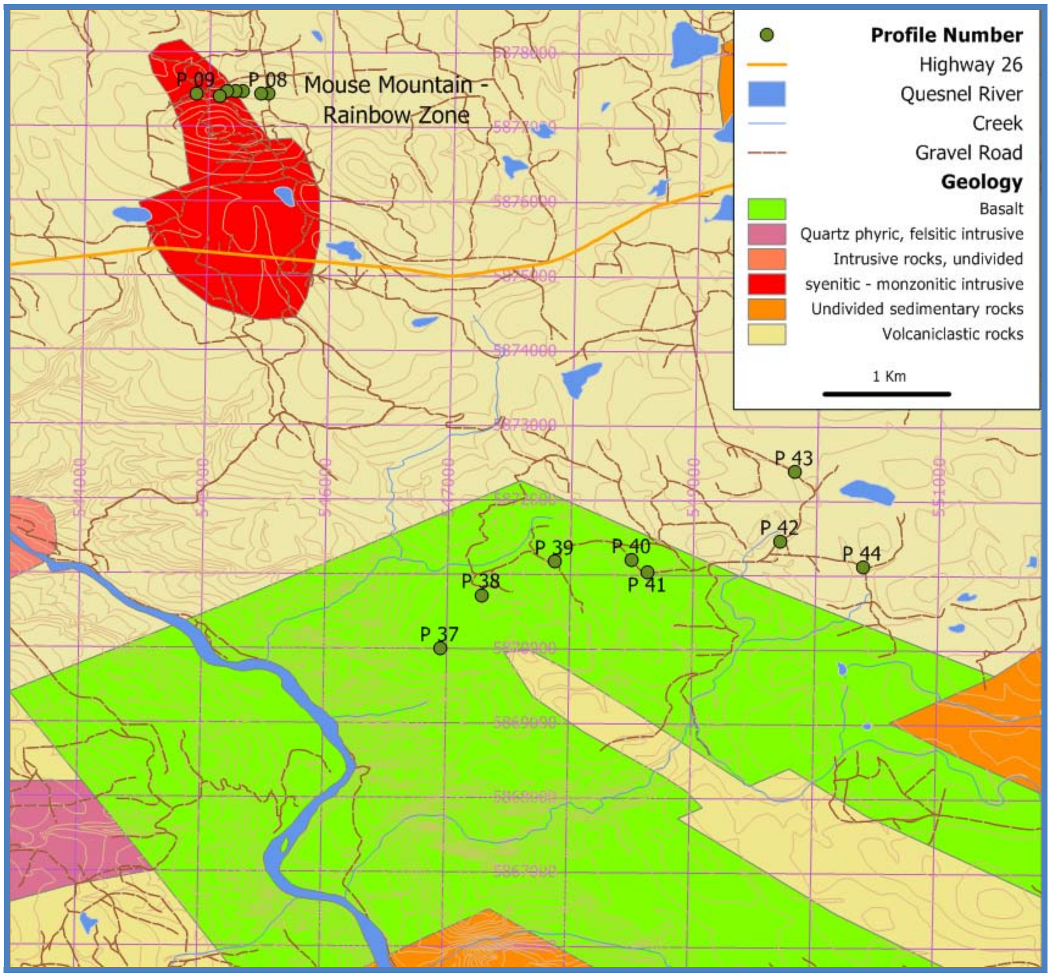

Figure 3.1.38: Sample profile locations south of Highway 26. Geology from Massey et al. 2005.

Profiles locations along a traverse south of Highway 26 (HW 26) are shown in Figure 3.1.38 and the variation of Cu in the soil in Figure 3.1.39. At Profile 40 there is a sharp B soil horizon Cu peak and smaller Lower B and Upper horizon peaks. Gold in Figure 3.1.41 displays a sharp C horizon peak with up to 70 ppb Au in the F-H soil horizon at Profile 39. However, no Au was detected by aqua regia-ICPMS of a C horizon sample at Profile 39 most likely due to an uneven distribution of larger Au grains in till. The presence 1-2 Au grains in the till heavy mineral concentrate from Profiles 39 and 41 supported this interpretation. Reshaped and modified Au grain shape suggests erosion over a longer transport distance or Au-bearing glacial sediment has been reworked.

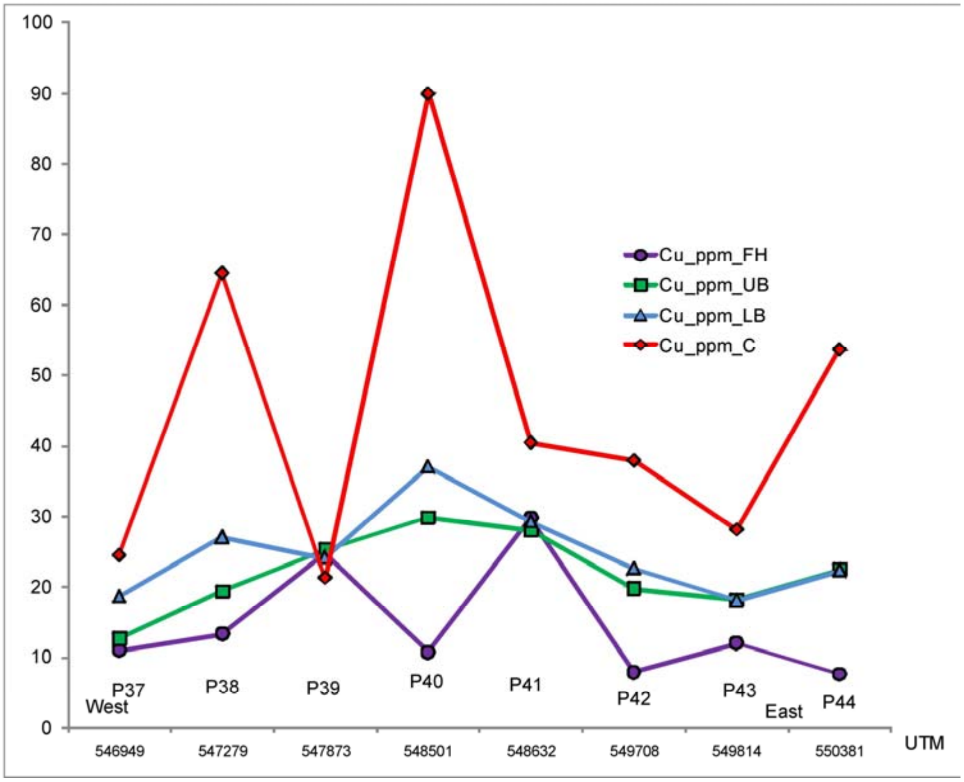

Figure 3.1.39 Copper in soil along the traverse South of HW 26.

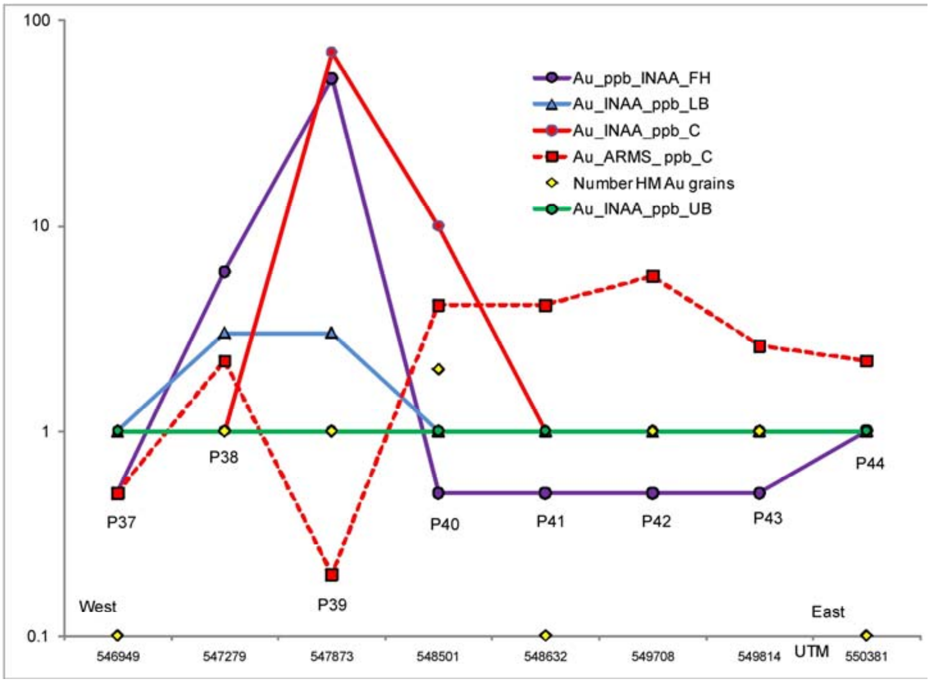

Figure 3.1.40 Gold by INAA and HMC Au grains in soil along the traverse South of HW 26.

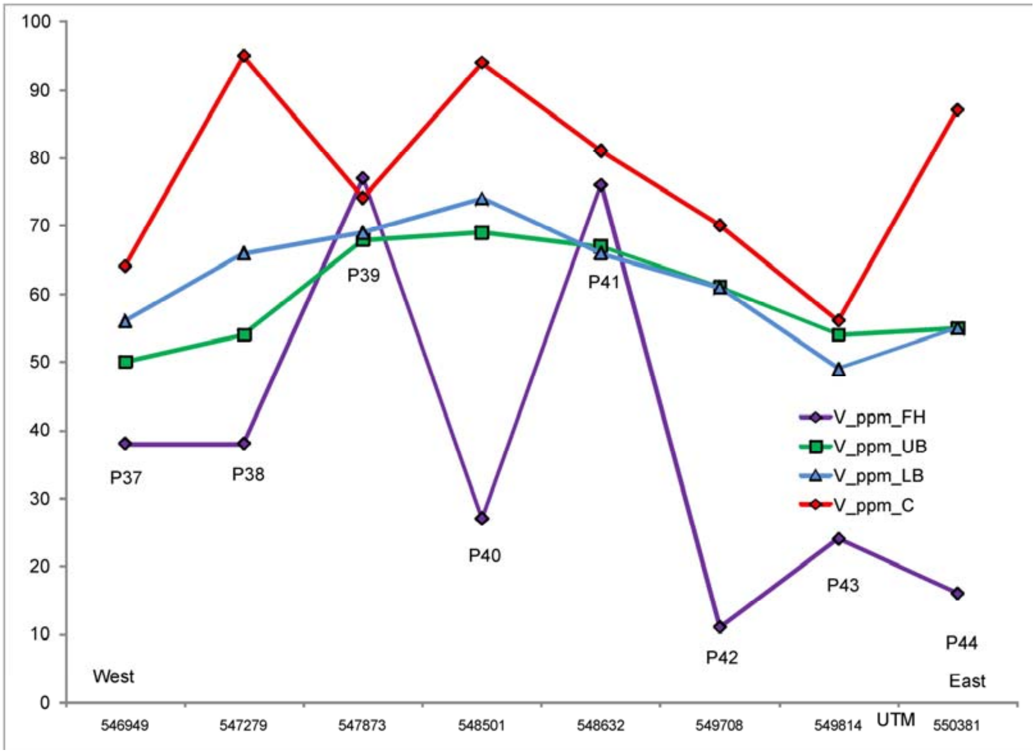

Figure 3.1.41: Variation of V by aqua regia-ICPMS in soil along the traverse South of HW 26 traverse.

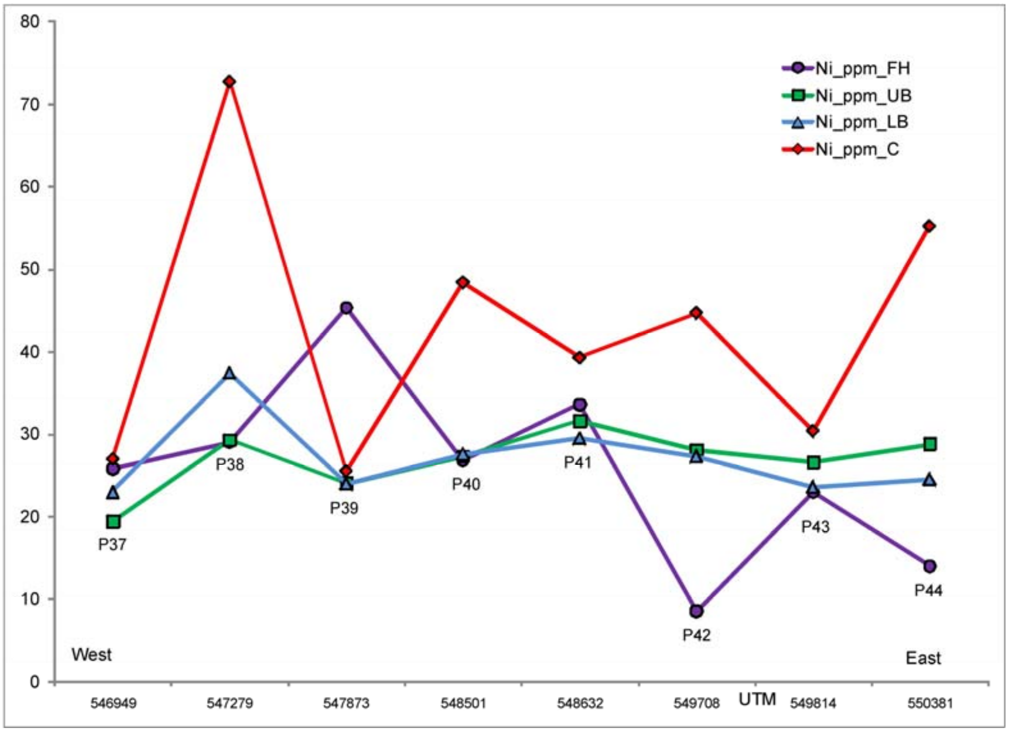

Figure 3.1.42: Variation of Ni by aqua regia-ICPMS in soil along the traverse South of HW 26 traverse.

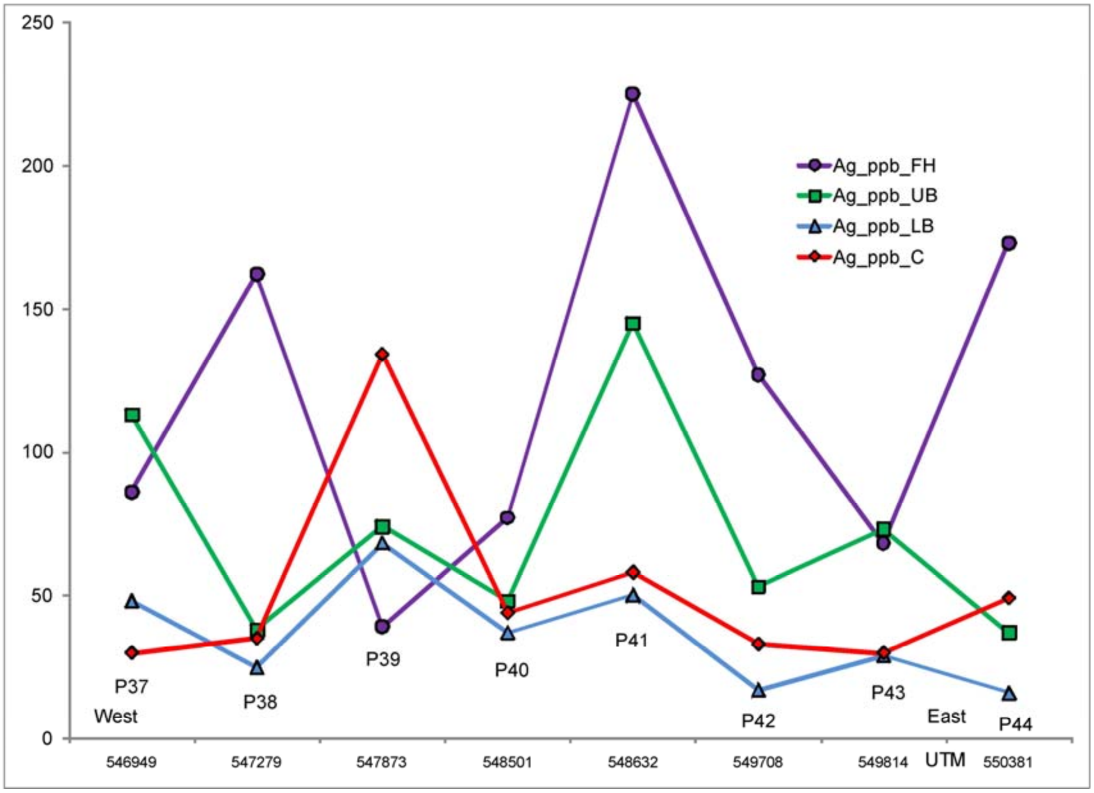

Figure 3.1.43: Silver by aqua regia-ICPMS in soil along the traverse South of HW 26 traverse.

Vanadium (Figures 3.1.41) and Ni (Figure 3.1.42) along the traverse follows Cu variation suggesting that the B soil horizon geochemistry reflects till geochemistry. There is very little relationship between the V and Ni F-H horizon and V and Ni in the B soil horizon. Silver, in Figure 3.1.43, varies rather erratically along the traverse, but there is a strong Ag peak in both F-H and B soil horizon at Profile 41. While no Hg was determined in F-H horizon samples Figure 3.1.44 shows that there is a sharp Hg peak at Profile 39 corresponding to the Au F-H and C soil anomalies. Possible causes for the high C soil horizon Hg and corresponding elevated Au are that the Hg indicates a Au mineralized vein beneath the till or that Hg is anthropogenic and the juxtaposition of the two elements is just a coincidence. Arsenic in Figure 3.2.45 displays an inverse C soil horizon relationship to Hg at Profile 39 and since As is a common Au pathfinder there is additional evidence that the Hg soil anomaly may be contamination from an unknown source. Molybdenum in Figure 3.1.46 is consistently higher in F-H horizon samples and there is a small Mo peak in the C horizon at Profile 40. Lead and Z in Figures 3.1.47 and 3.1.48 are also elevated in the F-H horizon compared to the B and C horizons and there is a marked F-H horizon Zn peak at Profile 43. Of the three partial leach methods only MMI^{TM} detects sufficient Au to provide appreciable contrast (Figure 3.1.49). The MMI^{TM} Au contrast is smaller than that by INAA analysis of C and F-H horizon soils and the peak of the MMI^{TM} Au is displaced east to Profile 40. The MMI^{TM} Cu contrast, shown on the traverse in Figure 3.1.50, is greater than Au and also Cu determined by other partial leaches including aqua regia-ICPMS.

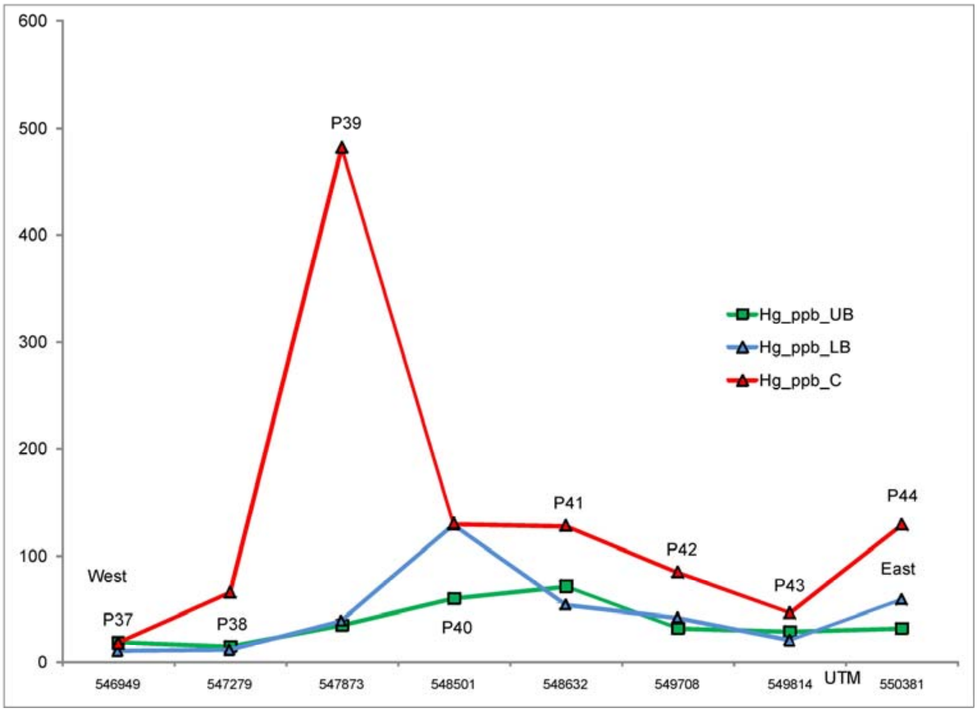

Figure 3.1.44: Mercury by aqua regia-ICPMS in soil along the traverse South of HW 26 traverse.

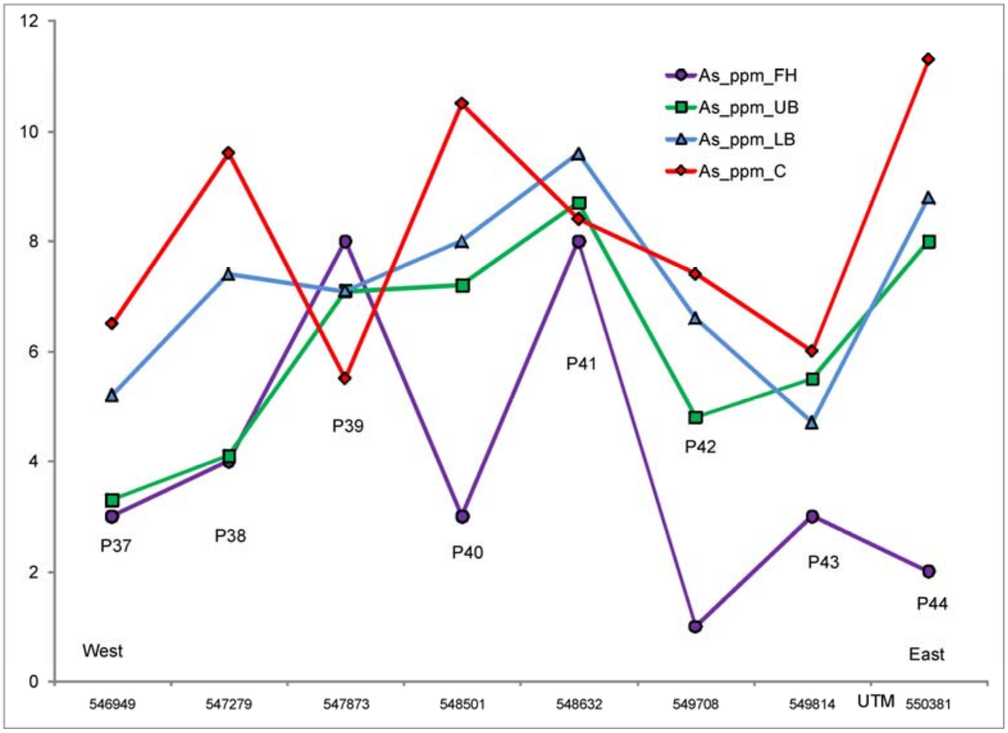

Figure 3.1.45: Arsenic by aqua regia-ICPMS in soil along the traverse South of HW 26 traverse.

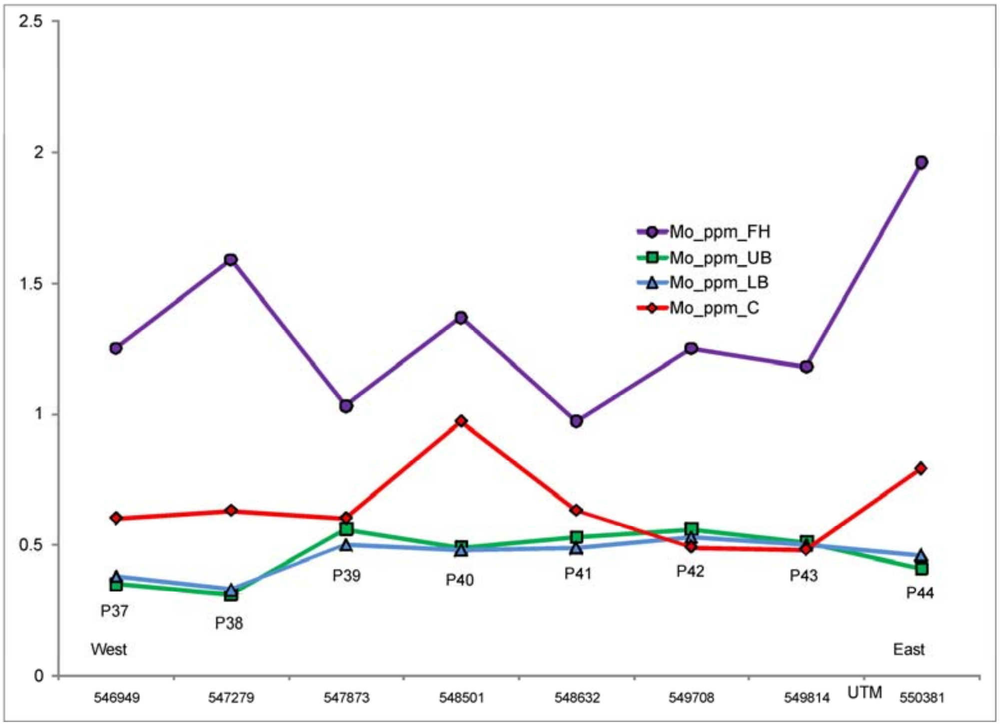

Figure 3.1.46: Molybdenum by aqua regia-ICPMS in soil along the traverse South of HW 26

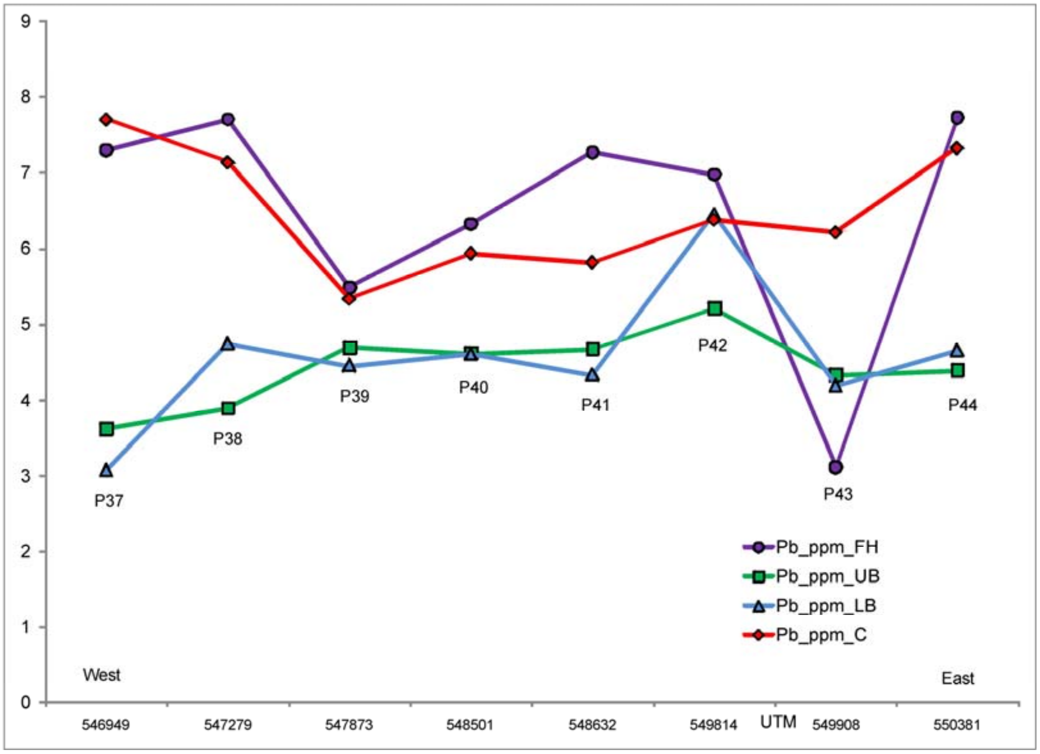

Figure 3.1.47: Lead by aqua regia-ICPMS in soil along the traverse South of HW 26

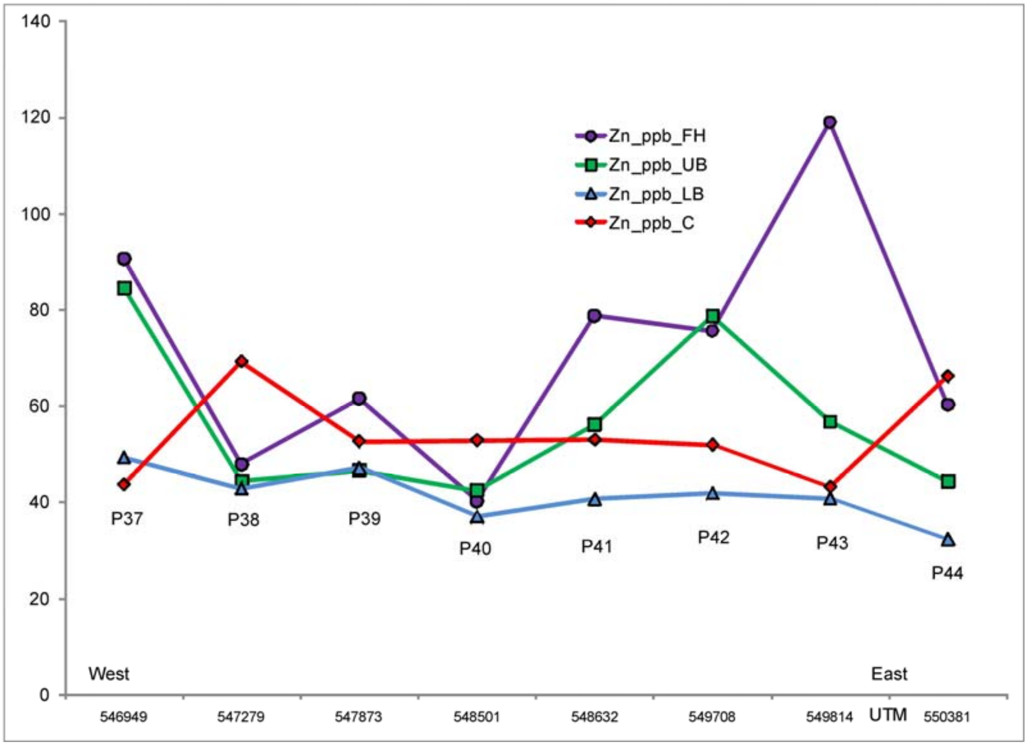

Figure 3.1.48: Zinc by aqua regia-ICPMS in soil along the traverse South of HW 26

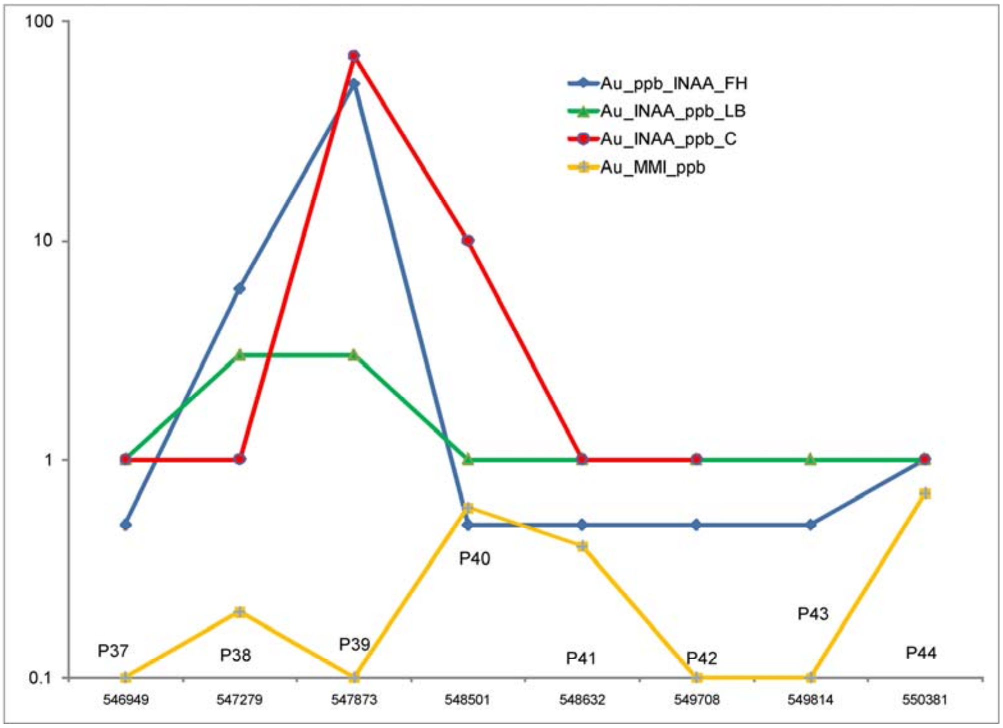

Figure 3.1.49: Gold by INAA and MMI^{TM} in soil along the traverse South of HW 26 traverse.

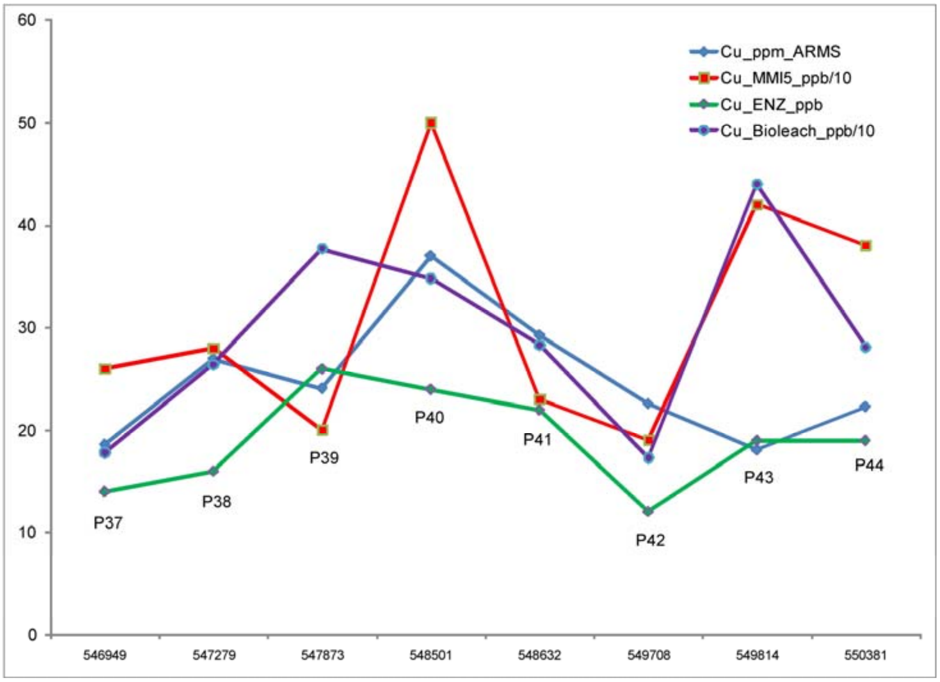

Figure 3.1.50: Copper by aqua regia-ICPMS, Enzyme Leach^{SM}, BioLeach ^{SM} and MMI^{TM} in soil along the traverse South of HW 26 traverse.

Sutherland and Hoffman, (2008) identify an apical SGH^{SM} anomaly above a reduced "chimney" centered on Profiles 39 along the traverse south of Highway 26. Based on a comparison of SGH data from the Rainbow traverse with the SGH soil geochemistry from existing Cu-Au deposits, Sutherland and Hoffman, (2008), rank the anomaly as 2 (on a scale of 1 to 6). The relationship of this anomaly to Ca (aqua regia-ICPMS, MMI^{TM}) and soil pH expressed as IDH is shown in Figure 3.1.51. The reduced chimney predicted by Sutherland and Hoffman corresponds to an Au C-soil horizon peak, MMI^{TM} Cu peak with a flanking asymmetric BioLeach^{SM} halogen peak (Figure 3.1.52), a low soil pH (IDH values) and higher soil LOI. However, placing significance on the existence of high or low element values in soil at a single, isolated location along a traverse can be misleading. Lower soil LOI and higher pH could reflect increased bacterial decomposition of soil organic matter in response to the presence of an electro-potential cell above a buried massive sulphide body. Conversely, higher LOI might reflect increased soil biomass through increased bacterial activity stimulated by higher alkane flux. Lower pH created by this hydrocarbon would increase mobility of metals and thus results in their depletion from the redox cell.

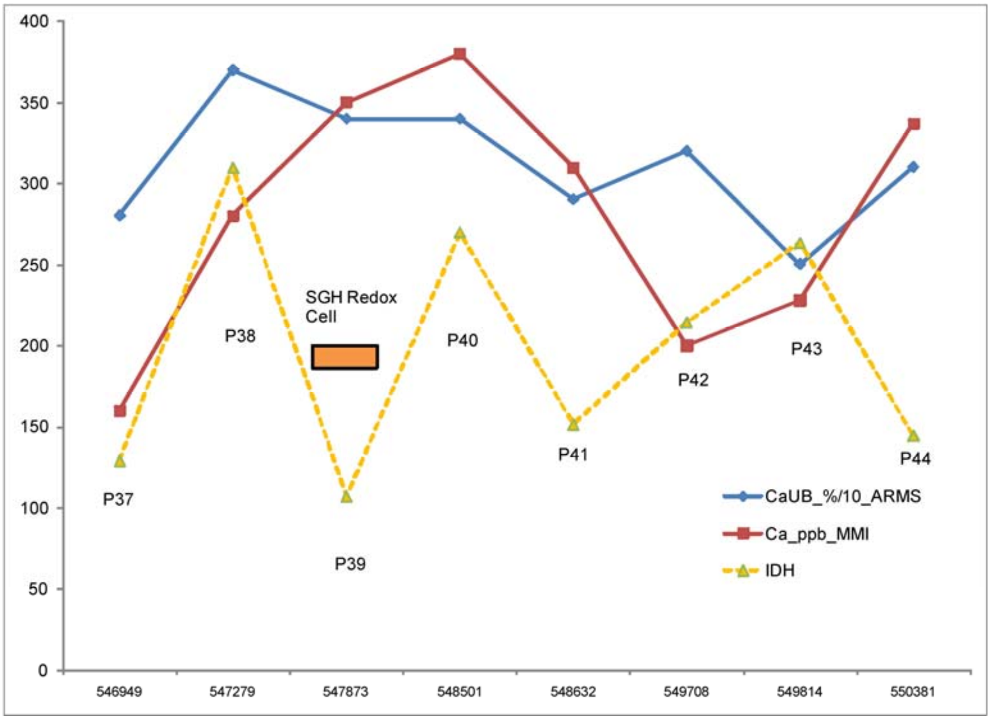

Figure 3.1.51: Variation of Ca and pH in soil along the traverse south of Highway 26.

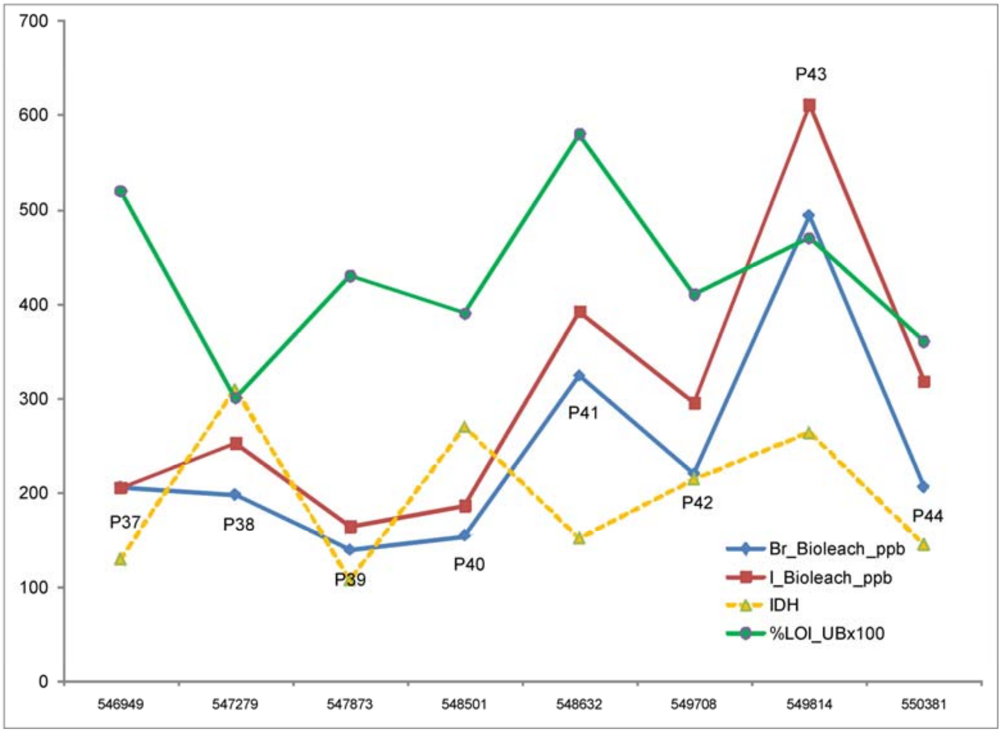

Figure 3.1.51: BioLeach Br and I, pH (IDH) and LOI in soil along the traverse south of BC Highway 26.

Element	Range	Peak value	Background (median)	Threshold (3rd quartile)	Contrast
Au_AR_FH	0.25 – 117 ppb	62.9 ppb	0.25 ppb	0.25 ppb	252
Au_AR_UB	0.2 – 12.9 ppb	8.8 ppb	1.1 ppb	1.95 ppb	4.5
Au_AR_LB	0.2 – 24 ppb	20.2 ppb	2.1 ppb	3.5 ppb	5.8
Au_AR_C	0.2 - 6.8 ppb	6.3 ppb	2.6 ppb	4.1 ppb	1.5
Au_MMI_LB	0.05 – 0.6 ppb	0.6 ppb	0.2 ppb	0.3 ppb	2.2
Ag_AR_FH	39 – 665 ppb	582.5 ppb	183 ppb	287 ppb	2.0
Ag_AR_UB	35 – 578 ppb	478 ppb	80 ppb	132 ppb	3.2
Ag_AR_LB	16 – 171 ppb	155 ppb	64 ppb	99 ppb	1.6
Ag_AR_C	30 – 211 ppb	183 ppb	53 ppb	64 ppb	2.9
Ag_MMI_LB	76 - 41 ppb	36 ppb	13 ppb	31 ppb	1.2
Ag_BioLeach_LB	0.1 – 0.5	0.5 ppb	0.1 ppb	0.1 ppb	5.0
As_AR_FH	0.5 – 2.4 ppm	2.2 ppm	1.2 ppm	1.7 ppm	1.3
As_AR_UB	2.1 – 10.5 ppm	9 ppm	4.9 ppm	6.5 ppm	1.4
As_AR_LB	2.8 – 9.8 ppm	9.3 ppm	5.8 ppm	6.3 ppm	1.5
As_AR_C	3.7 – 16.9 ppm	15.1 ppm	8.4 ppm	10.5 ppm	1.4
As_MMI_LB	5 - 40 ppb	35 ppb	5 ppb	35 ppb	1.1
As_BioLeach_UB	89 - 221 ppb	203 ppb	137 ppb	157 ppb	1.3
As_BioLeach_LB	34 - 214 ppb	204 ppb	163 ppb	181 ppb	1.1
As_EnzLeach_UB	4 - 7 ppb	7 ppb	5 ppb	6 ppb	1.1
As_EnzLeach_LB	3 - 7 ppb	7 ppb	6 ppb	7ppb	1.0
Cu_AR_FH	7.61 – 29.7 ppm	27.2 ppm	11 ppm	13.1 ppm	2.1
Cu_AR_UB	12.65 – 92.3 ppm	63.5 ppm	23.61 ppm	29.28 ppm	2.2
Cu _AR_LB	18.04 – 49.49 ppm	44.03 ppm	27.05 ppm	29.03 ppm	1.5
Cu_AR_C	19.61 – 123.47 ppm	106.7 ppm	40.41 ppm	63.98 ppm	1.7
Cu_MMI_LB	290 – 1110 ppb	720 ppb	330 ppb	720 ppb	1.0
Cu_BioLeach_UB	229 – 680 ppb	618 ppb	445 ppb	481 ppb	1.2
Cu_BioLeach_LB	147 – 595 ppb	580ppb	419 ppb	476 ppb	1.4
Cu_EnzLeach_UB	16 – 61 ppb	52 ppb	30 ppb	39 ppb	1.3
Cu_EnzLeach_UB	10 – 48 ppb	43 ppb	24 ppb	32 ppb	1.3
Co_AR_FH	1.6 – 11.2 ppm	10.8 ppm	3.2 ppm	4.1 ppm	2.6
Co_AR_UB	5.7 – 24.3 ppm	17.5 ppm	8.9 ppm	9.9 ppm	1.8
Co _AR_LB	6.8 – 11.9 ppm	11.5 ppm	9.7 ppm	10.4 ppm	1.1
Co_AR_C	5.8 – 20.0 ppm	17.8 ppm	11.2 ppm	14.8 ppm	1.2
Co_MMI_LB	2.5 – 179 ppb	169 ppb	61 ppb	133 ppb	1.2
Co_BioLeach_UB	21 – 155 ppb	133 ppb	78 ppb	91 ppb	1.5
Co_BioLeach_LB	31 – 126 ppb	121 ppb	81 ppb	111 ppb	1.1
Co_EnzLeach_UB	10 – 51 ppb	45 ppb	20 ppb	28 ppb	1.6
Co_EnzLeach_LB	7 – 24 ppb	23 ppb	13 ppb	15 ppb	1.5
Hg_AR_UB	11 – 71 ppb	65 ppb	34 ppb	46 ppb	1.4
Hg _AR_LB	11 – 129 ppb	109 ppb	38 ppb	52 ppb	2.1
Hg_AR_C	18 – 482 ppb	381 ppb	68 ppb	129 ppb	3.0
Mn_AR_FH	181 – 4130 ppm	3675 ppm	1540 ppm	2670 ppm	1.4
Mn_AR_UB	141 – 324 ppm	323 ppm	205 ppm	252 ppm	1.3
Mn _AR_LB	182 – 398 ppm	377 ppm	302 ppm	320 ppm	1.2
Mn_AR_C	195 – 828 ppm	763 ppm	367 ppm	556 ppm	1.4
Mn_Bioleach_UB	811 – 6811 ppb	6135 ppb	2520 ppb	4020 ppb	1.5

Mn_BioLeach_LB	972 – 5500 ppb	5415 ppb	3110 ppb	3698 ppb	1.5
Mn_EnzLeach_UB	160 – 4720 ppb	3145 ppb	668 ppb	921 ppb	3.4
Mn_EnzLeach_LB	324 – 1140 ppb	816 ppb	509 ppb	591 ppb	1.5
Mo_AR_FH	0.67 – 1.96 ppm	1.82 ppm	1.25 ppm	1.37 ppm	1.32
Mo_AR_UB	0.31 – 1.7 ppm	1.06 ppm	0.65 ppm	0.72 ppm	1.5
Mo _AR_LB	0.33 – 0.86 ppm	0.84 ppm	0.62 ppm	0.71 ppm	1.2
Mo_AR_C	0.38 – 1.33 ppm	1.1 ppm	0.63 ppm	0.78 ppm	1.4
Mo_MMI_LB	2.5 – 7 ppb	6.5 ppb	2.5 ppb	5.5 ppb	1.2
Mo_BioLeach_UB	3.9– 12.2 ppb	12.2 ppb	8.2 ppb	11 ppb	1.2
Mo_BioLeach_LB	3.3 – 17.3 ppb	16.3 ppb	9 ppb	11 ppb	1.5
Mo_EnzLeach_UB	3 – 18 ppb	15 ppb	5 ppb	9 ppb	1.8
Mo_EnzLeach_LB	2 – 9 ppb	9 ppb	5 ppb	6 ppb	1.6
Ni_AR_FH	3.9 – 45.3 ppm	39.45 ppm	13.7 ppm	22.9 ppm	1.7
Ni_AR_UB	11 – 36.1 ppm	30.5 ppm	24 ppm	26.6 ppm	1.1
Ni _AR_LB	18.8 – 37.4 ppm	34.7 ppm	24.5 ppm	27.3 ppm	1.3
Ni_AR_C	20.5 – 72.2 ppm	64 ppm	34.7 ppm	44.7 ppm	1.4
Ni_MMI_LB	56 – 266 ppb	236 ppb	171 ppb	198 ppb	1.2
Ni_BioLeach_UB	47 – 129 ppb	123 ppb	78 ppb	90 ppb	1.4
Ni_BioLeach_LB	28 – 104 ppb	102 ppb	70 ppb	95 ppb	1.1
Ni_EnzLeach_UB	13 – 39 ppb	38 ppb	22 ppb	28 ppb	1.3
Ni_EnzLeach_LB	12 – 30 ppb	29 ppb	22 ppb	25 ppb	1.2
Pb_AR_FH	3.11 – 11.1 ppm	11 ppm	7.71 ppm	9.03 ppm	1.2
Pb_AR_UB	3.62 – 6.0 ppm	5.92 ppm	4.95 ppm	5.29 ppm	1.1
Pb _AR_LB	3.07 – 6.5 ppm	6.46 ppm	4.65 ppm	5.04 ppm	1.3
Pb_AR_C	4.05 – 10.82 ppm	9.88 ppm	6.18 ppm	7.19 ppm	1.4
Pb_MMI_LB	5-230 ppb	190 ppb	100 ppb	120 ppb	1.6
Pb_BioLeach_UB	7.2 – 141 ppb	128 ppb	24 ppb	81 ppb	1.6
Pb_BioLeach_LB	7 – 52 ppb	46 ppb	26 ppb	33 ppb	1.4
Zn_AR_FH	32 – 261 ppm	245 ppm	89.4 ppm	173 ppm	1.4
Zn_AR_UB	41.3 –93.4 ppm	93.1 ppm	65.3 ppm	77.2 ppm	1.2
Zn _AR_LB	32.3– 75.6 ppm	764.6 ppm	52.3 ppm	63.9 ppm	1.3
Zn_AR_C	37.3 – 91.8 ppm	54.5 ppm	53 ppm	66 ppm	1.4
Zn_MMI_LB	10 – 1130 ppb	950 ppb	440 ppb	570 ppb	1.7
Zn_EnzLeach_UB	5 – 130 ppb	120 ppb	30 ppb	68 ppb	1.8
Zn_EnzLeach_LB	5 – 460 ppb	270 ppb	35 ppb	50 ppb	5.4
Zn_BioLeach_UB	62 – 769 ppb	638 ppb	285 ppb	396 ppb	1.6
Zn_BioLeach_LB	18– 1070 ppb	1065 ppb	320 ppb	629 ppb	1.7
Br_BioLeach_UB	220 – 684 ppb	571 ppb	315 ppb	393 ppb	1.5
Br_BioLeach_LB	236 – 513 ppb	448 ppb	321 ppb	359 ppb	1.2
I_BioLeach_UB	261 – 759 ppb	628 ppb	448 ppb	478 ppb	1.3
I_BioLeach_LB	302 – 476 ppb	460 ppb	391 ppb	440 ppb	1.0

Table 3.3: Anomaly contrast for Au, Ag, As, Cu, Co and Mo in FH, Upper B, Lower B and C soil horizon samples calculated from combined data from the Mouse Mountain Rainbow Zone and traverse south of Highway 26.

Anomaly Definition

Among factors that define a geochemical anomaly are contrast, spatial size and the multi-element association. Anomaly contrast can be simply expressed as the average of the two highest element concentrations in a survey dataset ratioed to a threshold that might represent the 95th percentile or 3rd quartile value (Cook and Dunn, 2005). Stanley and Nobel (2008) applied a student t test to the mean value of successive sample pairs along a geochemical traverse for predicting the optimum geochemical anomaly contrast. Their technique allows a much more objective contrast estimate using survey data but may not be suitable where there numerous, isolated single samples anomalies such as those revealed in the geochemical patterns along the Mouse Mountain Rainbow zone and south of BC Highway 26 traverses. Anomaly contrast for Au, Ag, As, Cu, Co and Mo estimated from the geochemical data combined from the two traverses is estimated by the more simple approach i.e. ratio of average two highest values to a 3rd quartile threshold. Table 3.3 shows that the anomaly contrast for elements determined by aqua regia-ICPMS ranges from 250 for Au in the F-H soil horizon to 1.1 for Co in the lower B horizon and there seems no relationship between contrast for different elements and soil horizon. Anomaly contrast for metals determined by MMI™ is typically larger than those by bioleach although for some elements (e.g. Ag) a greater contrast is possible with aqua regia extraction. Bromine and I contrast ranges from 1.3 to 1.6 and shows little difference in upper B horizon samples compared to the lower B horizon. Soil organic matter and pH influence the distribution of elements in the upper B soil along both Rainbow and Highway 26 traverses as shown by the association of increased LOI and higher concentration of several metals (e.g. Cu). Cobalt, Cr, Ni, V variation most likely is closer indication the till geochemistry whereas Au, Ag, As, Cu, Hg, Pb and Zb are pathfinders to Cu-Au mineralization.

3.2 Soda Creek

Location : NTS – 93B 08 LAT. 52°16'00" UTM NORTH – 5791000
LONG. - 122°21'00" UTM EAST – 544000

MINFILE Status*: None: Geochemical anomaly (regional stream sediment).*

Geology: Soil samples, collected west of Soda Creek, cross an area that is covered by the Chilcotin Group basalt. Under the plateau basalt are most likely Permian to Triassic marine sediments and volcanics forming the Cache Creek Complex. The Chilcotin volcanics may be more than 100 metres thick because of the area is near the Fraser River valley (Mihalynuk, 2007).

Alteration and Mineralization: No mineral occurrences have been reported in the area although Cache Creek rocks are known to host volcanic massive sulphide (VMS) mineralization.

Local Environment: Numerous lakes, poorly defined marshy stream channels and drumlin-like landforms are common features of this gently undulating plateau that has an average elevation of 1000 metres ASL. To the east of the area sampled the plateau surface has a steep slope towards the Fraser River valley. Tipper, 1972, interpreted the few drumlin-like landforms visible on air photographs to reflect a south to north ice-flow during the most recent advance of the Fraser Glaciation. Diamicton, exposed in road-cuts, is a silt-clay textured basal till and at one sample location it proved to have enough carbonate for the till to react with dilute hydrochloric acid. Soil ranges from bruisols on better drained till to organic around wetlands. Vegetation comprises a mainly Interior Douglas-Fir (*Pseudotsuga menziesii glauca),* White Spruce *(Picea glauca),* Lodgepole Pine *(Pinus contorta latifolia),* Trembling Aspen (*Populus tremuloides*) and Paper Birch (*Betula papyrifera*) canopy. Willow (*Salix*) and Alder (*Alnus*) grow commonly near wetlands. Figure 3.2.1 shows the location of the Soda Creek community, the Fraser River, principal lakes, soil profile sites and the site of a region geochemical stream sediment collection in 1980 and 2007.

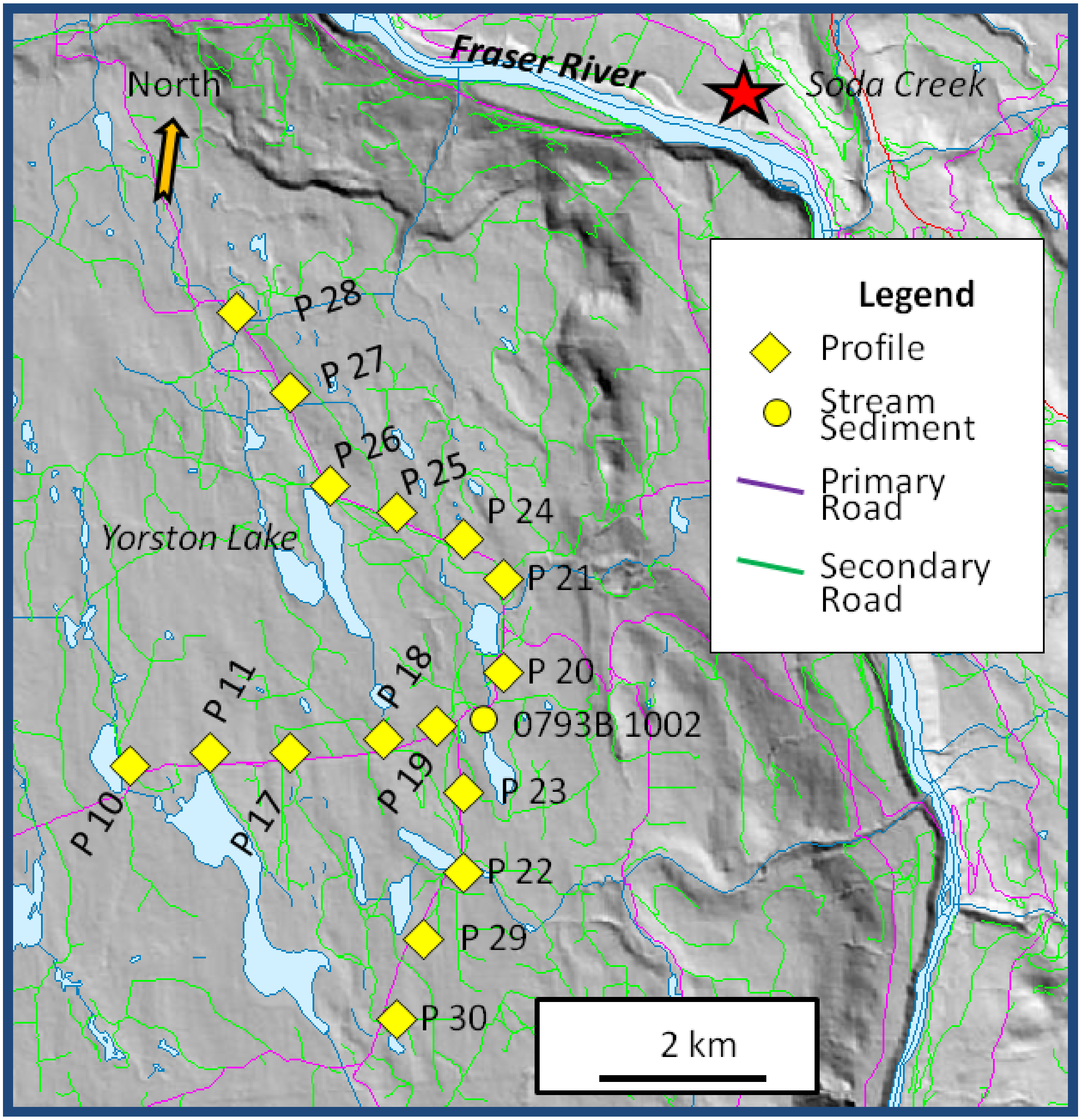

Figure 3.2.1: Landforms of the Soda Creek survey area. Soil sample profile locations are identified by a P prefix and a stream sediment samples collected at a historical BC regional geochemical survey site is labelled 0793B 1002. Base map digital elevation model image captured from Map Place (BC Geological Survey, 2010).

Soda Creek Geochemistry

Lithogeochemistry

No rock samples were collected for analysis and there is no previously published lithogeochemical data.

Drainage geochemistry

Sample_ID	93B805009	93B071002	95th Percentile for NTS 93B
Latitude	52.27753	52.27738	
Longitude	-122.35346	-122.35343	
Elevation	900		
pH	8.2		
Zn_ppm	94	83.9	86
Cu_ppm	164	33.44	44
Pb_ppm	2	3.22	4
Ni_ppm	190	72.3	71
Co_ppm	13	21	18
Ag_ppm	0.2	0.055	0.1
Mn_ppm	200	786	2900
Fe_%	2.00	3.53	4
Mo_ppm	1	0.39	2
U_ppm	4.5	0.7	5.5
Hg_ppb	50	20	120
As_ppm	2.0	1.3	10
Sb_ppm	0.4	0.15	1
V_ppm	nd	48	
LOI_%	nd	15	
Au_ppb_ICPMS	nd	0.8	
Au_ppb_INAA	2		9

Table 3.4 Geochemistry of 1980 and 2007 regional survey samples from Coyote Creek compared to a regional thresholds at the 95th percentile for NTS 93B. Sample 93B805009 was analysed by a combination of aqua regia-atomic absorption spectrophotometry, delayed neutron counting (U) and instrumental neutron activation (Au). Sample 93B071002 was analysed by aqua regia digestion-inductively coupled plasma mass spectrometry and for loss on ignition (LOI) at 500^{o}C

Elevated Cu values in a regional stream survey sediment sample from Coyote Creek stimulated an interest in a Cu-Ni mineralized bedrock source for the anomaly in an area west of Soda Creek (Jackaman, 2001). A re-sampling of the creek in 2007 during the soil geochemical study revealed that the sediment contained background Cu levels but elevated Ni. The elevated Cu and Ni is explained by sediment from a small first order stream channel that has negligible water flow, an abundance of basalt boulders along the creek bank close to the sample site and the high organic content (15% LOI) of the sediment. Table 3.4 shows element values and LOI for the samples. The elevated Ni is most likely caused by metal weathered from olivine in the basalt and concentrated by the organic-rich sediment.

Soil geochemistry

Element Associations

Element associations with the Soda Creek soil geochemical data that are indicated by high positive (or negative) correlations coefficient (> +0.8 or – 0.8) tested for significance with scatter plot graph are:

F-H: Horizon: (1) V-Ce-Co-Cr-Fe-Hf-La-Ni-Sm-Mg-Eu; (2) Ba-Mn; (3) Zn-As (negative)
Upper B Horizon: (1) V-Ca-Ag-Cu-Cr-Co-Fe-Ni-La.
Lower B Horizon: (1) Ti-Co-Sc
C horizon: (1) Ti-Al-Cr-Fe-Al-Ga-Sc-Co.

Soil Horizon Geochemical Comparisons

Statistics (mean, median, quartiles, range) calculated from the geochemical data from the soil samples collected in Soda Creek area reveal only Cu, Ni, Cr and Ca are anomalous. Few of the samples have any detectable Au (INAA) and the highest Au values are 14 ppb in the Lower B horizon at Profile 11; 14 ppb in the Upper B horizon at Profile 23 and 8 ppb in the C soil horizon at Profile 21. These samples do not appear to follow any clearly defined trend and most likely they represent a random scatter Au values.

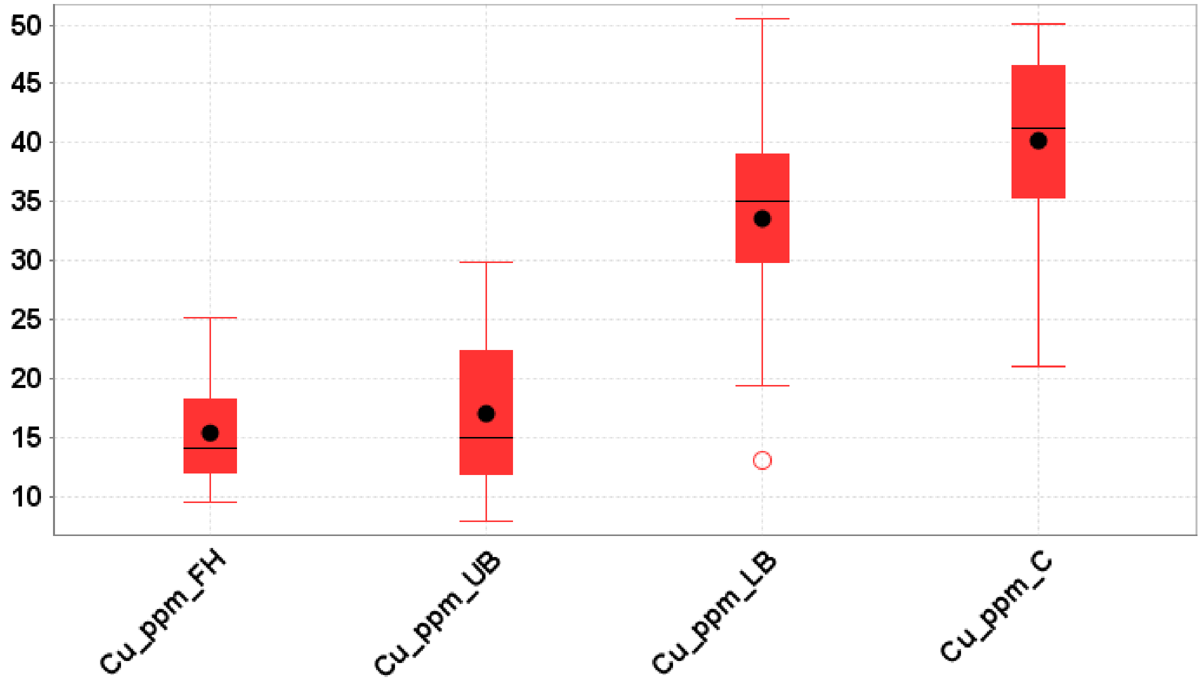

Figure: 3.2.2. Box plot showing the distribution of Cu in 16 soil samples from C, lower B, Upper B and F-H horizons analysed by aqua regia-ICPMS.

The box plot in Figure 3.2.2 shows the distribution of Cu in soil horizons using the data combined from the north-south and east-west sample traverses. Copper increases from the F-H to the C horizon and the increase is most evident in the transition from the upper B to the lower B soil horizon. Nickel (Figure 3.2.3), and V (Figure 3.2.4) distributions are similar to Cu and, again, there is a noticeable increase metal from the upper B to lower B horizon. Figure 3.2.3 also shows that the lower B horizon soil range has the highest Ni content (> 120 ppm) although median Ni increases from lower B into the C horizon. Variation of Cr by INAA from F-H to C horizon is more gradual than that of Ni and the lower B horizon has a similar Cr content to the C horizon. Major elements (e.g. Mg – Figure 3.2.6) also increase from F-H into the C soil horizon and the high (2.8%) Ca content of the C horizon (Figure 3.2.7) can be explained by a carbonate rich till sampled at Profile 11.

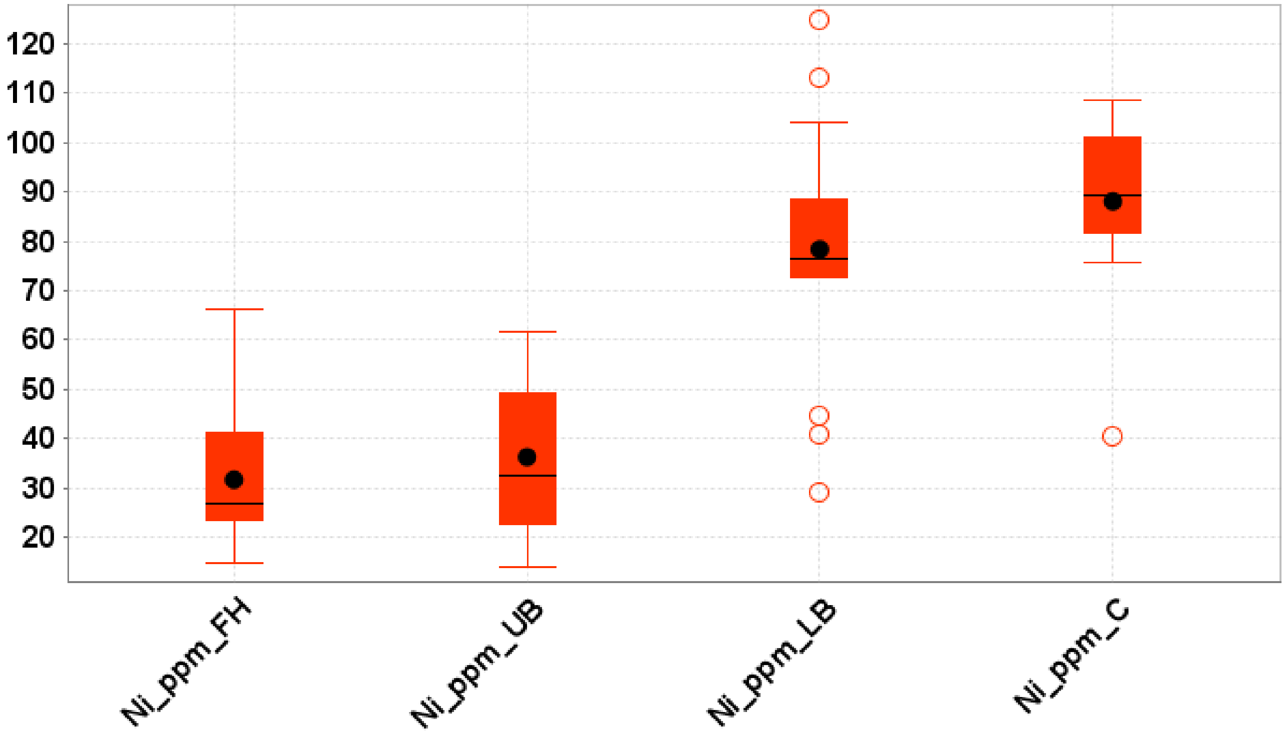

Figure: 3.2.3. Box plot showing the distribution of Ni in 16 soil samples from C, lower B, Upper B and F-H horizons analysed by aqua regia-ICPMS.

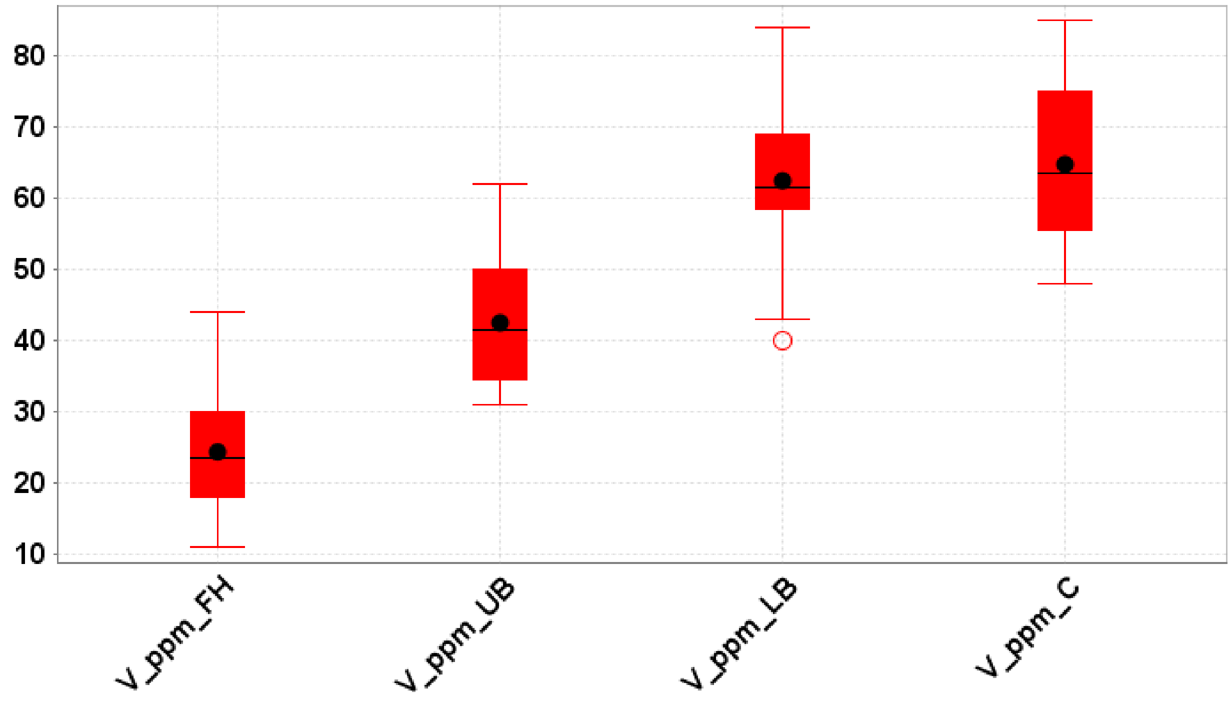

Figure: 3.2.4. Box plot showing the distribution of V in 16 soil samples from C, lower B, Upper B and F-H horizons analysed by aqua regia-ICPMS.

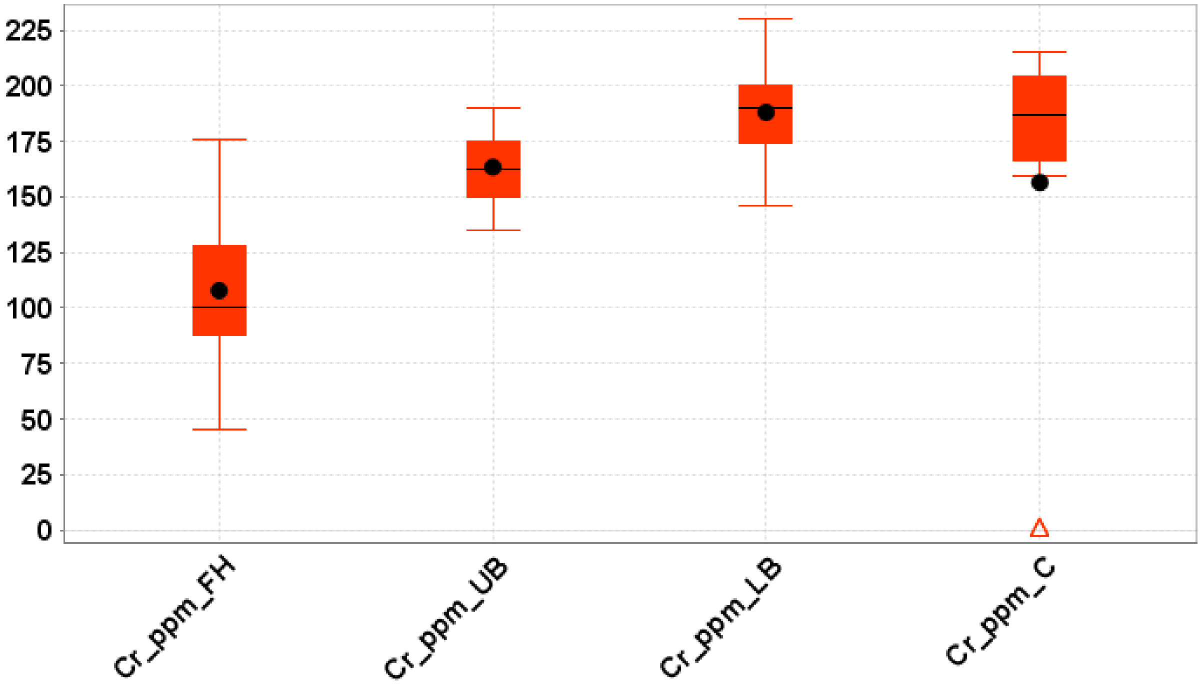

Figure: 3.2.5. Box plot showing the distribution of Cu in 16 soil samples from C, lower B, Upper B and F-H horizons analysed by INAA.

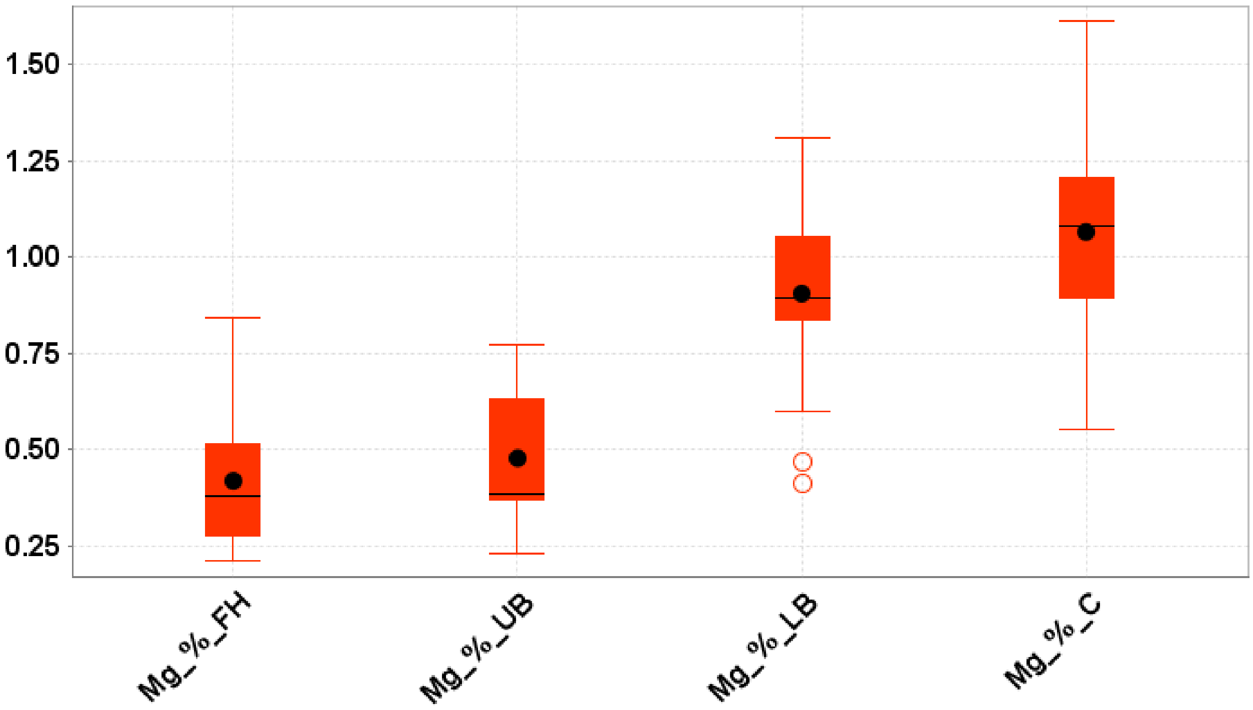

Figure: 3.2.6. Box plot showing the distribution of Mg in 16 soil samples from C, lower B, Upper B and F-H horizons analysed by aqua regia-ICPMS.

Figure 3.2.7 shows the results of the t-test applied to Au, Ag, Cu, Co, Cr, Hg, Fe, Mn, Mo, Ni, Pb, V, Zn data for the F-H horizon compared to element data for the upper B soil horizon; element data for the upper B compared to element data for the lower B soil horizon and element data for the lower B horizon compared to the element data for C soil horizon. There is no obvious pattern of a difference (at the 0.05 significance level) or a similarity between population means for the elements. There is a difference in the means for most of the elements in the FH soil horizon compared to the Upper B soil horizon. The is a difference between the means for Cu, Cr and Ni for the C soil horizon compared to the Lower B soil horizon could be explained by the anomalous chemistry of the till compared to the soil. The differences in the means for other elements in the horizons most likely reflect the chemistry of each element.

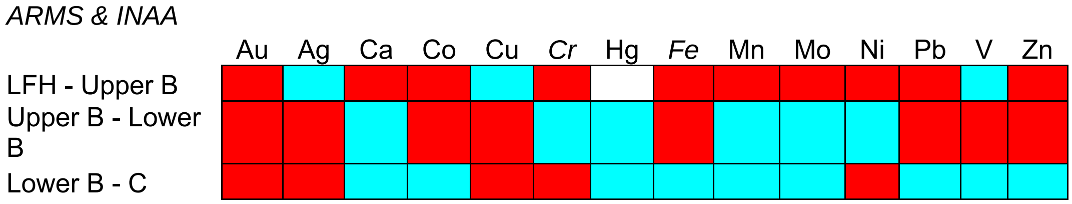

ARMS & INAA

	Au	Ag	Ca	Co	Cu	*Cr*	Hg	*Fe*	Mn	Mo	Ni	Pb	V	Zn
LFH - Upper B	🟥	🟦	🟥	🟥	🟦	🟥		🟥	🟥	🟥	🟥	🟥	🟦	🟥
Upper B - Lower B	🟥	🟥	🟦	🟥	🟥	🟦	🟦	🟥	🟦	🟦	🟦	🟥	🟥	🟥
Lower B - C	🟥	🟥	🟦	🟦	🟥	🟥	🟦	🟦	🟦	🟦	🟥	🟦	🟦	🟦

Figure 3.2.7: Summary of a t-test applied to establish if there is a difference at the 0.05% significances level for Au, Ag, Ca, Cu, Cr, Hg, Fe, Mn, Mo, Ni, Pb, V and Zn means in the F-H horizon compared to the upper B soil horizon, the upper B compared to lower B soil horizon and the lower B horizon compared to the C soil horizon by aqua regia_ICPMS and by INAA (INAA determined elements are in italics). A blank square indicates that there were insufficient values above detection limit for a test to be applied. Red square indicates a significant difference at the 0.05 significance level between the means.

Soil Sampling Results

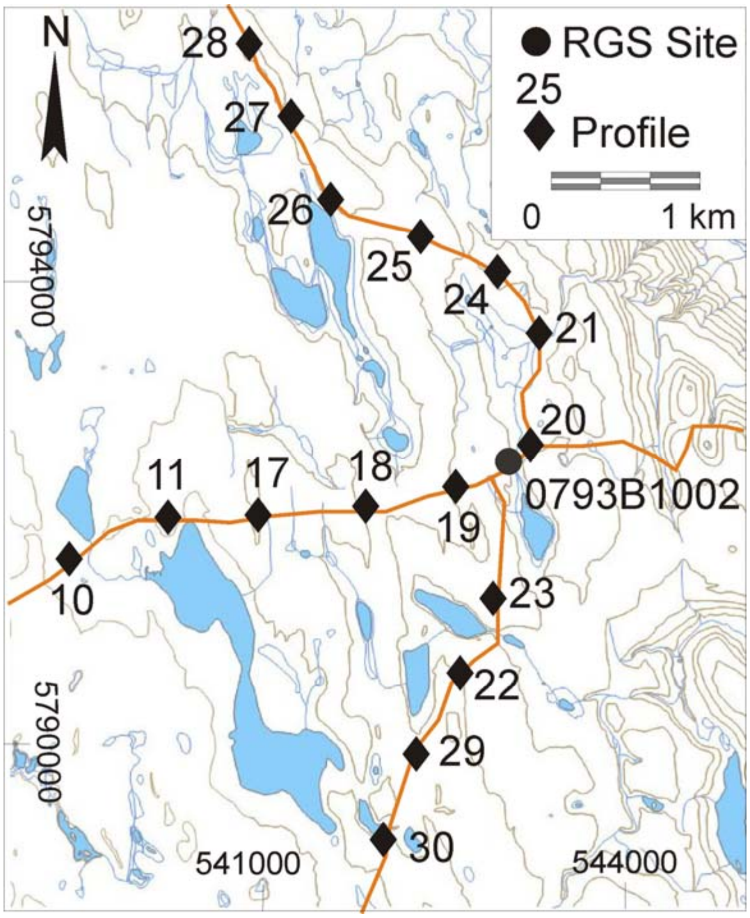

Figure 3.2.8: Soda Creek sample profile locations. Location map topography from MapPlace (BC Geological Survey, 2010).

Figure 3.2.8 shows the Soda Creek sample profile locations and the soil Cu geochemistry along the north-south and east west traverses is displayed in Figures 3.2.9 and 3.2.10.

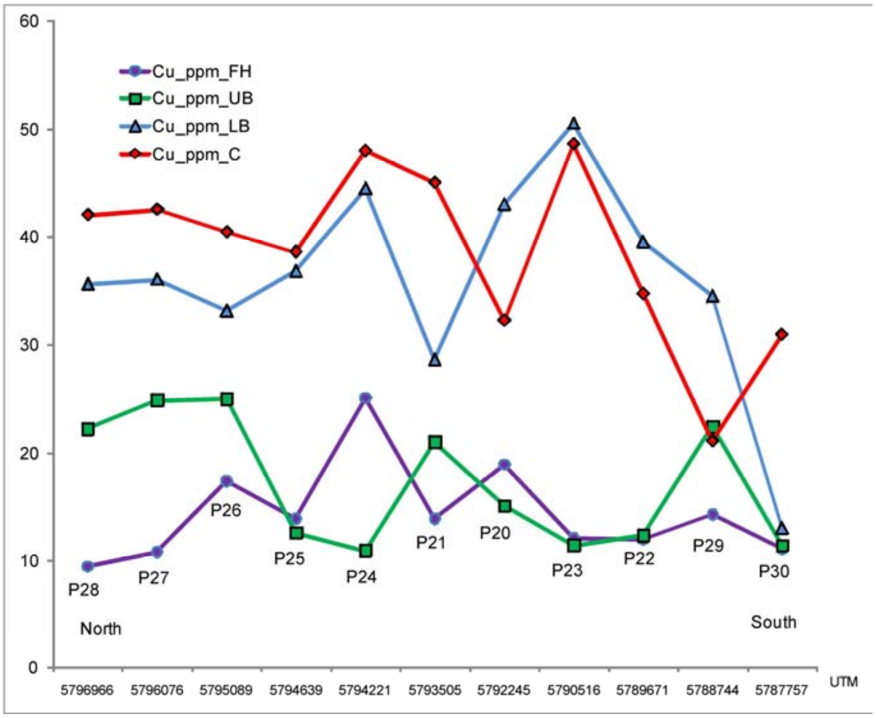

Figure: 3.2.9. Soda Creek north to south traverse Cu soil geochemistry.

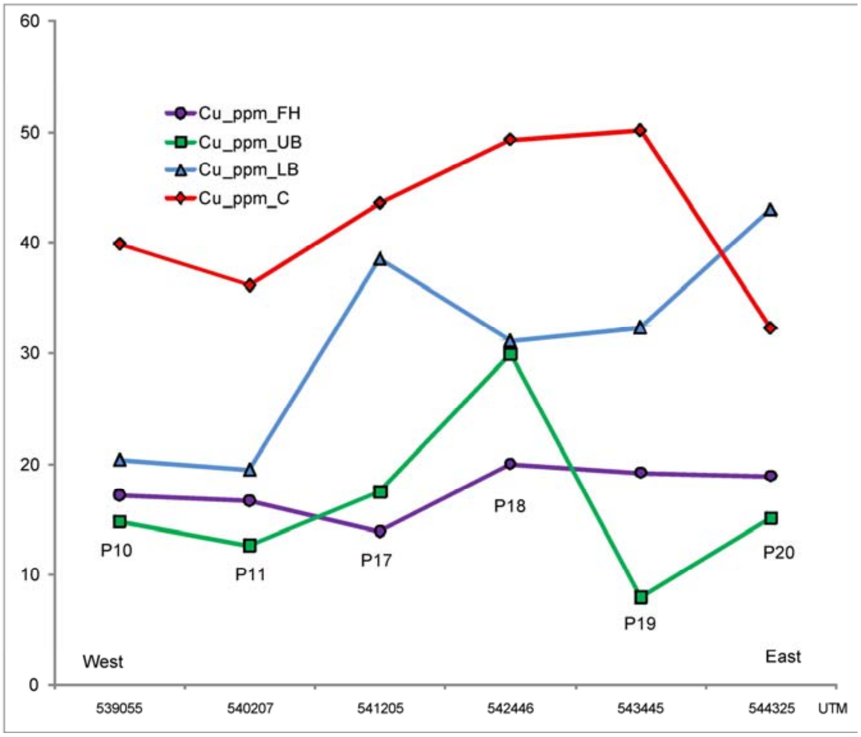

Figure: 3.2.10. Soda Creek west to east traverse Cu soil geochemistry.

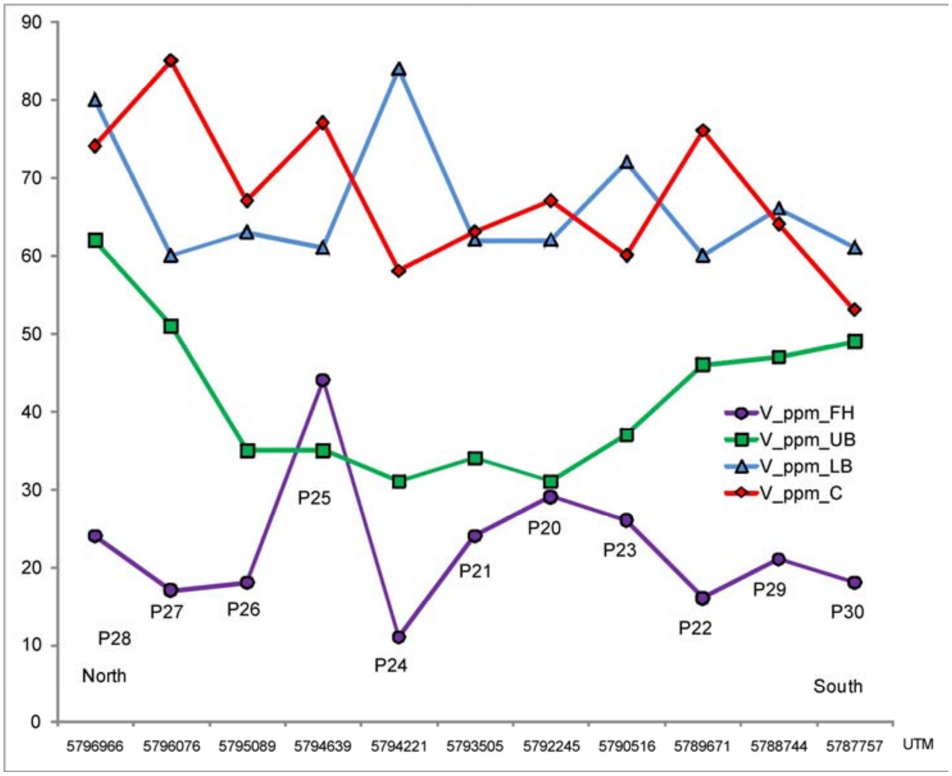

Figure: 3.2.11 Soda Creek north to south traverse V soil geochemistry.

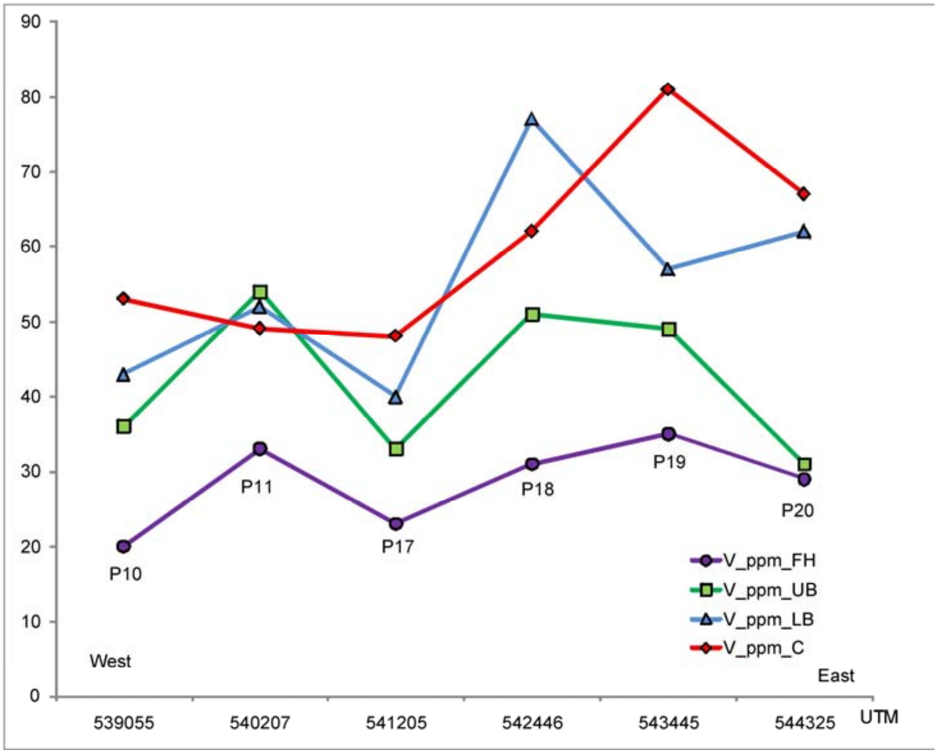

Figure: 3.2.12 Soda Creek west to east traverse V soil geochemistry.

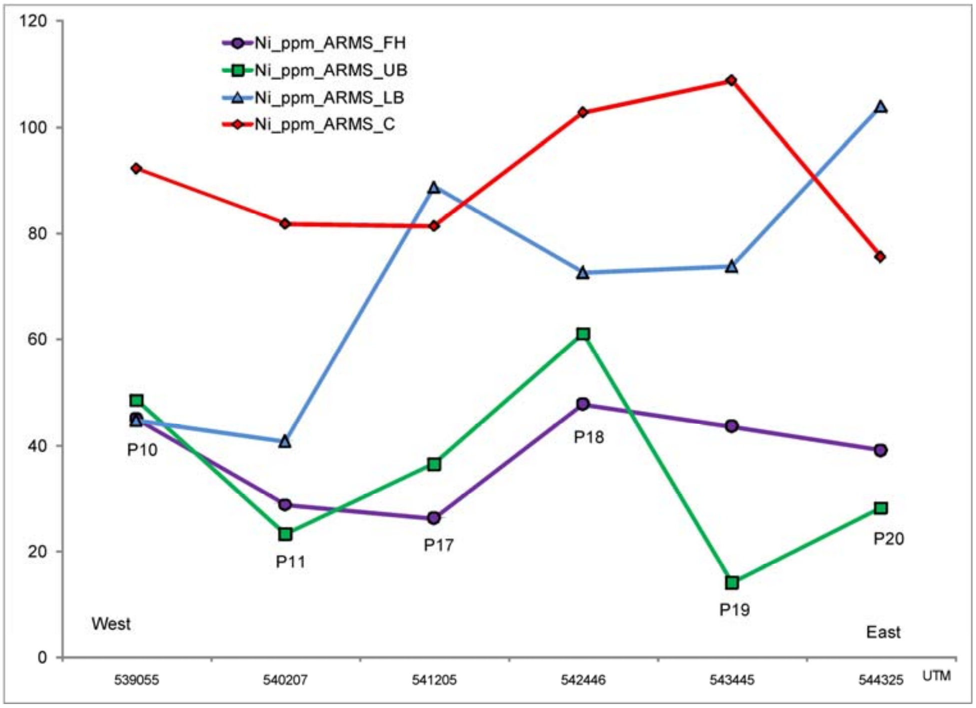

Figure: 3.2.13 Soda Creek west to east traverse Ni soil geochemistry.

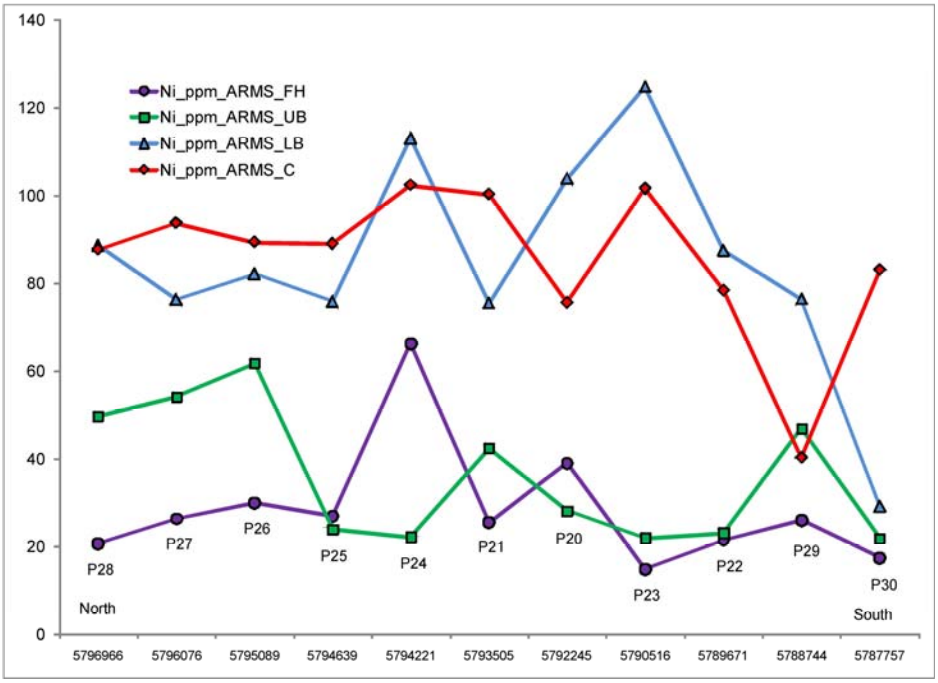

Figure: 3.2.14 Soda Creek north to south traverse Ni soil geochemistry.

Copper, Ni and V variations in the C soil horizon along the north to south traverse are similar to those in the Lower B soil horizon, but are visibly different from the Upper B and F-H horizon geochemistry (Figures 3.2.9 to 3.2.14). For example, concentrations of the elements are higher in the Lower B and C horizons compared to levels in the Upper B and F-H horizon. There are marked Cu and Ni peaks in the C and Lower B horizons at Profiles 23 and 24 with a corresponding F-H horizon at Profile 24. Vanadium levels in the C and Lower B horizons are similar although the north to south pattern is erratic and there are no obvious peaks. The V pattern in the Upper B horizon differs in that values decrease progressively from the north end of the traverse (Profile 28) to a minimum at Profile 20 and then increase to the south end of the traverse. There is a marked V peak in the F-H horizon at profile 25. Along the east-west traverse the C soil horizon Cu and Ni values, shown in Figures 3.2.9 and 3.2.13, increase from west to east to a peak at Profile 19 and the convex shape of pattern resembles a glacial dispersal geochemical profile in a till deposited by ice flowing from east to west. However, there is convincing evidence from surface features that ice flow is from south to north and the element patterns most likely reflect a variation of drumlin sediment geochemistry across the drumlin landform axis. Vanadium C soil horizon geochemistry is similar to Cu and Ni in that values rise to a peak at Profile 19, but the shape is concave rather than convex (Figure 3.2.11). Copper, Ni and V are lower in B and F-H horizons and the soil patterns are less reflective of those in the C horizon most likely due to redistribution of elements through soil forming processes

Cache Creek Group marine sedimentary and volcanic rocks could be concealed beneath the plateau basalt and these volcanics potentially can host VMS and vein-type Au mineralization. Variation of geochemical pathfinders for VMS and precious metal mineralization such as Au, Ag, Zn and Hg in soil may indicate mineralization. Figure 3.2.15 shows that variation of Au in soil from north to south is erratic and that there are isolated Au peaks in the B soil horizon. Highest Au concentration is 14 ppb in the soil and a single Au grain was isolated from a C horizon heavy mineral concentrate. This grain is described in the Overburden Drilling report as having a “reshaped” rather than “pristine” shape and this suggests a remote source for the Au with reworking of the grain during transport. Silver, in contrast to Au, shows a sharp, isolated F-H horizon peak at Profile 21 and minimum values in all horizons at Profile 24 (Figure 3.2.16). Highest Hg values are in the Upper B horizon at Profile 28 and the variation displayed an inverted “rabbit ear” pattern from north the south. There is very little Hg variation in the deeper mineral horizons (Figure 3.2.17). The most visible feature of the Zn geochemistry is a double peak in the F-H horizon unrelated to Zn variation in the underlying mineral soil horizons (Figure 3.2.18).

The trend of decreasing element concentrations towards a “low” in the middle of the north to south sample traverse is reflected in the soil pH pattern expressed as IDH (inverse hydrogen difference). Figure 3.2.19 shows calculated IDH values from Upper B soil pH, loss on ignition, BioLeach^{SM} I and Br. Lower IDH and LOI values correspond to higher BioLeach^{SM} I and Br and this pattern may reflect changes in soil bacteria activity. Secondary soil Ca has been suggested as a reflection of a reduced “chimney” above an oxidizing mineral sulphide body. Variation of Soil Ca by aqua regia digestion and MMI^{TM} leach along the north to south traverse in Figure 3.2.20 shows that the aqua regia extractable Ca and, to a lesser extent, IDH values, display a mid-traverse “low” at Profile 24, but the MMI^{TM} Ca displays a “high” over the same interval and values generally decrease with higher aqua regia-Ca.

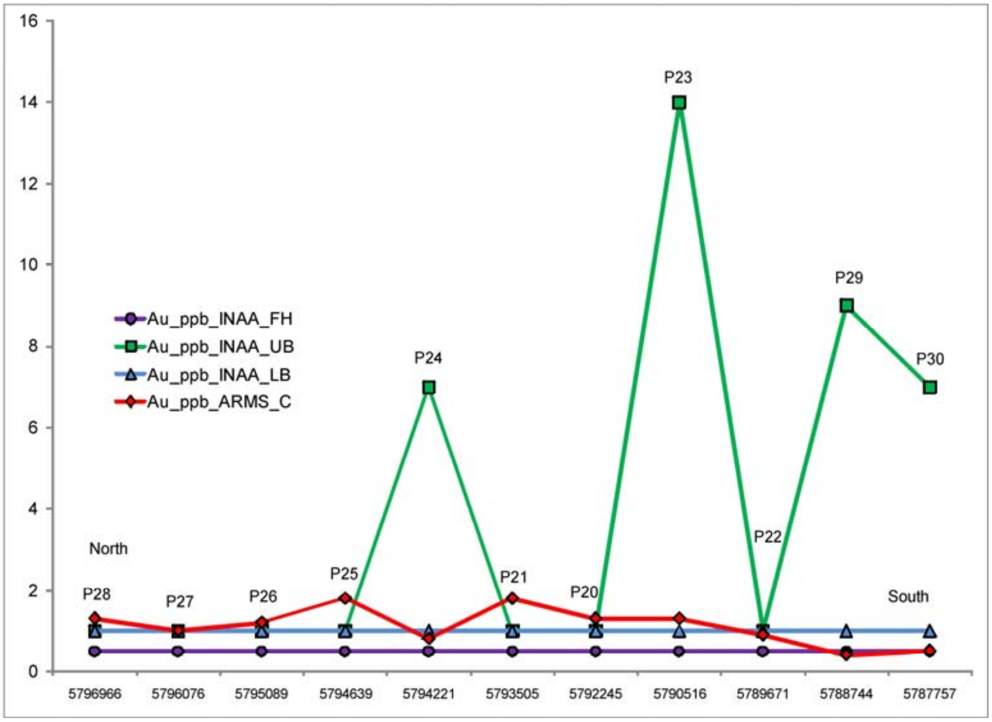

Figure: 3.2.15 Soda Creek north to south traverse Au soil geochemistry.

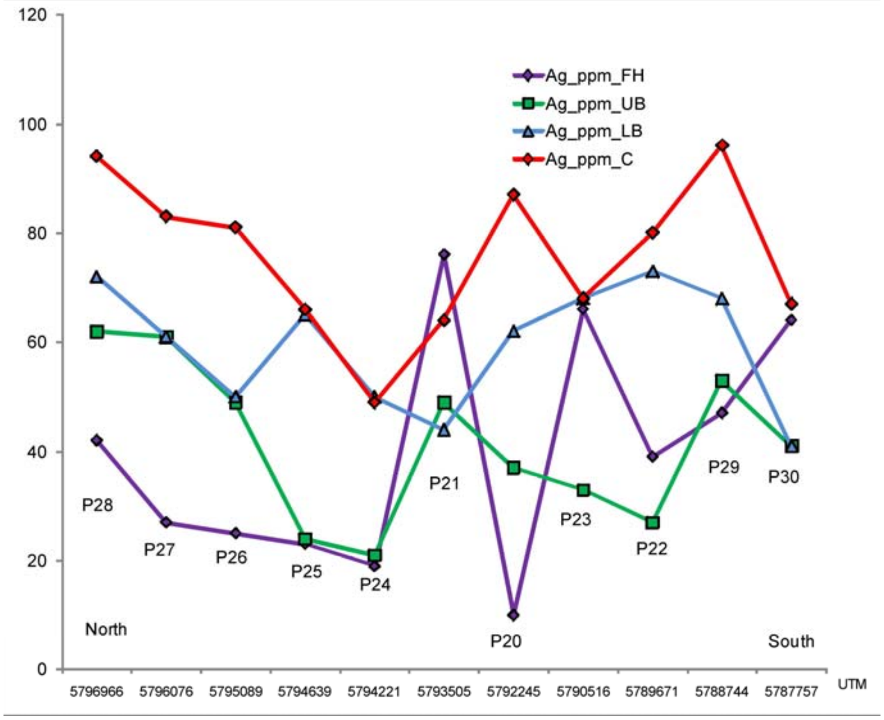

Figure: 3.2.16 Soda Creek north to south traverse Ag soil geochemistry.

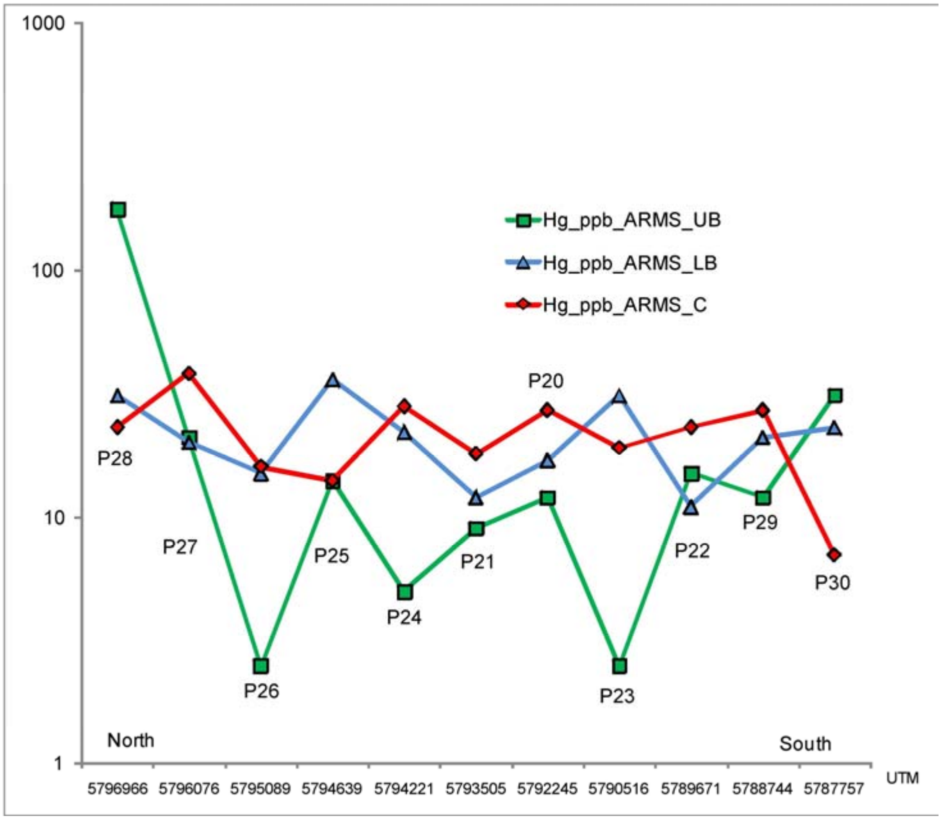

Figure: 3.2.17 Soda Creek north to south traverse Hg soil geochemistry.

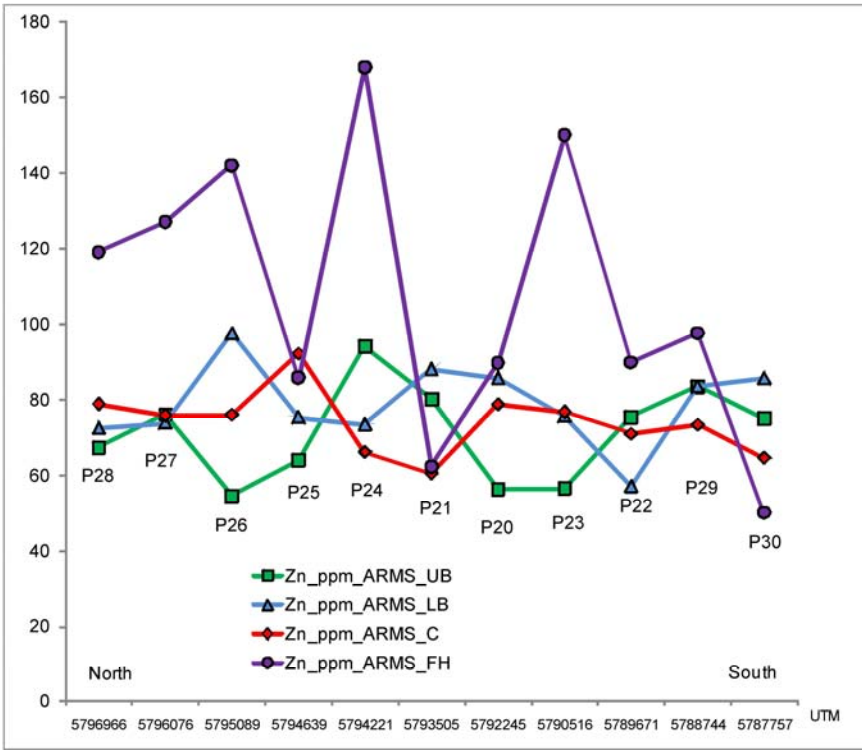

Figure: 3.2.18. Soda Creek north to south traverse Zn soil geochemistry.

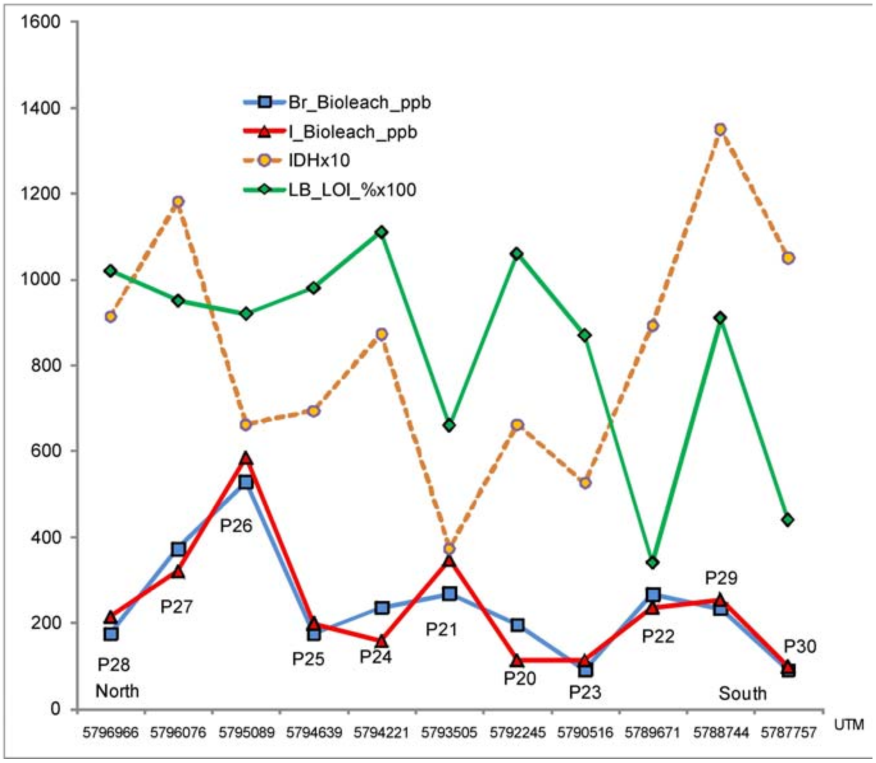

Figure: 3.2.19. Soda Creek north to south traverse B, I & LOI soil geochemistry.

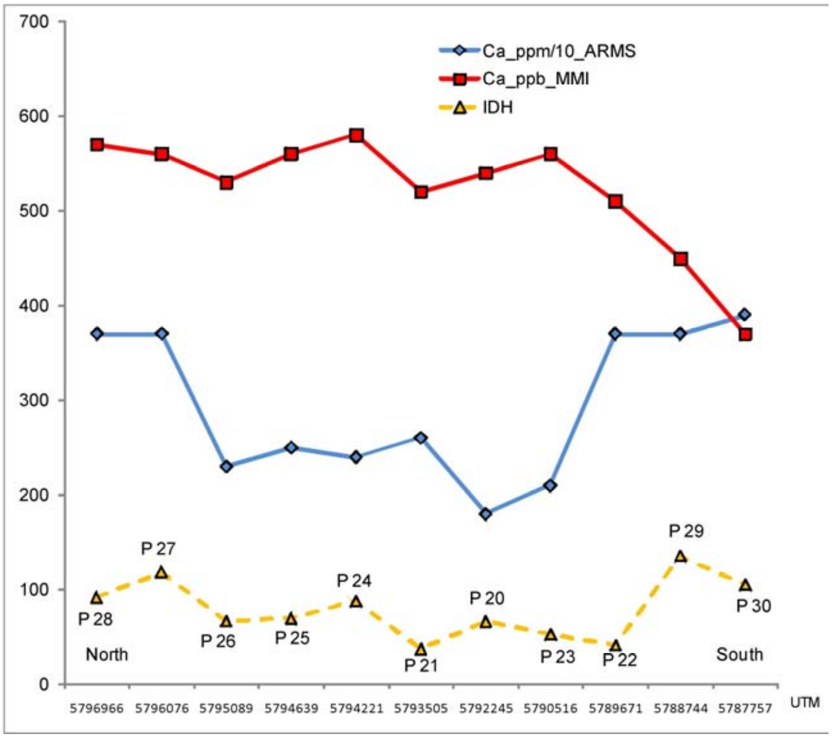

Figure: 3.2.20. Soda Creek north to south traverse Ca & IDH geochemistry.

There is a single Au peak on the east-west traverse with a value of 14 ppb in the lower B soil horizon at Profile P11 and no corresponding Au increase in the other horizons (Figure 3.2.21). A single Au grain, described in the Overburden Drilling report as being “reworked” was isolated from the C soil heavy mineral concentrate at Profile 18. Since this grain is reworked rather than “pristine” a distant rather than local source is suggested from the grain shape. Variation of Ag in Figure 3.2.22 along the east-west traverse is more complex. For example, there is a marked C horizon Ag “low” at Profile 17, an F-H horizon peak at the same Profile and a B soil horizon peaks at Profile 18. Mercury in Figure 3.2.23 also displays a peak at C horizon peak at Profile 18 and a “low” at Profile 17 in C and lower B horizons. Figure 3.2.24 shows that there is a subdued C and lower B horizon Zn peak at Profile 18 whereas upper B and F-H horizon Zn values increase from east to west reaching a maximum towards the west end of the traverse. In Figure 3.2.25 there are higher LOI, Bioleach Br and Bioleach I values in the Upper B soil at Profile 18 and the correlation between LOI with elevated Ag, Hg and Zn could be explained by enhancement of these elements in the increased soil humic content.

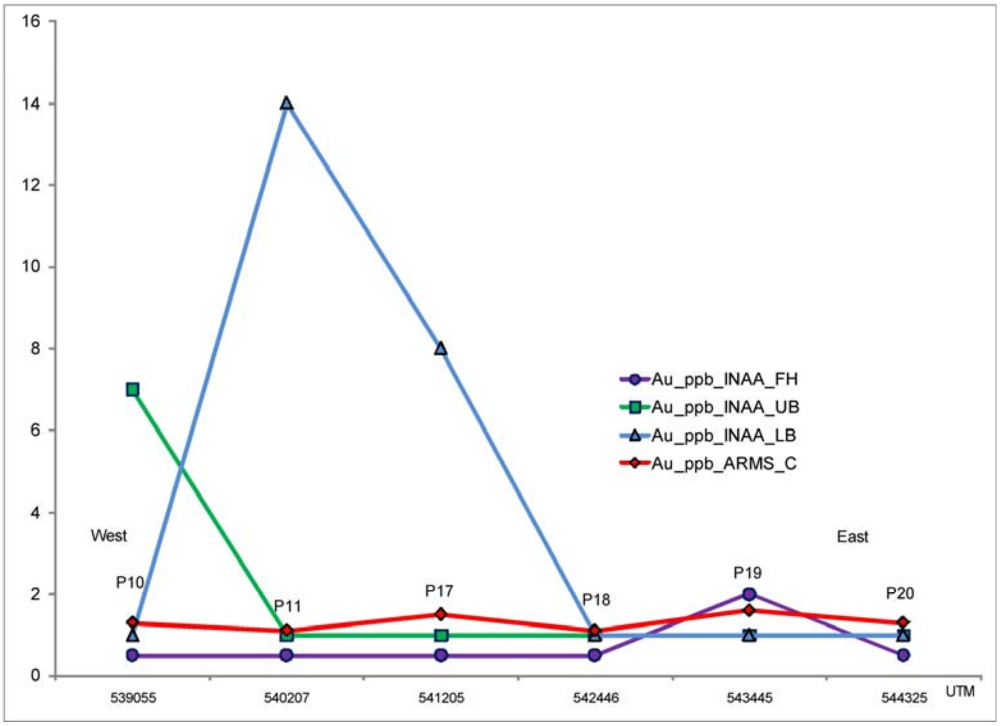

Figure3.2.21. Soda Creek west to east traverse Au soil geochemistry.

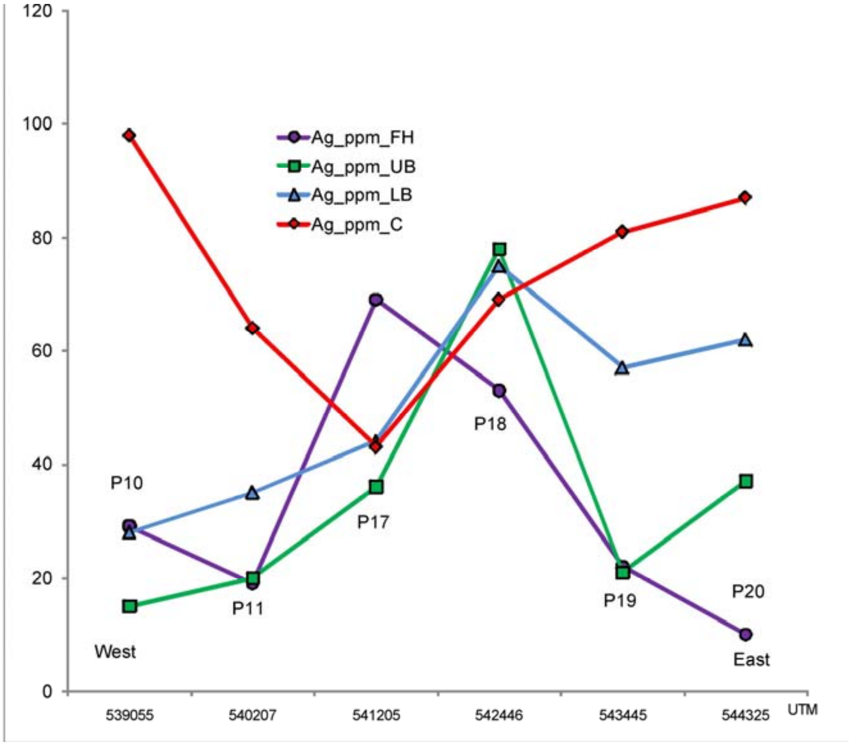

Figure3.2.22. Soda Creek west to east traverse Ag soil geochemistry.

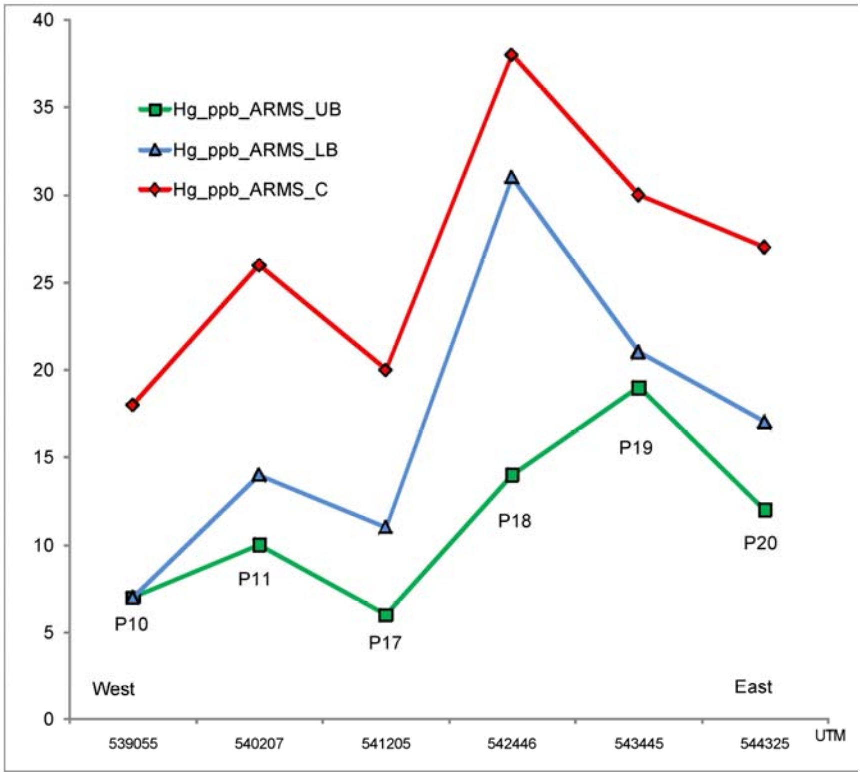

Figure: 3.2.23. Soda Creek west to east traverse Hg soil geochemistry.

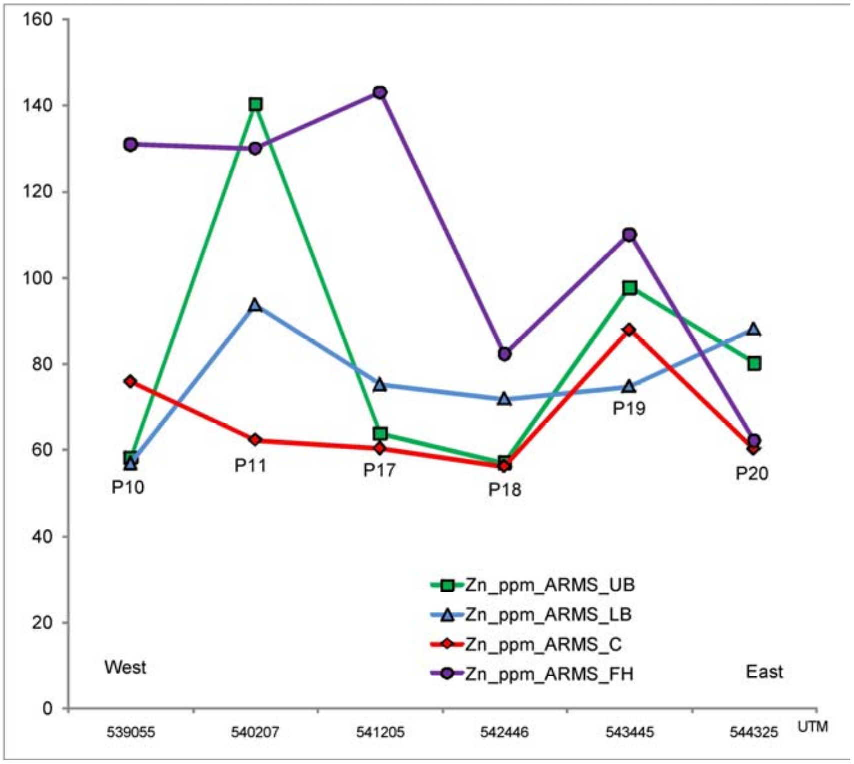

Figure: 3.2.24 Soda Creek west to east traverse Zn soil geochemistry.

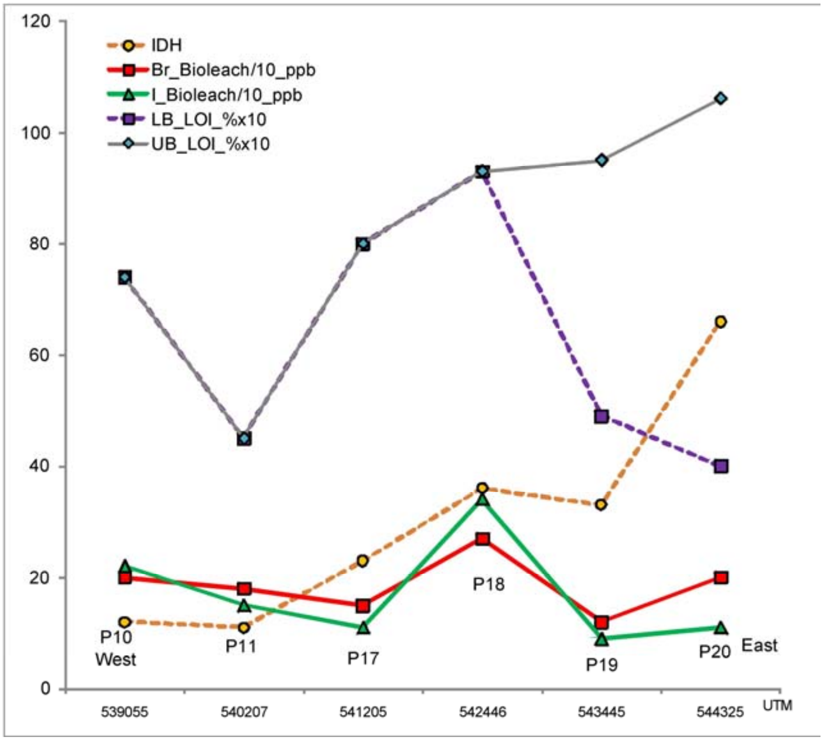

Figure: 3.2.25. Soda Creek west to east LOI & BioLeach^{SM} Br and I.

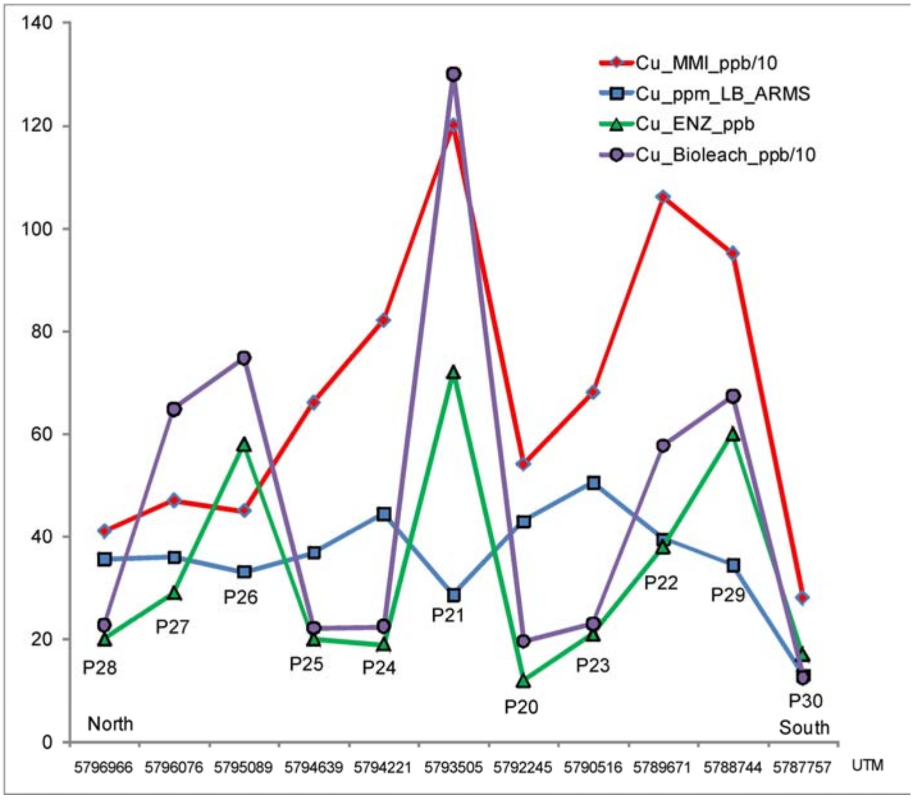

Figure: 3.2.26 Soda Creek north to south traverse Cu partial leach geochemistry.

Figure 3.2.26 shows partial leach Cu in the lower B soil horizon samples along the north-south traverse. Copper by aqua regia-ICPMS analysis is displayed by comparison to Cu by BioLeach^{SM}, MMI^{TM} and Enzyme Leach^{SM}. BioLeach^{SM} and MMI^{TM} Cu patterns are similar especially the sharp Cu peak by both methods at Profile 21, but there is no correlation between these methods and with aqua regia-ICPMS Cu. Nickel in Figure 3.2.27 is similar to the Cu variation with Bioleach^{SM} and Enzyme Leach^{SM} peaks at Profile 21 and 26. There is also very little correlation of partial leach Ni with aqua regia-ICPMS Ni values. However, unlike Cu, there is a marked Bioleach^{SM} Ni peak at profile 20. Figure 3.2.28 reveals only detectable Bioleach^{SM}, and MMI^{TM} Au in soil and that the while there is some correlation between the MMI^{TM} and aqua regia-ICPMS Au patterns as far as the peaks area are coincident the aqua regia-ICPMS Au contrast is much larger than that for MMI^{TM}. Patterns in Figure 3.2.29 also show that there is almost no relationship between MMI^{TM} Au and soil pH (IDH). In Figure 3.2.29 aqua regia-ICPMS Ca values decrease along the north to south traverse to a “low” at Profile 20 and there is a correlation to IDH. However there is no obvious correlation of MMI^{TM} Ca with IDH and with aqua regia Ca so it likely that the Ca patterns are a reflection of till chemistry rather than a near surface pattern caused by buried, weathering sulphides.

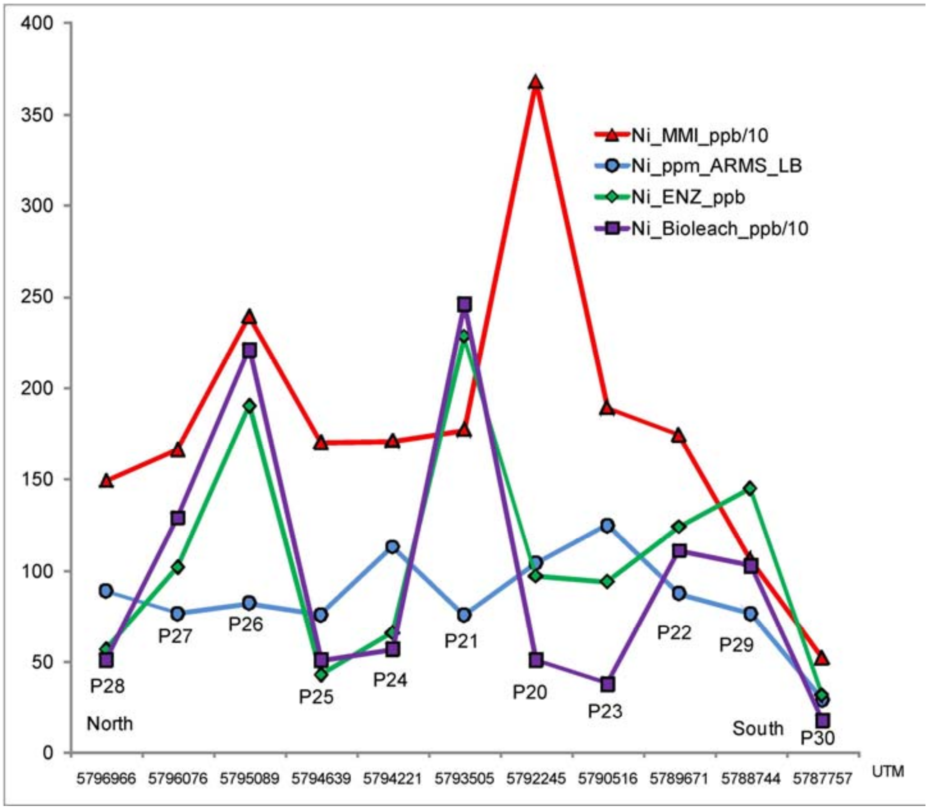

Figure: 3.2.27. Soda Creek north to south traverse Ni partial leach geochemistry.

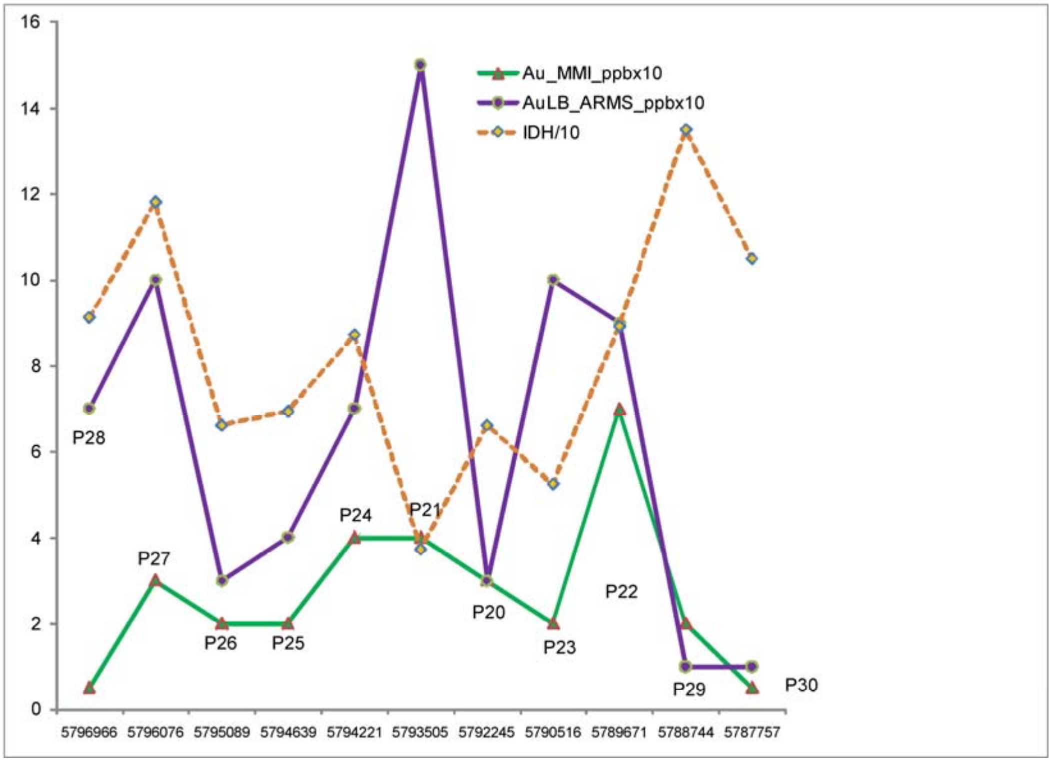

Figure: 3.2.28. Soda Creek north to south traverse Au partial leach geochemistry.

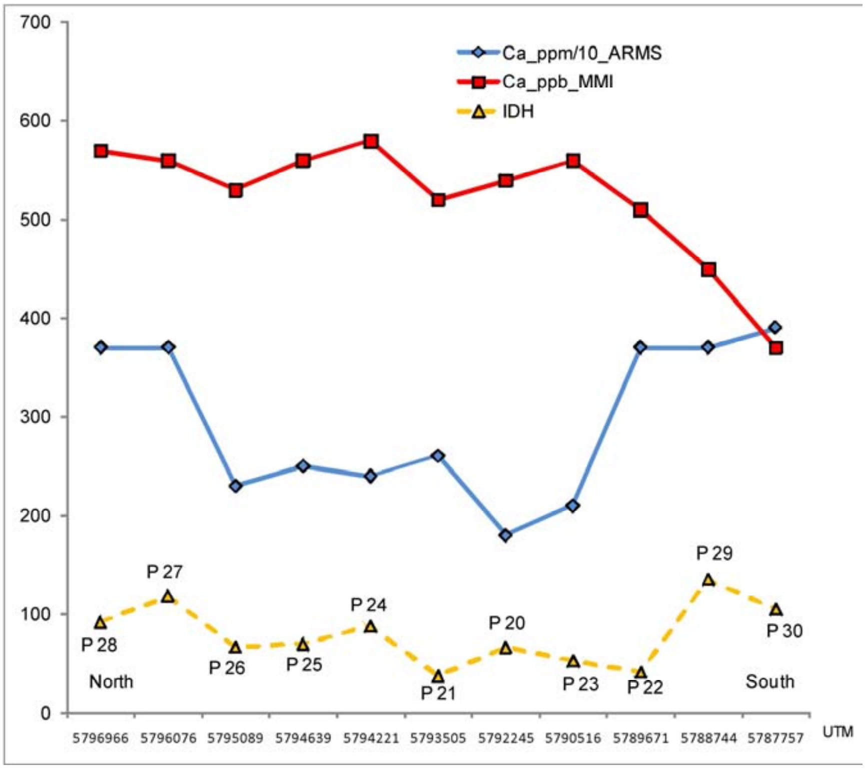

Figure: 3.2.29. Soda Creek north to south traverse Ca partial leach geochemistry.

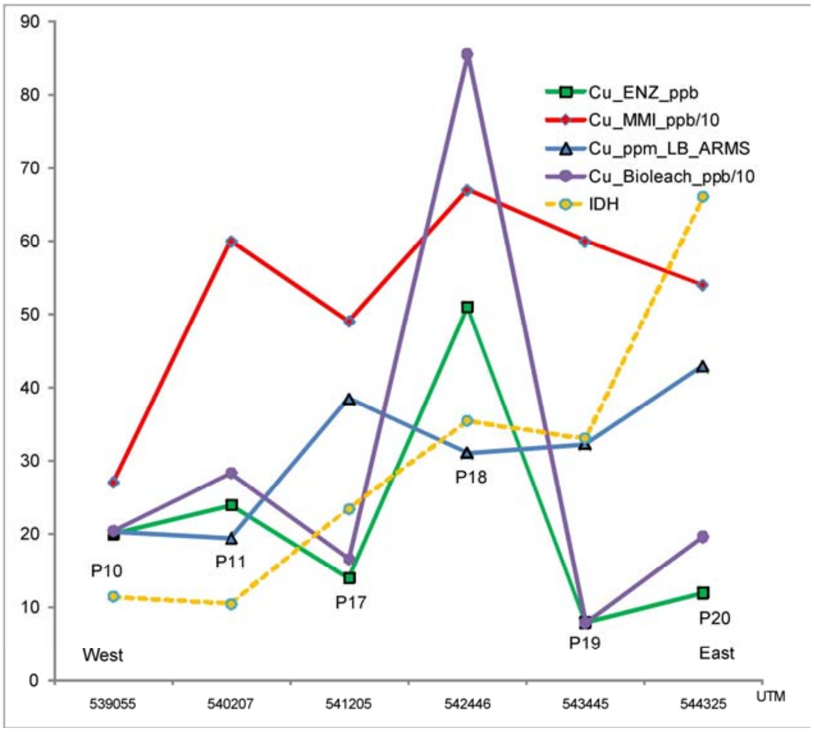

Figure: 3.2.30 Soda Creek west to east Cu partial leach geochemistry.

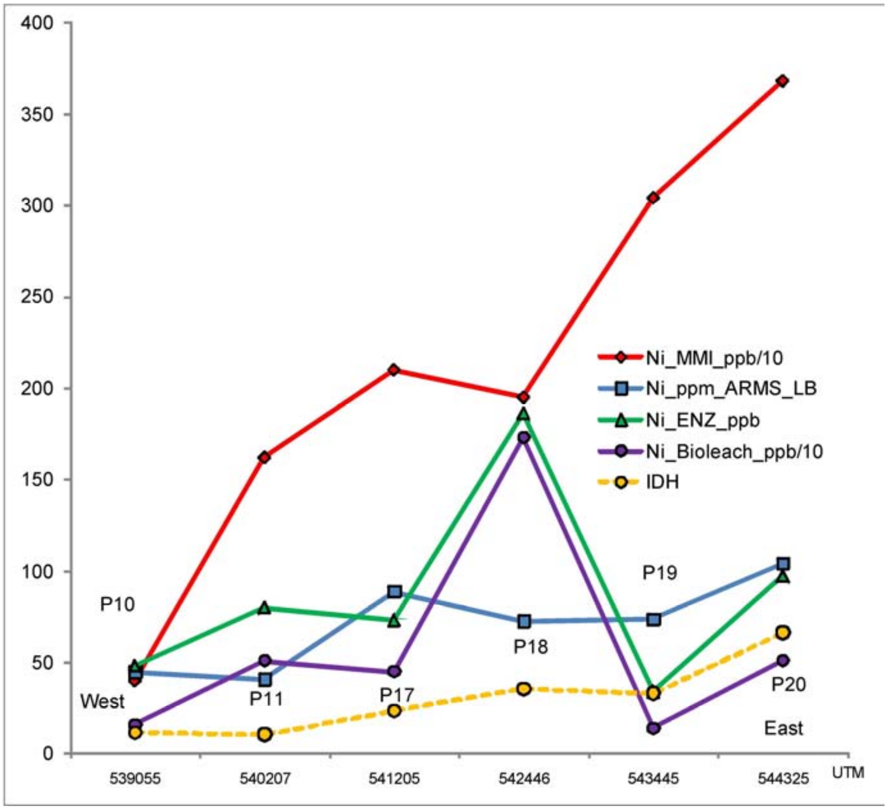

Figure: 3.2.31 Soda Creek west to east Ni partial leach geochemistry.

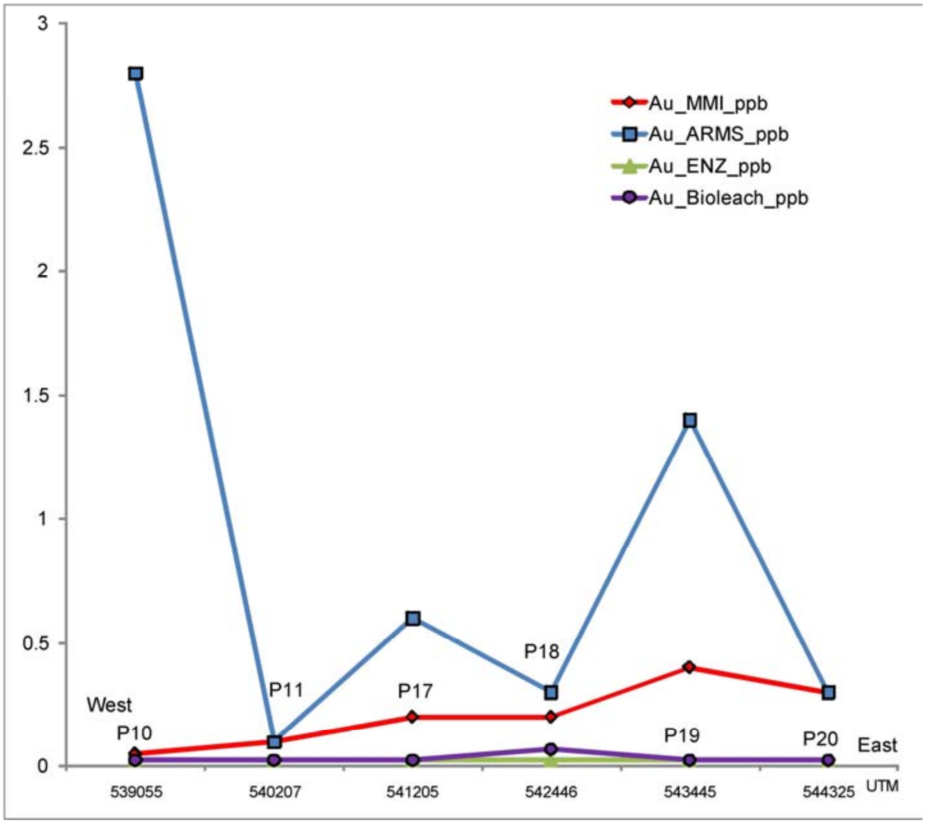

Figure: 3.2.32 Soda Creek west to east Au partial leach geochemistry.

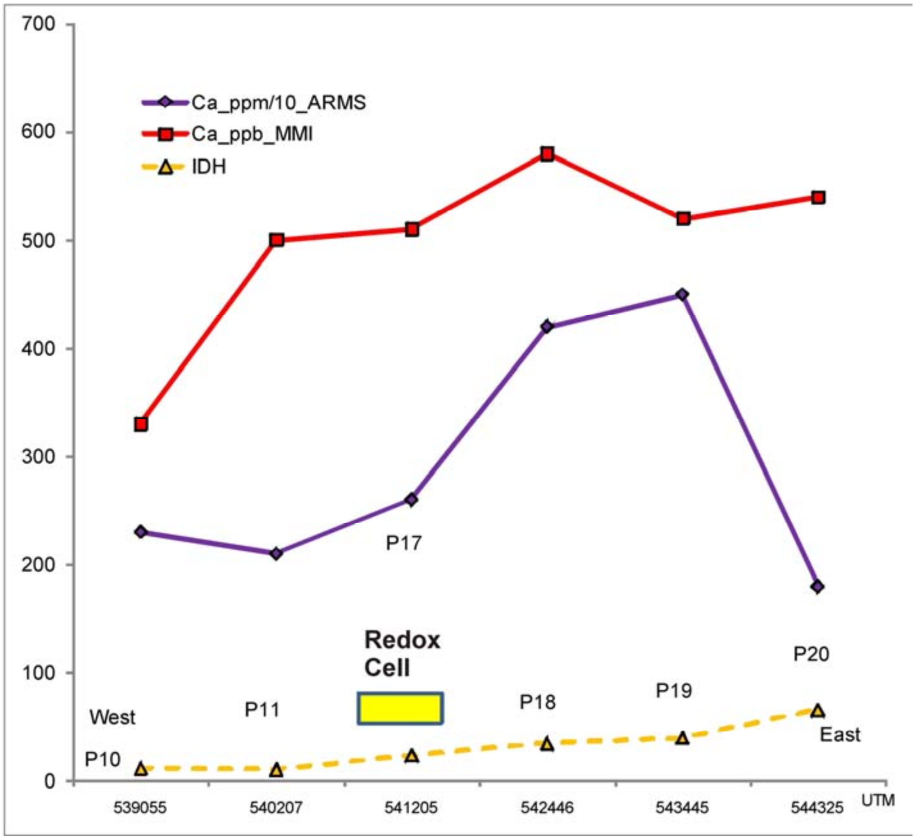

Figure: 3.2.33 Soda Creek west to east Ca, IDH and SGH^{SM}.

Along the east-west traverse there is a close association between BioLeach^{SM} and Enzyme Leach^{SM} Cu and between BioLeach^{SM} and Enzyme Leach^{SM} Ni especially a coincident peak at Profile 18, but very little correlation of these element patterns with MMI^{TM} extractable results (Figures 3.2.30 and 3.2 31). Partial leach Au (Figure 3.2.32) is similar to that displayed by patterns along the north-south traverse in that the aqua regia values show the largest contrast. In Figure 3.2.33 shows variation of aqua regia-ICPMS Ca, MMI^{SM} Ca and location of an SGH^{SM} apical anomaly along the west to east traverse. Sutherland and Hoffman, 2008 interpret the apical SGH^{SM} anomaly as evidence of a reduced "chimney" or redox cell at Profile 17. From a comparison of SGH^{SM} data from the Soda Creek west to east traverse with the SGH^{SM} soil geochemistry from existing Cu-Au deposits, Sutherland and Hoffman, (2008), rank the anomaly as 4 (on a scale of 1 to 6). While there are no obvious element or pH variations over the redox cell it is flanked to the east at Profile 18 by marked Ca by aqua regia-ICPMS and by Cu and Ni partial leach peaks. The soil geochemical patterns could therefore reflect one half of a twin peak (rabbit ear) anomaly induced by a subtle redox effect over buried sulphides in the bedrock beneath till and basalt.

Anomaly Definition

Table 3.6 lists threshold, range and contrast for selected elements by aqua-regia-ICPMS and partial leach methods in the Soda Creek samples.

Element	Range (min-max)	Peak Value	Background (median)	Threshold (3rd quartile)	Contrast
Au_AR_FH	*				
Au_AR_UB	*				
Au_AR_LB	0.2 – 2.8 ppb	2.1 ppb	0.7 ppb	0.8 ppb	2.7
Au_AR_C	0.2 – 1.8 ppb	1.7 ppb	1.3 ppb	1.4 ppb	1.2
Au_MMI	0.05 – 0.7 ppb	0.6 ppb	0.2 ppb	0.3 ppb	2.0
Au_BioLeach	0.05 – 0.07 ppb	0.07 ppb	0.03 ppb	0.03 ppb	2.1
Ag_AR_FH	10 – 76 ppb	73 ppb	34 ppb	56 ppb	1.3
Ag_AR_UB	15 – 78 ppb	70 ppb	34 ppb	76 ppb	1.0
Ag_AR_LB	28 – 75 ppb	73 ppb	55 ppb	68 ppb	1.1
Ag_AR_C	43– 98 ppb	97 ppb	75 ppb	84 ppb	1.2
Ag_MMI	4 - 29 ppb	26 ppb	16 ppb	18 ppb	1.4
Ag_BioLeach	0.1 – 0.6	-	-	-	-
Cu_AR_FH	9.5 – 25.1 ppm	22.2 ppm	14.1 ppm	17.8 ppm	1.6
Cu_AR_UB	8 – 29 ppm	27 ppm	15 ppm	22.3 ppm	1.8
Cu _AR_LB	13 – 50.5 ppm	47.5 ppm	35.1 ppm	38.8 ppm	1.4
Cu_AR_C	21.1 – 50.2 ppm	49.7 ppm	41.2 ppm	45.7 ppm	1.0
Cu_MMI	270 – 1200 ppb	1125 ppb	600 ppb	620 ppb	1.9
Cu_BioLeach	79 – 1300 ppb	1100 ppb	257 ppb	692 ppb	4.2
Ni_AR_FH	14.9 – 66.3 ppm	57.1 ppm	26.7 ppm	47.2 ppm	2.1
Ni_AR_UB	14.1 – 61.8 ppm	61.5 ppm	32.4 ppm	48.8 ppm	1.9
Ni _AR_LB	29.2 – 124.8 ppm	114.3 ppm	76.4 ppm	88.7 ppm	1.5
Ni_AR_C	40.3 – 108.7 ppm	105.7 ppm	89.3 ppm	103.7 ppm	1.2
Ni_MMI	402 – 3680 ppb	3360 ppm	1740 ppb	1950 ppb	1.9
Ni_BioLeach	135 – 2460 ppb	2335 ppm	539 ppb	1035 ppb	4.3
V_AR_FH	11 – 44 ppm	40 ppm	24 ppm	30 ppm	1.6
V_AR_UB	31 – 62 ppm	58 ppm	42 ppb	50 ppm	1.4
V _AR_LB	40 – 84 ppm	82 ppm	62 ppb	68 ppm	1.3
V_AR_C	48 – 85 ppm	83 ppm	64 ppb	75 ppm	1.3
V_MMI	-	-	-	-	-
V_BioLeach	143 – 2340 ppb	2325 ppb	682 ppb	1573 ppb	1.5
Br_BioLeach_UB	76 – 528 ppb	450 ppb	195 ppb	266 ppb	2.3
Br_BioLeach_LB	143 – 448 ppb	436 ppb	424 ppb	446 ppb	1.0
I_BioLeach_UB	90 – 584 ppb	465 ppb	198 ppb	253 ppb	2.3
I_BioLeach_LB	173 – 1130 ppb	1120 ppb	1110 ppb	1120 ppb	1.0

Table 3.6: Anomaly contrast for Au, Ag, Cu, Ni and V in FH, Upper B, Lower B and C soil horizon samples calculated from the Soda Creek west to east and north to south traverse combined data. Bromine bioleach and I bioleach contrast is also listed in Table 3.3. The peak value is calculated from the average of the two highest values and values below detection limit are set and 0.5 detection limit. Values shown as "-" in Table 3.6 indicate there were insufficient determinations above detection limit to calculate a statistic.

3.3 Alexandria

Location: NTS – 93B 09 LATITUDE. 52°40'00" UTM NORTH – 5835000
LONGITUDE. - 122°35'00" UTM EAST – 539000

MINFILE Status: *None* **Commodities:** *None*

Mineral Deposit Profile: *None*

Significant and Associated Minerals*: None*

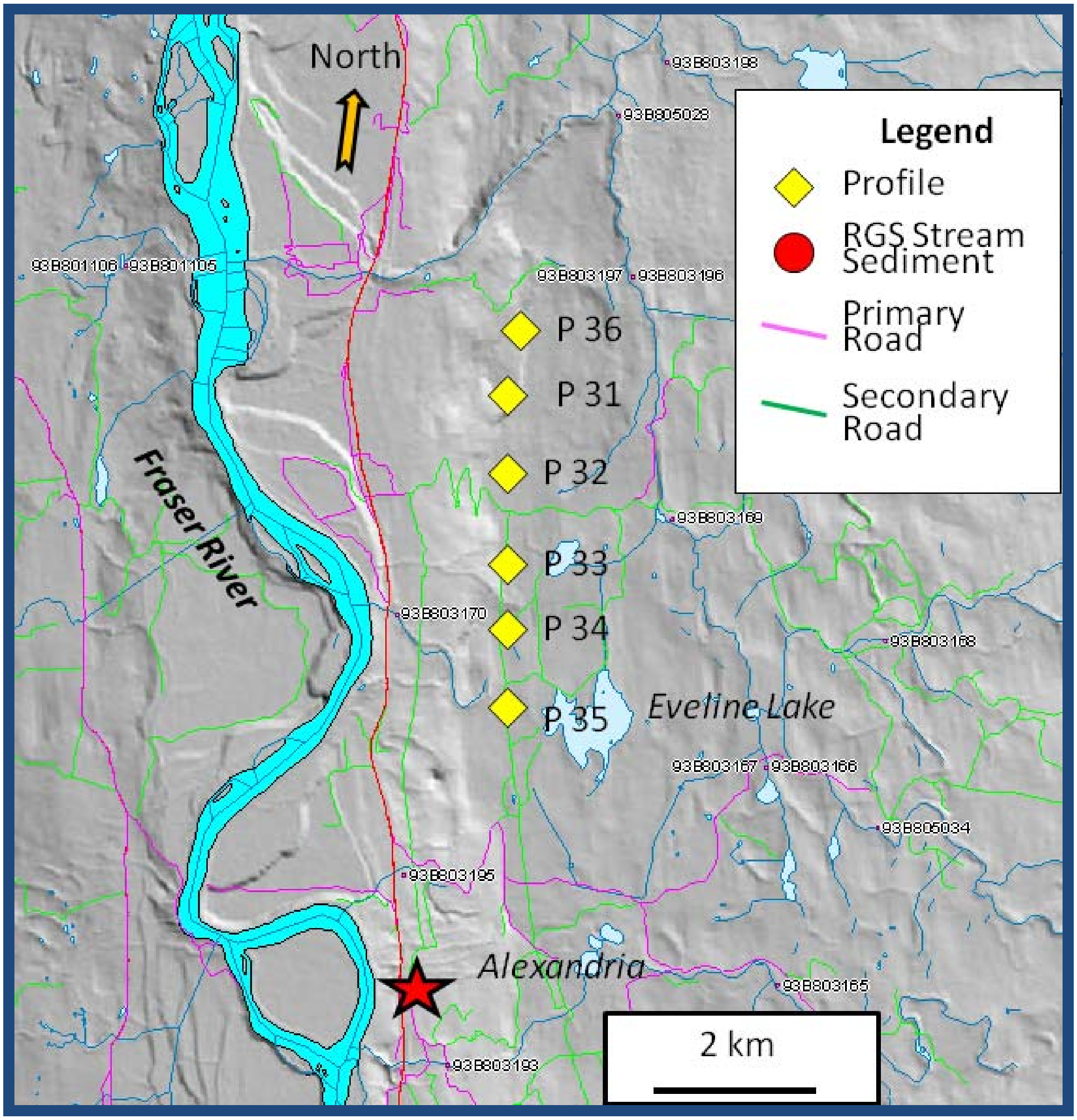

Figure: 3.3.1 Alexandria area profile locations. Base map digital elevation model image captured from Map Place (BC Geological Survey, 2010).

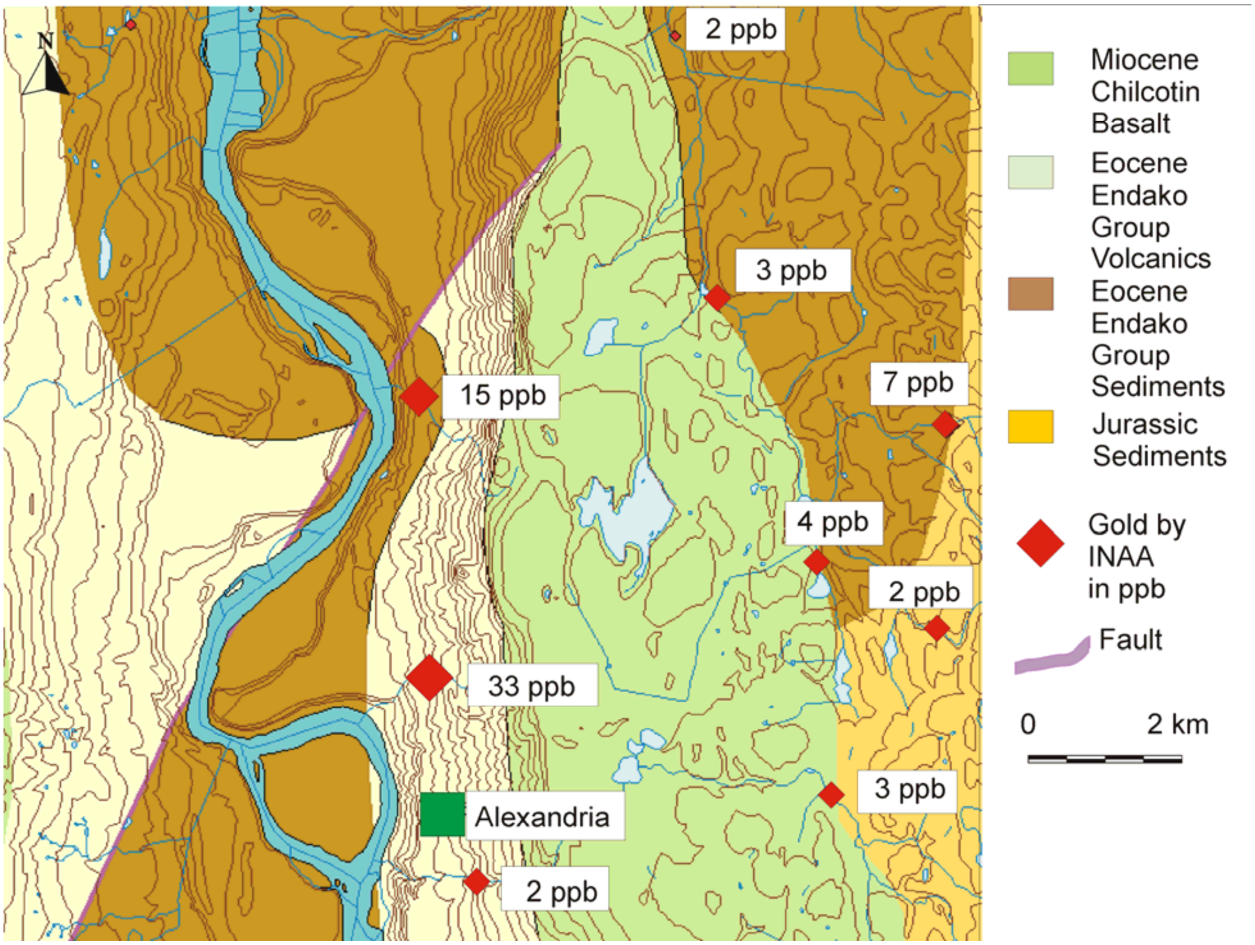

Figure: 3.3.2 Alexandria area geology from Massey et al. 2005.

Geology: Soil samples, collected from six profiles along a power line right of way north of Alexandria, are from an area that is underlain by Tertiary rocks. The sampling aimed to detect any surface geochemical expression over a north east trending fault identified on the digital geology map by Massey *et al.*, (2005); to interpret a stream sediment Au anomaly in Windt Creek and to compare background soil geochemistry with that established for the Soda Creek area. Rouse and Mathews, (1979), recognised five Tertiary rock units from mapping along the Fraser River valley between Quesnel and the Marguerite Ferry. In the survey area along the eastern scarp of the Fraser River valley the two bedrock units are the Middle to Late Miocene Crownite Formation and Late Miocene Plateau Basalts. The Crownite Formation consists of up to 12 metres of massive, almost pure diatomite with minor clay layers. Above the diatomite are up to 80 metres of vesicular, columnar basalt. The Tertiary rocks conceal the contact between Lower to Mid Jurassic Nicola Group sediments east of the Fraser River and Cache Creek Group sediments to the west. A glacial deposit of consisting of sandy loose sediment covering the basalt is most likely reworked till.

Alteration and Mineralization: No metallic mineral occurrences have been reported in the area but Crownite Formation diatomite has been mined economically in an open pit south west of Quesnel.

Local Environment: The eastern scarp of the Fraser River valley in the Alexandria area is at an elevation of 780 and 800 metres. East of the scarp the land surface slopes gently into an extensive marshy plateau where there are numerous lakes and poorly defined marshy stream channels. Drainage is predominantly to the east although a few, short streams have breached the escarpment and flow west into the Fraser River. Predominantly bruisolic soils have developed on a sandy textured diamicton and there are organic soils in wetland areas with a mainly white spruce and lodgepole pine vegetation. Although the sample profiles were located in a relatively undisturbed, forested area along the escarpment there may be some contamination from power line maintenance. Figure 3.3.1 shows the profile sites, location of the Alexandria community, the Fraser River, and the power line right of way. Figure 3.3.2 shows bedrock geology and location of two regional stream sediment sample sites with the Au content detected by analysis of the sediment.

Alexandria Geochemistry

Lithogeochemistry

No rock samples were collected for analysis and there is no previously published lithogeochemical data.

Drainage geochemistry

Sample ID	93B803170	93B803195	95th Percentile for NTS 93B
Latitude	52.68041	52.64885	
Longitude	-122.44937	-122.45043	
Elevation_m	540	560	
Water pH	7.9	8.2	
U_water_ppb	0.16	2	
F_water_ppb	140	160	
Zn_AAS_ppm	36	32	86
Cu_AAS_ppm	15	15	44
Pb_AAS_ppm	1	1	4
Ni_AAS_ppm	20	18	71
Co_AAS_ppm	10	8	18
Ag_AAS_ppm	0.1	0.1	0.1
Mn_AAS_ppm	300	270	2900
Fe_AAS_%	1.2	1.5	4
Mo_AAS_ppm	1	1	2
U_NADNC_ppm	1.5	1	5.5
W_COL_ppm	1	1	
Hg_AASF_ppb	60	20	120
Au_NA_ppb	15	33	9
As_NA_ppm	2	3	1
Ba_NA_ppm	460	530	
Cr_NA_ppm	120	190	
Co_NA_ppm	14	15	
Ni_NA_ppm	36	43	
Zr_NA_ppm	300	400	

Table 3.7 Geochemistry of 1980 and 2007 regional survey samples from Coyote Creek compared to a regional thresholds at the 95th percentile for NTS 93B.

Only Au is anomalous in two alkaline streams draining west from the escarpment into the Fraser River.

Alexandria soil geochemistry

Element Associations

A correlation matrix determined using the soil horizon data can give rather misleading indications of soil geochemical associations because only samples from six profiles in the Alexandria area were analysed. In the C, lower B and Upper B horizons there is an association between Cu-Ni-Co-Ca-Cr-Mg-Fe-Sc although As and Hg are also part of the signature in the C horizon and LOI is also included in the Lower and Upper B horizons. The high, positive correlation coefficients can be explained by one profile where all of the elements are elevated in the mineral soil. A Ni-Co-Cr-Fe-Sc signature is also revealed in the FH horizon correlation matrix, but there are also positive relationships between Zn and Cu, Mo and Ag and negative relationships between Cu and Pb and with Cu and Te.

Soil Horizon Geochemical Comparisons

Element mean, median, quartile and range for the Alexandria area soils show that only Cu, Ni and are anomalous. None of the samples have any detectable Au or other pathfinders such as As and Hg.

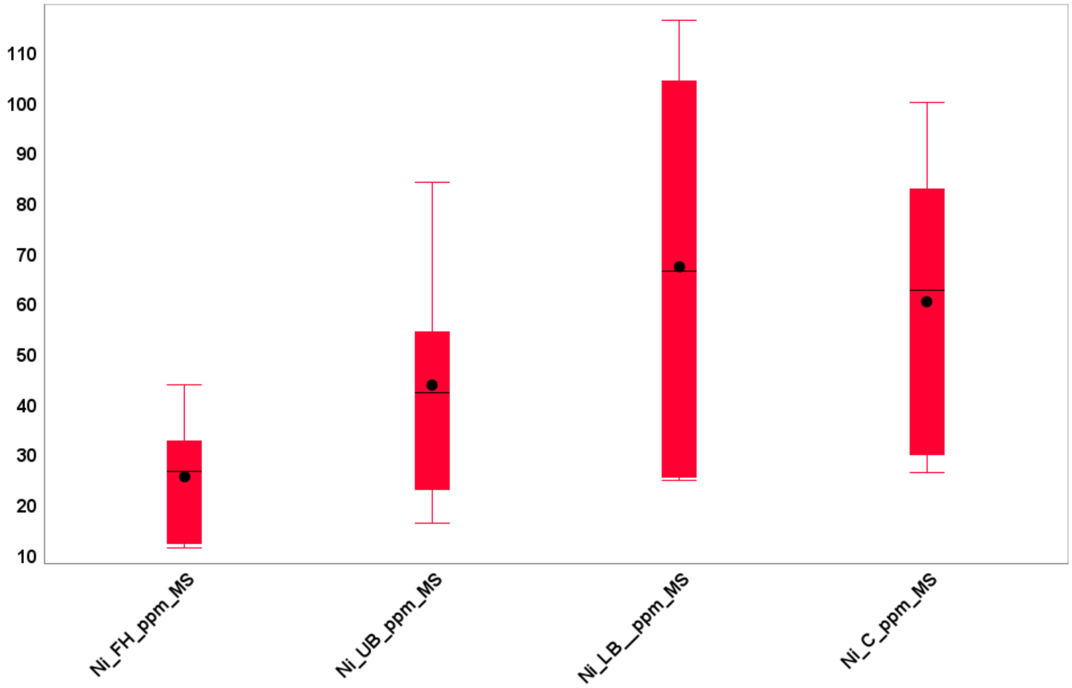

Figure: 3.3.3. Box plot for Ni by aqua regia-ICPMS in 6 soil samples from the C, lower B, Upper B and F-H horizons.

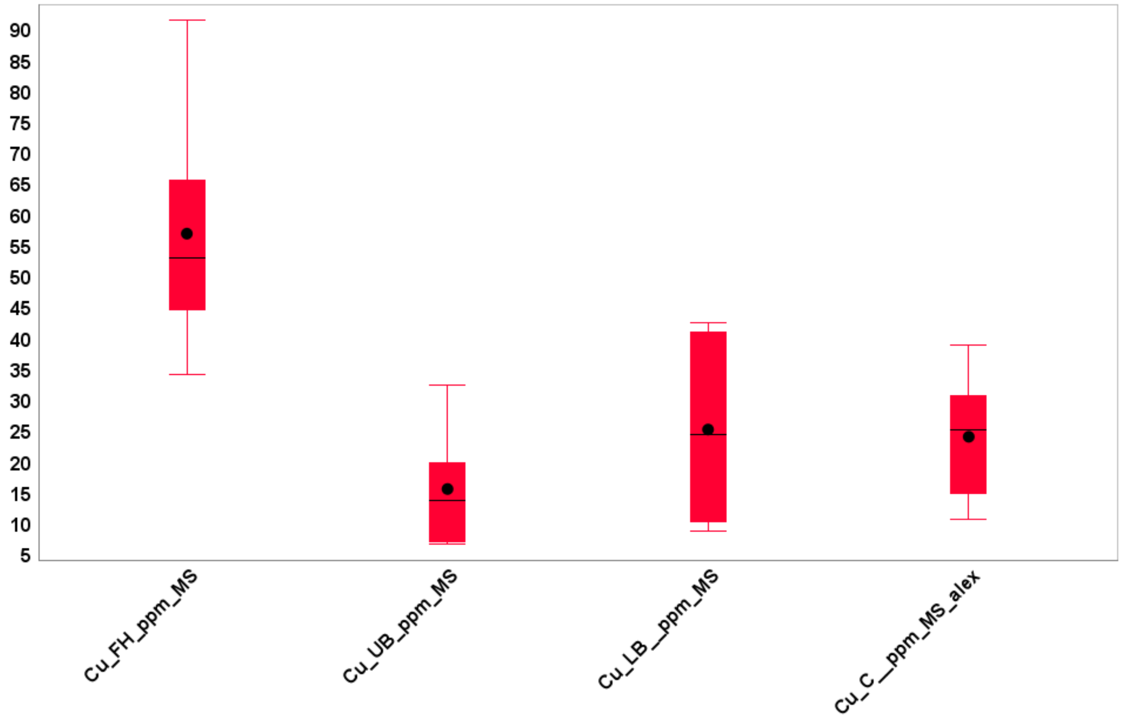

Figure: 3.3.4. Box plot for Cu aqua regia-ICPMS in 6 soil samples from the C, lower B, Upper B and F-H horizons.

Figure 3.3.3 shows that the Ni in the soil increases from the F-H to the C horizon and that the highest Ni values (up to 120 ppm) are in the lower B soil horizon. However, variation of Cu, in Figure 3.3.4, indicates that Cu is higher in the F-H horizon compared to levels in the B and C horizons. Vanadium variation in Figure 3.3.5 resembles Ni suggesting that the soil chemistry for both elements is influenced by the parent glacial sediment. A t-test applied to determine if there is a difference at the 0.05 confidence level between C soil horizon means of Cu, Ni and V for the Soda Creek C soil horizon samples (16) compared to the Alexandria samples (6) reveals that there is no difference for Ni and V but there is a significant difference for Cu. This could suggest a similar source for the C horizon Ni and Ni chemistry in the two areas.

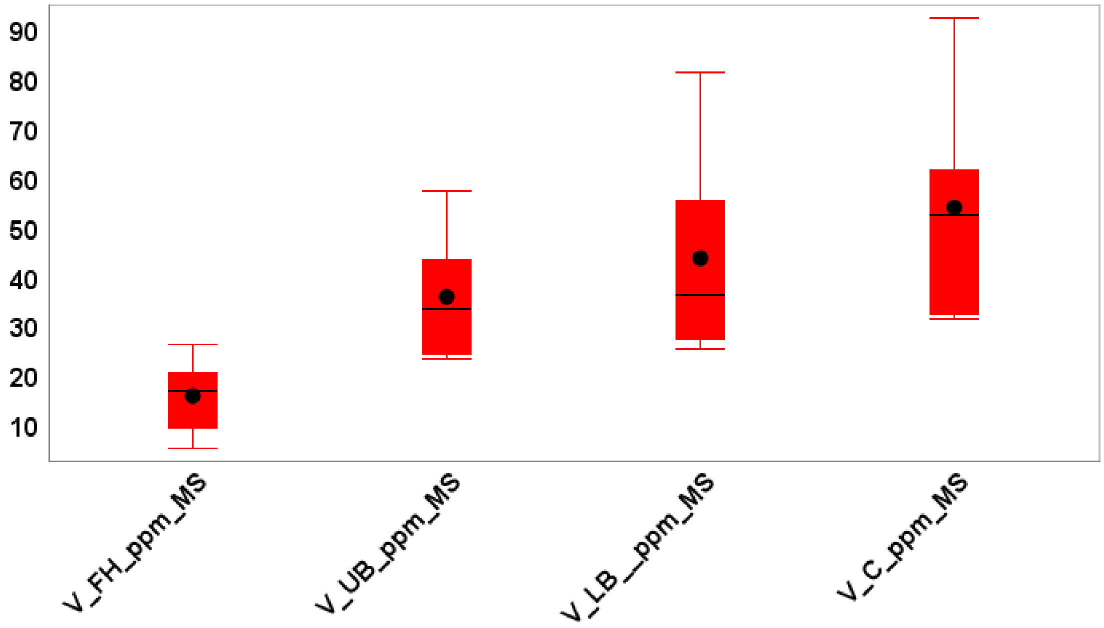

Figure: 3.3.5. Box plot for V by aqua regia-ICPMS in 6 soil samples from the C, lower B, Upper B and F-H horizons.

Soil Sampling Results

Figures 3.3.6 to 3.3.12 show the distribution of Cu, Ni, V, Fe, Cr, Pb and Zn in soil from north to south along the Alexandria sample traverse. Copper, Ni, V, Fe, Cr, and Zn all show a sharp peak in the C and B soil horizons at Profile 33. While most F-H horizon elements patterns are more subdued and the variations do not reflect those in the underlying B and C horizons, there are Cu and Zn horizon anomalies at Profile 34. Several of the elements (e.g. V, Ni, Cr) in the B and C horizon have asymmetric-shaped patterns along the traverse and this shape may reflect the geochemistry of a till deposited by a south to north ice flow. The upper B soil at Profile 33 has a much higher LOI (> 14%) and there is increased BioLeach^{SM} I and BioLeach^{SM} Br (Figure 3.3.13). Figure 3.3.14 shows that samples from Profile 33 also have increased MMI^{TM} and BioLeach^{SM} metals (e.g. Ni) compared to aqua regia-ICPMS determined elements. In Figure 3.3.15 the highest Au, is in the F-H horizon sample at Profile 36 and in Upper B soil at Profile 31. Figure 3.3.16 shows that there is an aqua regia-ICPMS Ca peak at Profile 33, but no corresponding MMI^{TM} Ca peak. At Profile 33 there are IDH values and an interpretation by Sutherland and Hoffman, 2008, from the SGH chemistry that of a redox cell. However, Sutherland and Hoffman, (2008), rank the SGH anomaly at Profile 33 of 1 (low) on scale of 6 (high). The “anomalous” soil at Profile 33 with its higher LOI values, increased metal content and elevated BioLeach^{SM} may reflect higher soil organic content compared to that in the surrounding sediment. Figure 3.3.17 shows darker, more clay-rich sediment in Profile 33 contrasting to more-sandy, grey coloured sediment in Profile 35. The geochemical patterns could be due to a change in surface drainage or sediment filling a buried channel crossing the plateau because an east-west gulley with an intermittent creek is visible between Profiles 33 and 34 on Figure 3.3.1. Erosion in this valley may have exposed till with chemistry different to the sediment typical of the plateau cover.

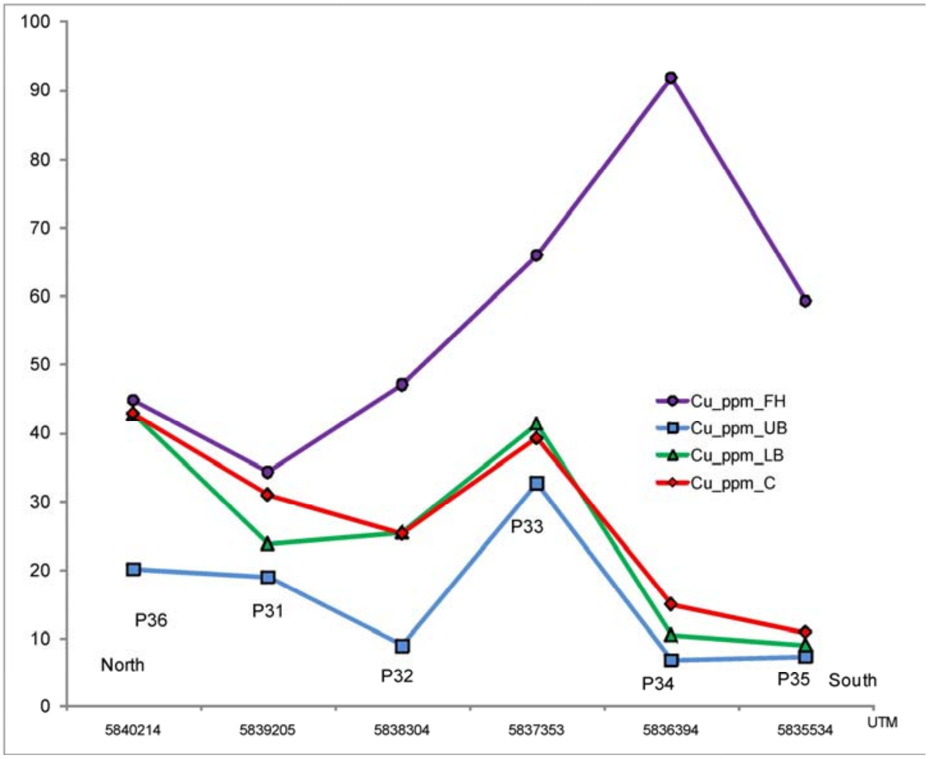

Figure: 3.3.6. Copper soil geochemistry along Alexandria north to south traverse.

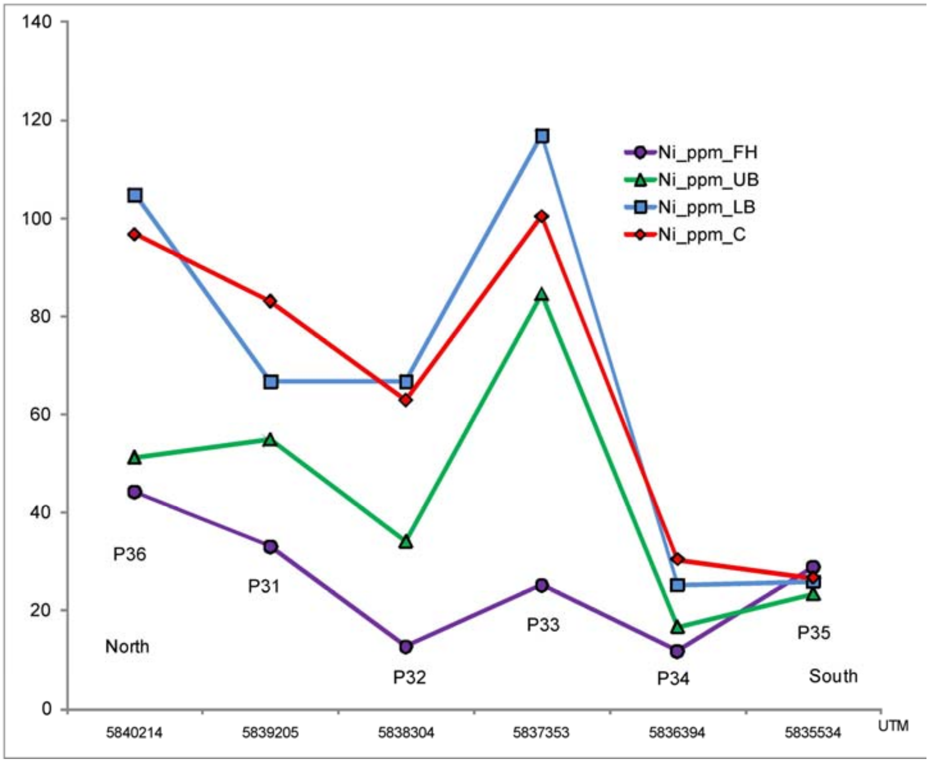

Figure: 3.3.7. Nickel soil geochemistry along Alexandria north to south traverse.

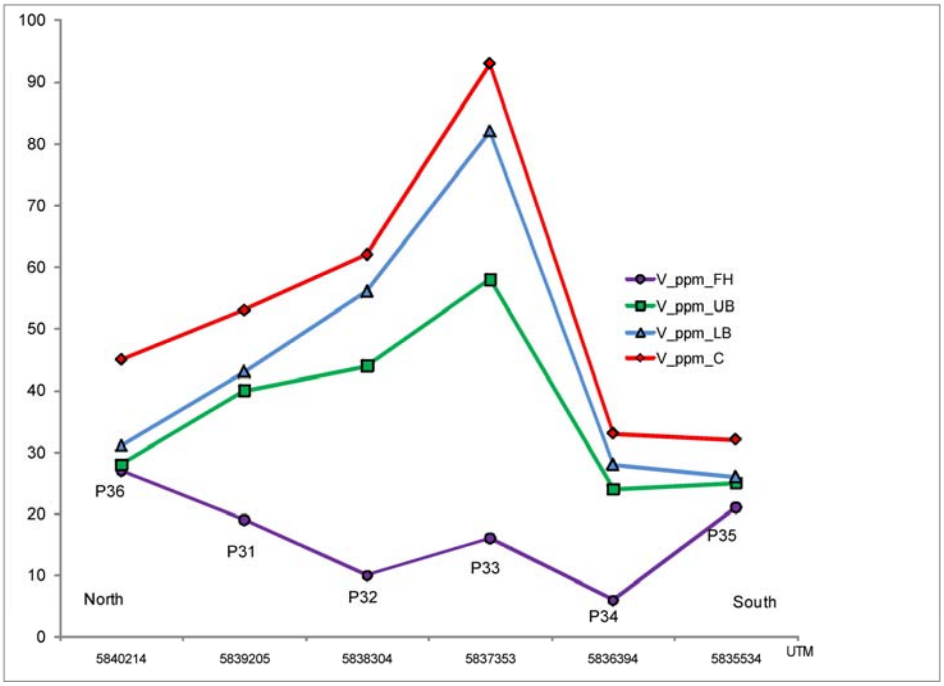

Figure: 3.3.8. Vanadium soil geochemistry along Alexandria north to south traverse.

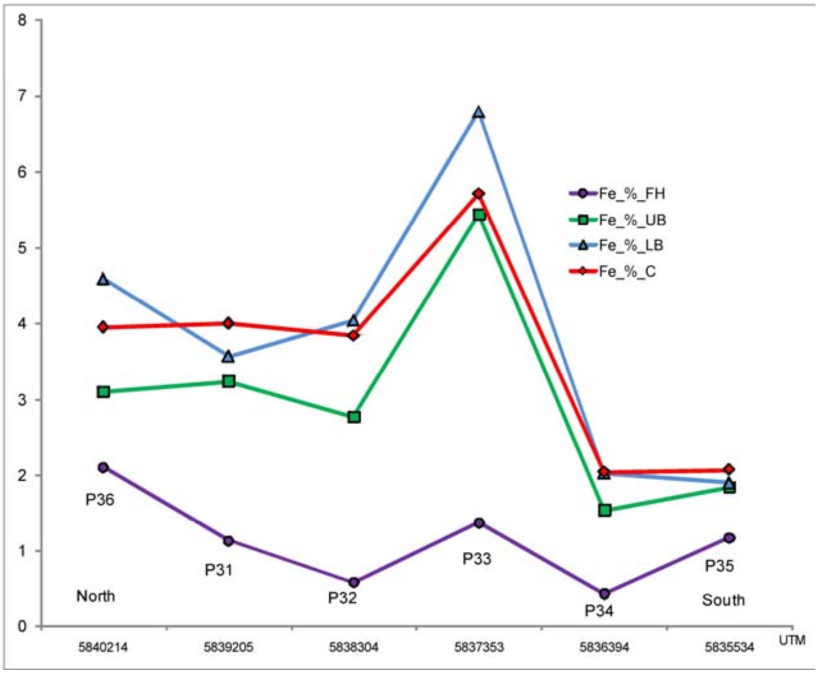

Figure: 3.3.9. Iron soil geochemistry along Alexandria north to south traverse.

.

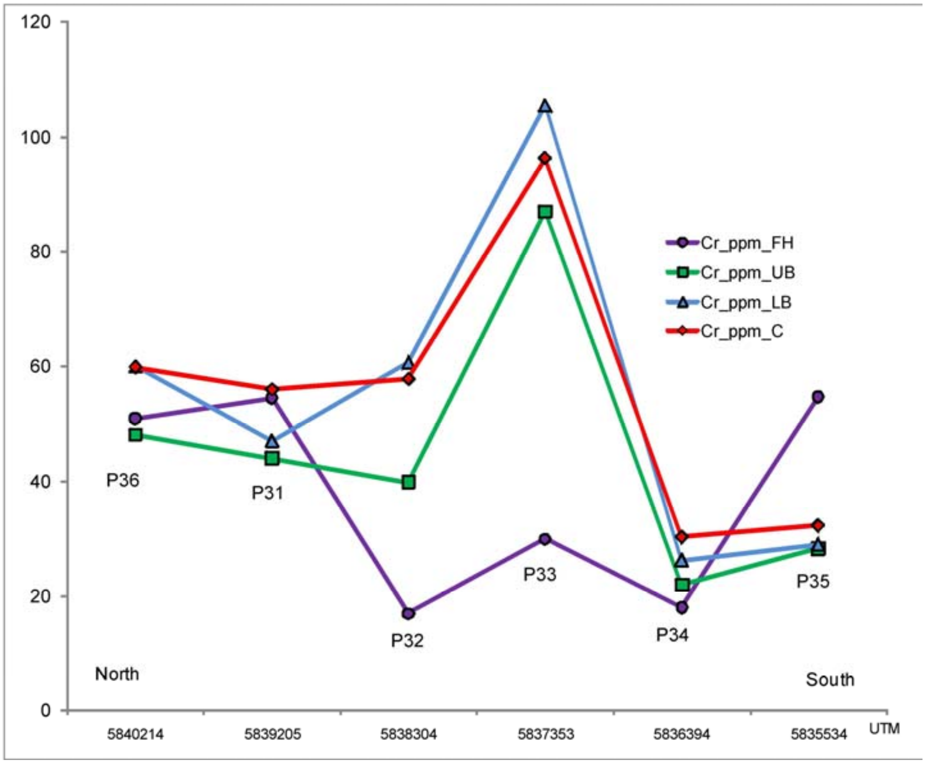

Figure: 3.3.10. Chromium soil geochemistry along Alexandria north to south traverse.

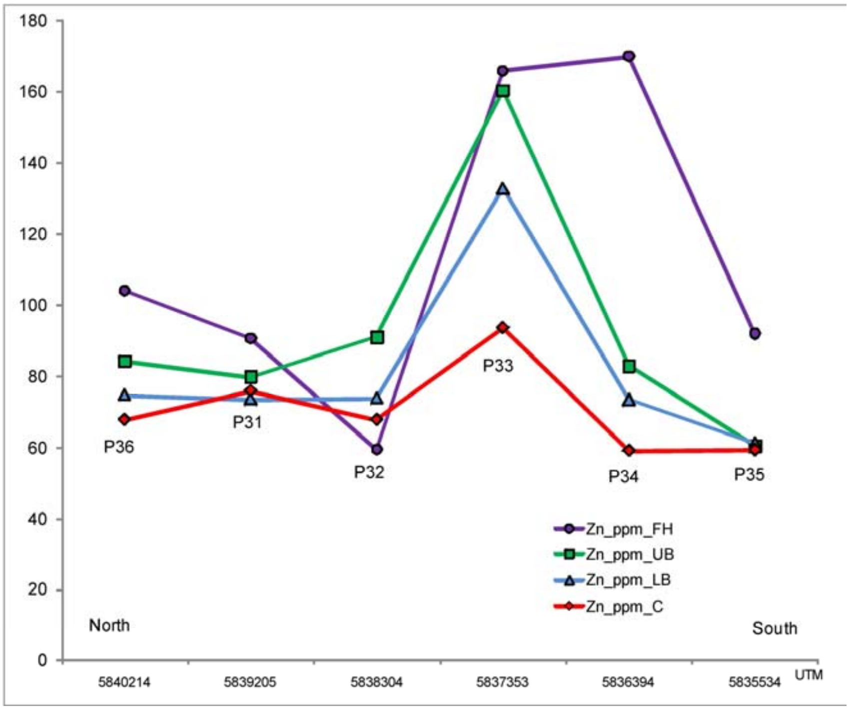

Figure: 3.3.11. Zinc soil geochemistry along Alexandria north to south traverse.

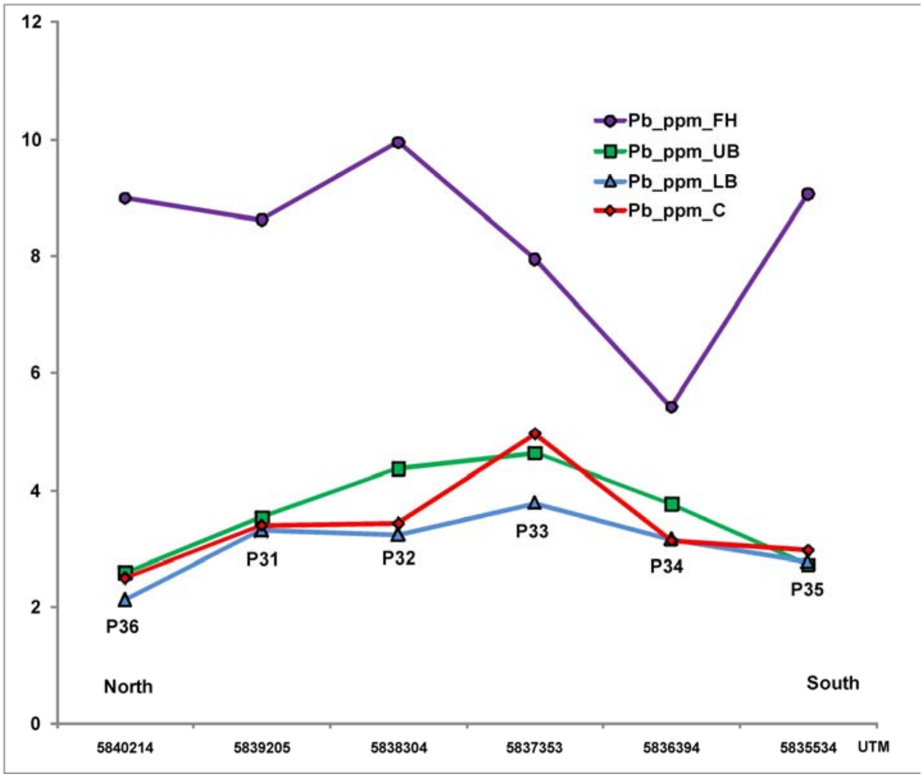

Figure: 3.3.12. Lead soil geochemistry along Alexandria north to south traverse.

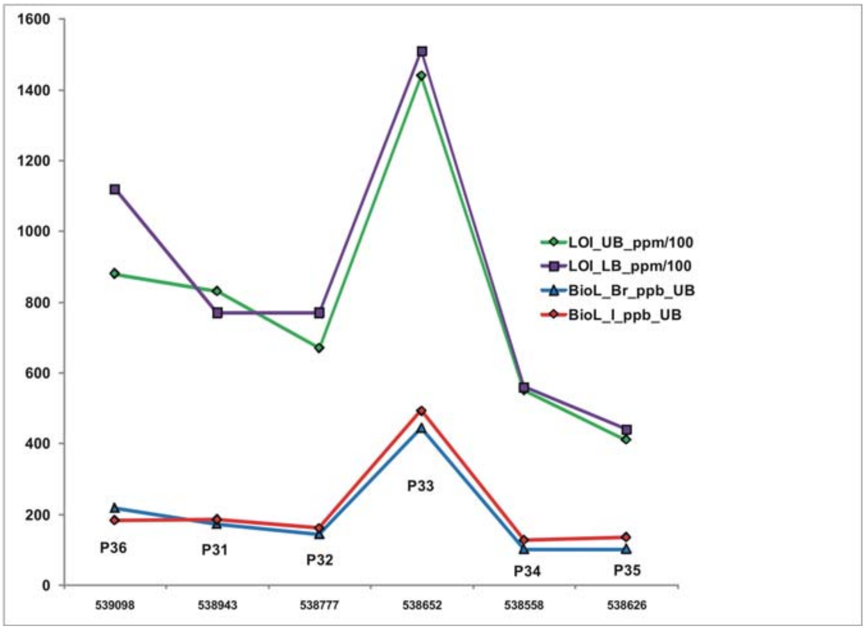

Figure: 3.3.13. Soil pH, Br, I geochemistry along Alexandria north to south traverse.

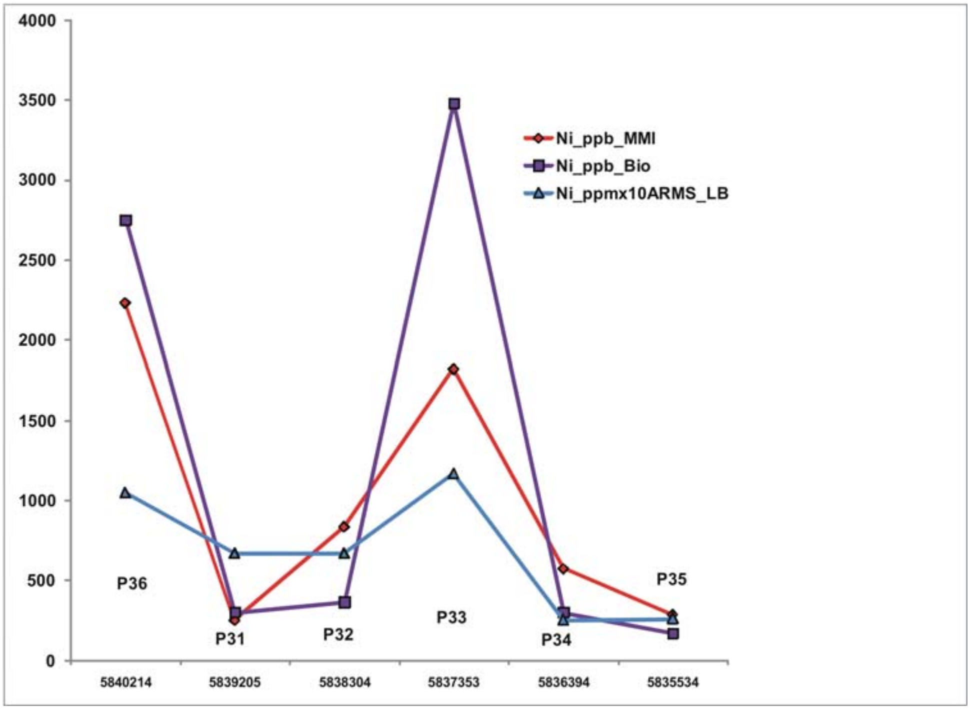

Figure: 3.3.14. Nickel by partial leach along Alexandria north to south traverse.

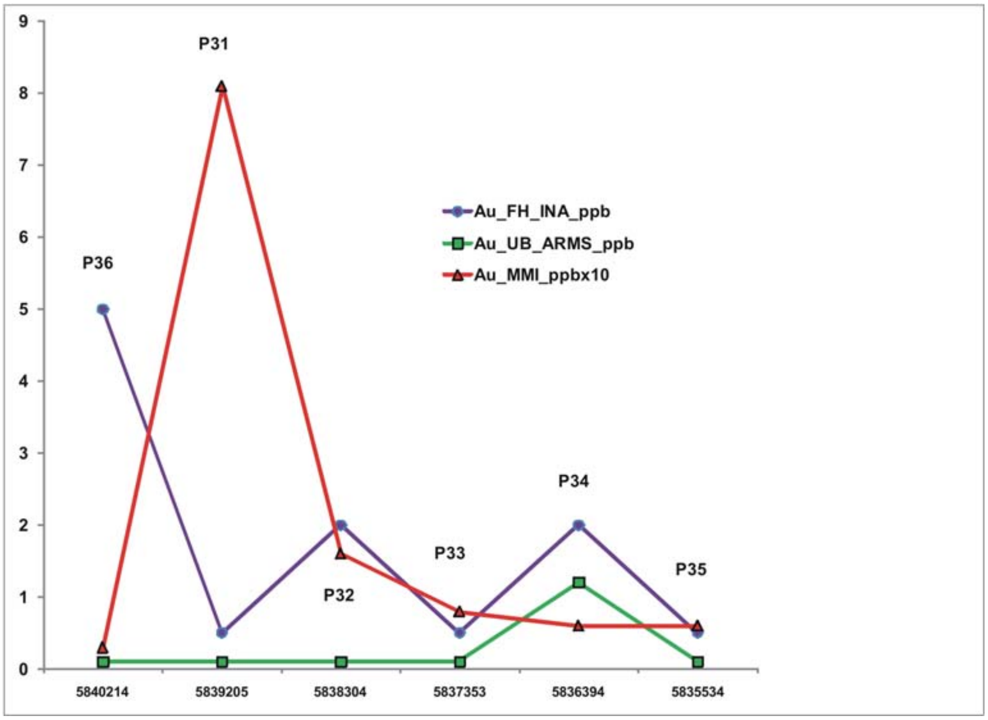

Figure: 3.3.15. Gold by INAA (F-H) horizon, aqua regia-ICPMS and MMI^{TM} partial leach along Alexandria north-south traverse.

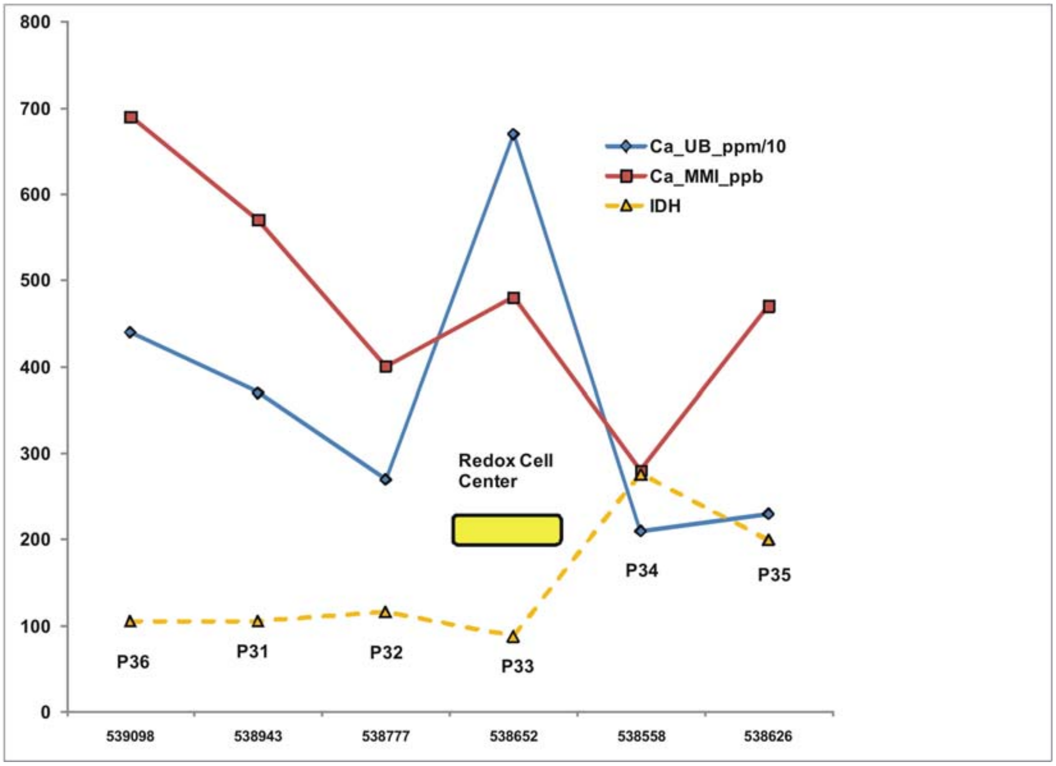

Figure: 3.3.16. Calcium soil geochemistry and pH (IDH) along the north to south traverse.

Figure: 3.3.17. Profile 33 (Left) and Profile 35 (Right).

3.4 SHIKO LAKE

Deposit Name: Red Gold - Shiko Lake **MINFILE Number: 093A 058**

Location: NTS – 93A 06W	LAT. 57°27'50" LONG. - 121°29'03"	UTM NORTH – 5813716 UTM EAST – 602981

MINFILE Status: *Occurrence* **Commodities***: Cu, Au, Zn*

Mineral Deposit Profile: *L03 – Alkalic porphyry Cu-Au*

Significant and Associated Minerals*: Chalcopyrite, bornite, pyrite, sphalerite, magnetite, chlorite, epidote, calcite, actinolite, biotite, amphibolites.*

Regional Geology: The Shiko Lake property is located in a belt of predominantly volcanic rocks with associated intrusive complexes that have been interpreted from previous bedrock mapping and lithogeochemical studies to be the products of a magmatic island-arc that developed off-shore from Ancestral North America from the late Triassic to early Jurassic. Collectively, these island-arc related rocks form the Quesnelia and Stikine terranes that extend along the whole length of the Cordillera through central British Columbia. Because of the potential for small, complex silica-under saturated, alkaline intrusive rocks within Quesnelia to host porphyry Cu +/-Au mineralization they have been a focus of numerous past mapping and mineral deposit projects such as those by Bailey, (1988 a, b), 1990; Panteleyev, (1988), Panteleyev and Hancock, (1989); Panteleyev *et al*., (1996), and by Logan and Bath, (2006). The Quesnel Terrane between the city of Quesnel and Horsefly Lake is bounded to the west by coeval rocks of the oceanic Cache Creek Terrane and to the east by older rocks of the pericratonic Kootenay Terrane. Cache Creek rocks that have been metamorphosed to blueschist facies are field evidence for an easterly dipping subduction plate associated with the Mesozoic magmatism. Jurassic to Cretaceous batholiths mark the tectonic boundary between Quesnellia and the Kooteny Terrane.

Age dating of intrusive rocks has demonstrated that the Quesnelia arc magmatism migrated from west to east starting at about 212 Ma and terminating with the emplacement of 195 Ma calc-alkaline intrusions. At the Mount Polley mine 8 km north of the Shiko lake property the Cu-Au mineralization of high-level alkaline intrusive complex close to the central axis of the magmatic arc occurred during complex emplacement over a relatively short (~ 3Ma) time interval (Logan *et al.,*2007). Quesnelia lithologies within the belt north and south of Mount Polley are represented by the Nicola Group rocks. The two, main lithostratigraphic divisions of the Nicola Group are an older, fine grained sedimentary facies that is conformable with a younger, alkali, shoshonitic volcanic facies. West of the arc axis, the rocks are mainly volcaniclastic sediments. Augite porphyry basalt and andesite flows, volcanic brecccia and volcaniclastic sediments up to 5 km thick fill a 20 km wide belt along the arc axis. The volcanic rocks are mainly subaqueous with minor subarial facies. East of the arch axis are black phyllites, clastic sediments such as greywacke and conglomerate. Intrusive rocks, such those at Mount Polley and Shiko Lake, range from pyroxinite sills, quartz porphyritic dikes to multiphase monzonite-syentite-diorite stocks.

Local Geology: Geology, alternation and Cu-Au mineralization described here is based on an account in the MINFILE database (BC Geological Survey, 2010) and geological studies reported by Logan and Mihalynuk, (2005). The Shiko Lake property is centred on a Lower Jurassic intrusive complex known as the Shiko Lake or Shiko stock composed of diorite grading into syenite and monzonite. This stock is surrounded by older and coeval and comagmatic sedimentary and volcanic units. The intrusive complex displays a high magnetic signature and the sedimentary and volcanic stratigraphy represents local areas of high chargeability due to increased sulphide content. The stock has intruded the Nicola Group volcanic and sedimentary rocks. Nicola Group rocks that have been intruded by the Shiko stock (syenite- monzonite-diorite-gabbro) and by mafic-felsic dikes consist of augite basalt (interlayered augite-bearing basaltic flows-tuffs-wackes), felsic heterolithic breccias, massive to locally laminated tuffaceous sediment mapped as siltstone and maroon, analcite- bearing possibly subaerial basaltic flows. A simplified geology map of the area where samples were collected is shown in Figure 3.4.1. There is a long history of exploration over the property including geochemical and geophysical surveys and diamond drilling. Most recently (2007) Novagold's program included overburden drilling, diamond drilled 11 of holes totalling 2293 metres and 12 line kilometres of ground-based, deep-sensing, IP/resistivity survey.

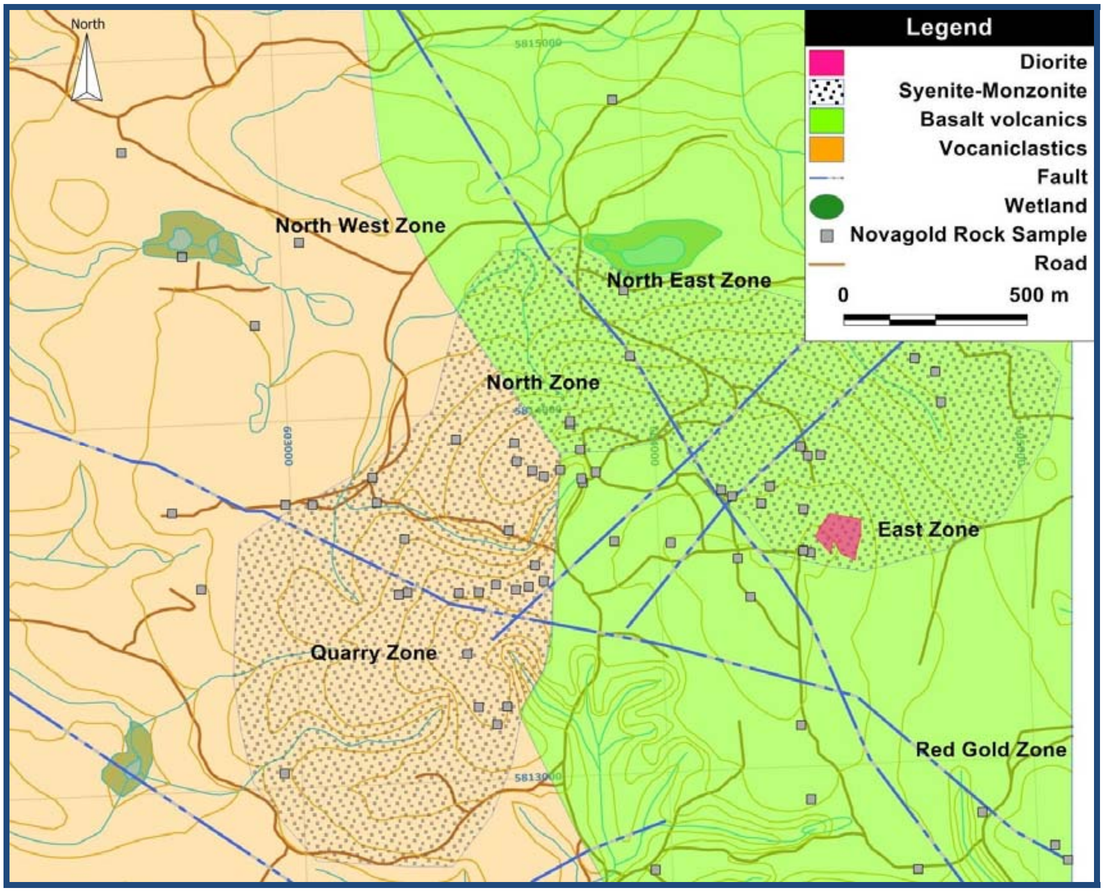

Figure: 3.4.1 Shiko Lake property geology and location of Novagold rock samples. Note that the geological contract between the intrusive and basalt is approximate.

Alternation and Mineralization: Hydrothermal activity associated with the intrusion of the stock has produced pods and lenses of epidote-chlorite-calcite alteration within basaltic rocks and alteration of wall rock adjacent to fractures within the stock. This propylitic alteration assemblage is locally accompanied by chalcopyrite-pyrite-bornite mineralization. Chalcopyrite, bornite and gold occur in veins and as coarse disseminations mainly in the youngest quartz syenite but are also found in the other intrusive phases. Fracture controlled pervasive potassium alteration and epidote alteration of the volcaniclastic rocks is associated with the Cu mineralization. Earlier potassium and epidote alternation has been cut by late stage calcite-filled veinlets (Logan and Mihalynuk, 2005).

Assays from drill core reported in 1974 ranged from 0.01 to 0.10 per cent copper and typically around 0.034 gram per tonne gold. The copper values were low and sporadic with very low gold values (Assessment Report 5540). In 1984, Falconbridge Copper Corporation completed sampling on the property with rock chip samples returning up to 2000 ppm copper and 1350 ppb gold (Property File Rimfire Durfeld, R.M., 1984). Areas of Cu-Au mineralization identified and outlined by exploration of the property are the North, Quarry, North East, East-Redgold and Northwest Zones.

North Zone: This zone covers the northeast extension of the main Shiko Lake diorite and its contact with host rocks of felsic breccia. Diamond drilling by Phelps Dodge intercepted widespread potassic alteration (K-spar-biotite-amphibole-magnetite) with anomalous copper-gold values. Higher values of gold and copper occur locally as well (DD Hole P-1 intersected 10 metres of 720 ppb gold and 0.47 per cent copper). In 2007, drilling by Novagold (Assessment Report 29999) successfully duplicated the highly anomalous metal values seen in early percussion hole P-1, yielding three significant intercepts from drillhole DDH-07-0003:

- 8.1 metres grading 0.74 per cent copper and 2.3 grams per tonne gold (3.9-12 m)
- 28.5 metres grading 0.39 per cent copper and 1.0 grams per tonne gold (29-57.5 m)
- 8.0 metres grading 0.09 per cent copper and 1.7 grams per tonne gold (89-97 m)

Quarry Zone; Copper and Au mineralization occur as fracture-fill and disseminations in a composite alkalic intrusion which ranges in composition from augite monzonite to syenite. The main intrusive complex consists of an older pyroxene diorite, which has been cut by a younger composite pyroxene monzonite to syenite body. An albite-quartz, strongly sodic, porphyry dike cutting the monzonite and syenite is the final phase of the intrusive activity. Trenching and drilling of the Quarry zone revealed up to 1.9 grams per tonne Au and 0.11 per cent Cu over 11.9 metres (DDH 96-2). More recent sampling by Novagold confirmed high metal values associated with actinolite-biotite-chalcopyrite-bornite fracture fillings. Highly anomalous values were obtained in similar rocks approximately 400 metres east of the Quarry zone (drillholes 80-1 to 80-3).

Northeast Zone: Pervasive epidote-calcite alteration overprinted by intense magnetite–epidote-K-feldspar alteration has been intersected by diamond drilling. An intersection of 12 metres of 0.36 gram per tonne Au with 0.22 per cent Cu was reported in DDH 90-5.

Redgold Zone: The East and Redgold showings are poorly explored occurrences of highly anomalous copper-gold mineralization along the northwest trending, possibly fault displaced portion of the main lithocap. Extensive zone of epidote–calcite–pyrite-K-feldspar altered augite basalt where elevated concentrations of Cu occur in rocks “hardened” by garnet-diopside skarn formation which are subsequently brecciated and quartz veined is characteristic of the Redgold Zone. The nearest drill hole (DDH 91-20, collared 300 metres northeast of the zone) intersected 159 metres of disseminated sulphide mineralization in pervasively propylitized basalt grading 358 ppm Cu and 199 ppb Au. Trace to 2 per cent medium to coarse-grained chalcopyrite was disseminated throughout this hole with anomalous Cu and Au associated with aggregates of coarse-grained calcite, sphalerite, and chalcopyrite. Grab samples from previously excavated trenches yielded concentrations of Cu as high as 1.08 per cent and Au to 1.6 grams per tonne.

East Zone: The East zone is located 750 metres northwest of the Redgold target, and was reportedly discovered by prospecting in 2004 when trenching exposed potassic altered “igneous” breccias (monzonite, syenite) in a complex contact with augite basalt. The East zone sits on the flank of a composite monzonite–syenite cupola and consists of brecciated augite basalt and “hybridized” syenite/monzonite possibly intrusive breccia over an area approximately 10 by 30 metres in rubblecrop. Intrusive fragments in breccia are strongly magnetic and exhibit secondary K-feldspar and biotite alteration. Copper and Au mineralization is hosted by intrusive breccias with best values associated with disseminated sulphide and hairline quartz-K-feldspar (chalcopyrite, bornite) veinlets. Initial grab samples analysed up to 0.61 per cent Cu and 1.1 grams per tonne Au, with a subsequent two-metre chip in a shallow trench yielding 0.78 per cent Cu and 9.6 grams per tonne Au.

Northwest Zone: Anomalous to highly anomalous soil samples occur along the northwest contact of the Shiko Lake stock in an area tested by percussion hole P-5 (diorite) and DDH 90-4 (felsic breccia). Summary logs for these holes indicate strong pyrite with long intervals of 500-1000 ppm Cu on both sides of the contact (averaging about 700 ppm).

Local Environment: Detailed soil sampling on the Shiko Lake property focused on a partly drift-covered, steep-sided ridge located 2 kilometres south of Mitchelle Bay on Quesnel Lake. The northwest trending ridge crest at 1020 metres ASL elevation is typical of the undulating Fraser Plateau to the west whereas to the east are the more mountainous Quesnel Highlands (Holland, 1964). The original land surface was modified by a Pleistocene continental ice-sheet the flowed west from the Cariboo Mountains. Tipper, (1971), interpreted glacial landforms to the north and west of Quesnel Lake as evidence for two major Pleistocene continental glacier advances across the area. Given the proximity of Shiko Lake to the Cariboo Mountains the glacial sediments on the Shiko Lake property were most likely deposited by the most recent advance and subsequent deglaciation of the Late Wisconsin Fraser Glaciation.

A predominantly sandy till was deposited by east to west advancing ice and on steeper slopes this has been reworked into colluvium. Rare striations and lunate rock gouges on polished outcrop indicate ice-flow between 280 to 300^o from the south-east. A steeper northwest facing slope of the ridge suggests that it is a Roche moutonnée glacial landform formed by ice erosion across the landscape. Sand and gravel deposited during deglaciation have accumulated in the major valleys such as the Horsefly River valley to the south of Shiko Lake. Levson and Giles, (1993), describe a section north of Horsefly where a Late Wisconsin diamicton and glacio-fluvial sand and gravels that deposited by high-gradient and braided streams cover Ag-bearing Miocene gravels.

Humo-ferric podzolic and brunisolic soils have developed on the better drained sandy till whereas organic and gleysolic soils are common in poorly drained depressions. Western red cedar, white spruce and Douglas fir, lodgepole pine, common paper birch, black cottonwood and trembling aspen form the canopy. Willow, alder and devils club grow thickly in poorly drained areas. The ridge and surrounding area has been extensively logged and presently Mountain Pine beetle has damaged much of the remaining timber.

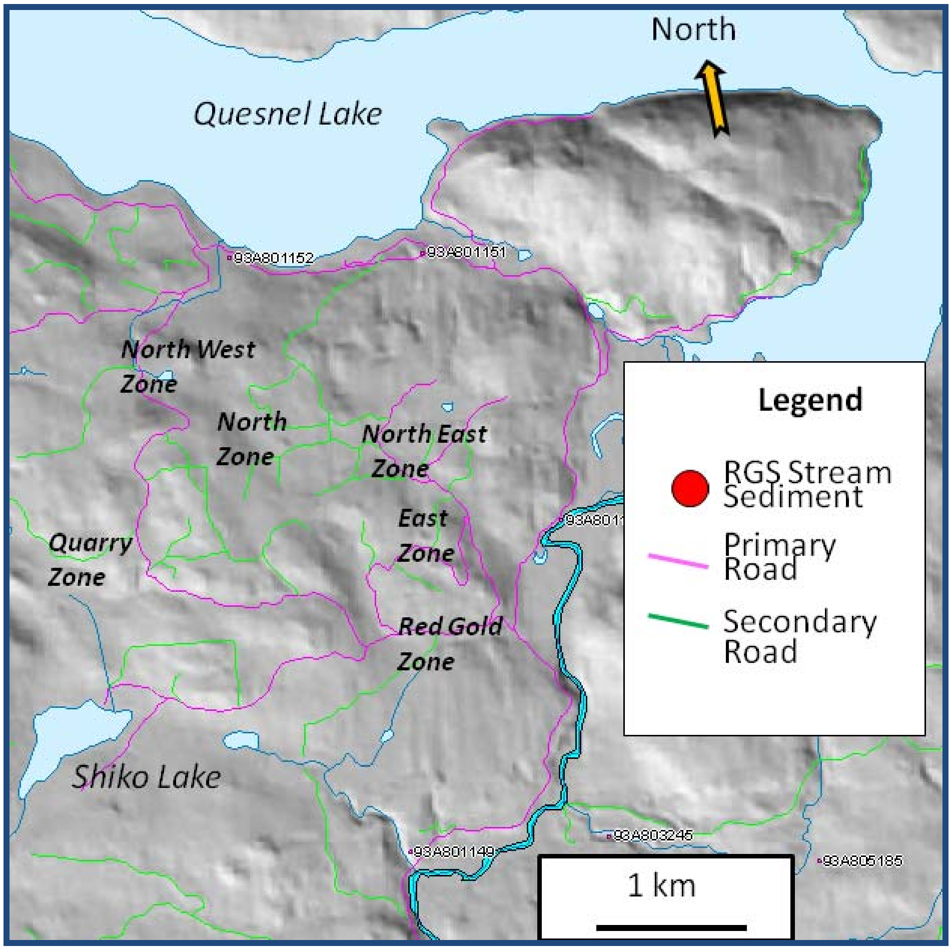

Figure: 3.4.2. Mineralized zones and landforms, Shiko Lake property. Base map digital elevation model image captured from Map Place (BC Geological Survey, 2010).

Lithogeochemistry

No rock samples were collected for analysis in 2007, but there are published geochemical data for Cu-Au mineralized intrusive and volcanic rocks sampled by Logan and Mihalynuk, (2005), from the area around the Mount Polley and Shiko Lake properties. These samples were analysed by ICPMS and ICPES for a trace, minor and major elements after HF-HCLO$_4$-HNO$_3$-HCl digestion. The results show that there are geochemical differences between volcanic and the Cu-Au mineralized intrusive rocks. The box plot in Figure 3.4.3 compares median, quartile and range for Au, Ag, Cu, Mo, Ni, Sr and V in basalt samples with the statistics for intrusive syenite-monzonite samples. While median values for Au, Cu, V and Ni are higher in basalts compared to the syenite-monzononite, Figure 3.4.3 shows that maximum values for Ag, Au, Cu, Mo and Ni are much higher in the intrusive rocks compared to the volcanics.

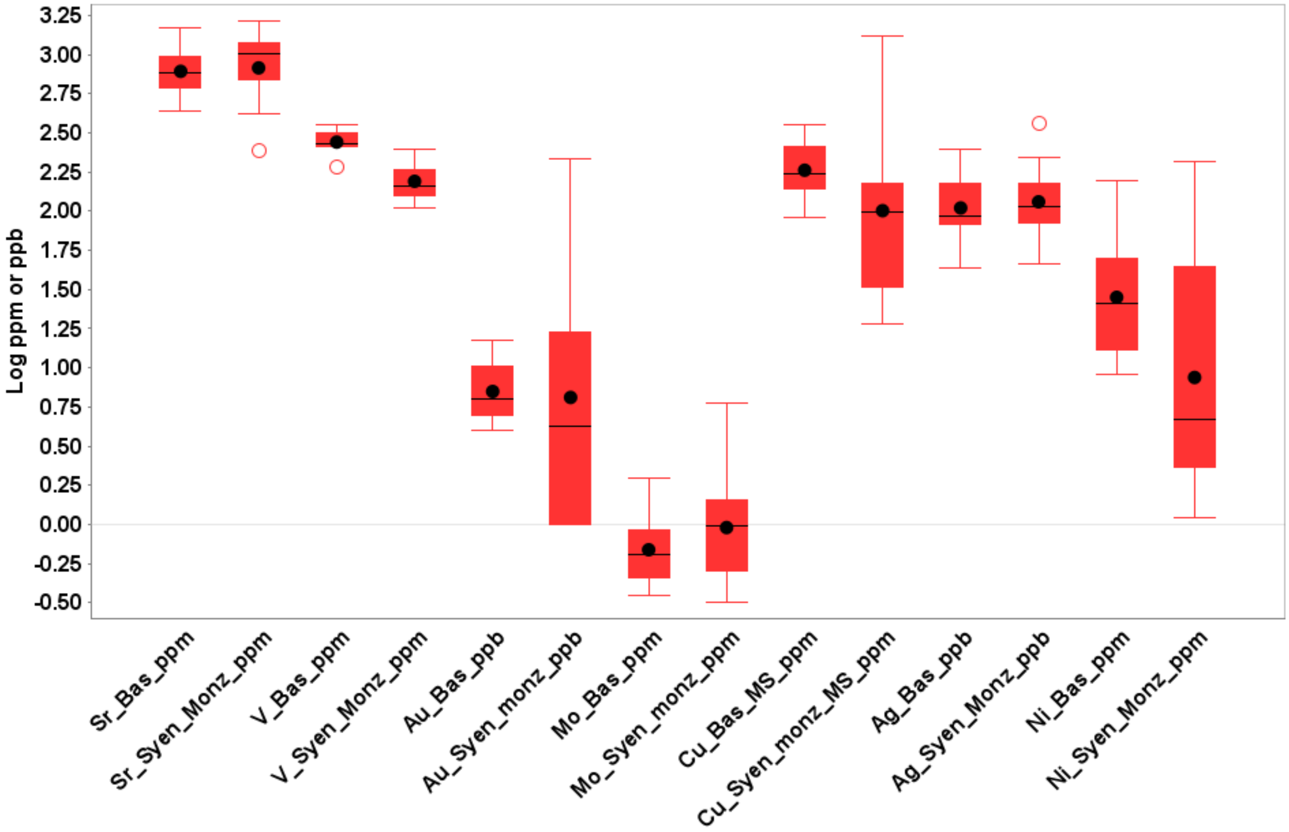

Figure: 3.4.3 Box plot for selected elements by HF-HCLO$_4$-HNO$_3$-HCl digestion – ICPMS/ES in basalt and syenite-monzonite from the Shiko Lake area.

The results of rock samples collected by in Petsel (2006) the Shiko Lake property and analysed for 49 elements by aqua regia-ICPES/ICPMS complement the data generated by Logan and Mihalynuk, (2005). However, a caution should be used when making a direct comparison of the two data set to estimate variations in bedrock geochemistry and regional element backgrounds because the HF-HClO$_4$-HNO$_3$-HCl-ICP/MS analyses reported by Logan and Mihalynuk are near-total whereas a suite the data produced by Petsel (2006), is by a less rigorous, partial aqua regia digestion.

Element	Min.	Max.	Median	3rd Quartile	U_Fence	Max/U_Fence
Au_ppb	2.5	2460	2.5	14	32	78.7
Te_ppm	0.025	1.29	0.025	0.038	0.56	28.3
Cu_ppm	2.5	6480	119	170	297	21.2
Pb_ppm	0.25	247	4.7	606	11.4	21.7
Bi_ppm	0.005	1.13	0.02	0.03	0.07	16.7
Ag_ppb	5	3040	90	140	260	11.7
Re_ppb	1	54	1	3	6	9
Hg_ppb	5	2180	50	125	238	7.7
Cd_ppm	0.03	1.92	0.11	0.155	0.23	7.6
Cs_ppm	0.025	22.3	0.97	1.835	3.8	5.9
Mo_ppm	0.18	14.5	0.64	1.23	2.4	5.8
Sb_ppm	0.05	6.22	0.29	0.635	1.3	4.7
S_%	0.005	4.96	0.07	0.44	1.07	4.6

Table 3.7. Minimum, maximum, median, 3rd quartile and upper fence (3rd Quartile+[Interquartile distance x1.5]) statistics for elements with a Maximum to Upper Fence ratio > 4. The statistics are calculated from aqua regia-ICPMS data for 167 rock samples reported by Petsel, (2006).

Table 3.7 lists minimum, maximum, median, 3rd quartile and upper fence (3rd Quartile+[Interquartile distance x1.5]) statistics for elements with a Maximum:Upper Fence ratio greater than 4 calculated from aqua regia-ICPMS data for 167 rock samples reported by Petzel, 2006. The table shows that An, Te, Cu, Pb, Bi, Ag and Re are among elements most elevated in the Shiko Lake bedrock samples based on Maximum:Upper Fence (threshold) value ratios. However, element ranges and median values vary markedly with rock type as shown by Cu, Au and Pb in Figure 3.4.3, 3.4.4 and 3.4.5. Copper is clearly enhanced in diorite compared to other rock types whereas Pb is elevated in both basalt and diorite. The contrasting distribution of these two elements in host rocks could reflect an association of the Cu mainly in the sulphide mineralized diorite compared to the Pb as galena veins hosted by the basalt. Molybdenum and Re (Figures 3.4.6 and 3.4.7) are concentrated in siltstone compared to other rock types but an interpretation of the statistics should be viewed with caution because the number of samples used to create the plots range from over 50 basalt samples to only 6 siltstones. Vanadium, Figure 3.4.8, is clearly most enhanced in basalt and diorite whereas in Figure 3.4.9 Ag is higher in the monzonite compared to the other rock types. Figures 3.4.10 and 3.4.11 show the spatial variation of Cu and Au in bedrock. Clusters of rock samples with the highest values occur near the north and Quarry zone close to the intrusive contract.

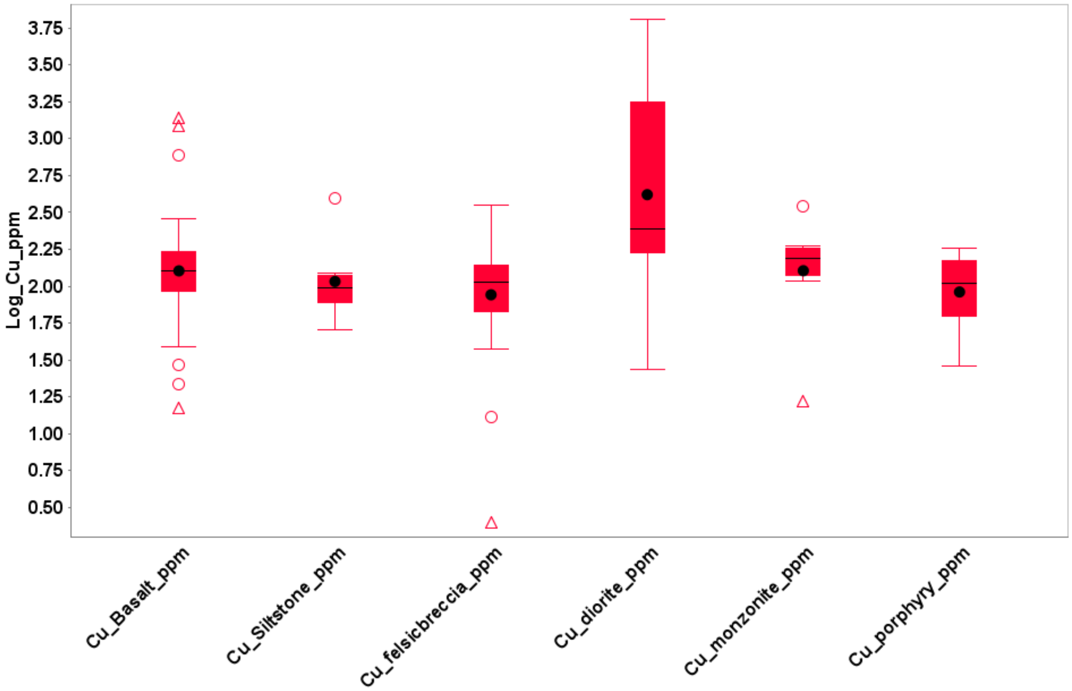

Figure: 3.4.3. Box plot for Cu by aqua regia digestion – ICPMS/ES in rock samples collected by Petsel, (2006), from the Shiko Lake property.

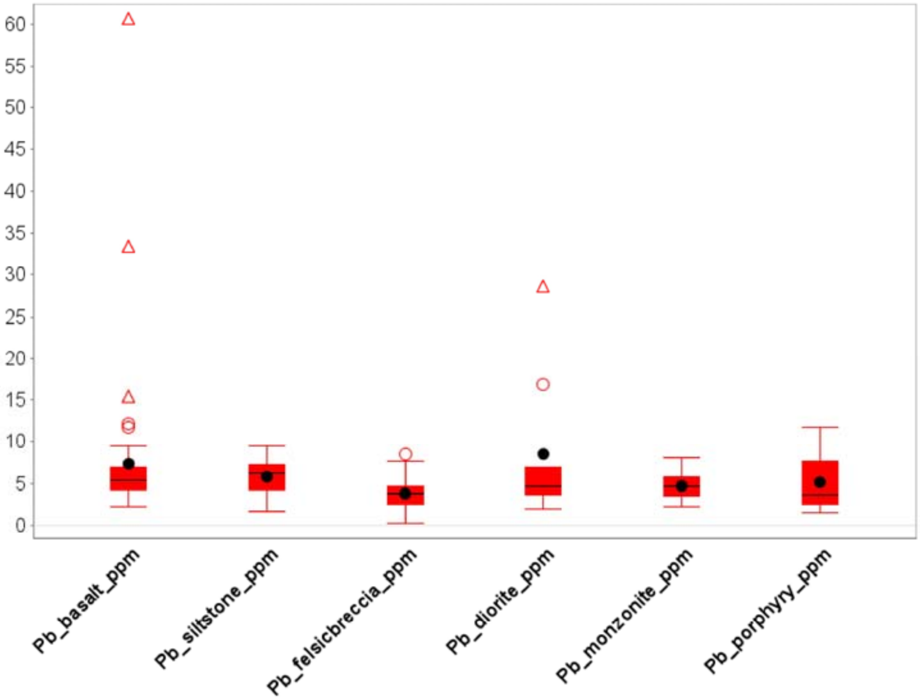

Figure: 3.4.4. Box plot for Pb by aqua regia digestion – ICPMS/ES in rock samples collected by Petsel, (2006), from the Shiko Lake property.

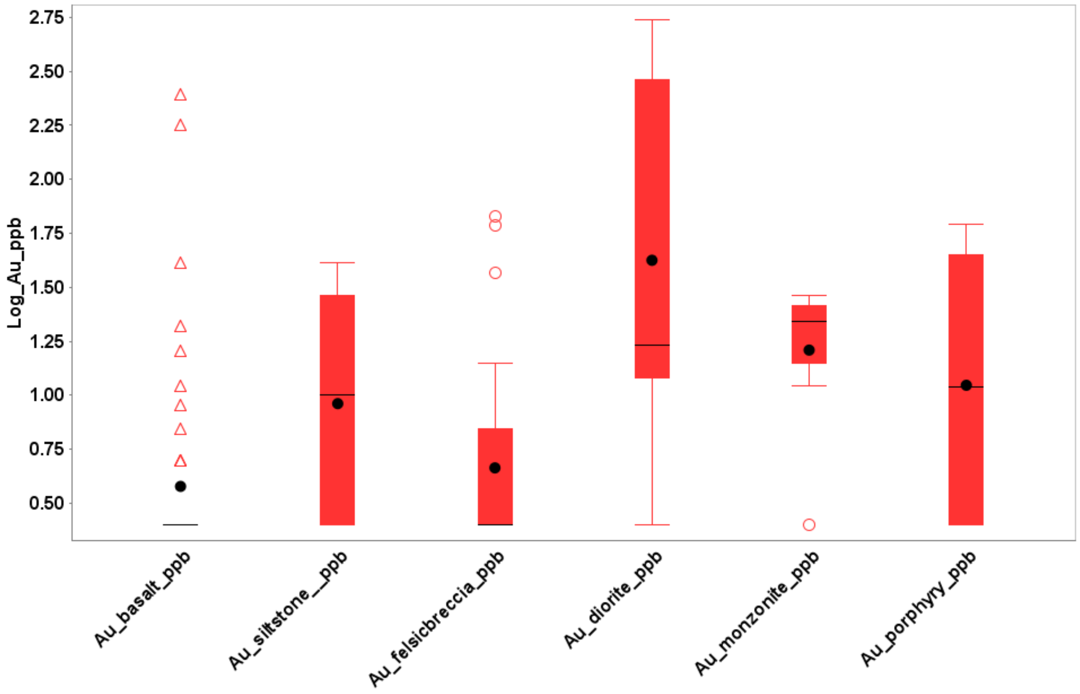

Figure: 3.4.5. Box plot for Au by fire assay- ICPES in rock samples Shiko Lake rock samples.

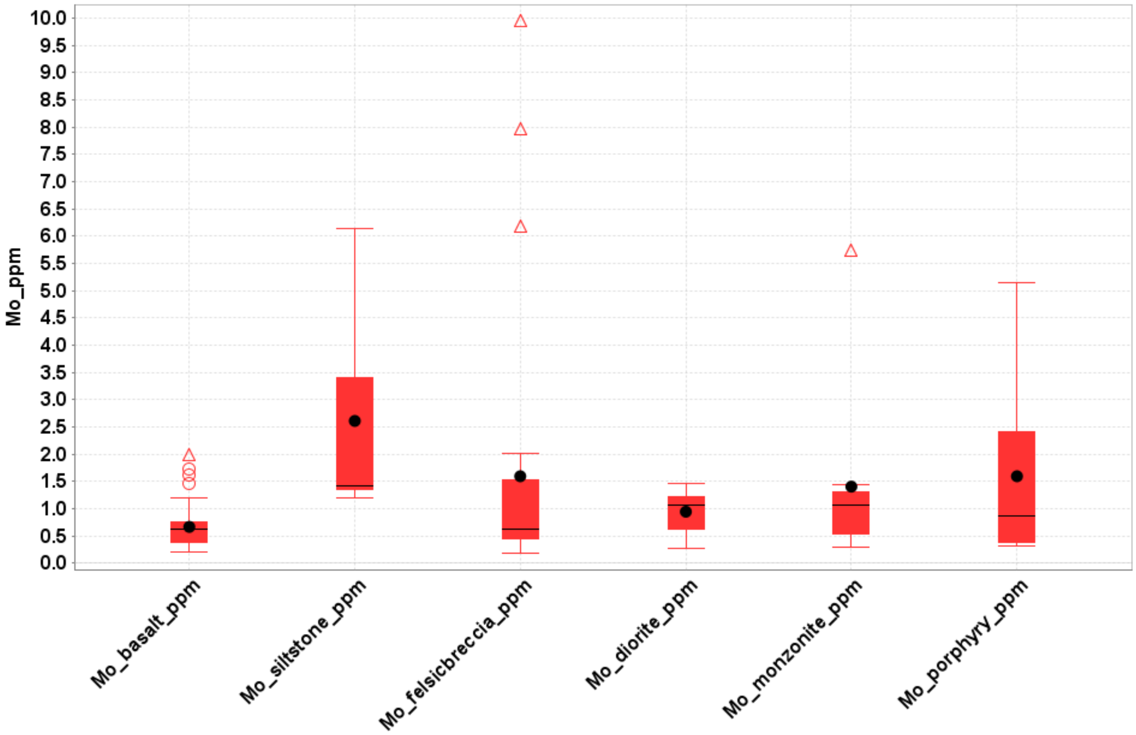

Figure: 3.4.6. Box plot for Mo by aqua regia digestion – ICPMS/ES in rock samples collected by Petsel, 2006, from the Shiko Lake property.

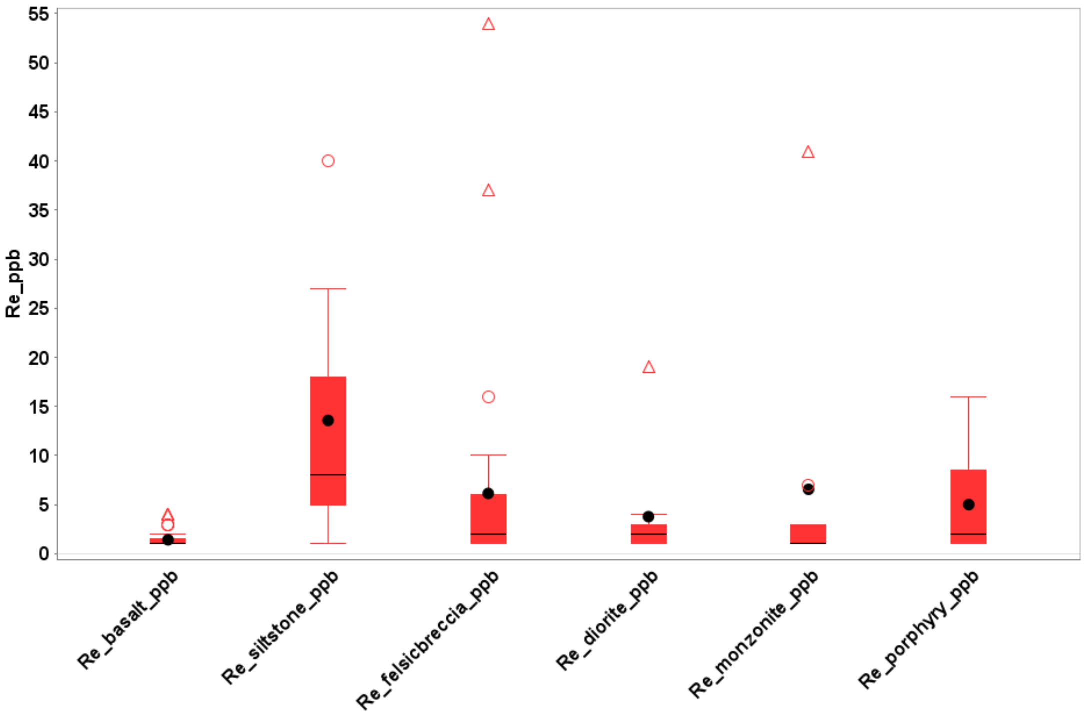

Figure: 3.4.7. Box plot for Re by aqua regia digestion – ICPMS/ES in rock samples collected by Petsel, 2006, from the Shiko Lake property.

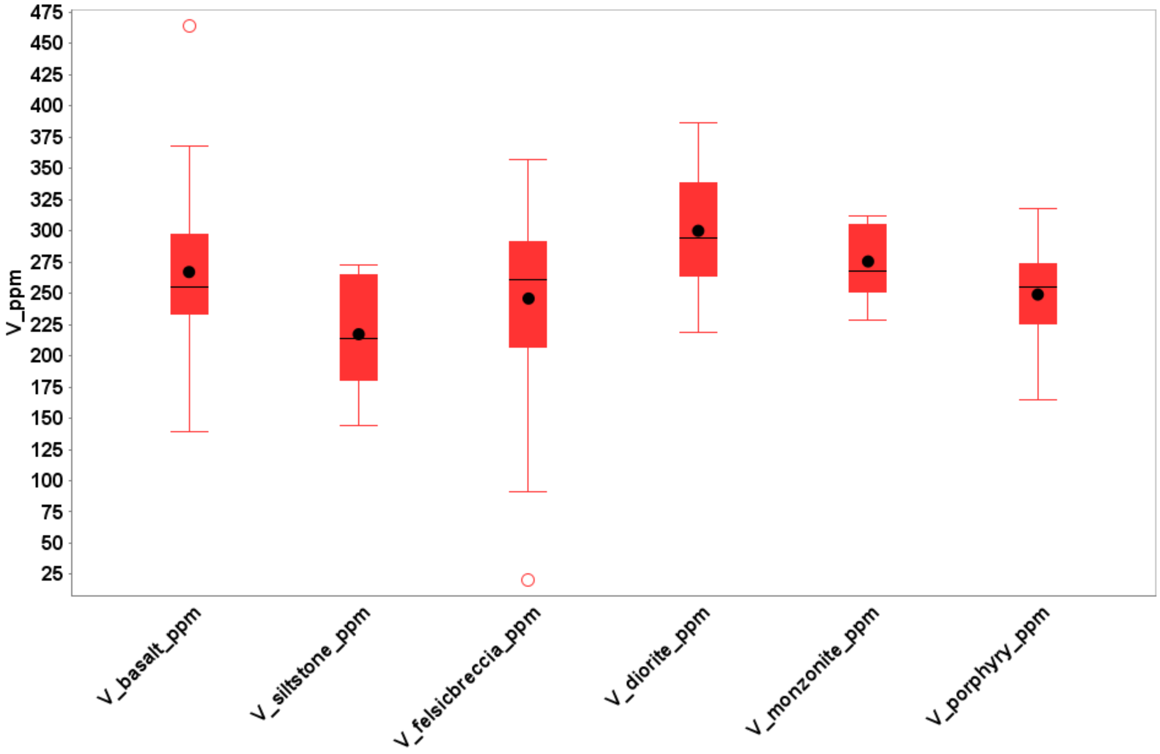

Figure: 3.4.8. Box plot for V by aqua regia digestion – ICPMS/ES in rock samples collected by Petsel, 2006, from the Shiko Lake property.

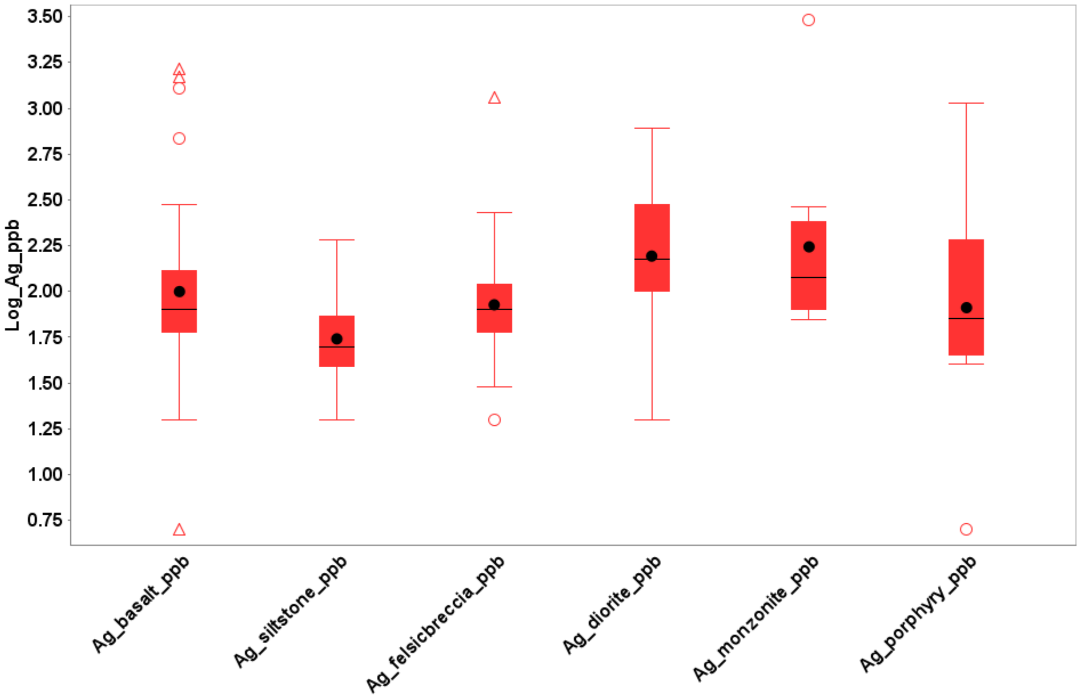

Figure: 3.4.9. Box plot for Ag by aqua regia digestion – ICPMS/ES in rock samples collected by Petsel, 2006, from the Shiko Lake property.

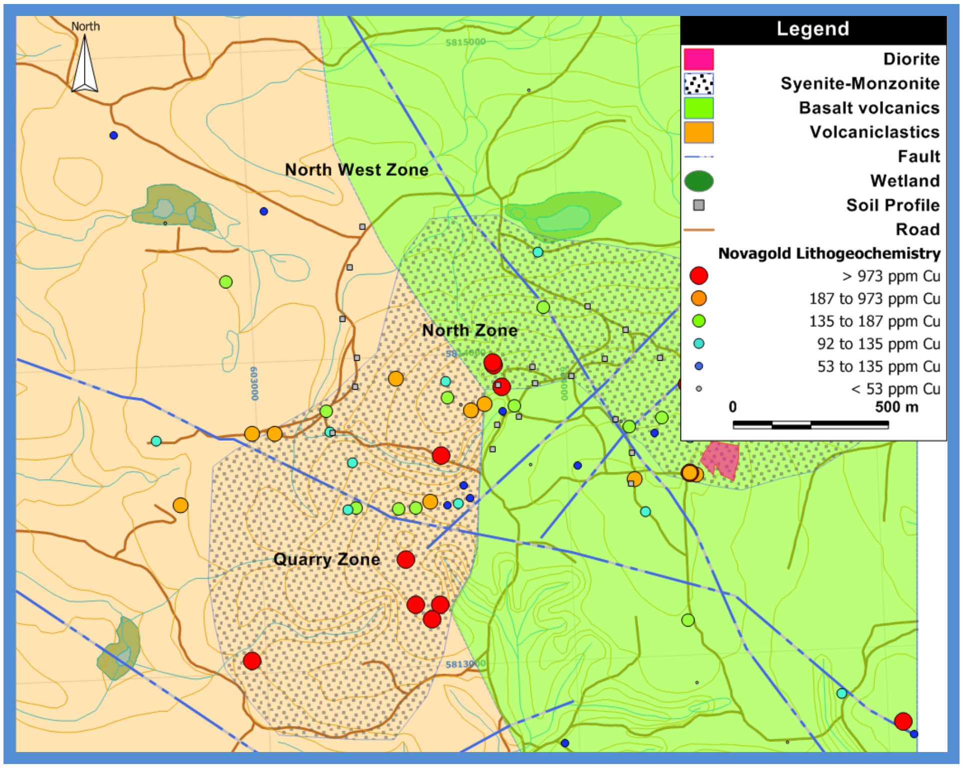

Figure: 3.4.10 Copper by aqua regia digestion – ICPMS/ES in rock samples collected by Petsel, 2006, from the Shiko Lake property. Geology from Petsel, 2006.

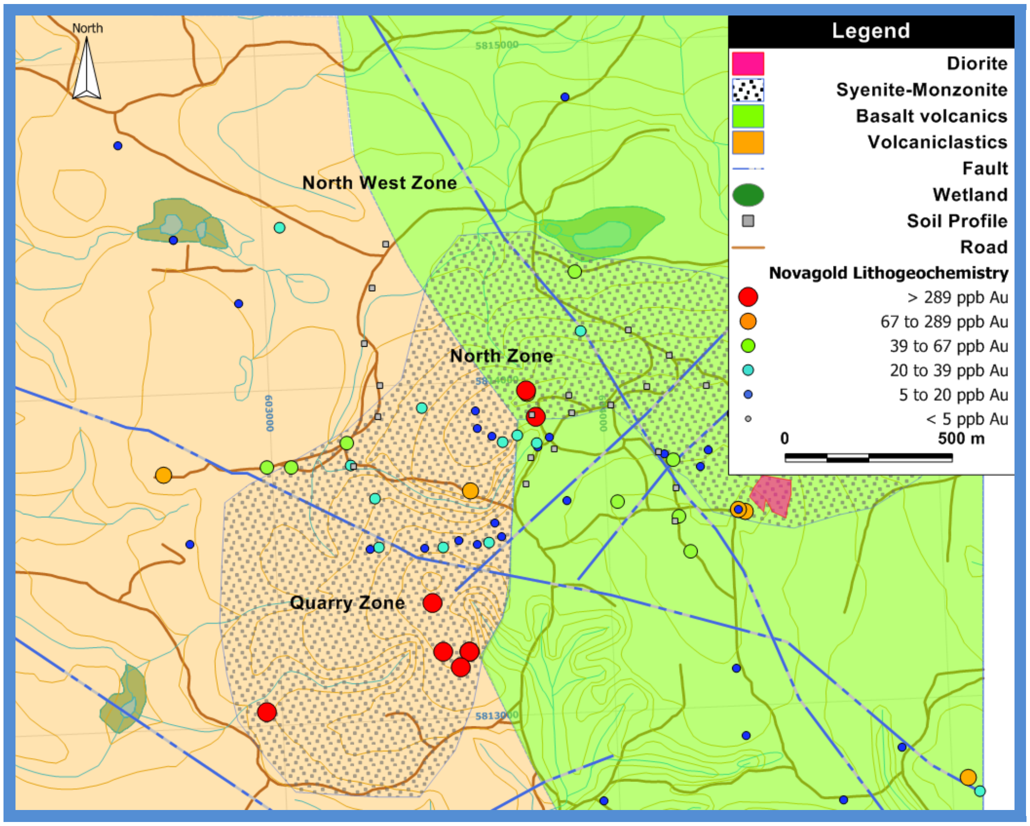

Figure: 3.4.11 Gold by fire assay – ICPES in rock samples from the Shiko Lake property.

Drainage Geochemistry

Five drainage sediment and one moss mat sediment samples were collected from streams flowing north from the Shiko Lake property into Quesnel Lake. Figure 3.4.12 identifies location of these samples and other sites where sediment was collected during a 1980 BC government regional geochemical survey (Jackaman, 1999). Also shown on Figure 3.4.12 are the profile sites where soil samples were collected in 2007 as part of this study. Sediment collected in 1980 was air, sieved through an 80 mesh (0.177 mm) screen and the minus 80 mesh fraction analysed for Ag, As, Cd, Co, Cu, Fe, Mn, Mo, Pb, V, Sb and Zn with an aqua regia digestion (3 ml concentrated. HNO_3: 1 ml concentrated HCl v/v) and atomic absorption spectrophometry (AAS). Silver, Cd, Co, Cu, Fe, Mn, Pb, Sb and Zn were measured by AAS with an air-acetylene flame with application of background correction for Pb, Ni, Co, Ag and Cd. Arsenic was determined by atomic absorption using a hydride evolution method; Mo and V were determined by AAS using a nitrous oxide acetylene flame. A separate 0.5 gram sample of the minus 0.177 mm fraction was analysed for Hg by reacting the sediment minus 80 mesh fraction with 20 ml concentrated HNO_3 and 1 ml concentrated HCl in a test-tube for 10 minutes at room temperature followed by a 2 hour digestion at 90C and, finally, dilution to 100 ml with metal free water . The Hg present was reduced to the elemental state by the addition of 10 ml 10% W/V $SnSO_4$ in M H_2SO_4 and the Hg vapour generated flushed by a stream of air into an absorption cell mounted in the light path of an atomic absorption spectrophotometer. Gold in the minus 80 mesh fraction was measured with instrumental neutron activation (INAA). Sediments taken in 2007 were also air dried and the analysed for Au and 36 elements including Zn, Cu, Pb, Ni, Co, Ag, Mn, As, Mo, Fe, Hg, V, Cd, Sb and Zn by leaching 1 gram of the sample with a HCl-HNO_3-H_2O (2:2:2 v/v) mixture at 95°C for one hour and then measuring the concentration of 37 elements in the diluted solution by ICPMS.

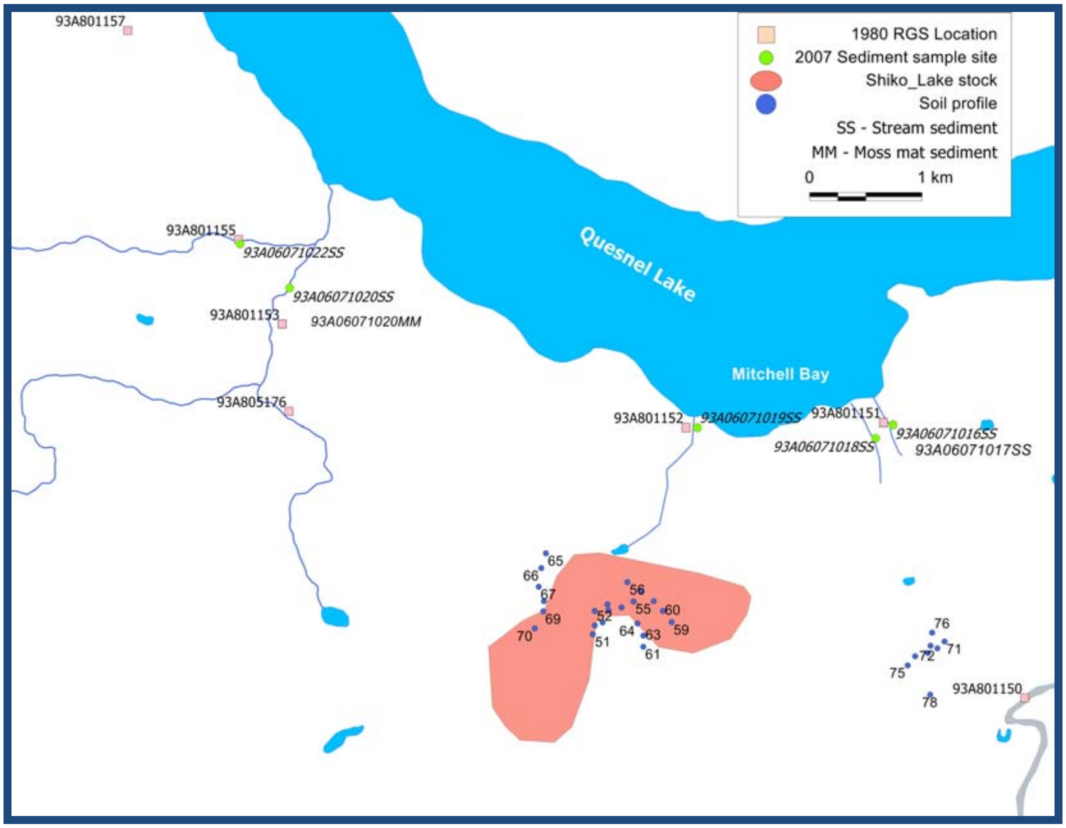

Figure: 3.4.12. Stream and moss mat sediment sample locations. The samples shown in italics were collected in 1980; the others were taken in 2007. A sample identification suffix ss indicates stream sediment and mm indicates moss mat sediment. The numbers are for the soil profiles. Geology from Massey et al. 2005.

	71016	**71017D**	***801151***	**71018S**	***801152***	**71019**	**71020**	**71020MM**	**71022**	***801155***	**93A_M**	**93A_3Q**	**NV_M**	**NV_3Q**
Ag_ppb	48	69	***100***	67	***100***	55	49	42	61	***100***	57	105	123	241
As_ppm	3.7	3.6	***3***	5.8	***3***	2.9	9.1	7.1	6.1	***4.5***	2.9	6.6	5.8	10.3
Au_ppb	0.7	0.6	***2***	0.7	***-1***	0.6	1.1	1.3	12.2	***8***	0.9	1.6	1.5	2.5
Bi_ppm	0.1	0.11	***nd***	0.08	***nd***	0.09	0.09	0.08	0.09	***nd***	0.15	0.25	0.1	0.14
Cd_ppm	0.25	0.36	***nd***	0.35	***nd***	0.16	0.18	0.15	0.28	***nd***	0.14	.32	0.4	0.8
Co_ppm	7.2	7.6	***7***	7.6	***8***	8.1	9.4	8.9	9.7	***7***	12.7	17	12.3	16
Cr_ppm	26.2	26.7	***nd***	26.6	***nd***	29.1	30	37.1	28.6	***nd***	29.9	44.8	42.4	64.6
Cu_ppm	28.85	49.97	***32***	26.2	***96***	20.31	20.59	18.98	39.64	***24***	24.95	36.5	32.7	48.8
Fe_%	1.76	1.8	***1.70***	2.03	***2.70***	1.99	2.21	2.4	2.21	***1.60***	2.48	3.16	2.48	3.03
Hg_ppb	40	57	***50***	46	***230***	217	29	34	64	***60***	35	55	47	68
Mn_ppm	388	566	***410***	1864	***1040***	596	509	567	723	***420***	449	679	618	856
Mo_ppm	0.32	0.41	***1***	0.6	***1***	0.4	0.48	0.43	0.57	***1***	0.51	0.95	1.0	1.9
Ni_ppm	17	18.7	***14***	15.7	***24***	18.4	19.7	19.1	21.7	***9***	30.5	42.7	30.2	42.8
Pb_ppm	5.44	5.77	***4***	4.72	***4***	5.09	5.19	4.85	5.66	***1***	7.1	12.4	5.9	7.9
Sb_ppm	0.38	0.62	***0.4***	0.51	***-0.2***	0.23	0.32	0.33	0.38	***0.2***	0.14	0.4	0.3	0.8
V_ppm	30	30	***nd***	41	***nd***	46	53	62	53	***nd***	29	49	47	70
Zn_ppm	38.8	43.3	***36***	50	***64***	41.1	42.1	42.4	53.8	***38***	56.3	74	59.5	84.4
pH	7.36		***8.7***	7.82	***8.7***	7.91	8.03		7.75	***8.4***				
F_W_ppb			***72***		***58***					***68***				

Table: 3.8. Stream and moss mat sediment chemistry. Data reported in italics prefix "80" are for the 1980 RGS samples analysed by an aqua regia digestion and AAS. Gold was determined by INAA. Values for samples prefix 7 are for the 2007 samples analysed for all elements by aqua regia digestion-ICPMS. A sample identification suffix s indicates a stream sediment and m a moss mat sediment. Values marked "-"are below detection limit and values marked "nd" were not determined. The columns labelled "93A_M" and "93A_3Q" are median and third quartile values calculated from 966 analyses of RGS samples collected in NTS 93A in 1980 (Jackaman, 1980). The columns labelled "NV_M" and "NV_3Q" are median and third quartile values calculated from 255 analyses of RGS samples collected in NTS 93A from rock draining Nicola Group rocks (uTrNC) in 1980.

In Table 3.8 data for seventeen common trace elements detected in the 2007 survey samples are compared to the chemistry of the 1980 RGS samples. Median and third quartile values for each element calculated from RGS data for NTS 93A (Jackaman, 1999) and for streams in NTS map sheet 93A that drain Nicola Group rocks are also included in the table as a guide to geochemical backgrounds. Samples 71016 and 71017 were collected at the same site and for some elements (e.g. Cu, Ag) there is a substantial difference between the amounts measured in the two samples. This disparity could reflect a sample that is largely sand (less than 0.18 mm size) rather than finer silt clay deposited in the high energy, steep gradient stream channel. Most elements have concentrations in the median to "upper fence" range and only Hg appears anomalous in both 1980 and 2007 samples. Copper in anomalous in the original RGS sample but only background levels were found in the 2007 sample from the steam draining the Shiko Lake North mineralized zone.

	71017	**71018**	**71019**	**71020**	**71020D**	**71022**
Al_water_ppb	2	1	5	8	17	8
As_water_ppb	-0.5	-0.5	-0.5	1.7	1.9	0.6
B_water_ppb	21	15	72	18	19	17
Ba_water_ppb	6.25	10.68	8.21	20.61	20.78	9.54
Ca_water_ppb	66273	68179	45778	32560	32329	31072
Ce_water_ppb	-0.01	-0.01	0.01	0.02	0.06	0.01
Cu_water_ppb	0.5	0.2	1.2	1.5	1.7	1.4
Fe_water_ppb	-10	-10	-10	16	31	-10
K_water_ppb	680	897	860	1106	1151	531
Li_water_ppb	0.5	0.8	0.3	0.7	0.9	0.4
Mg_water_ppb	5999	6846	5888	11718	11693	5715
Mn_water_ppb	0.44	0.18	0.9	2.76	3.12	1.65
Mo_water_ppb	0.3	0.7	0.7	1.3	1.3	0.9
Na_water_ppb	3333	3116	3818	8063	8382	5549
Ni_water_ppb	-0.2	-0.2	-0.2	0.3	0.9	-0.2
P_water_ppb	43	38	52	48	42	60
Pb_water_ppb	-0.1	-0.1	0.1	-0.1	0.4	-0.1
S_water_ppb	8	6	4	3	3	7
Se_water_ppb	-0.5	-0.5	-0.5	-0.5	-0.5	0.5
Si_water_ppb	5212	5204	6046	4363	4426	4095
U_water_ppb	0.14	0.25	0.14	0.19	0.54	0.11
V_water_ppb	-0.2	-0.2	0.2	0.2	0.2	0.5
Zn_water_ppb	1.3	0.8	2.3	1.3	1.4	-0.5
pH	7.36	7.82	7.91	8.03	8.03	7.75

Table: 3.9. Element values listed in the Table 3.9 are for elements measured by ICP-MS in filtered, acidified (HNO_3) stream water samples. Silver, Be, Bi, Cd, Cr, Co, Te, Ti, Tl, Sb, and W values are all below instrument detection limit and are not reported in the Table.

Table 3.9 shows elements detected in filtered, acidified stream water samples by ICPMS. Weakly alkaline stream water draining the Shiko Lake north mineralized zone has concentrations of pathfinder metals (e.g. As, Cu, Mo, Pb, Zn) that are all below 3 ppb. Metals are slightly higher in the water from larger streams draining the area north west of the Shiko Lake property.

Shiko Lake Geochemistry

Element Associations

Element associations with the Shiko Property soil geochemical data that are indicated by high positive correlations coefficient (> +0.8 or – 0.8) tested for significance with scatter plot graph are:

F-H: Horizon: (1) Ni-V-Mg-Sc-Cr; (2) La-Nd-Sm-U;

Upper B Horizon: (1) Fe-Co-P-Ti-V; (2) Ce-Hf

Lower B Horizon: (1) Ba-Al; (2) Co-Cu; (3) Sr-Hg (4) Ca-V-Sr

C horizon: (1) Nd-La-Lu-Th-Sm (2) Au-Cu (3) V-Ti

Soil Horizon Geochemical Comparisons

Figure 3.4.13 shows a consistent Cu increases from the F-H through the upper B and Lower B into the C horizon although this may, in part, reflect the finer grain size (<0.063mm) of the C samples analysed. The highest Cu detected (> 1000 ppm) occurs as outlier values in the B soil horizon although there are also several > 100 ppm in the F-H horizon. Zinc values typically show little variation down soil profiles.

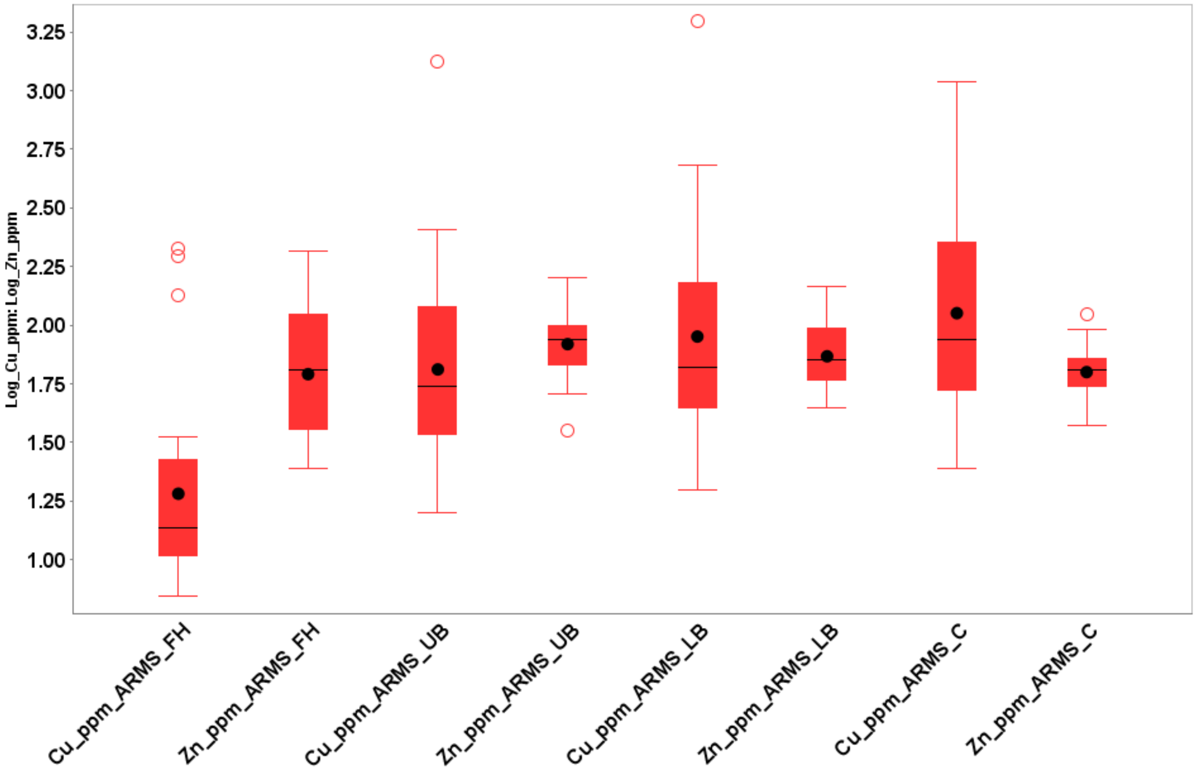

Figure: 3.4.13. Box box plot for Cu and Zn by aqua regia-ICPMS data in 28 soil samples from the C, lower B, Upper B and F-H horizons.

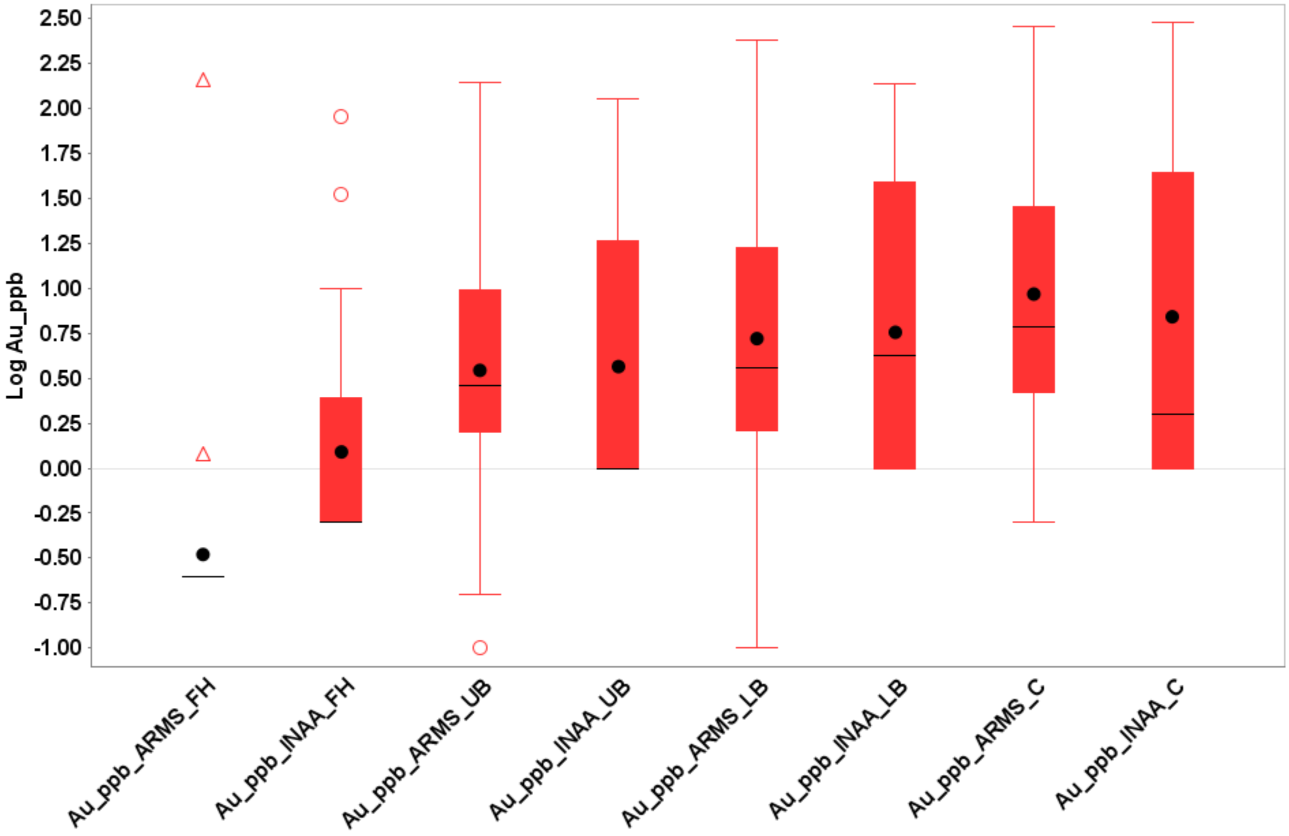

Figure: 3.4.14. Box plot for Au by INAA and by aqua regia_ICPMS in 28 soil samples from the C, lower B, Upper B and F-H horizons.

Figures 3.4.14 shows variation of Au by aqua regia-ICPMS and by INAA in the soil. Gold also increases with depth in soil profiles although there are more extreme INAA Au outliers in the FH horizon than in the mineral horizons. Both methods detect more than 90 ppb Au in all soil horizons. Nickel and V (Figure 3.4.15) variation is similar to Cu in that both elements increase with depth in the soil. While Mo medians, shown in Figure 3.4.17 decrease with depth in the soil from the F-H horizon, the maximum values increase to the C horizon.

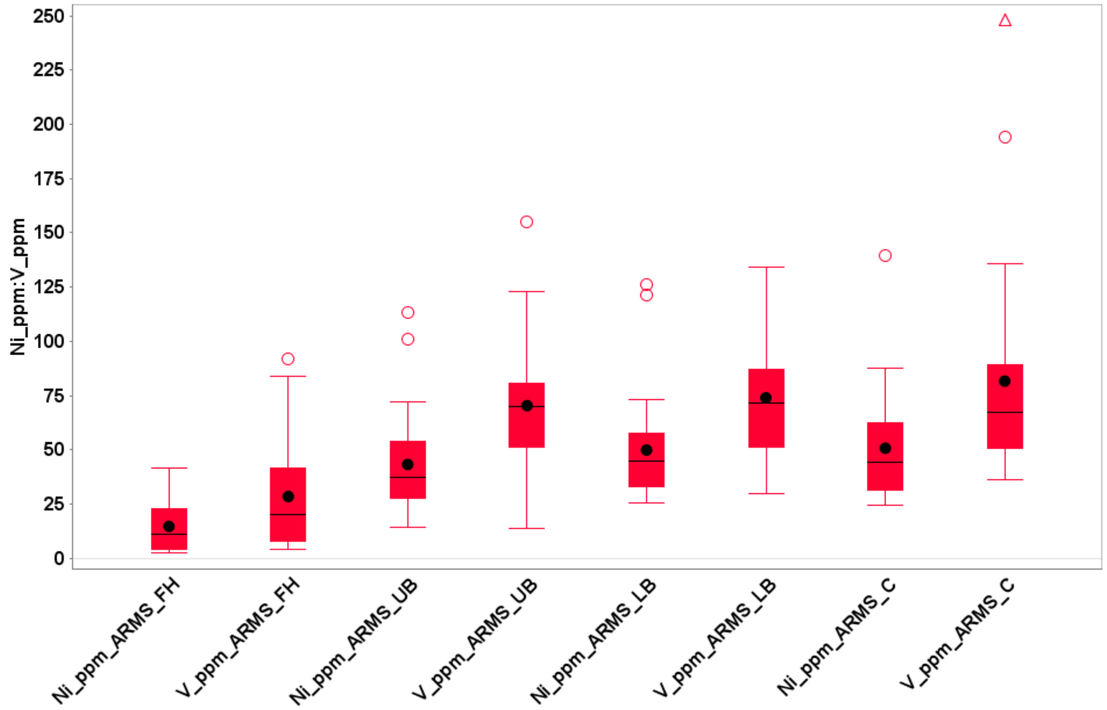

Figure: 3.4.15. Box plot for Ni and V by aqua regia-ICPMS in 28 soil samples from the C, lower B, Upper B and F-H horizons.

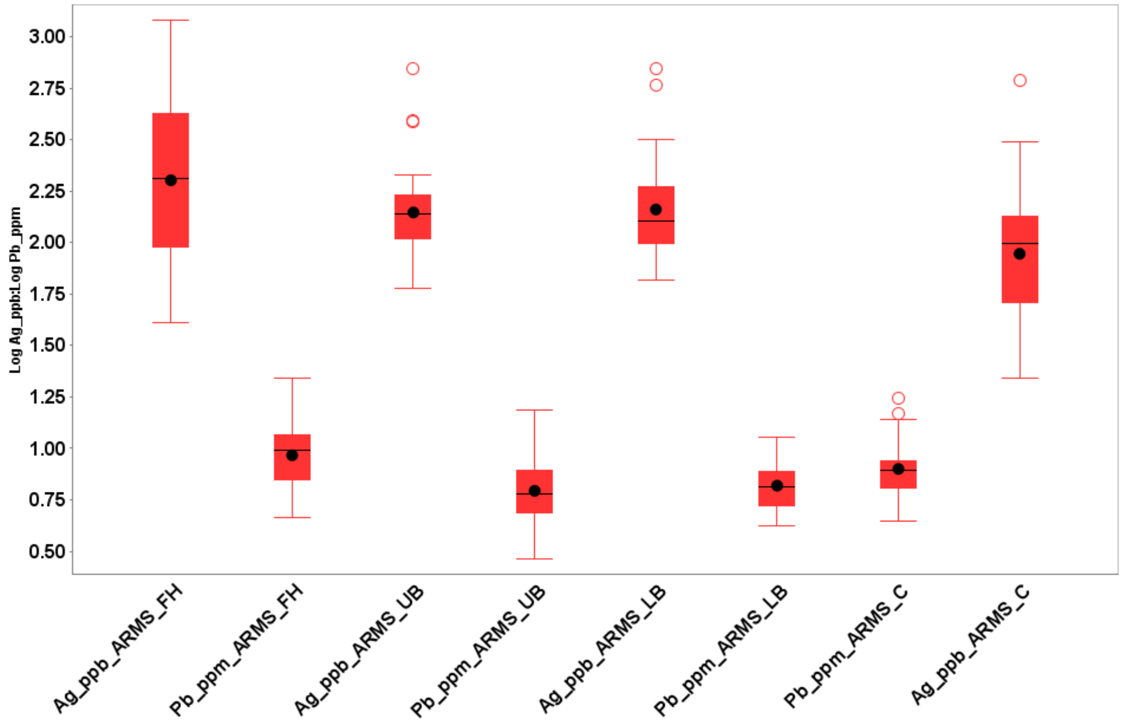

Figure: 3.4.16. Box plot for Ag and Pb by aqua regia-ICPMS in 28 soil samples from the C, lower B, Upper B and F-H horizons.

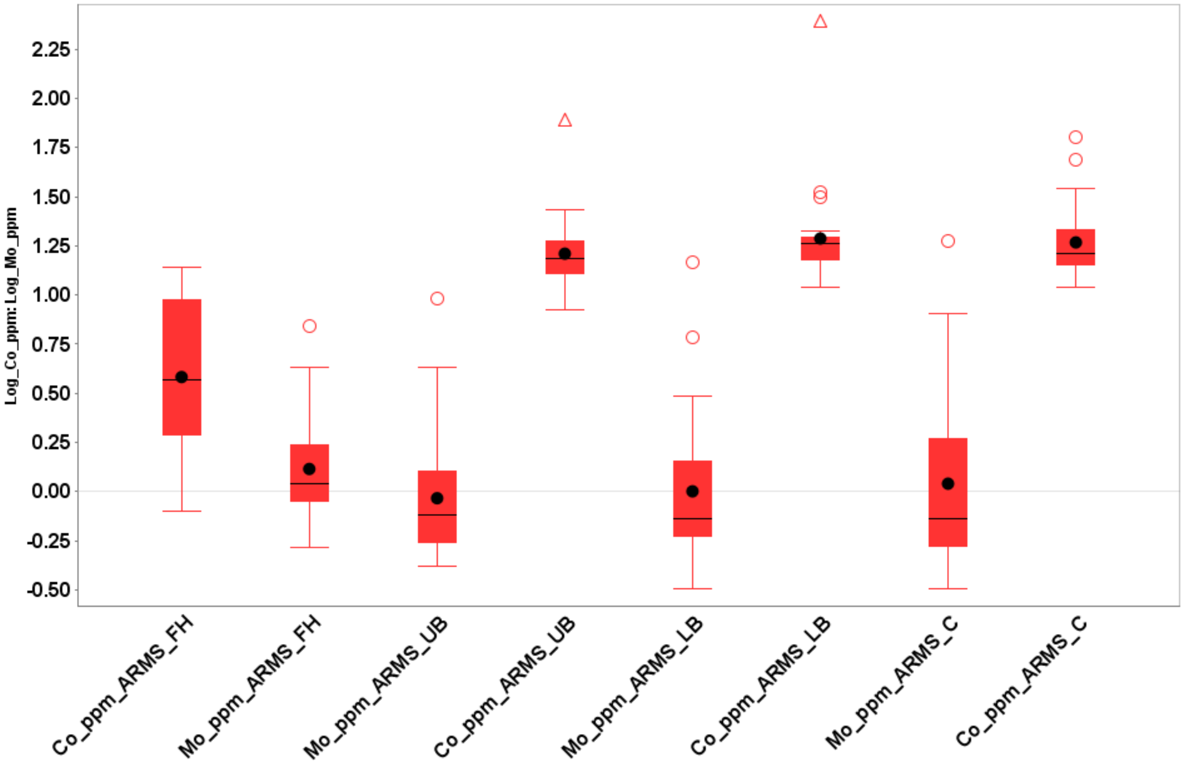

Figure: 3.4.17. Box plot for Mo and Co by aqua regia-ICPMS created in 28 soil samples from the C, lower B, Upper B and F-H horizons.

Figure 3.4.16 shows that Ag and Pb medians and means decrease from the F-H into the C horizon in contrast to Cu and Au patterns. V and Ni soil geochemistry, shown in Figure 3.4.10 and 3.4.11, resemble Cu although medians, quartiles and ranges are similar for all three of the mineral horizons. While Mo, shown in Figure 3.4.17 tends to be decrease with depth from the F-H horizon there are high outlier values in the mineral soil horizons. Cobalt, also shown in Figure 3.4.17 follows the more common trend of increase with depth displayed by Cu, Ni, Au and V in the soil. Figure 3.4.18 shows the variation of Cu, and Au in B soil horizon samples determined by MMI^{TM}, Bioleach^{SM} and Enzyme leach^{SM} partial extration methods. Bioleach^{SM} and MMI^{TM} extract similar amounts of Cu from the soil, but more Au is liberated by MMI^{TM} compared to bioleach. In Figure 3.4.19 MMI^{TM} liberates higher Ag compared to Co.

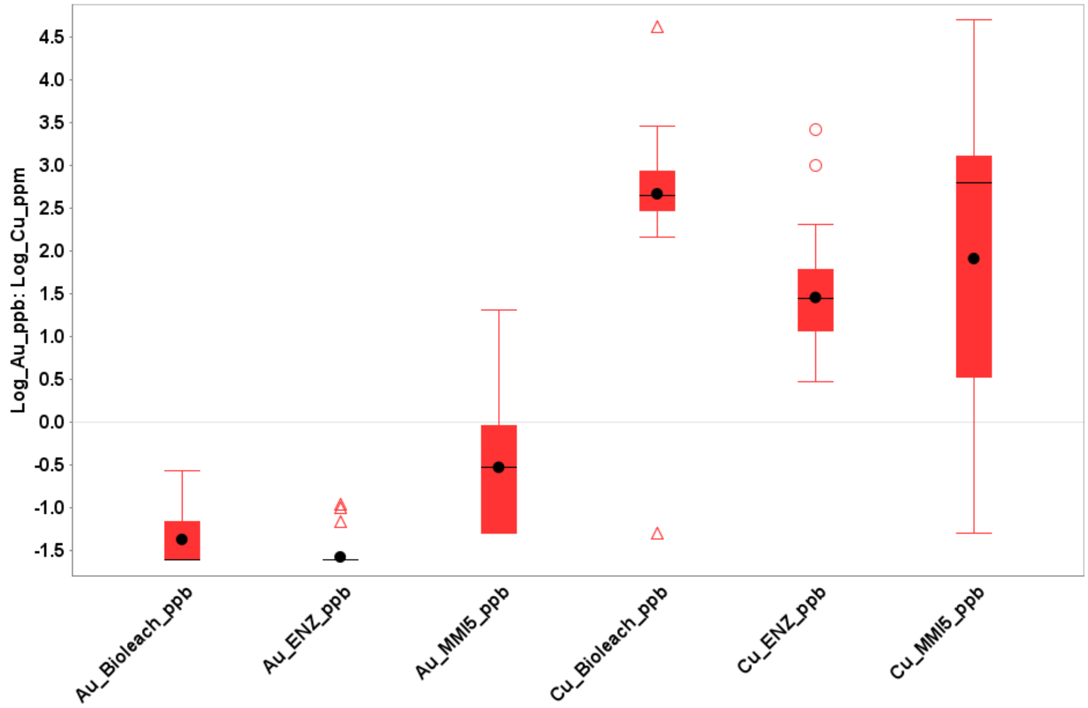

Figure: 3.4.18. Box plot for Cu and Au extracted with mobile metal ion (MMI), Bioleach and Enzyme leach from B soil horizon samples.

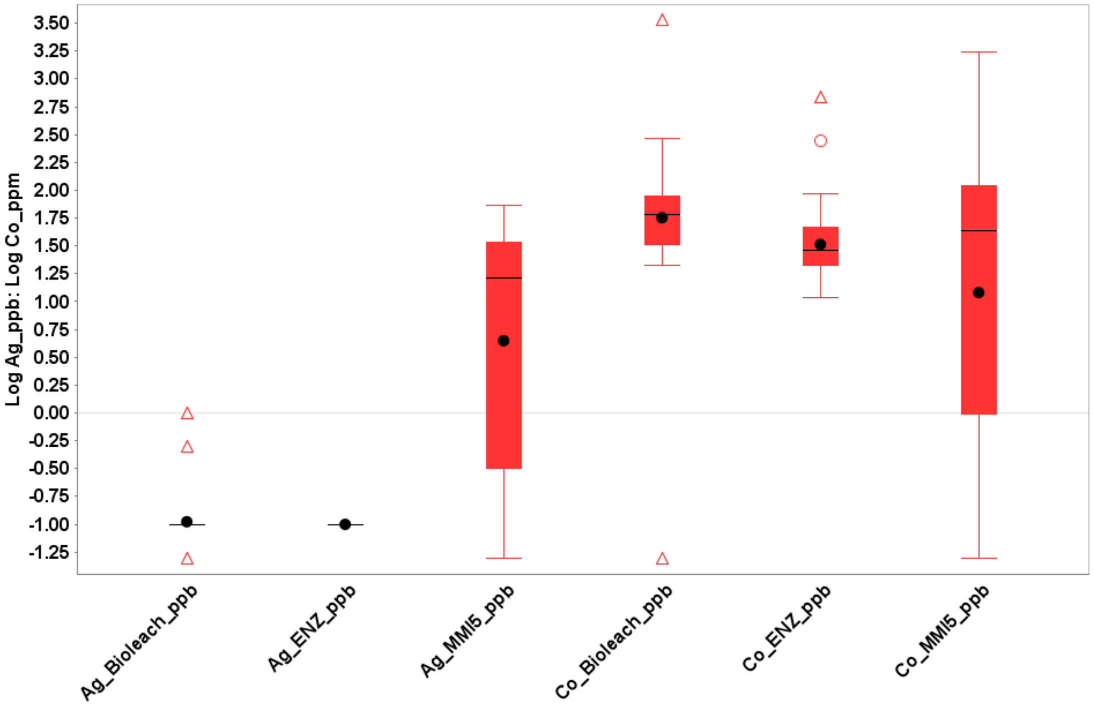

Figure: 3.4.19. Box plot for Co and Ag extracted with mobile metal ion (MMI), Bioleach and Enzyme leach from B soil horizon samples.

Geochemical differences among soil horizons

A two sample t-test determines if there is a statistical difference at the 0.05 percent significance level between population means for the pathfinder elements Au, Ag, As, Cu, Co, Hg, Mn, Mo, Ni, Pb, V, Zn by ICPMS and Br, Cr, Fe by INAA in the F-H horizon compared to the upper B horizon, the upper B horizon compared to the lower B horizon and the lower B horizon compared to the C soil horizon. The t test is determines if there is a statistical difference at the 0.05 percent significance level between population means for loss on ignition (LOI), pH and elements by Leach^{SM} and Bio Leach^{SM} and MMI^{SM} in the upper B soil horizon compared to the lower B horizon. All of values (except Fe) were log transformed and an F-test applied before the t test to establish if the variance of populations was equal or unequal. Figure 3.4.20 summarises the results of the t-test and reveals that there is a difference (at the 0.05 significance level) between population means for all elements except Ag and Mo in the F-H horizon tested against Ag in the upper B-horizon. However, there is no significant difference between populations means for upper B soil horizon elements, LOI and soil pH compared to lower B soil horizon. The t test for lower B soil horizon chemistry compared to the C-soil horizon chemistry identified the Ag, As, Mn and Zn populations as having significantly different means.

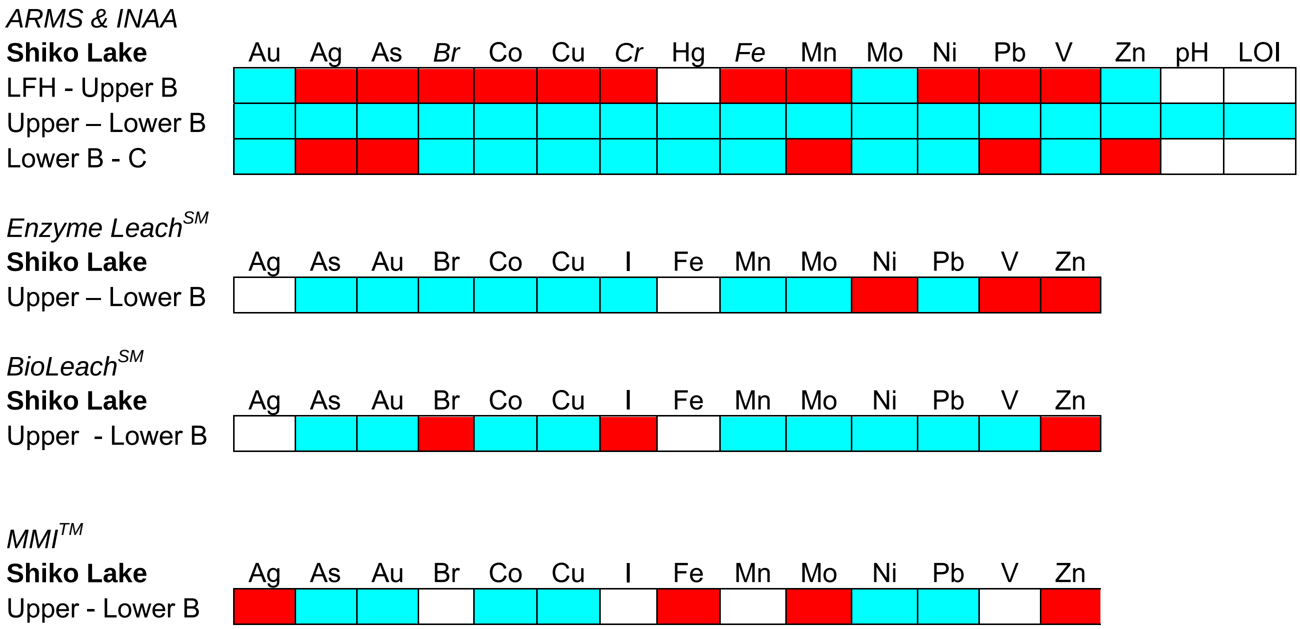

ARMS & INAA

Shiko Lake	Au	Ag	As	*Br*	Co	Cu	*Cr*	Hg	*Fe*	Mn	Mo	Ni	Pb	V	Zn	pH	LOI
LFH - Upper B	🟦	🟥	🟥	🟥	🟥	🟥	🟥		🟥	🟥	🟦	🟥	🟥	🟥	🟦		
Upper – Lower B	🟦	🟦	🟦	🟦	🟦	🟦	🟦	🟦	🟦	🟦	🟦	🟦	🟦	🟦	🟦	🟦	🟦
Lower B - C	🟦	🟥	🟥	🟦	🟦	🟦	🟦	🟦	🟦	🟥	🟦	🟦	🟥	🟦	🟥		

Enzyme Leach^{SM}

Shiko Lake	Ag	As	Au	Br	Co	Cu	I	Fe	Mn	Mo	Ni	Pb	V	Zn
Upper – Lower B		🟦	🟦	🟦	🟦	🟦	🟦		🟦	🟦	🟥	🟦	🟥	🟥

BioLeach^{SM}

Shiko Lake	Ag	As	Au	Br	Co	Cu	I	Fe	Mn	Mo	Ni	Pb	V	Zn
Upper - Lower B		🟦	🟦	🟥	🟦	🟦	🟥		🟦	🟦	🟦	🟦	🟦	🟥

MMI^{TM}

Shiko Lake	Ag	As	Au	Br	Co	Cu	I	Fe	Mn	Mo	Ni	Pb	V	Zn
Upper - Lower B	🟥	🟦	🟦		🟦	🟦		🟥		🟥	🟦	🟦		🟥

Figure 3.4.20: Summary of a t-test applied to establish if there is a difference at the 0.05% significances level for Au, Ag, As, Br, Co, Cu, Cr, Hg, Fe, Mn, Mo, Ni, Pb, V and Zn means in the F-H horizon compared to the upper B soil horizon, the upper B compared to lower B soil horizon and the lower B horizon compared to the C soil horizon by aqua regia_ICPMS and by INAA (INAA determined elements are in italics). Also shown are results of a t-test for pH and loss on ignition (LOI) in the upper B horizon compared to the lower B horizon and elements determined by mobile metal ion (MMI)^{TM}, Enzyme Leach^{SM} and BioLeach^{SM} in the upper B horizon compared to the lower B horizon. A red square indicates that there is a significant difference at the 0.05 significance level between the means. A blank square indicates that there were either insufficient values above detection limit for a test to be applied or that the element was not measured.

A t-test applied to the population means of Enzyme Leach^{SM}, BioLeach^{SM} and MMI^{SM} extracted Ag, Au, As, Br, Cu, I, Fe, Mo, Mn, Pb, V and Zn from upper B horizon soils compared lower B horizon soils shows that there is no significant difference for most of the elements including Au and Cu and only Zn by the three methods shows is consistently different.

Figure 3.4.20 might imply that where there is a significant geochemical difference between two horizons then the element patterns in each horizon are unrelated to each other. Ideally, the geochemistry of each horizon should be interpreting a link to a mineral source. In practice, there is more often a statistical correlation between soil horizon geochemistry more clearly revealed by the scatter plot for element values in one horizon plotted against another. For example, Figure 3.4.21 is a scatter plot for Cu in C horizon samples from Shiko Lake plotted against Cu values in lower B horizon samples. Except for one “anomalous” value there is an obvious sympathetic relationship between Cu in the two horizons. However, a strong, positive correlation between the lower B and upper B horizon Cu values shown in Figure 3.4.22 might only reflect a single high value and in the case of the upper B – F-H horizon comparison (Figure 3.4.23) there is some evidence of a negative correlation between the upper B – F-H horizon Cu values. Gold (by INAA) illustrates the caution needed when applying a statistical test to compare populations. Figures 3.4.24 to 3.4.26 are scatter plots showing the relationship between Au in the four horizons sampled at Shiko Lake. While there is some evidence of a C – lower B horizon correlation in Figure 3.2.24, the association is weaker between lower B and upper B (Figure 3.4.25) and an almost random scatter of values for upper B Au compared to F-H horizon Au (Figure 3.4.26). The disparity between t-test results and scatter plot in-horizon association for Au is most likely due to the large number of Au values that are below detection limit. Keeping in mind that Cu is a geochemically mobile element whereas as Au is not mobile except under conditions of extreme weathering (Mann, 1983), the scatter plots show that the C and Lowe B horizons can be treated as a similar sample medium, whereas the upper B and F-H horizon should be considered separately when sampling.

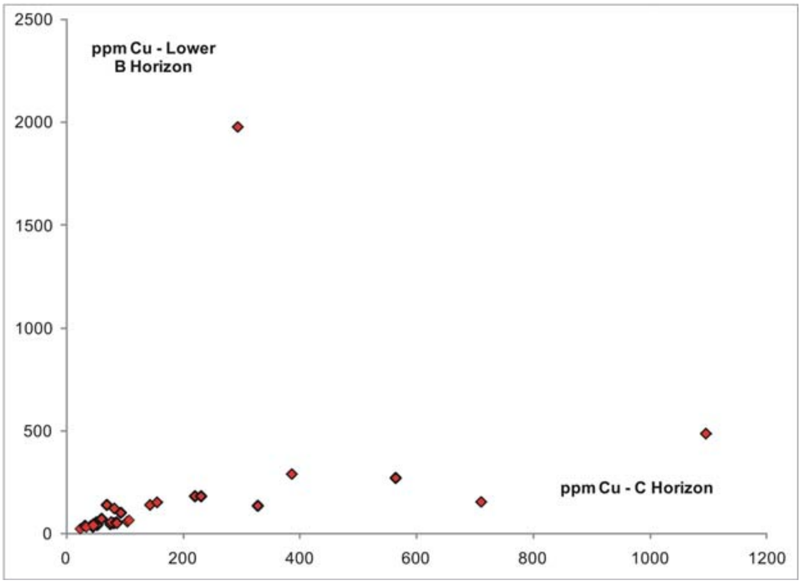

Figure: 3.4.21. Scatter plot of Cu in C horizon samples versus Lower B soil Horizon samples.

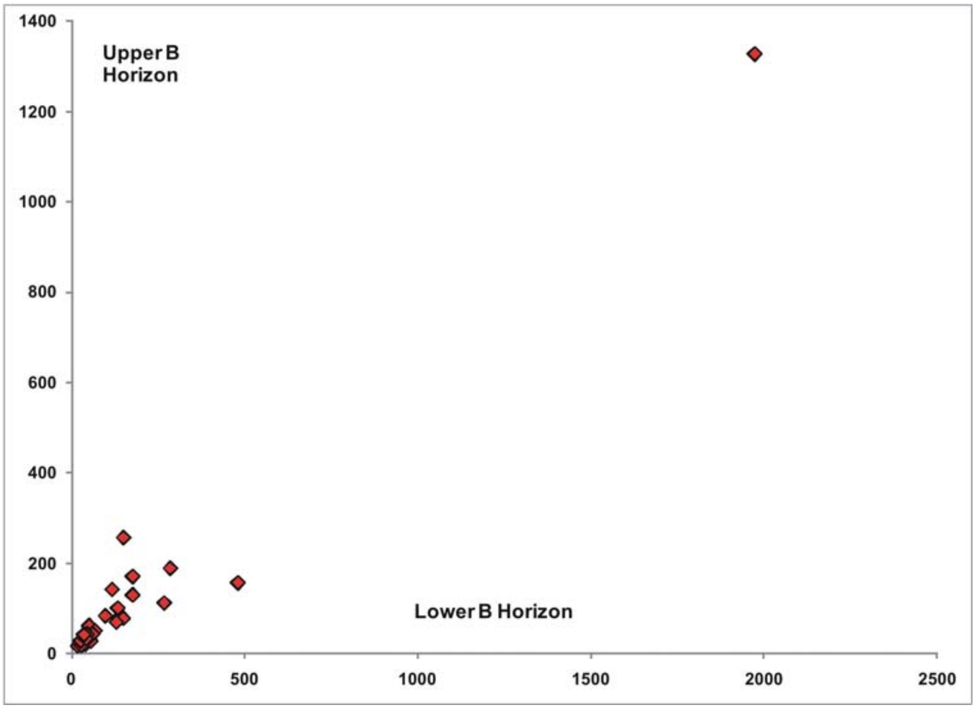

Figure: 3.4.22. Scatter plot of Cu in Upper B horizon samples versus Lower B soil Horizon samples.

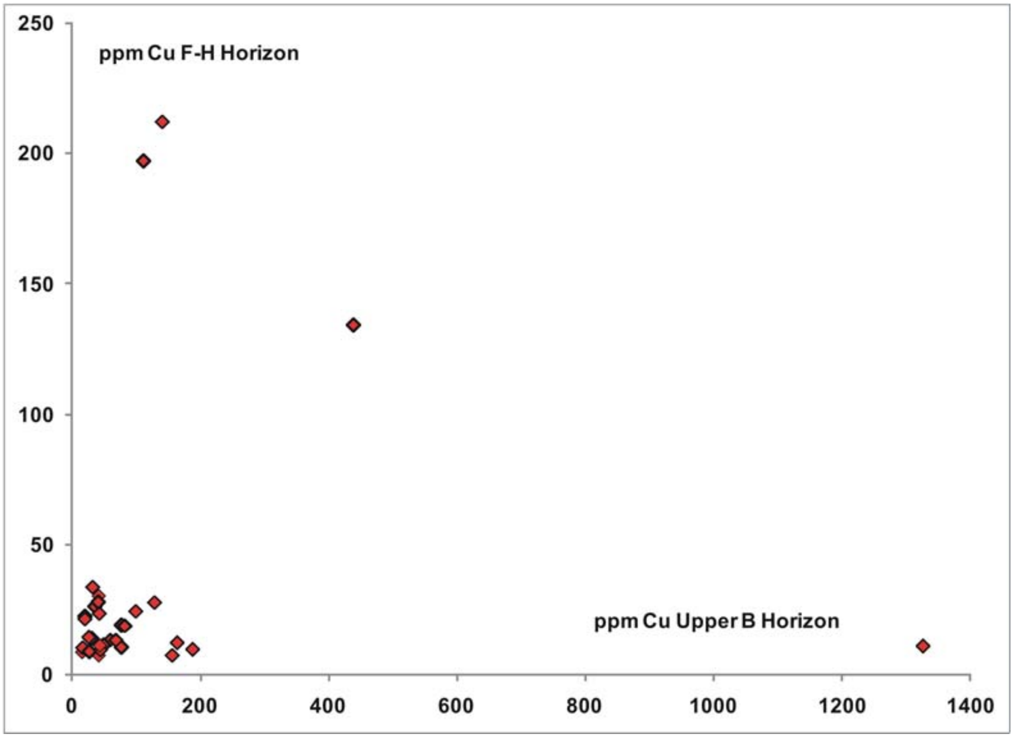

Figure: 3.4.23. Scatter plot of Cu in Upper B horizon samples versus F-H soil Horizon samples.

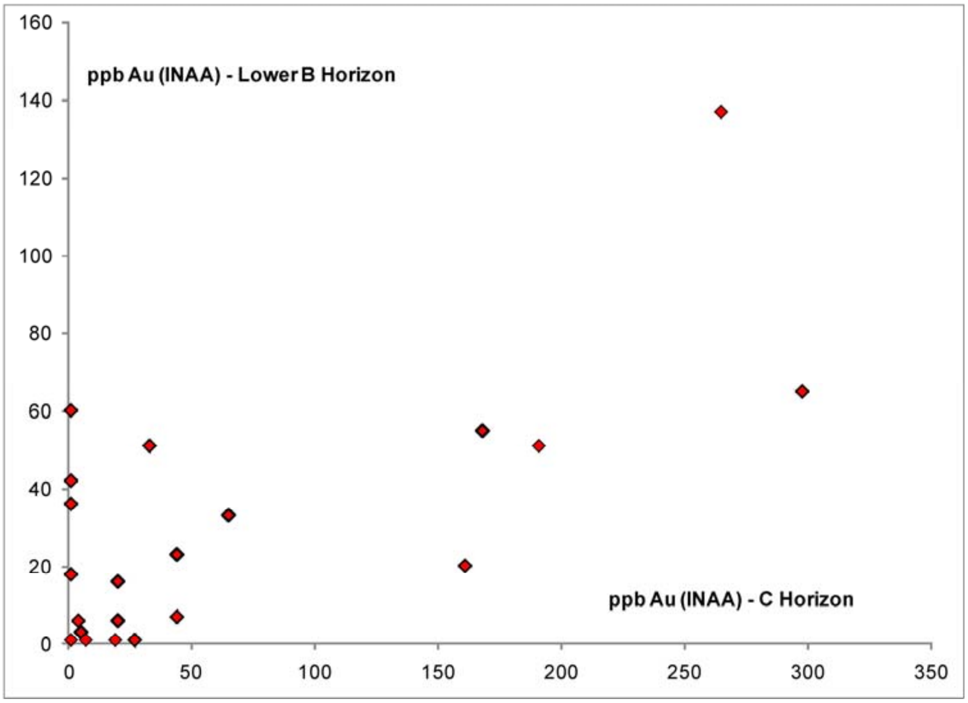

Figure: 3.4.24. Scatter plot of Au in C horizon samples versus Lower B soil Horizon samples.

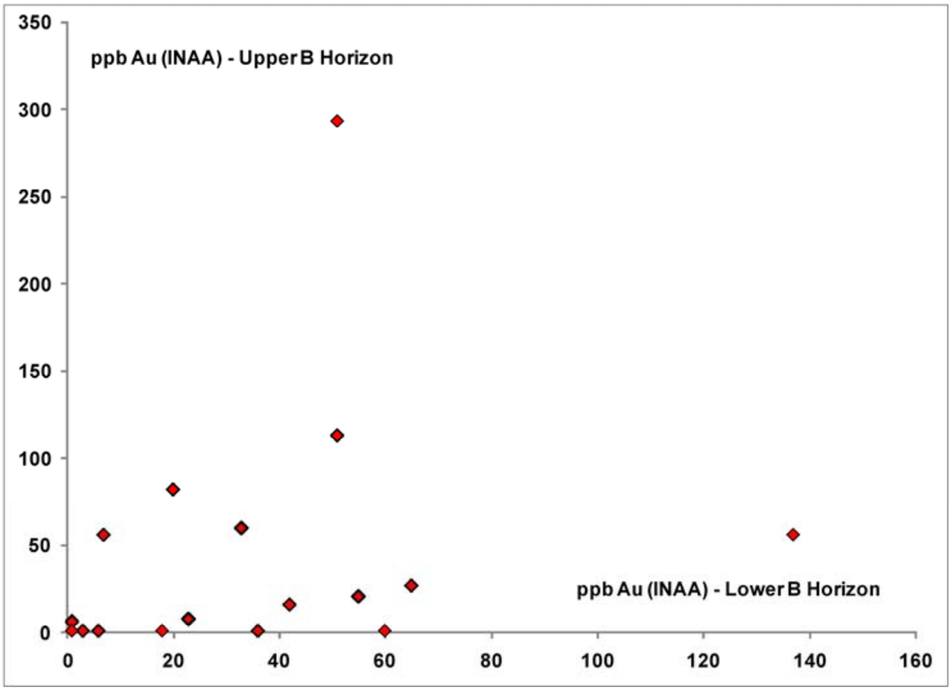

Figure: 3.4.25. Scatter plot of Au in Upper B horizon samples versus Lower B soil Horizon samples.

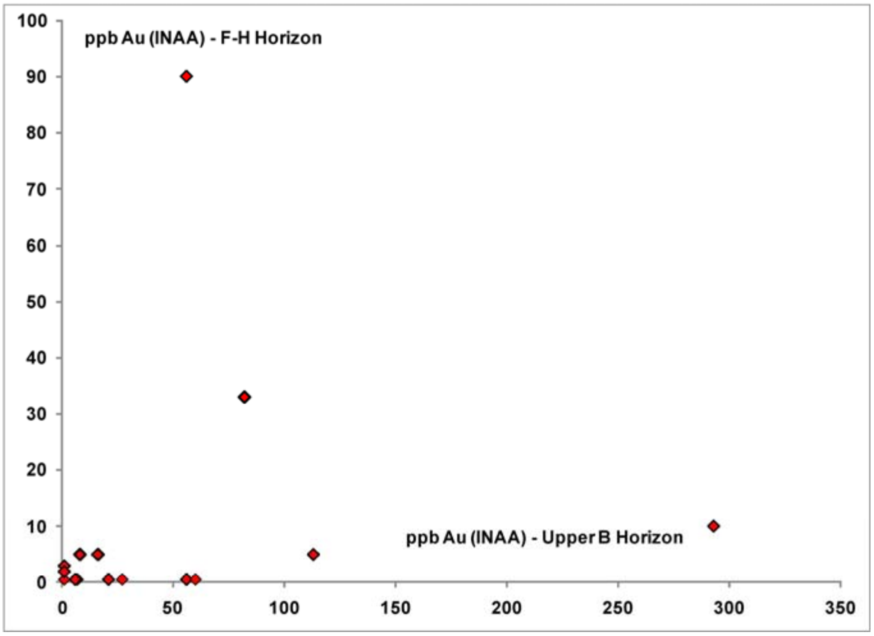

Figure: 3.4.26. Scatter plot of Au in Upper B horizon samples versus F-H soil Horizon samples.

Soil Sampling Results

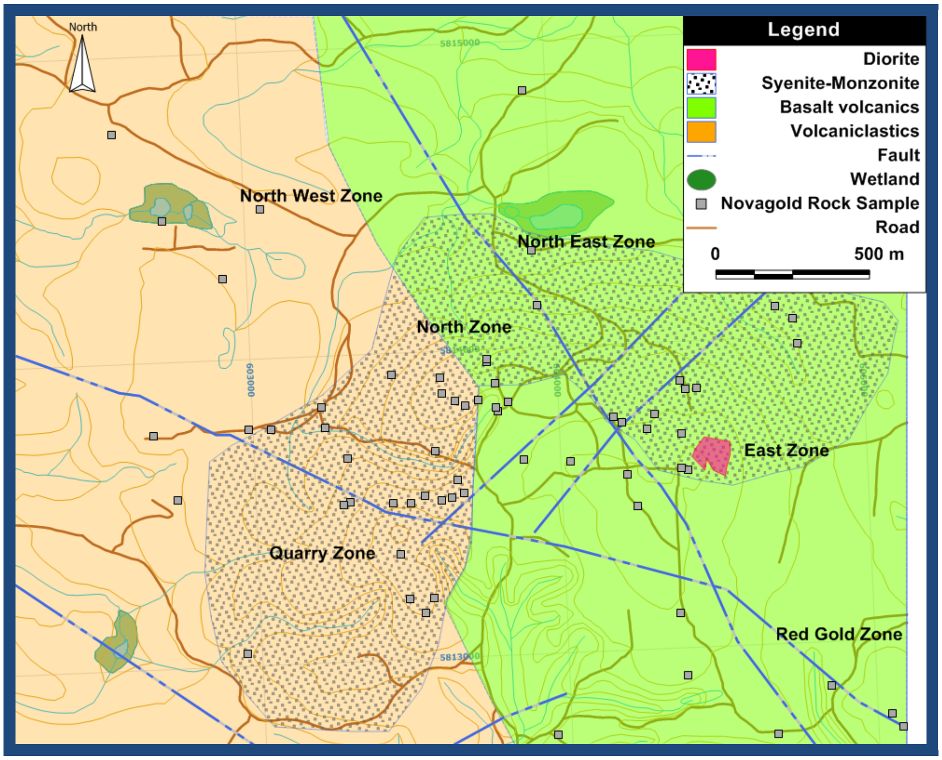

Figure: 3.4.27a. NovaGold soil samples and BCGS Profiles in the NW, N and NE zones.

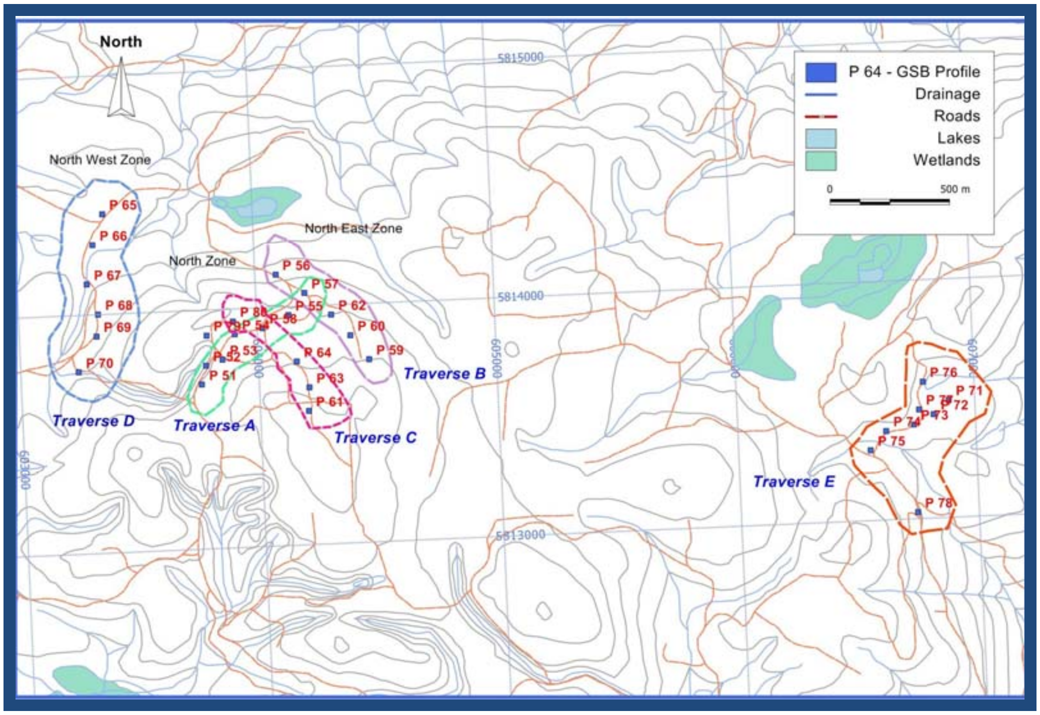

Figure: 3.4.27b.Sample Traverse locations and Profiles including Traverse E.

Figure 3.4.27**a** shows sample profiles and Novagold soil sample sites across the North West, North and North East mineralized zones on the Shiko Lake property and Figure 3.4.27**b** identifies the five Profile samples traverses including Traverse C in the area of the East Pb-Zn mineralized zone.

Traverse A: Traverse A, shown in Figure 3.4.27b, is close to a contract between basalt and the monzonite-diorite intrusive that is covered by till and colluvium. There are traces of chalcopyrite and pyrite in outcrop close to Profiles 79 and 80 and samples of rock ranging from diorite to feldspar porphyry that were collected by Petsel, (2006), have up to 1285 ppb Au, 0.445% Cu and 14 ppm Mo. In this area there is generally less than 1 metre of glacial sediment and soil above bedrock. Profiles 58 to 61, however, penetrate soil developed on a sandy till that ranges from more than 1 to less than 0.5 metre thick above basaltic bedrock. Ideally, the soil geochemistry in the profile samples along Traverse A should be a reasonably good reflection of Cu-Au sulphide mineralization given a close proximity to Cu-Au mineralized bedrock and a variable drift thickness from colluviums near Profile 79 to thicker till at Profile 51. In the soil the highest Cu is in the C horizon at 58 with values above 700 ppm. Figure 3.4.28 shows that there are lower Cu values in B and F-H horizon samples and that the C horizon geochemistry is best reflected in the Lower B, Upper B and F-H horizon variations of soil at Profile 58. Figure 3.4.29 shows Cu by MMI^{TM}, Enzyme Leach^{SM}, BioLeach^{SM} and aqua regia-ICPMS analysis in Lower B horizon samples. Figures 3.4.28 and 29 show similar Enzyme Leach^{SM}, BioLeach^{SM} Cu patterns especially where values peak at Profile 58 whereas MMI^{SM} Cu variation is closer Cu by aqua regia-ICPMS in Lower B horizon samples and there is no obvious increase at Profile 58. The highest B horizon MMI^{TM} Cu values are at Profile 79 and MMI^{TM} Cu displays the most Cu anomaly contrast of all the methods. The MMI^{TM} Cu is therefore a strong indicator of Cu-Au mineralization assuming that samples from Profiles 79 and 80 are near bedrock. Both Lower B and Upper B horizon soil samples from profiles along Traverse A have been analysed for metals, including Cu, by MMI^{SM}, Enzyme Leach^{SM}, BioLeach^{SM} and the results are shown in Figure 3.4.30. The Lower B horizon Cu MMI^{SM} patterns reflect upper B horizon Cu MMI^{SM} patterns, but anomaly contrast is clearly larger for Lower B horizon Cu MMI^{SM} determinations. Similarly, Lower B horizon BioLeach ^{SM} Cu patterns reflect upper B horizon Bioleach ^{SM} Cu patterns, but again, anomaly contrast is clearly greater in the Lower B horizon chemistry.

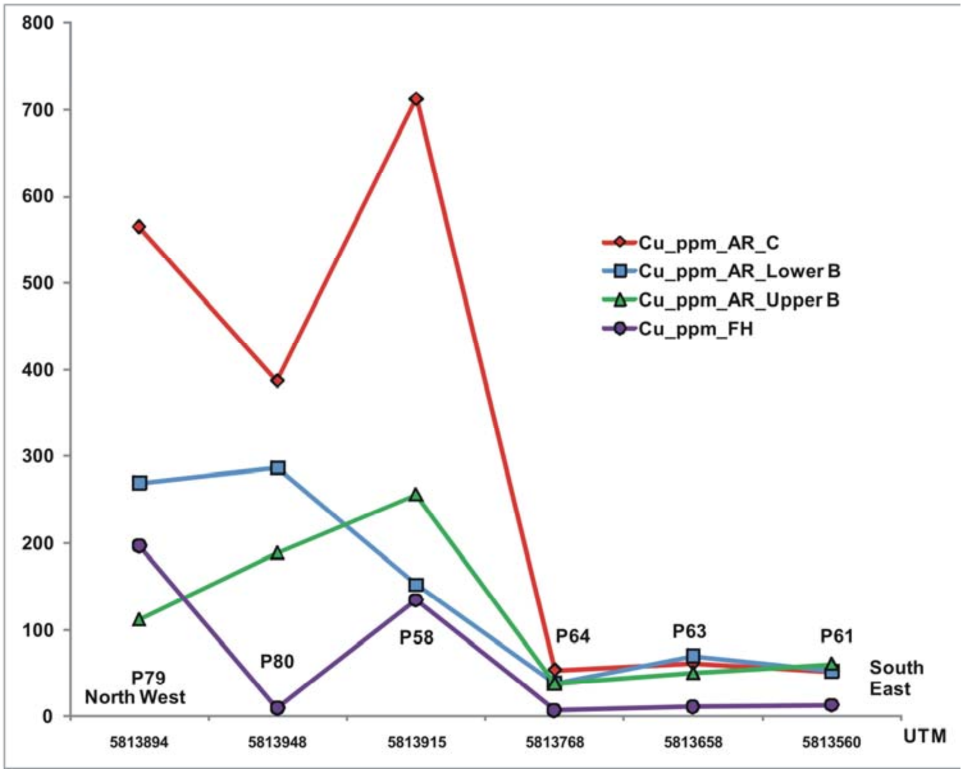

Figure: 3.4.28. Copper by aqua regia-ICPMS along Traverse A

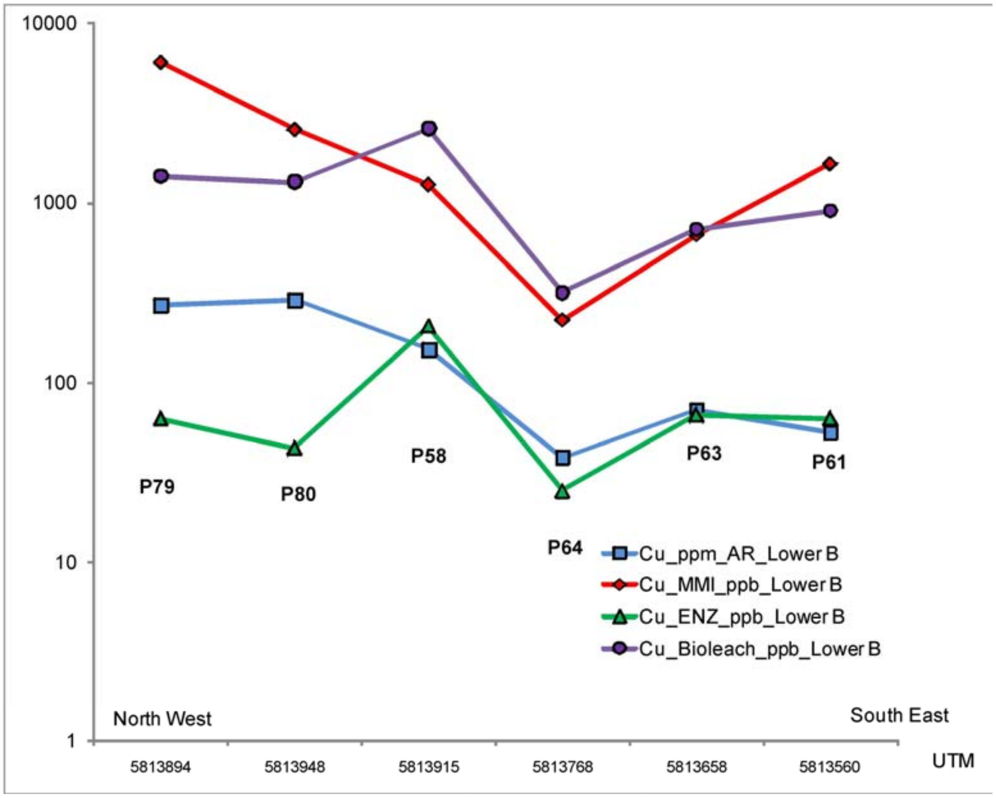

Figure: 3.4.29. Copper by aqua regia-ICPMS and partial leaches along Traverse A

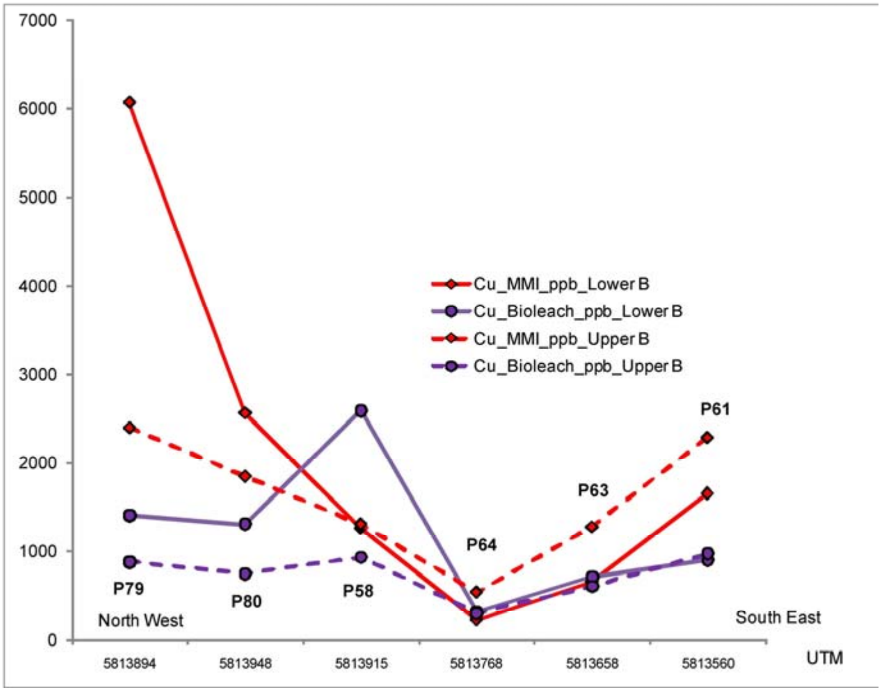

Figure: 3.4.30. Upper and Lower B Horizons Cu by MMI™ and Bioleach℠ along Traverse A.

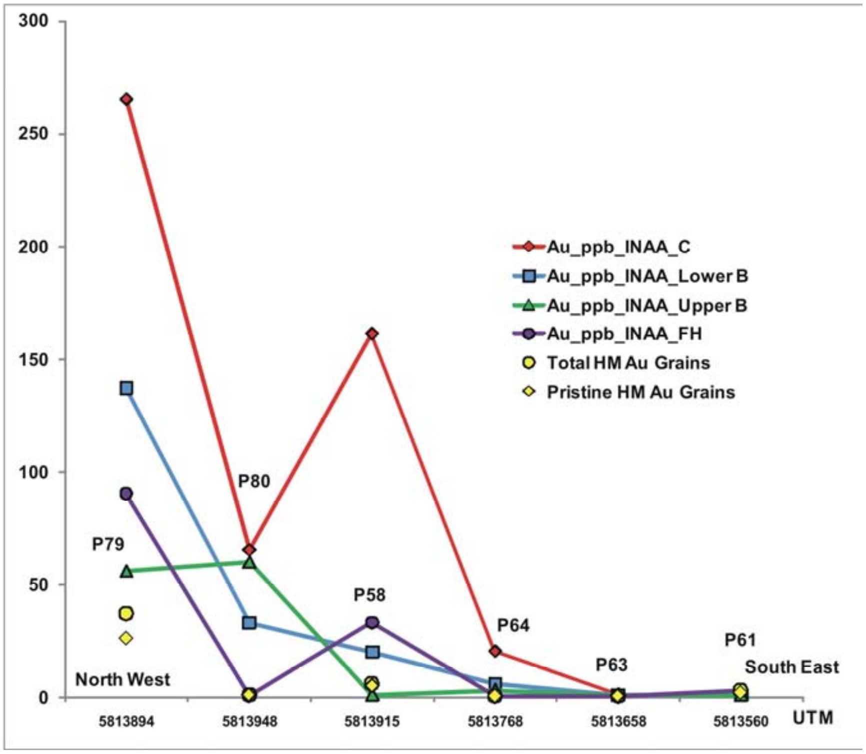

Figure: 3.4.31. Gold by INAA and HM Au grains along Traverse A.

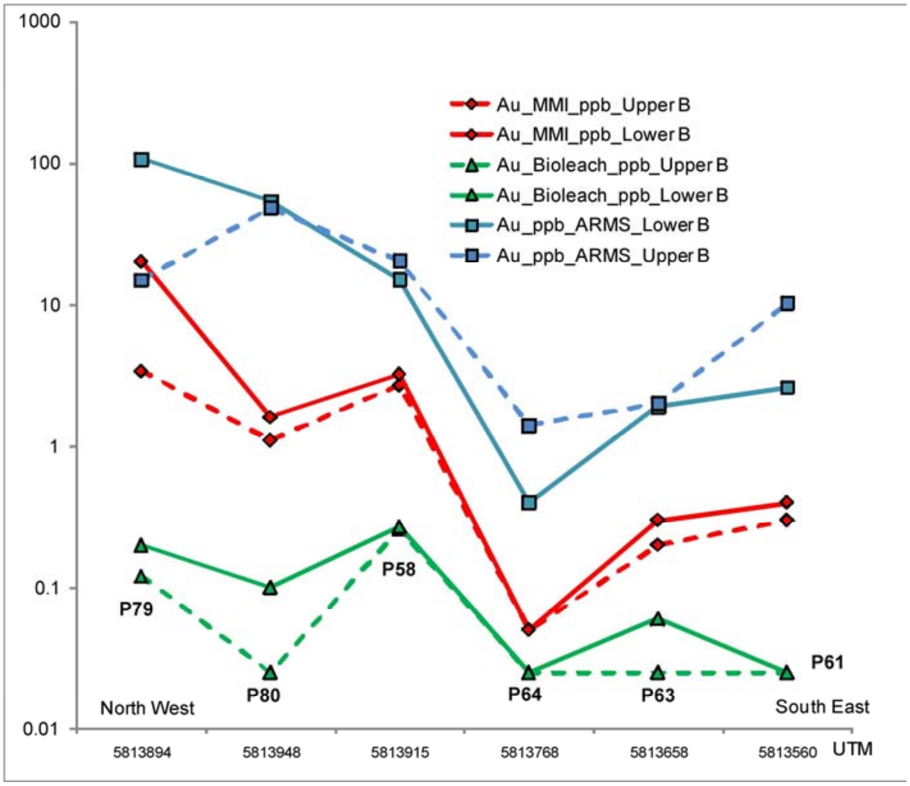

Figure: 3.4.32. Upper and Lower B horizon Au by aqua regia-ICPMS, MMI^{TM} and BioLeach^{SM}

Figure 3.4.31 shows variation of Au by INAA along Traverse A. Highest Au detected is in the C horizon soil at Profile 79 where there is 265 ppb Au, but lower values in B and F-H horizon samples. There are 37 Au grains in the C horizon heavy mineral concentrate of which more than 50 percent are described as “pristine” suggesting a near-by source for the Au particles. A smaller Au peak at Profile 58 has 6 grains in the C horizon, but of these grains 5 are “pristine”. Gold content falls below detection level in the soil south in Profiles 63 and 61. Figure 3.4.32 compares MMI^{TM} Au, BioLeach^{SM} Au and aqua regia-ICPMS Au in Upper and Lower B soil horizon samples. MMI^{TM} Au contrast is greatest in the Lower B horizon followed by aqua regia-ICPMS Au contrast and then BioLeach^{SM} Au contrast. Although BioLeach^{SM} Au contrast is smaller the Au variation detected by the two different partial leach methods is similar. Silver in Figure 3.4.33 is generally lower in the F-H horizon compared to B and C horizons, except at Profile 79 where there is a higher Ag in the F-H horizon. Silver values in the F-H horizon along Traverse A display a “low” at Profile 58 with increasing values towards the North West and South East. By contrast, there are higher Ag values in the C horizon at Profile 80 where the content decreases in the order C-Ag> F-H Ag> Upper B Ag > Lower B Ag. There are higher MMI^{TM} Ag values in lower B horizon samples from Profiles 79 and 80 compared to the Upper B MMI^{SM} Ag values, but contrast is larger for the Upper B MMI^{TM} Ag because of the low MMI^{TM} Ag content at Profile 64. Figure 3.4.34 shows that MMI^{TM} Ag and aqua regia-ICPMS Ag variations in the Upper horizon are generally similar to those in the Lower B horizon.

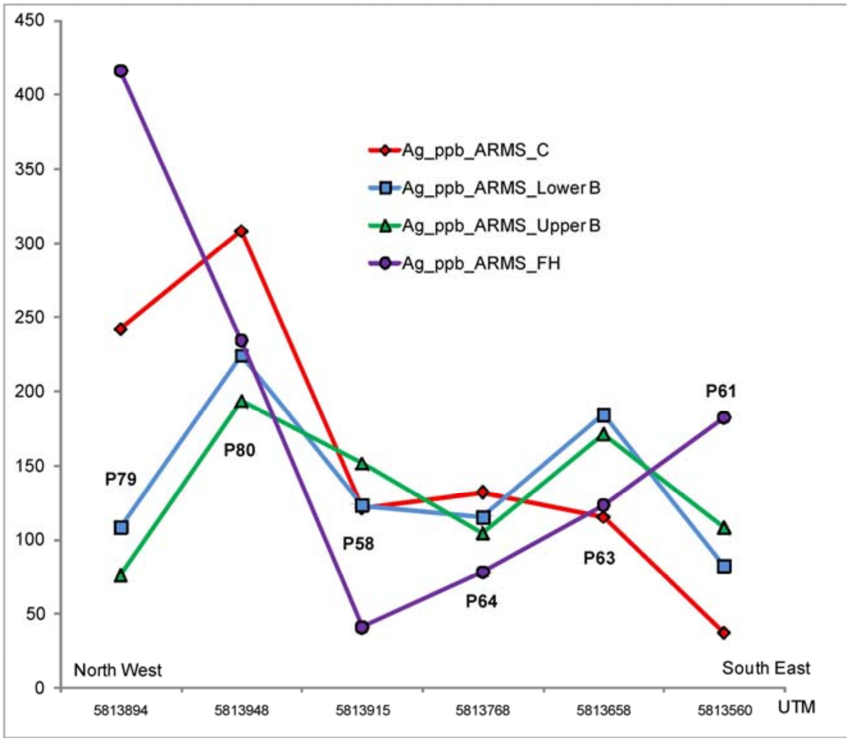

Figure: 3.4.33. Silver by aqua regia-ICPMS along Traverse A.

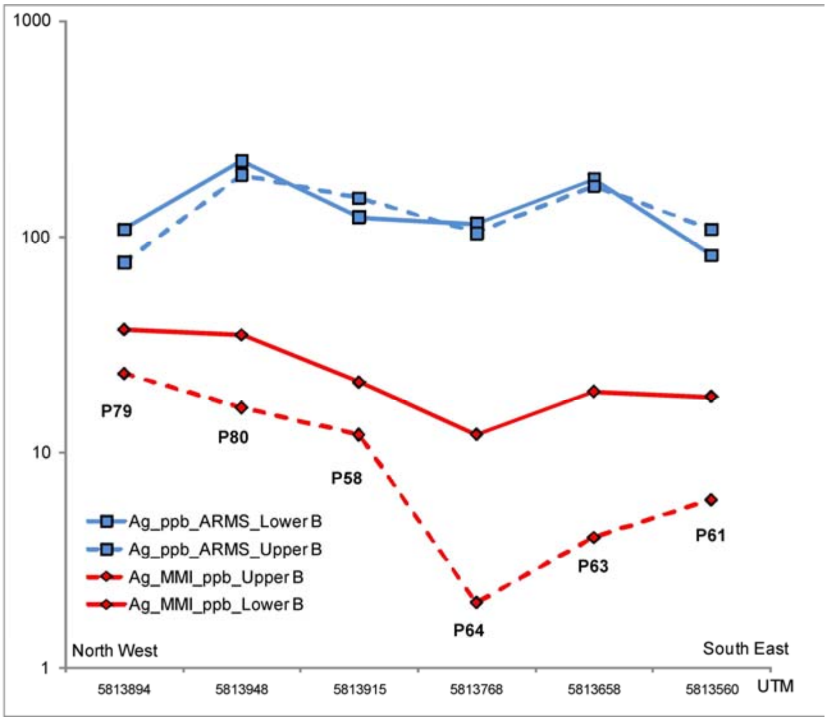

Figure: 3.4.34. Upper and Lower B horizon Ag by aqua regia-ICPMS, and MMI™

In Figure 3.4.35 Mo values reach 19 ppm in the C horizon at Profile 79 and there is a sharp Mo decrease in along Traverse A through Profile 80 and 58. At profile 79, the Mo content of the soil horizons is in the order C horizon Mo > Lower B horizon Mo > F-H horizon Mo > Upper B horizon Mo. Cobalt, shown in Figure 3.4.36, is similar to Ag with the highest Co values in C horizon samples and a Co peak at Profile 80. Soil Co content down Profile 80 follows the order of relative abundance of C horizon Co > Lower B horizon Co > Upper B horizon Co> F-H horizon Co. Figure 3.4.37 shows higher MMI™ Co values in Upper B soil samples compared to Lower B MMI™ and BioLeach℠ extractable Co. MMI℠ and BioLeach℠ Co values in Upper B soil samples increase to a peak between Profiles 63 and 64, but elevated MMI™ and BioLeach℠ Co levels do not correspond with the higher aqua regia-ICPMS Co in the B and C soils between Profiles 70 and 80. Vanadium in Figure 3.4.38 increases to a peak at Profile 58 with V abundance in order of C horizon V > Upper B horizon V > Lower B horizon V> F-H horizon V. Figure 3.4.39 shows that Mn content of the C horizon is similar to that of the B horizons and there is very little Mn variation in B and C soil along Traverse. However, Mn in the F-H horizon increases to a peak between Profiles 58 and 64 with values up to 2800 ppm Mn. In Figure 3.4.40 the B horizon Enzyme Leach℠ Mn variation is similar to the aqua regia F-H Mn variation although there is a difference in the size of the peaks in the two horizons. Variation of Upper B horizon Enzyme Leach℠ Mn, however, is very different because there is a deep Enzyme Leach℠ Mn “low” at Profile 58 that corresponds to the V multi-horizon peak.

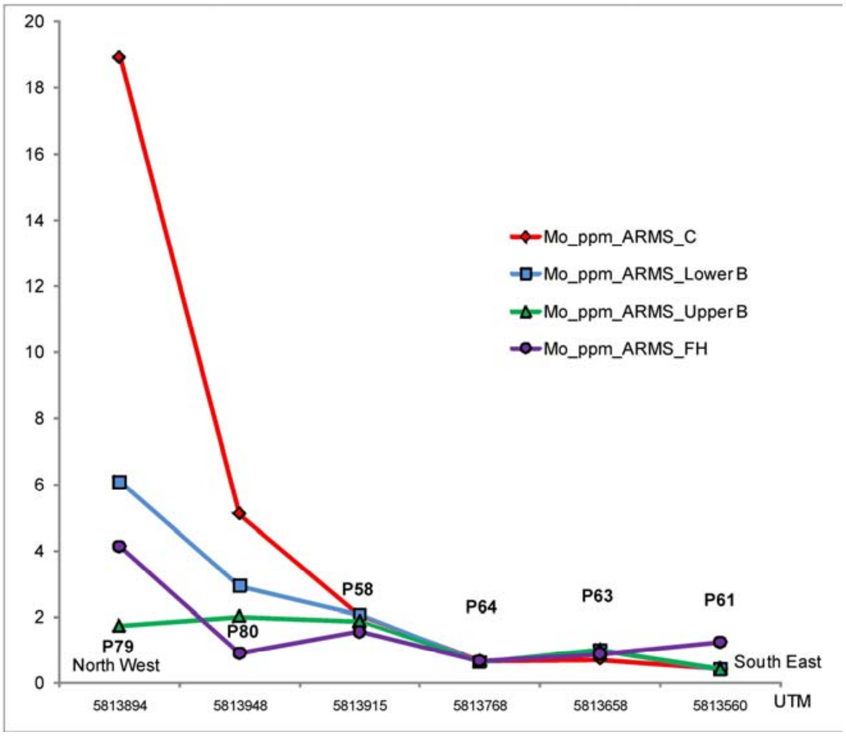

Figure: 3.4.35. Molybdenum by aqua regia-ICPMS along Traverse A.

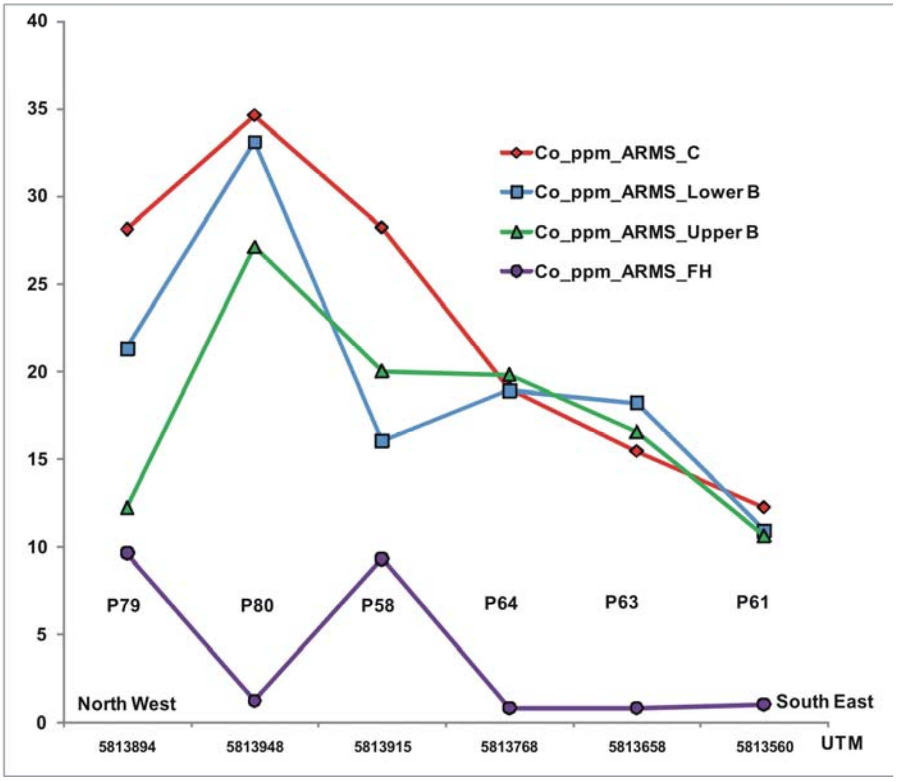

Figure: 3.4.36. Cobalt by aqua regia-ICPMS along Traverse A.

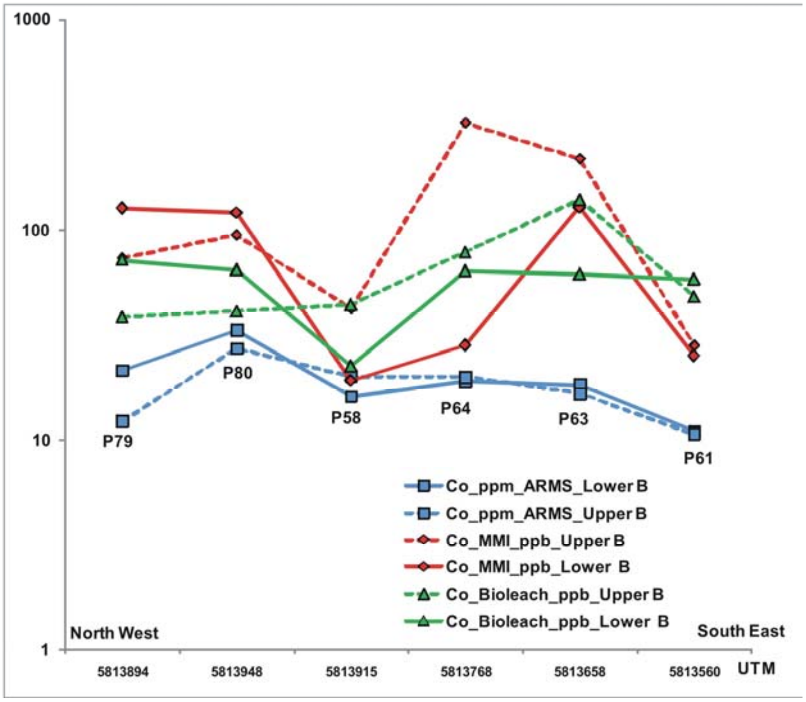

Figure: 3.4.37. Upper and Lower B Horizon Co by aqua regia-ICPMS, MMI^{TM} and BioLeach^{SM}

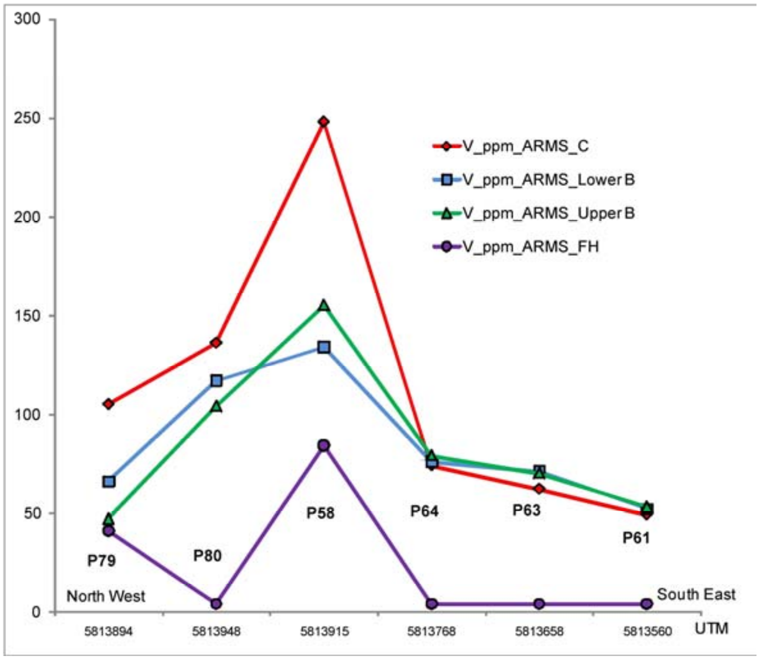

Figure: 3.4.38. Vanadium by aqua regia-ICPMS along Traverse A.

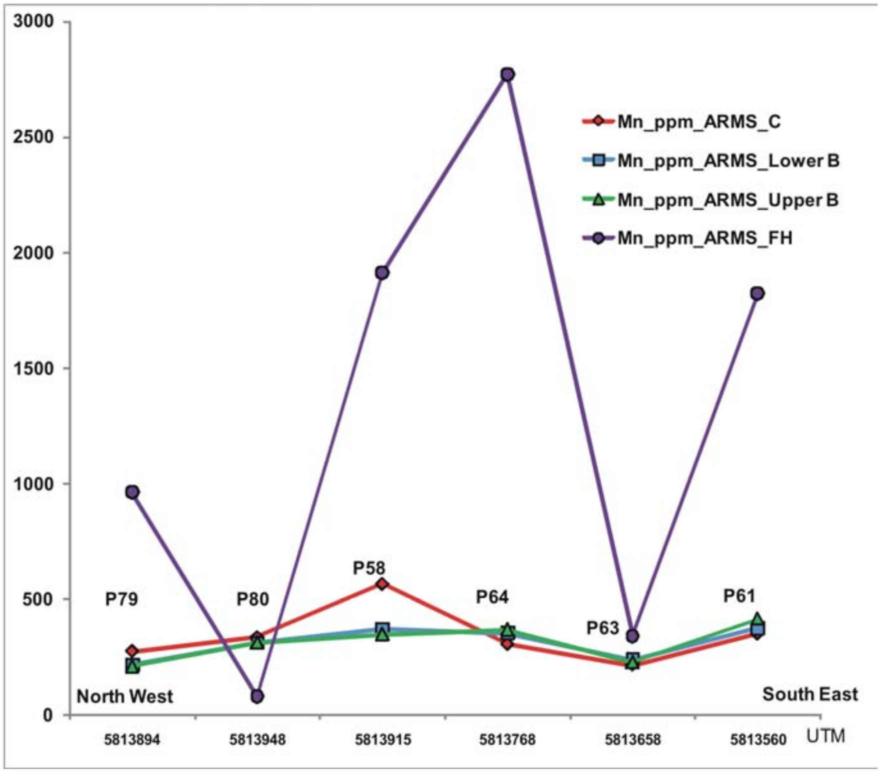

Figure: 3.4.39. Manganese by aqua regia-ICPMS along Traverse A.

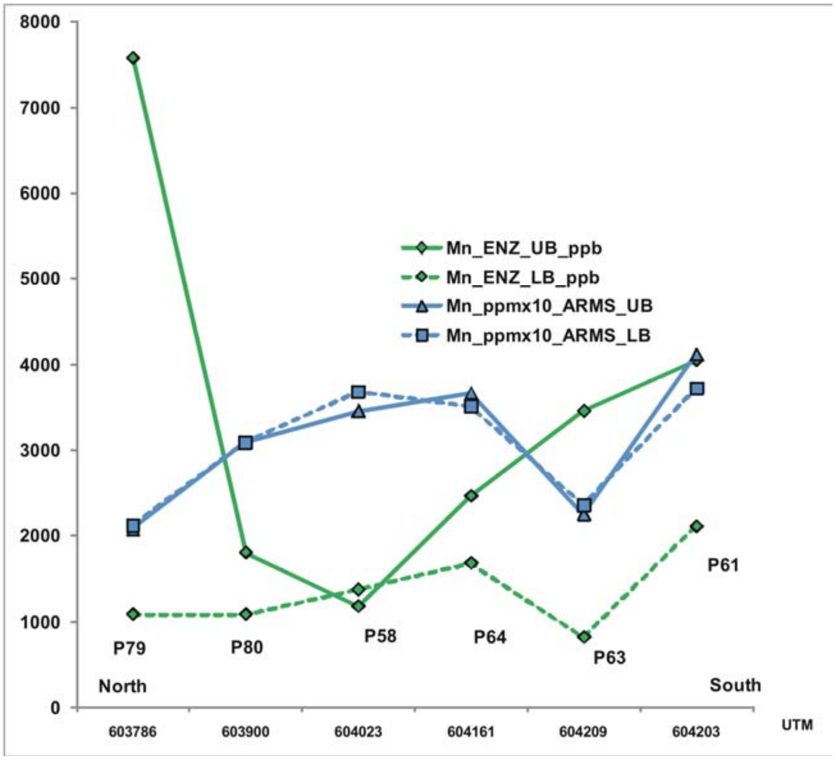

Figure: 3.4.40. Manganese by Enzyme Leach^{SM} along Traverse A.

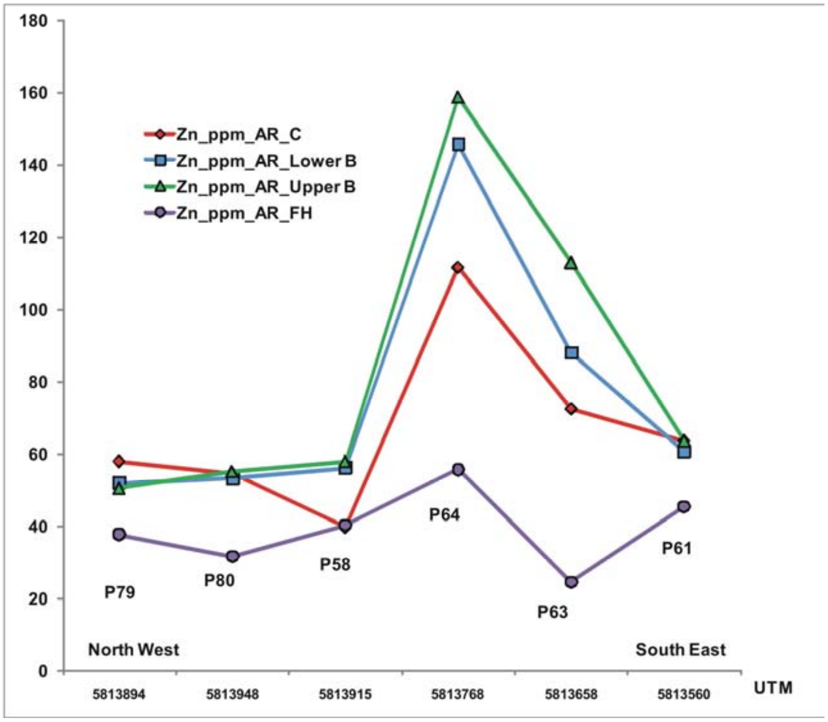

Figure: 3.4.41. Zinc by aqua regia-ICPMS along Traverse A.

In Figure 3.4.41 Zn increases a sharp, asymmetric peak at Profile 64 with relative Zn abundance in order of Upper B horizon Zn > Lower B horizon Zn > C horizon Zn> F-H horizon Zn. Figure 3.4.42 shows that there is a similar Pb variation to Zn in the B and C horizon although the peak at Profile 64 is more subdued and Pb in the F-H horizon has a pronounced “low” at Profile 64. Upper B horizon loss on ignition in Figure 3.4.43 increases steadily from northwest to southeast to a peak at Profile 63. The lower B horizon samples have smaller LOI and while the variation is more irregular the LOI pattern along Traverse A is similar to that in the Upper B horizon. There is a small decrease in field measured pH especially in Upper B horizon samples decreasing a “low” at Profile 64. Figure 3.4.44 shows that there is a spatial relationship between LOI and variation of BioLeach^{SM} Br and I along Traverse A especially where values increase to a peak between Profile 63 and 64. In this area there is elevated LOI, lower field measured soil pH and higher BioLeach^{SM} Br and I. In Upper B soil horizon samples there are “saw tooth” aqua regia-ICPMS and MMI^{TM} extractable Ca patterns in Figure 3.4.45 with peaks at Profiles 58 and 61 and an inverse difference hydrogen ion (IDH) at Profile 64. The Ca patterns in the Lower B horizon is similar although the regia-ICPMS Can peak at Profile 58 is offset from the MMI^{TM} extractable Ca peak at Profile 64 (see Figure 3.4.45). In addition to showing Upper and Lower B horizon Ca geochemistry the Figures 3.4.45 and 3.4.46 also show the centre of a redox cell that has been interpreted from the SGH data by Sutherland and Hoffman, (2008), who rank the SGH anomaly from data collected on the Shiko Lake property as 5 on a scale of 1 (low) on scale of 6 (high). Existence of bedrock sulphide mineralization near Profile 79 and 80, inverse difference hydrogen (IDH) values and the element geochemical patterns along Traverse A suggest that one part of a double peak halo anomaly centered on Profile 79.

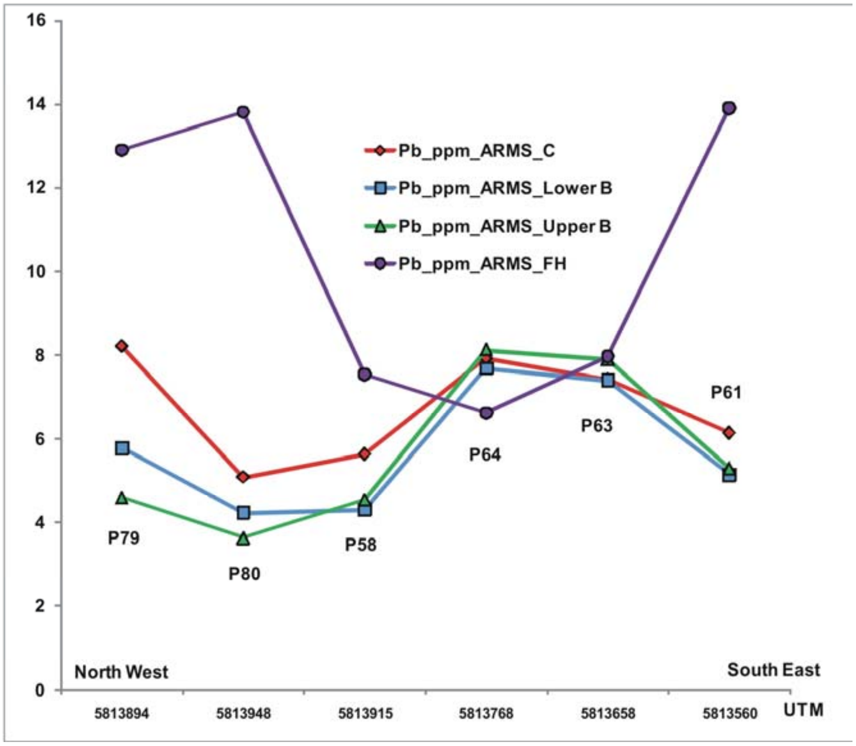

Figure: 3.4.42. Lead by aqua regia-ICPMS along Traverse A.

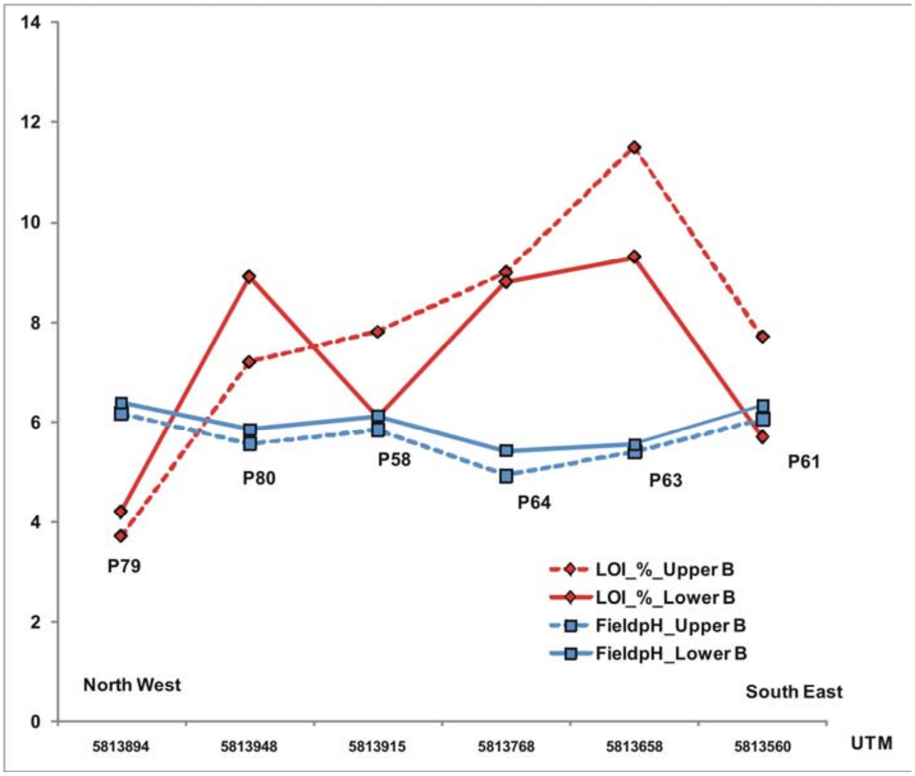

Figure: 3.4.43. Loss on ignition (LOI) and field pH along Traverse A.

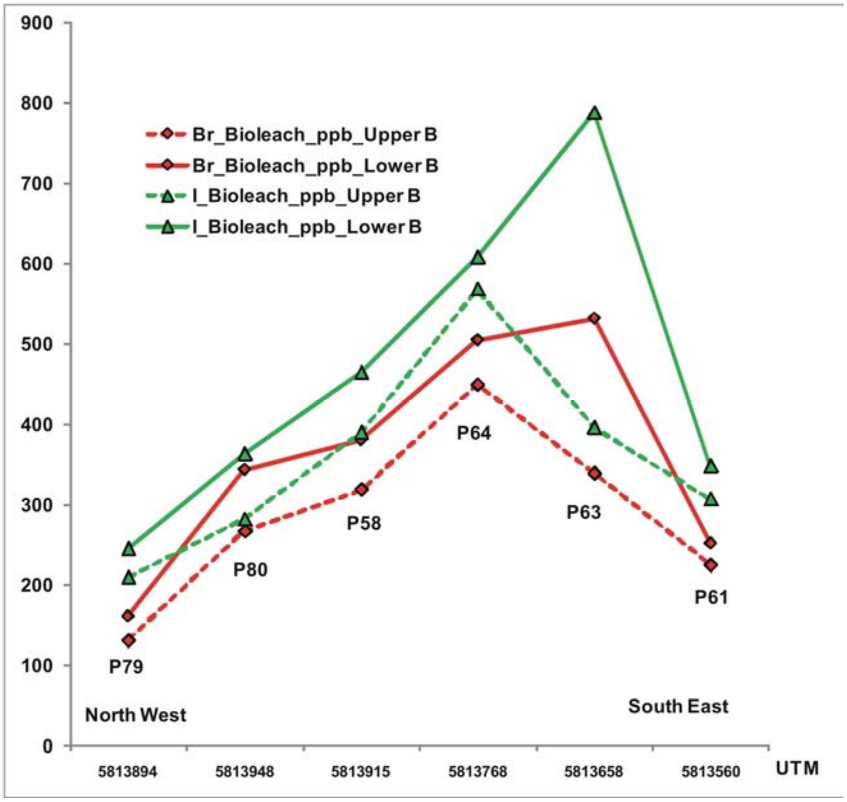

Figure: 3.4.44. BioLeach^{SM} Br and I along Traverse A.

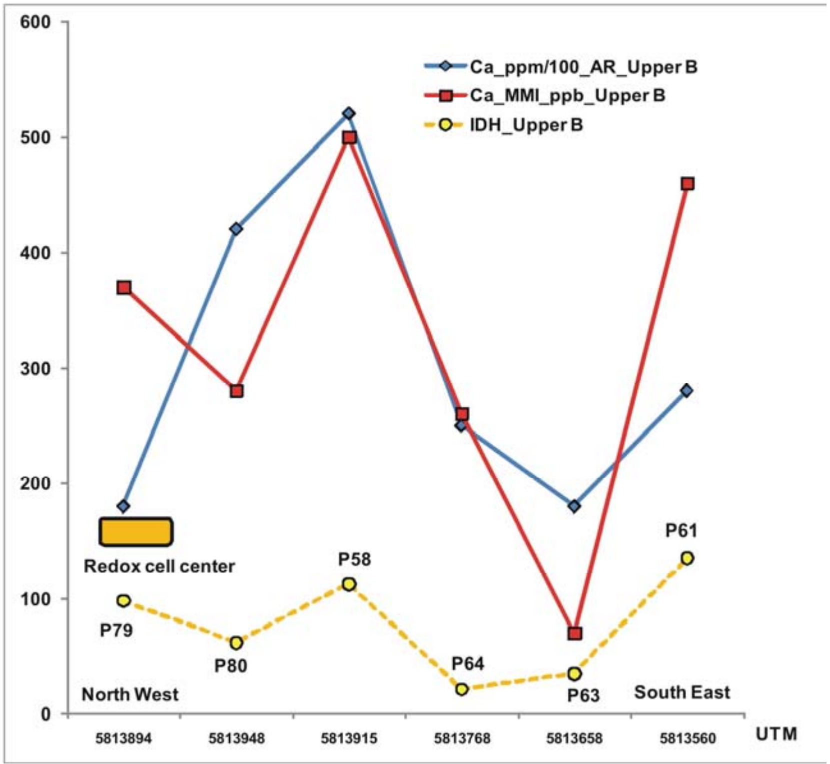

Figure: 3.4.45. Upper B soil MMI^{TM} aqua regia_ICPMS Ca and IDH along Traverse A.

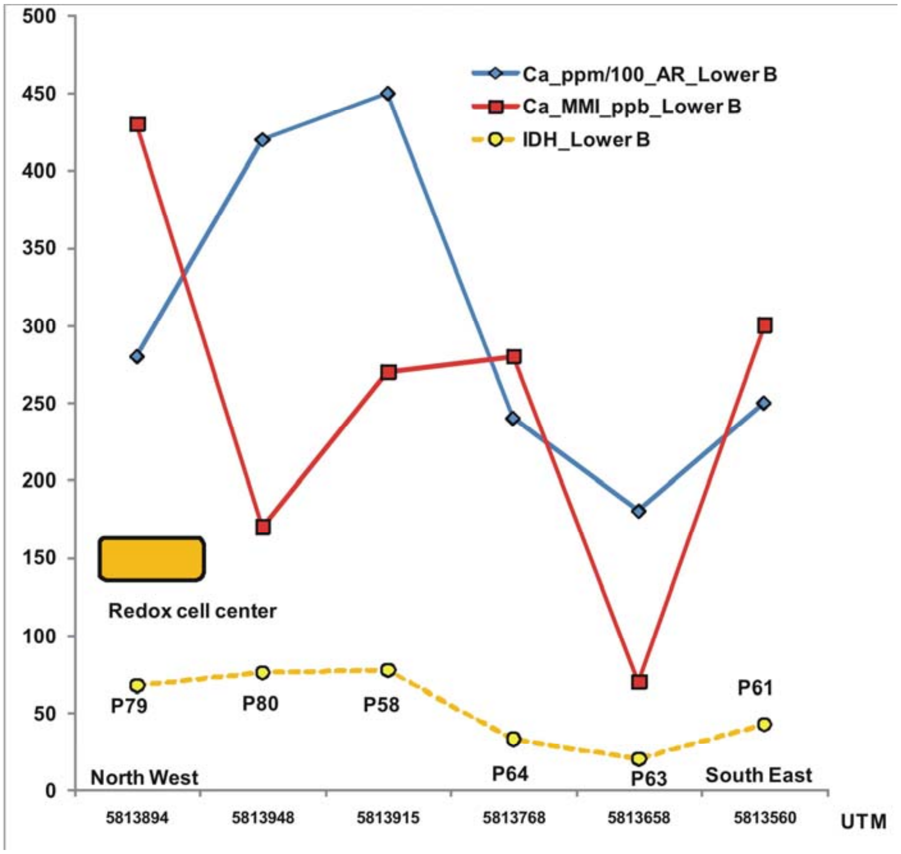

Figure: 3.4.46. Lower B soil MMI™ aqua regia_ICPMS Ca and IDH along Traverse A.

Traverse B: Figure 3.4.27**a** and **b** show location of sample traverse B that extends for more than 500 metres across the North East mineralized zone. Figure 3.4.47 displays C soil horizon Cu values along the traverse created by combining data from Lett and Sandwith, (2008) with the overburden geochemical data reported by Petsel, 2006. The C-soil horizon Cu shows the greatest anomaly contrast compared to Cu in other horizons and there is an asymmetric Cu peak at Profile 60. BioLeach℠ Cu contrast is greater than MMI™ Cu contrast and Enzyme Leach℠ Cu contrast at Profile 60, but there is a secondary Cu MMI™ anomaly at Profile 56 (See Figure 3.4.48). The Au pattern in the C soil horizon, in Figure 3.4.49 is similar to that displayed by Cu with INAA Au values up to 298 ppb at Profile 60 in the C soil horizon. Profile 60 also has a large number of total and pristine Au grains in the C horizon heavy mineral concentrate. A second, smaller Au peak at Profile 56 in the Upper B horizon, but not the C horizon has a marked MMI™ geochemical anomaly (Figure 3.4.50). The asymmetric shape of the Au and Cu peaks suggest a source of mineralized material in till deposited by ice flowing from north to south. Since this at variance to the regional ice-flow direction a likely explanation is that there is bedrock several sources for the Au in the till reflected in the multiple Au peaks along Traverse B.

In Figure 3.4.51, Ag displays a pattern that is similar to Cu and Au, but the Ag contrast at Profile 60 is higher in F-H horizon samples rather than for the mineral horizons. There is up to 5 ppm Mo in the C soil horizon at Profile 60 and this peak, shown in Figure 3.4.52, is reflected by a correspondingly smaller one in the Lower B Horizon. Unlike variation in the mineral horizon, the F-H horizon Mo displays no peak at Profile 60, but increases towards to north end of the traverse. Variation of Co by aqua regia-ICPMS in Figure 3.4.53 is similar to that displayed by Cu, Au and Mo and Co values increase to a sharp peak at Profile 60. This peak is reflected by Co MMI^{TM} and Co BioLeach^{TM} anomalies in the Lower B horizon samples (see Figure 3.4.54). Both Co by MMI^{TM} and Co by BioLeach^{SM} display almost identical patterns along Traverse B with Co BioLeach^{SM} showing the greatest contrast. In Figure 3.4.55 V levels in the C horizon soil horizon along Traverse B vary erratically and this variation most likely reflects a difference between the Novagold and GSB sample digestion methods. Vanadium values are higher in the C soil horizon than the B and F-H horizons. Unlike the multi-element B and C horizon peak at Profile 60 there a higher V in the F-H at Profile 62. Figure 3.4.56 shows higher BioLeach^{SM} Br and I in lower B soil horizon samples at Profile 62 with corresponding lower soil LOI, aqua regia Ca and MMI^{TM} Ca (Figure 3.4.57). The IDH (soil pH) values along Traverse B decrease from Profile 56 to a low at Profile 60 where there is a multi-element peak.

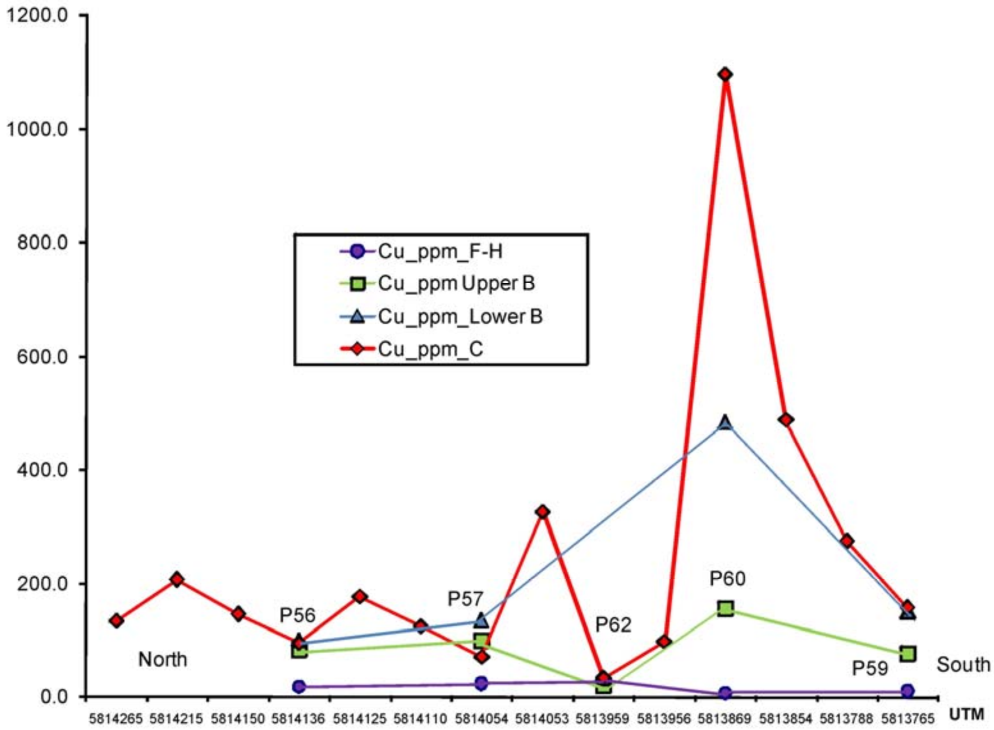

Figure: 3.4.47. Copper by aqua regia-ICPMS along Traverse B.

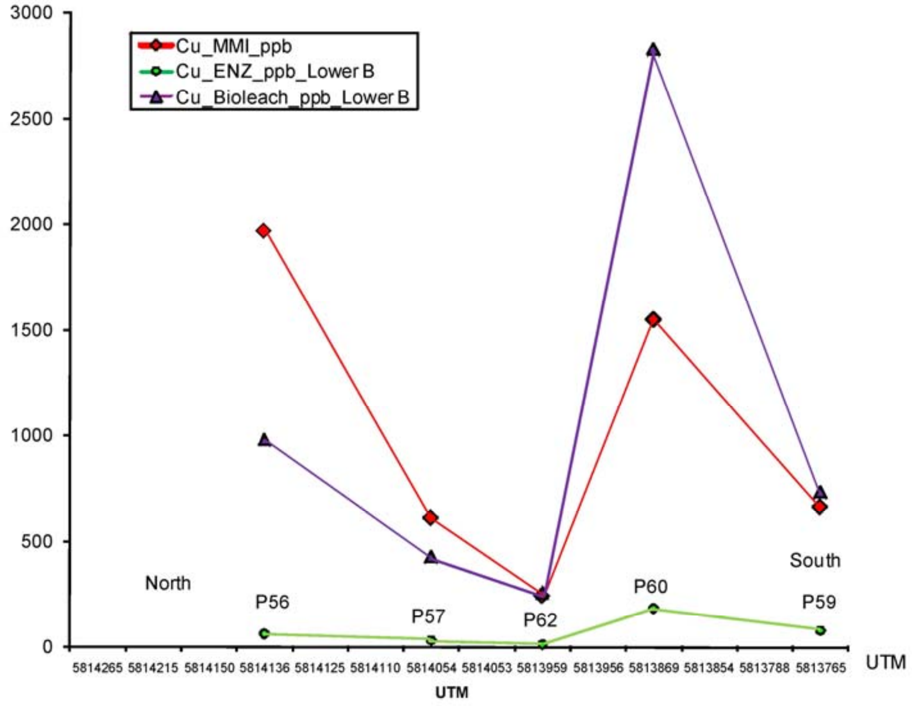

Figure: 3.4.48. Copper by partial leach along Traverse B.

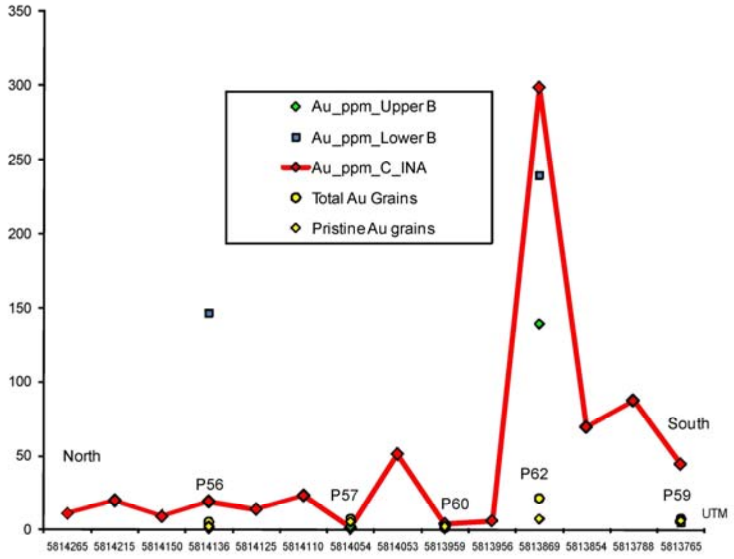

Figure: 3.4.49. Gold by INAA or fire assay-AAS (Novagold samples) along Traverse B.

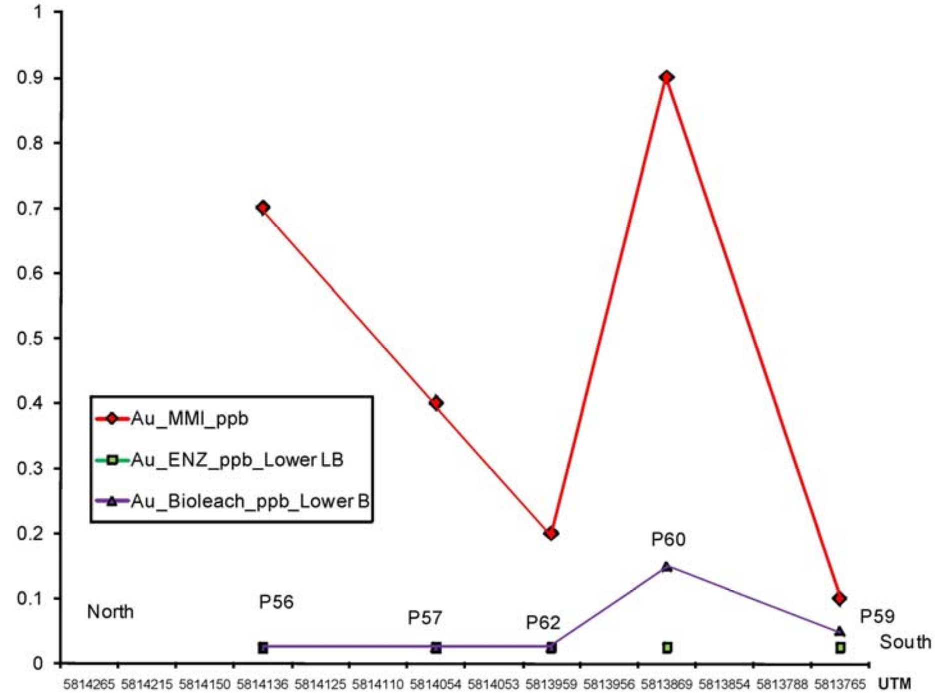

Figure: 3.4.50. Gold by partial leach along Traverse B.

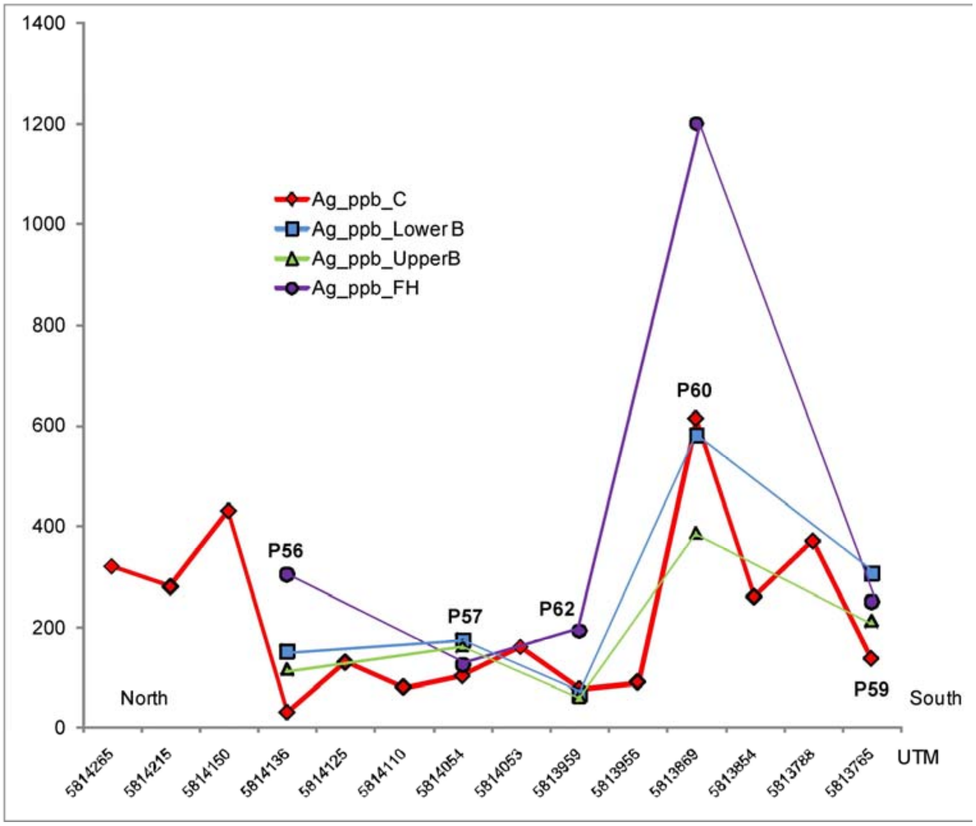

Figure: 3.4.51. Silver by aqua regia-ICPMS along the Traverse B.

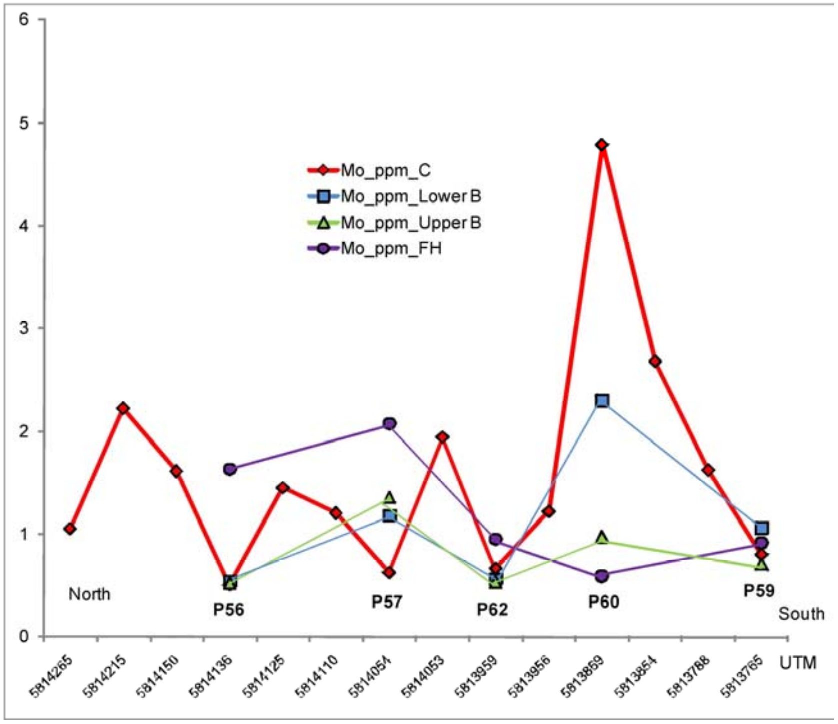

Figure: 3.4.52. Molybdenum by aqua regia-ICPMS along the Traverse B.

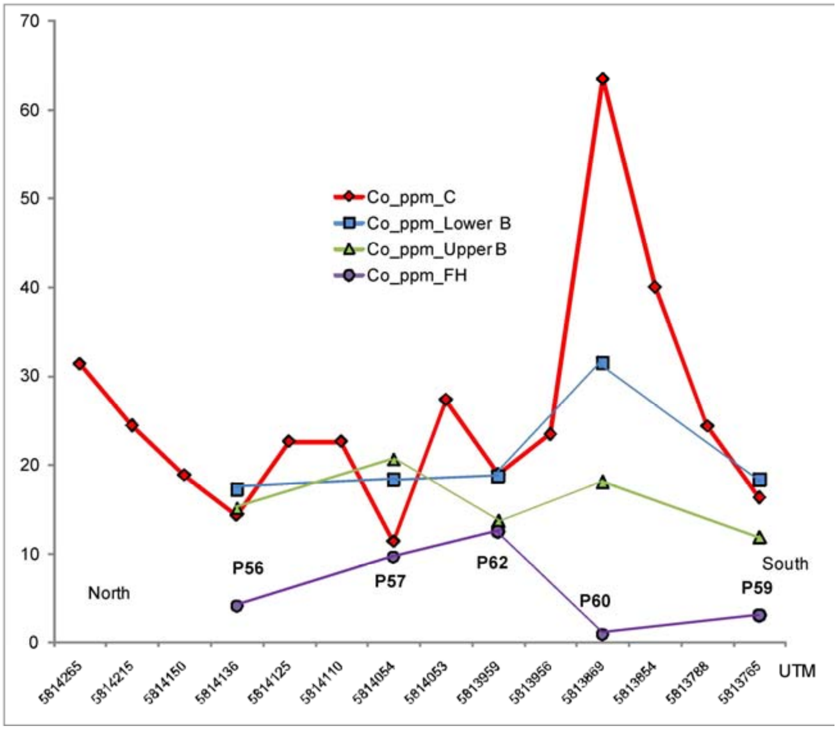

Figure: 3.4.53. Cobalt by aqua regia-ICPMS along Traverse B.

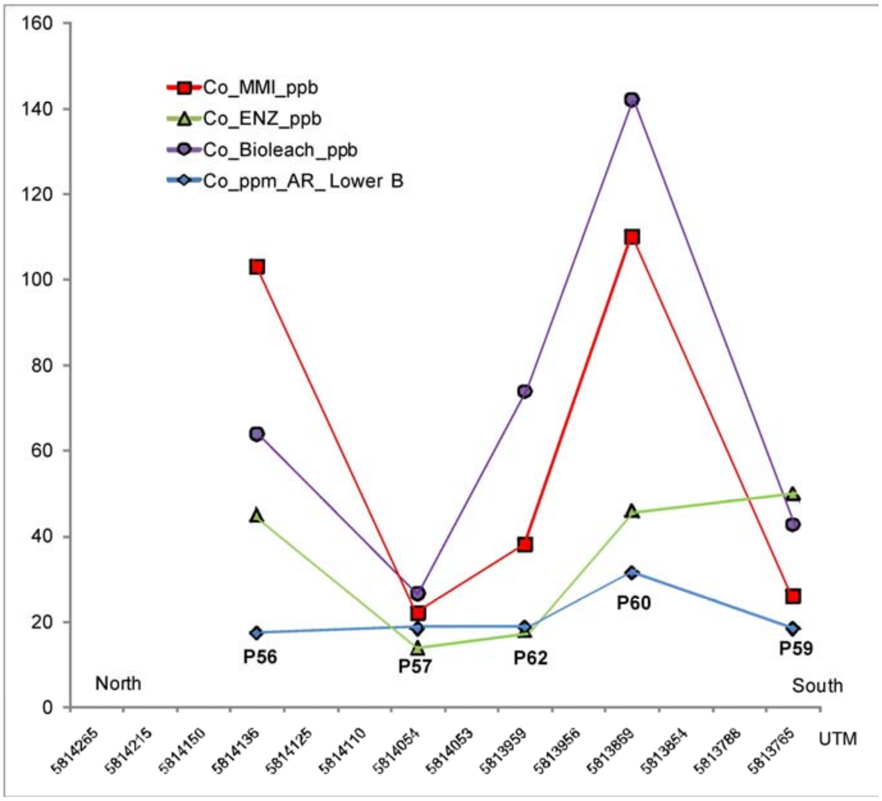

Figure: 3.4.54. Cobalt by partial leach along Traverse B.

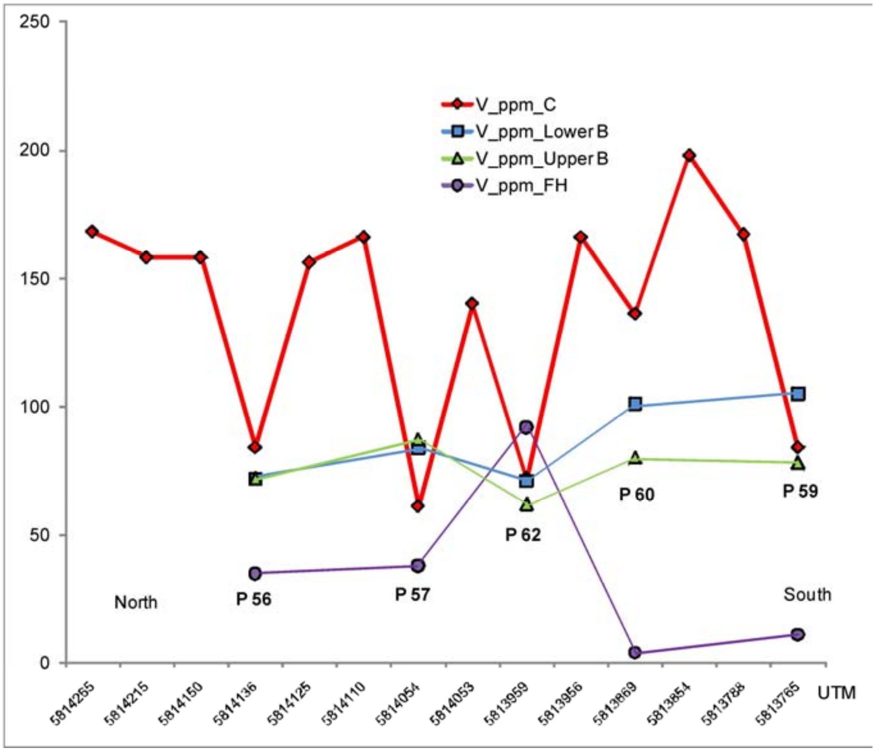

Figure: 3.4.55. Variation of V along Traverse B.

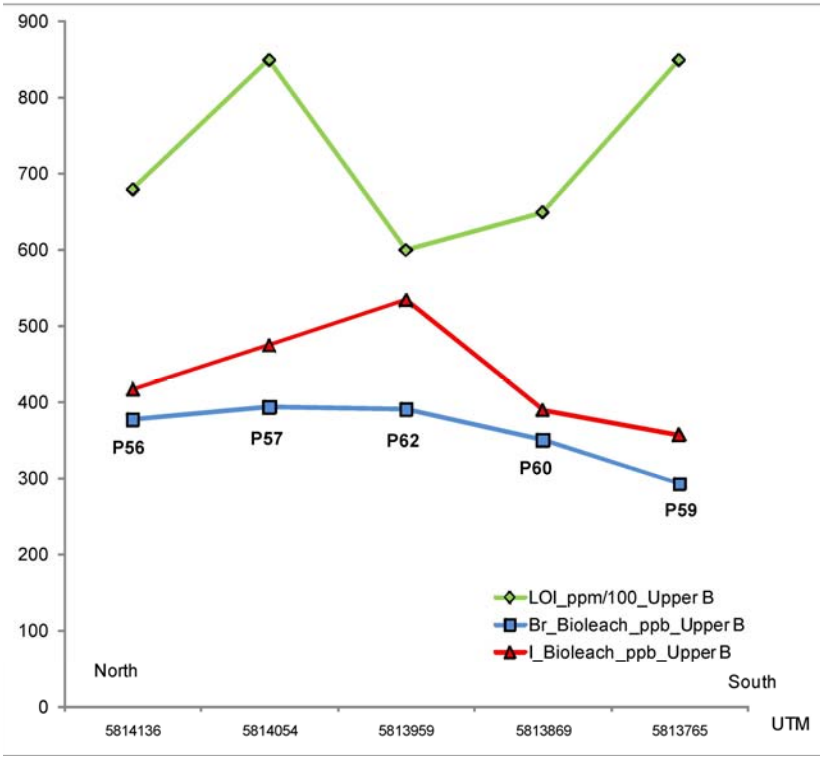

Figure: 3.4.56. Variation of LOI and BioLeach^{SM} Br and I along Traverse B.

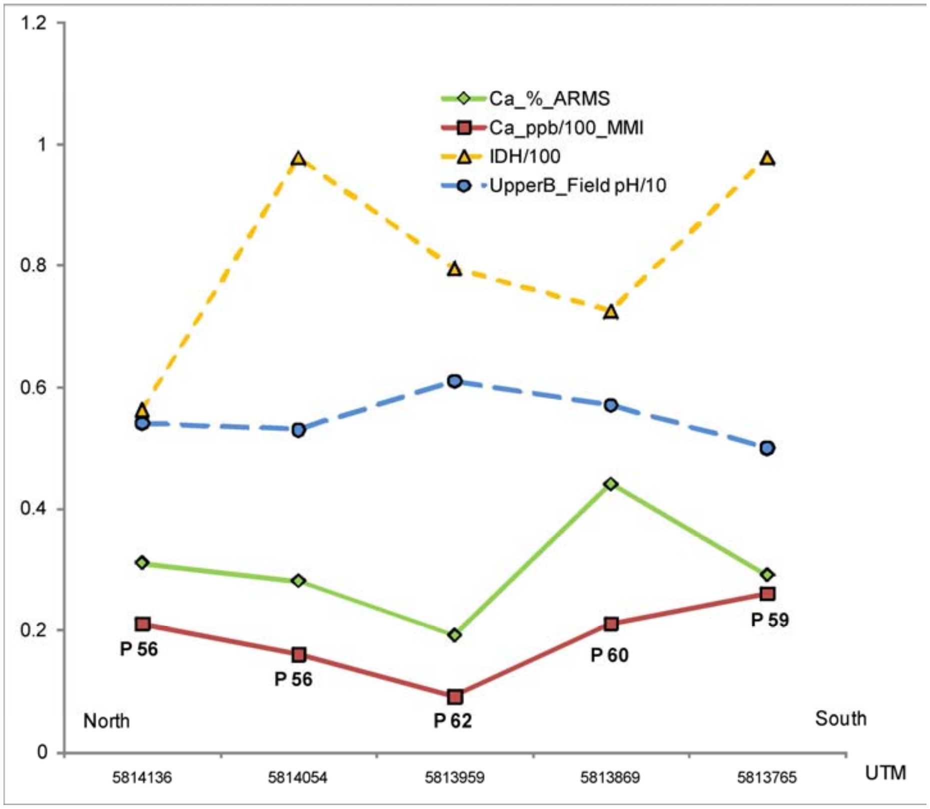

Figure: 3.4.57. Variation of aqua regia Ca, MMI^{TM} Ca and IDH along Traverse B.

Traverse C: Figure 3.4.27 shows the location of Traverse C that crosses the North Cu-Au mineralized zone extends into the North East mineralized zone. Copper variation in Figure 3.4.58 in the C soil horizon along the Traverse C represents data from sampling by Lett and Sandwith, (2008) combined with the soil-overburden geochemistry reported by Petsel, (2006). The C-soil horizon Cu shows the greatest anomaly contrast along the traverse compared to Cu contrast for the other horizons, but there is only a small Cu rise in the B and F-H horizon Cu corresponding to the C horizon Cu peak at Profile 58. However, there is a symmetric Cu peak at Profile 52 in both Upper and Lower B soil horizons with a much smaller Cu C horizon anomaly. In Figure 3.4.59 the Lower B horizon BioLeach^{SM} Cu and MMI^{TM} Cu anomaly contrast at Profile 52 is almost identical and the Enzyme Leach^{SM} Cu and aqua regia-ICMS Cu patterns are along the traverse are also very similar. There is a "saw tooth" Au pattern in the C soil horizon, shown in Figure 3.4.60 that might reflect both the difference between the INAA analysis of the Profile samples collected by Lett and Sandwith, 2008 compared to Novagold till samples that were analysed fire assay-AAS. The erratic Au pattern might be also due to the typical high variability of scattered Au grains in small samples. The most consistent Au anomaly is between Profiles 54, 58 and 55 and is has elevated Au in all of the soil horizons with up to 40 Au grains in the C soil horizon heavy mineral concentrate. Of these grains 30 percent have a "pristine" shape. While the largest numbers of Au grains are in the C soil horizon at Profile 55, the highest BioLeach^{SM} Au and MMI^{TM} Au and Enzyme Leach^{SM} Au values occur in the B soil horizon at Profiles 58 and 51. Gold anomaly contrast by the leach extraction follows the order MMI^{SM} Au > INAA Au > BioLeach^{SM} Au > Enzyme Leach^{SM} Au (see Figure 3.4.61).

In Figure 3.4.62 the highest C horizon Ag value are between Profiles 52 and 53 and are flanked by Lower and Upper B horizon peaks at Profile 52 and a single samples F-H horizon peak a Profile 55. In Figure 3.4.63 there is a concomitant increase of Mo with higher Ag, Cu and Au in the mineral horizons and an F-H Mo peak corresponding to Ag at Profile 55. Cobalt, shown in Figure 3.4.64) is also elevated at Profile 52 and the relative size of the anomaly contrast by aqua regia-ICPMS is in the order of Co-Lower B > Co-Upper B> Co-C > Co F-H. Partial leach analysis enhances the Co geochemical signal and the Co contrast for Lower B horizon samples taken at Profile 52 follows the order BioLeach^{SM} Co> MMI^{SM} Co > Enzyme Leach^{SM} Co > aqua regia Co (Figure 3.4.65). Vanadium in Figure 3.4.66, displays at broad peak between Profiles 54 and 55 in all of the soil horizons. Contrast for V is in the order V-C > V-Upper B =/> V-Lower B. High soil LOI is one reason for high Cu, Co and Mo values in the B horizon soils at Profile 52 and the large contrast partial leach anomalies in the soil. The high LOI values in Figure 3.4.67 indicate that the soil can be classified as organic (> 30%). In fact, the area around Profile 66 is a small forest wetland with a high water table and B horizon soil sampled is black, organic-rich material. In Figure 3.4.67 BioLeach^{SM} Br and I also increase with LOI suggesting that soil organic matter influences BioLeach^{SM} Br and I content. In Figure 3.4.68 the lower B horizon Ca by aqua regia-ICPMS and MMI^{SM} fall to a "low" at Profile 53 that is close to the centre of a redox cell interpreted from the SGH data by Sutherland and Hoffman, (2008) who rank the SGH anomaly as a guide to Cu-Au porphyry mineralization as 5 on a scale of 1 (low) on scale of 6 (high). Inverse difference hydrogen (IDH) values and field measured soil pH show very little change along the traverse suggesting that there has been minimal influence on the soil geochemistry from buried mineral sulphides.

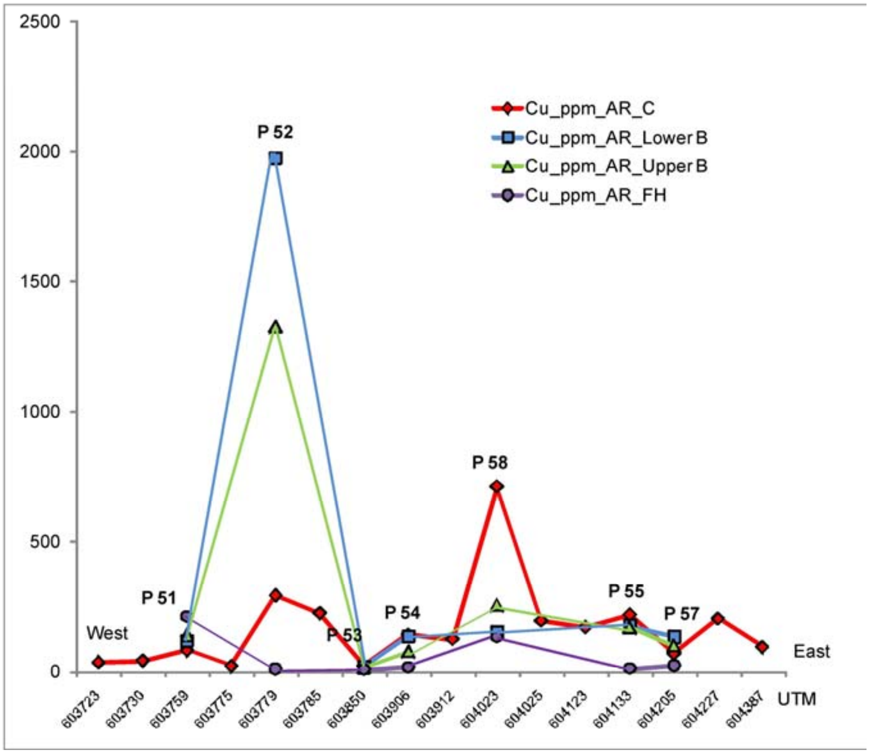

Figure: 3.4.58. Copper by aqua regia-ICPMS along Traverse C.

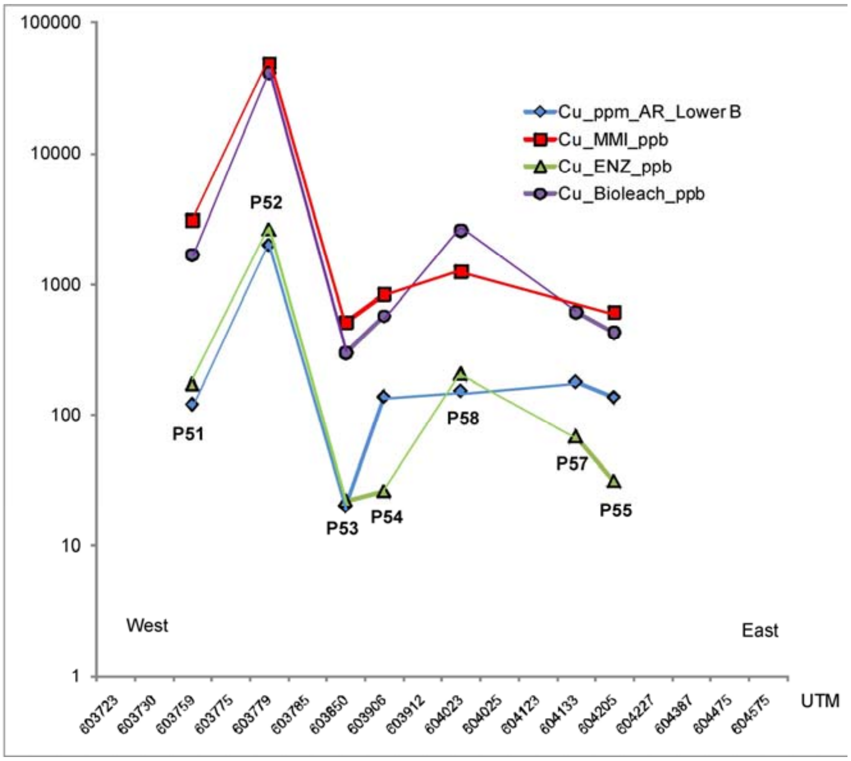

Figure: 3.4.59. Copper by partial leaches along Traverse C.

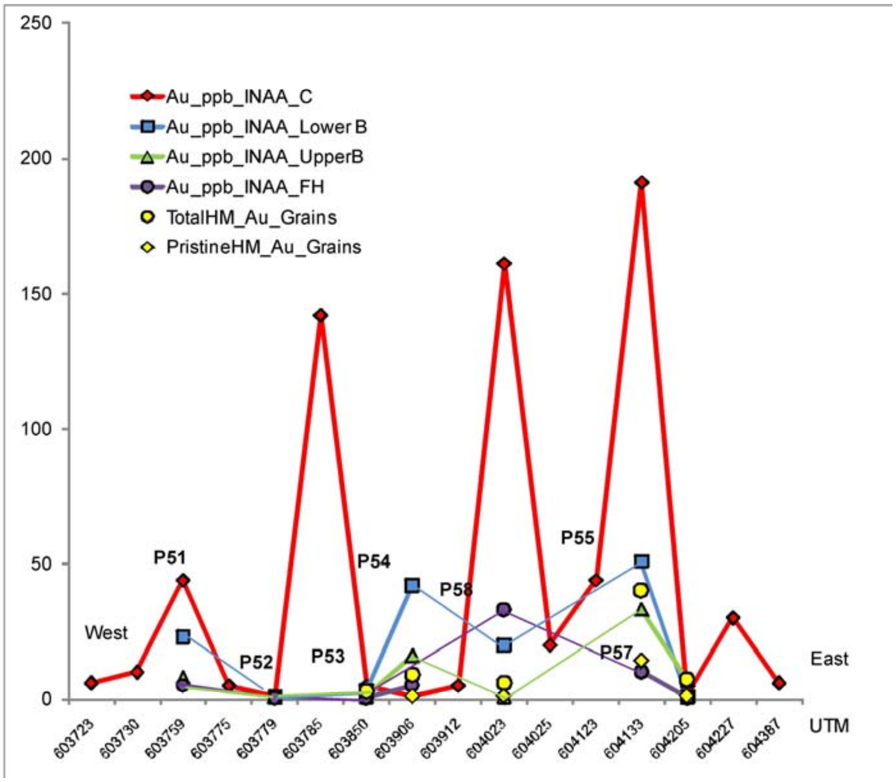

Figure: 3.4.60. Gold by INAA along Traverse C.

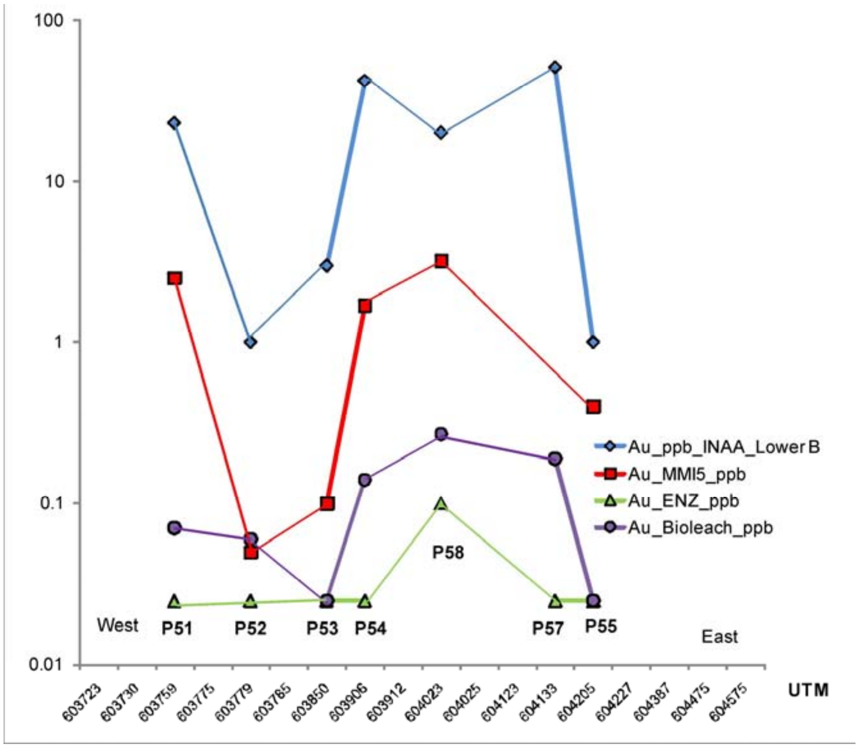

Figure: 3.4.61. Gold by partial leaches along Traverse C.

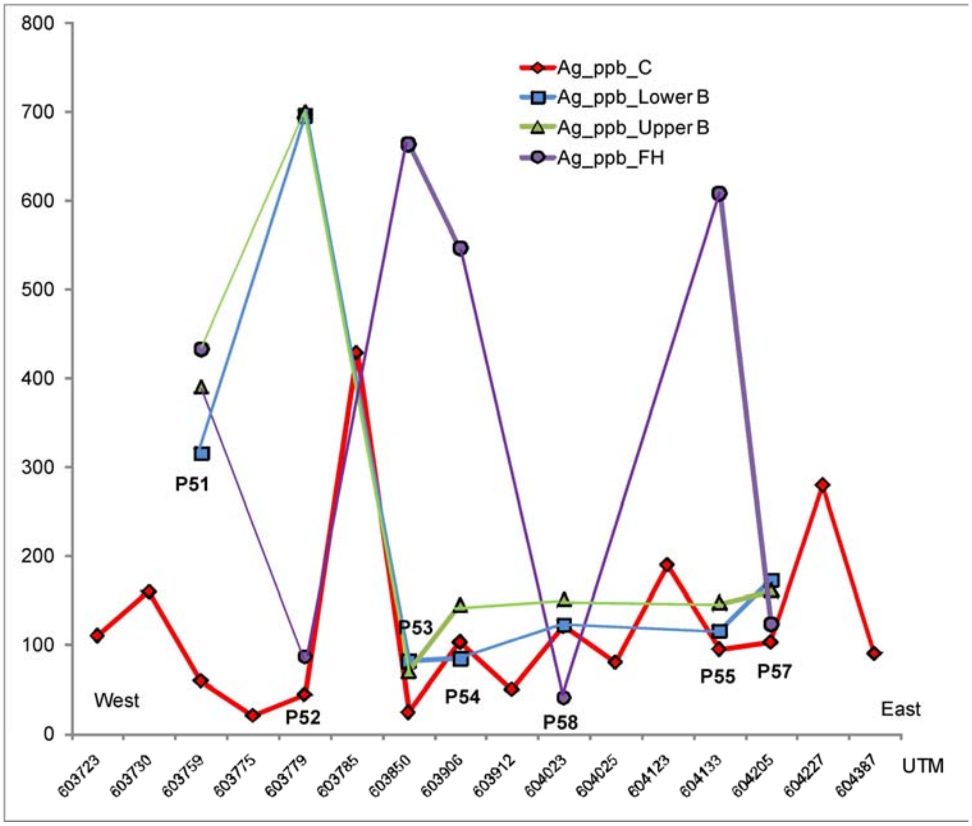

Figure: 3.4.62. Silver by aqua regia-ICPMS along Traverse C.

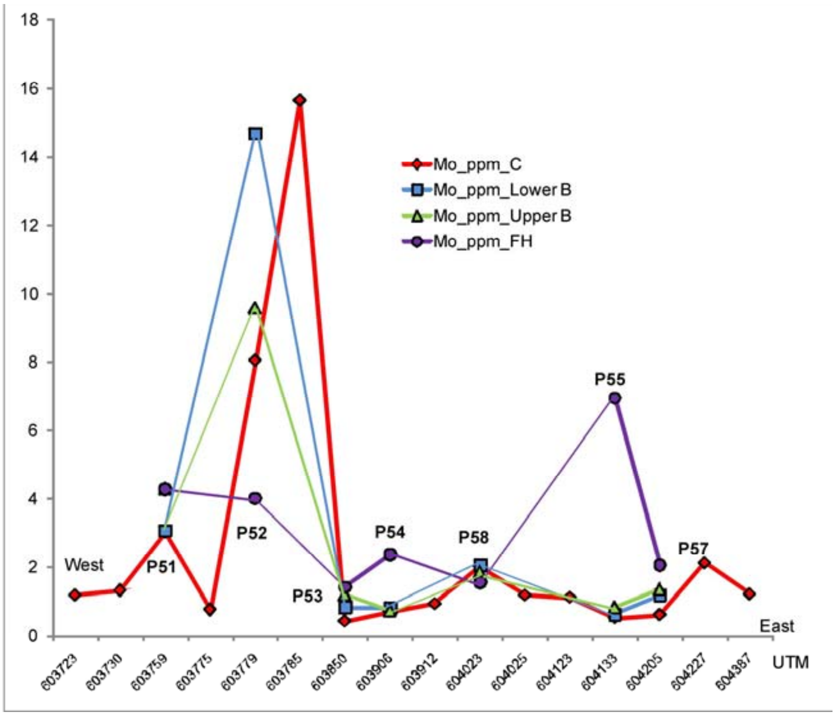

Figure: 3.4.63. Molybdenum by aqua regia-ICPMS along Traverse C.

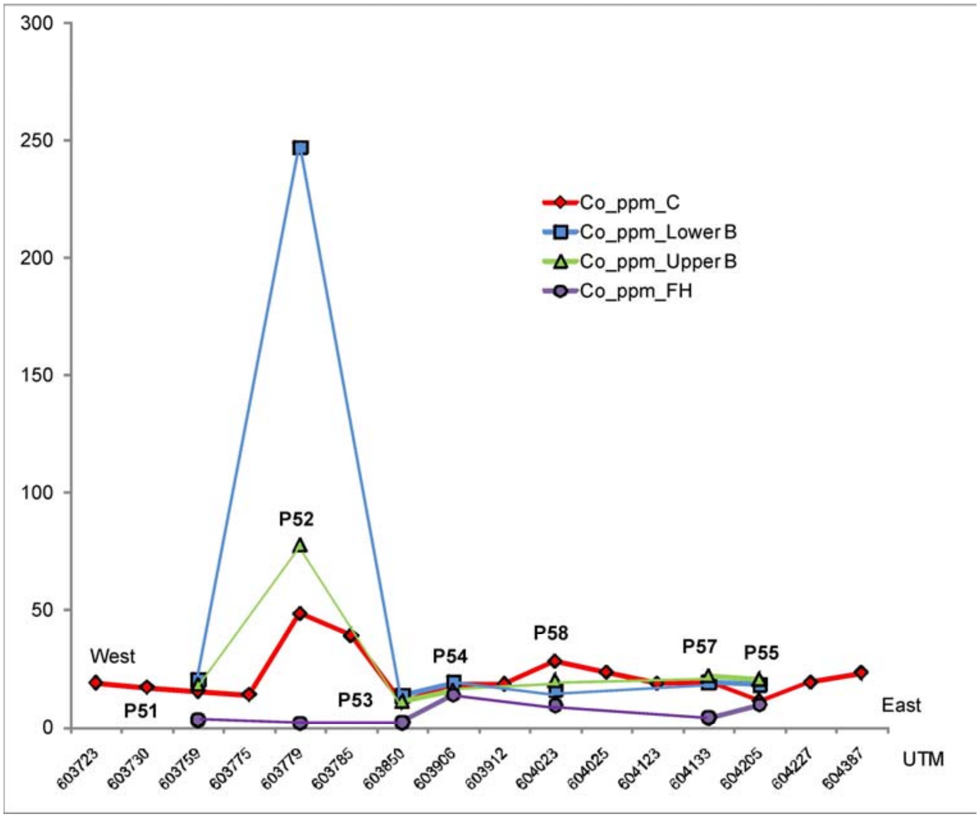

Figure: 3.4.64. Cobalt by aqua regia-ICPMS along Traverse C.

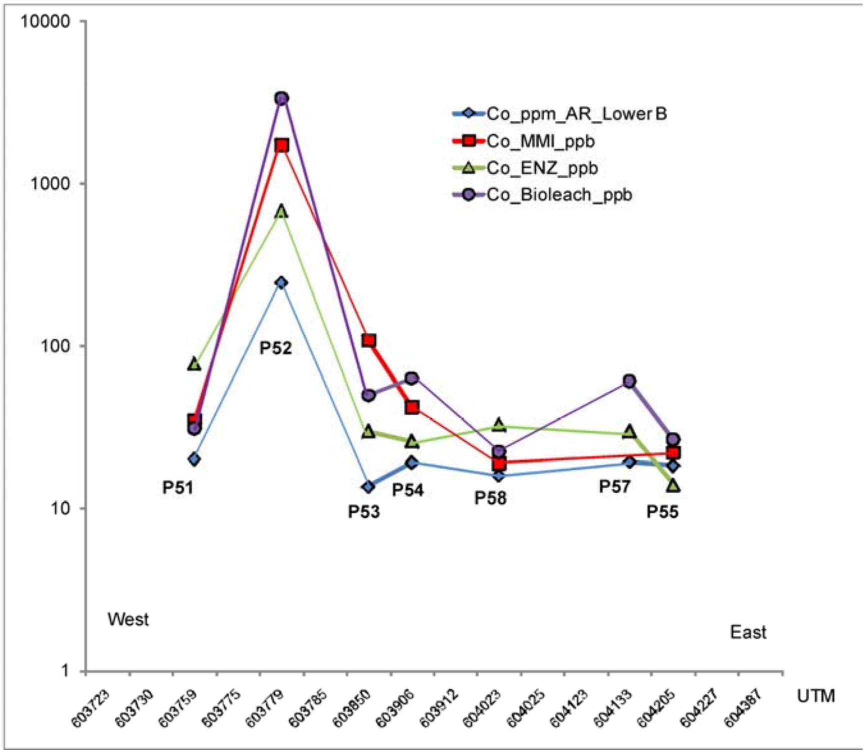

Figure: 3.4.65. Cobalt by partial leach analysis along Traverse C.

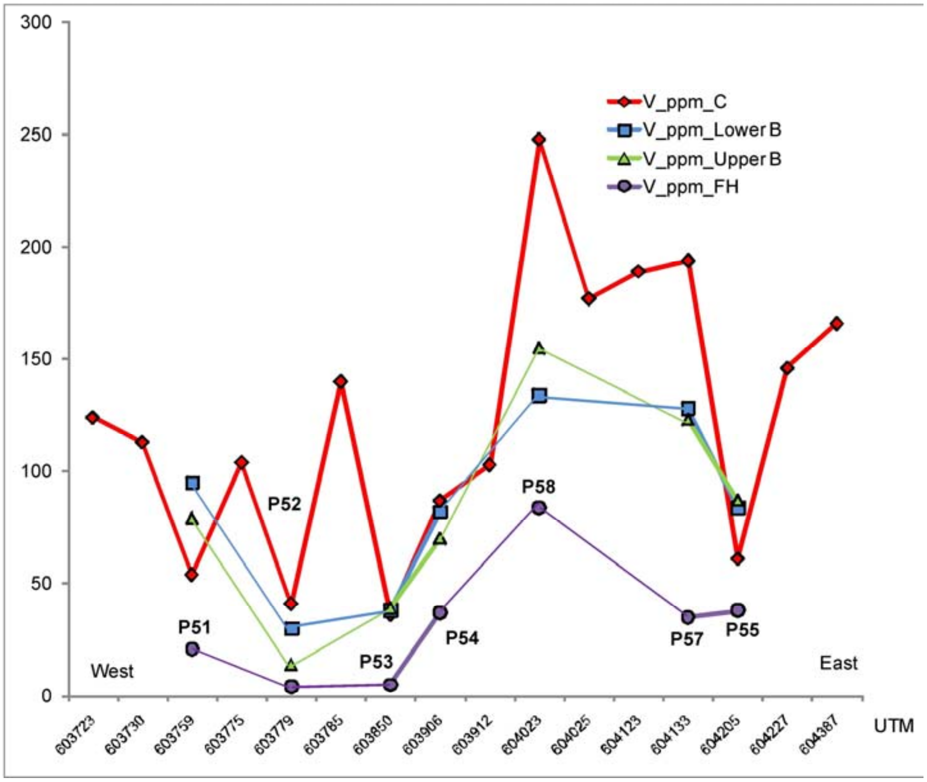

Figure: 3.4.66 Vanadium by aqua regia-ICPMS along Traverse C.

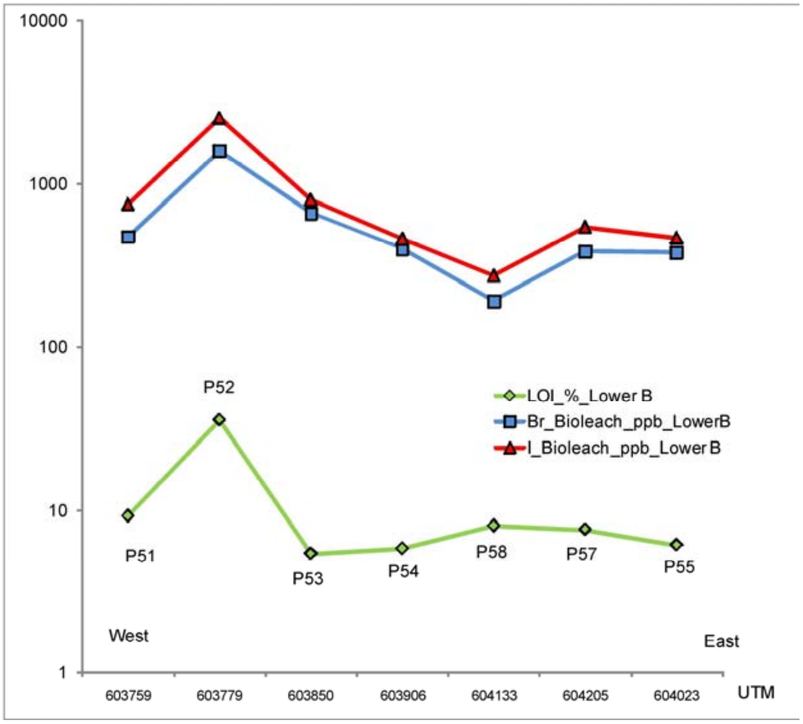

Figure: 3.4.67. Variation of LOI, BioLeach^{SM}, Br and I along Traverse C.

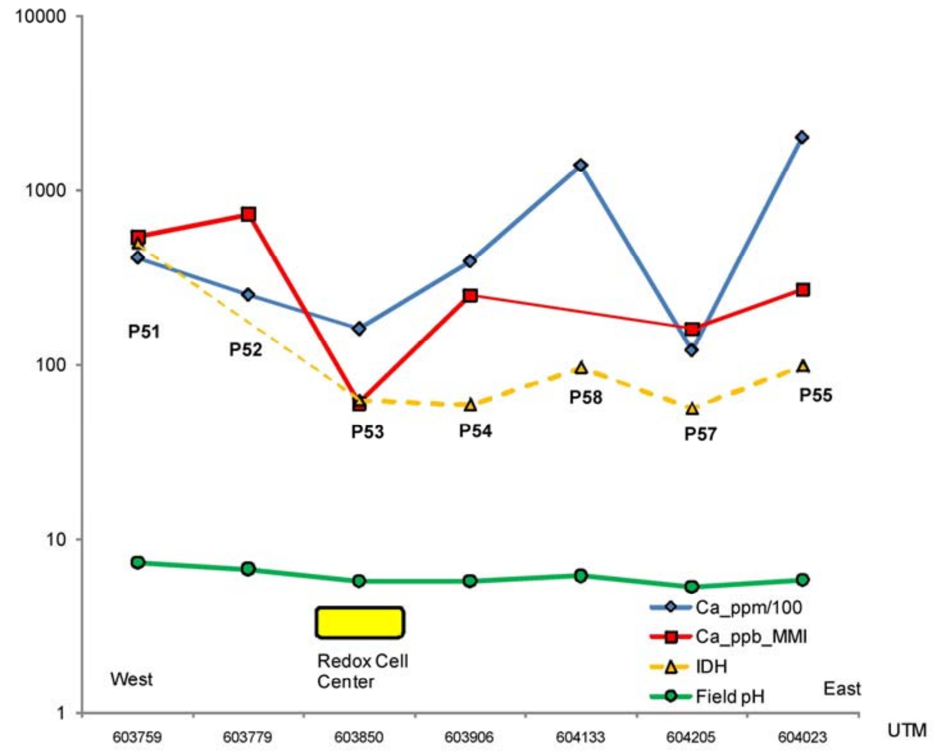

Figure: 3.4.68. Variation of Ca and IDH along Traverse C.

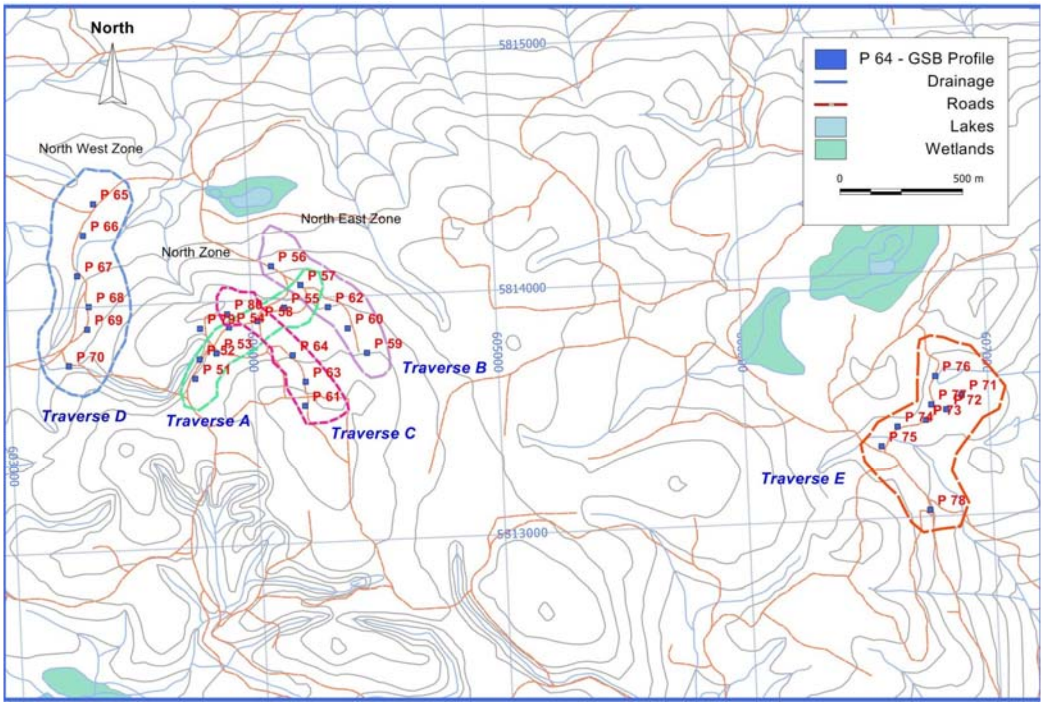

Figure: 3.4.69. Profile locations on Traverse D and E.

Traverse D: Location of Traverse D and A is shown on Figure 3.4.69 and Figure 3.4.70 displays Cu variation in soil over a distance of one kilometre along the Traverse D. The C soil horizon Cu patterns was created by combining the soil analyses from the profiles P65 to P70 sampled by Lett and Sandwith, (2008), with data reported by Petsel, (2006), from fire assay, atomic absorption and aqua regia digestion-inductively coupled plasma emission spectroscopy (ICPES) analysis of overburden samples. There is a marked C-horizon Cu anomaly over an interval of 400 metres between P65 to P68 reaching a peak value of 405 ppm Cu and the Cu anomaly contrast is greatest for the C-horizon and least for the F-H horizon. The C-Horizon Cu peak also has a distinctive asymmetric shape with a steep south-facing slope and a gentler north-facing slope. The Lower B horizon Cu-MMI^{TM}, Cu-Enzyme Leach^{SM} and Cu-BioLeach^{SM} profiles have a similar shape and anomaly contrast to the C-horizon Cu (Figure 3.4.71).

Figure 3.4.72 shows Au in soil along Traverse D revealing an anomaly resembling Cu, but with a more symmetrical shape. Again, the C-horizon Au contrast is larger than for Au in the B horizon Au (no Au was detected in the F-H samples). Also shown in the Figure are the total number of Au grains and pristine Au grains in the C-horizon sample heavy mineral concentrates from P65 to P70. A nearby bedrock source for the Cu-Au mineralization would explain the high number of pristine (irregular shape) Au grains with a geochemical Au anomaly in the < 0.063 mm fraction of the C horizon. While there are abundant Au grains, no sulphide grains were reported in the C-horizon heavy mineral concentrates at Profiles 66 and 69. However, a grain of cinnabar was identified at Profile 67 and two grains of electrum at Profile 68. There is no increased Hg in the C-horizon at Profile 67. Figure 3.4.73 indicates a MMI^{TM} Au anomaly with a peak at P66 but with almost no corresponding increase for either Enzyme Leach^{SM} or BioLeach^{SM} Au over the same interval. The MMI^{TM} Au anomaly peak at P66 corresponds to greatest number of total and pristine Au grains counted in a heavy mineral concentrate of the C soil horizon. The MMI^{TM} Au peak at P 69 has a corresponding total and pristine Au grain anomaly, but only background Au in the < 0.063 mm fraction of the C horizon sample.

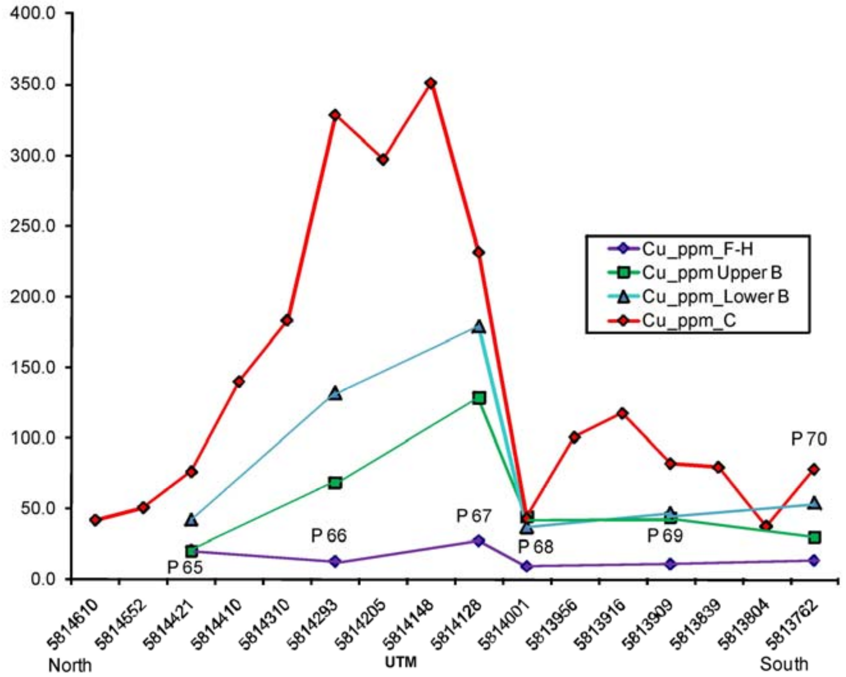

Figure: 3.4.70. Copper by aqua regia-ICPMS along Traverse D.

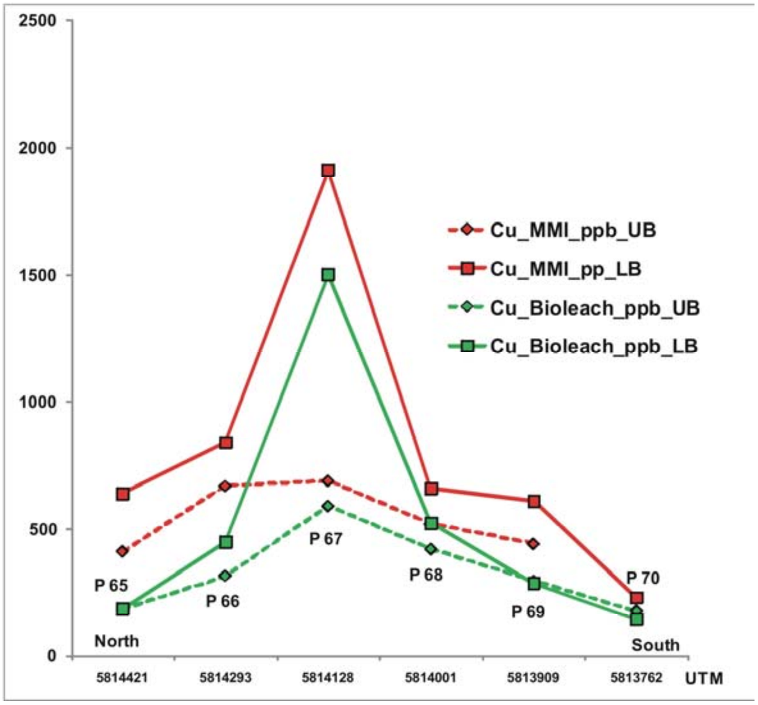

Figure: 3.4.71. Copper by partial leach analysis along Traverse D.

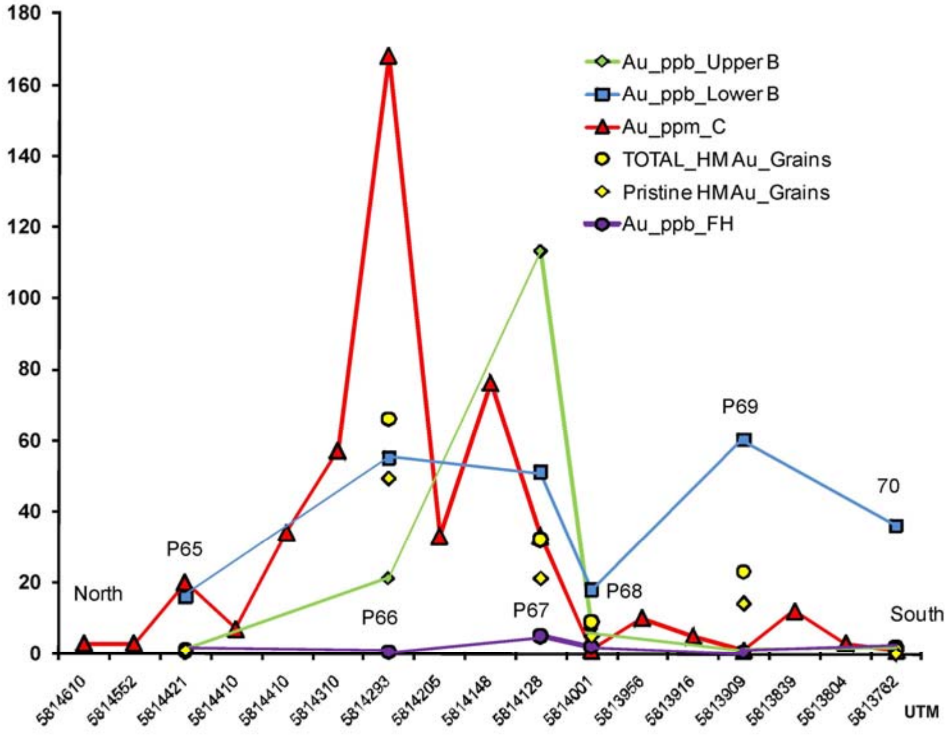

Figure: 3.4.72. Gold by INAA and HM Au grains along Traverse D.

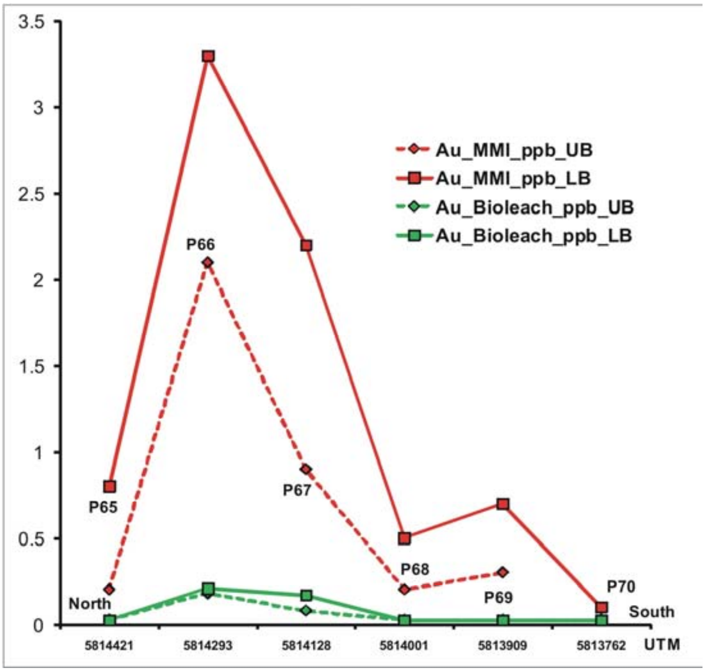

Figure: 3.4.73. Gold by partial leach analysis along Traverse D.

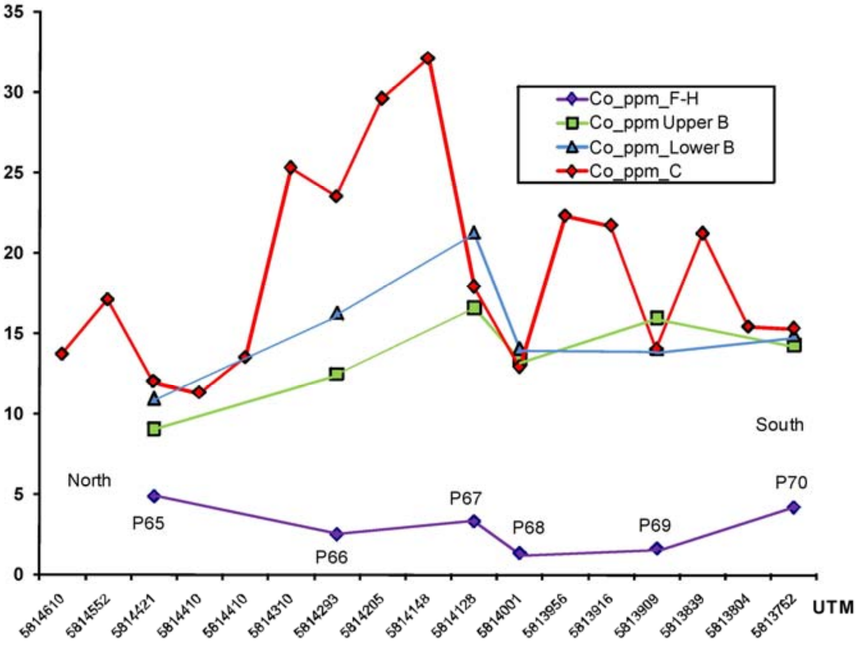

Figure: 3.4.74. Cobalt by aqua regia-ICPMS along Traverse D.

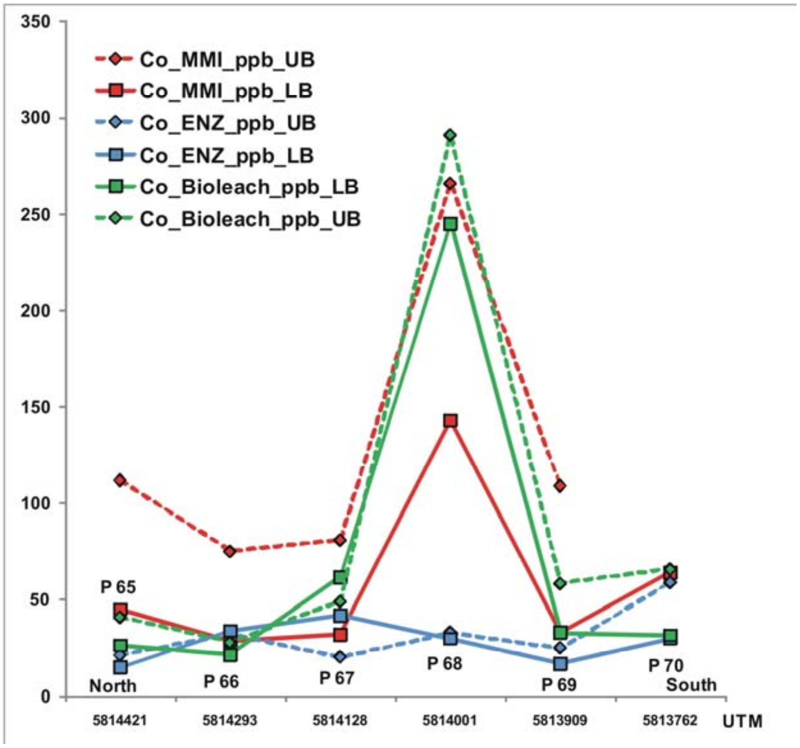

Figure: 3.4.75. Cobalt by partial leach analysis along Traverse D.

Figure 3.4.74 shows that Co variation in soil along Traverse D is similar to Cu although the C-horizon Co contrast is smaller and the anomaly shape more symmetrical between P68 and P70. Selective extraction profiles in Figure 3.4.75 show that the mobile metal ion Co and Bio Leach^{SM} Co anomaly peaks at P68 are displaced to the south of the C-horizon peak. The mobile metal ion Co contrast is smaller than the BioLeach^{SM} Co contrast although the anomalies have a similar pattern. Silver, shown in Figure 3.4.76, is higher in the F-H horizon compared to the mineral horizons and the Ag pattern in the C and to lesser extent B follows that of Cu and Co. There are only detectable MMI^{TM} Ag values and comparison of the MMI^{SM} Ag with lower B horizon Ag, shown in Figure 3.4.77) reveals a similarity between the two patterns. A rather "saw tooth" erratic V pattern in Figure 3.4.78 may very well reflect different digestion methods used to generate the Novagold C horizon data compared to that used for the till samples analysed by Lett and Sandwith, 2007. However, an asymmetric V peak at Profile 67 in all soil horizons is still visible and the peak is reflected by both aqua regia and Enzyme Leach^{SM} analyses (Figure 3.4.79). The Mo C soil variation in Figure 3.4.80 has similar to Cu in that there is an asymmetric Mo peak with a steeper south face between Profiles 66 and 67. Other horizons have lower Mo levels, but a similar variation to the C horizon values except that the F-H Mo levels increase towards Profile 65 rather than decrease.

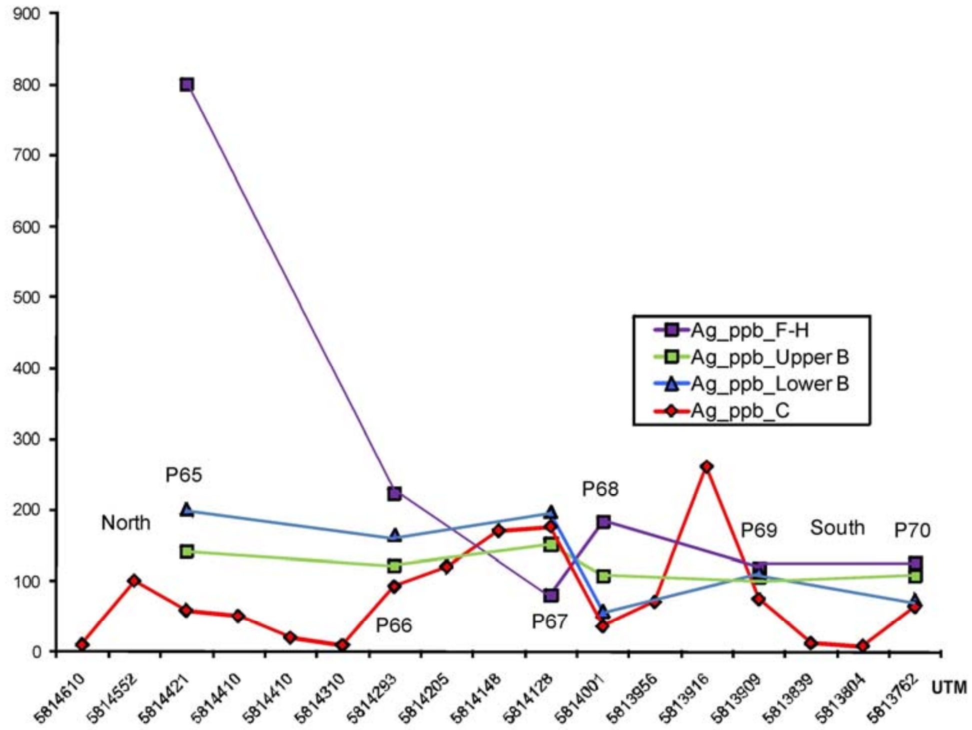

Figure: 3.4.76. Silver by aqua regia-ICPMS along Traverse D.

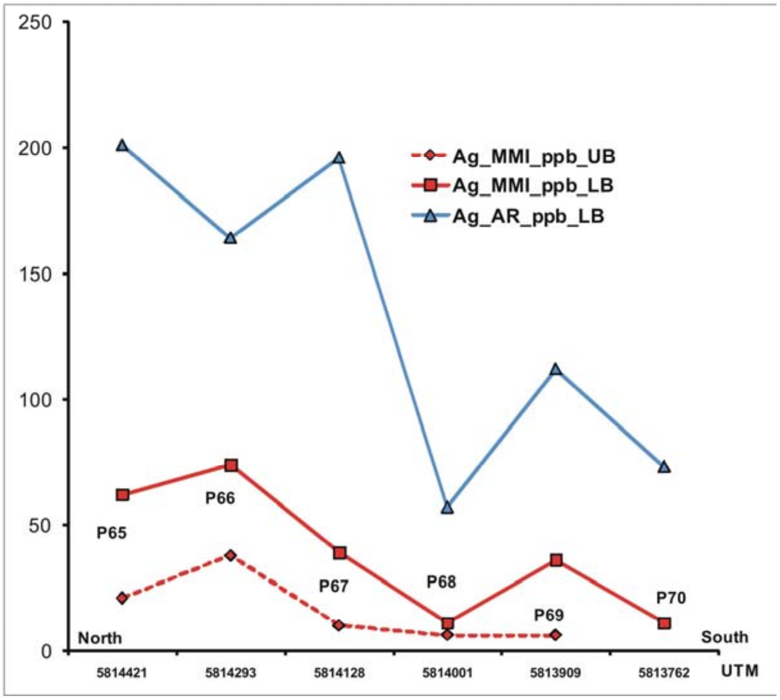

Figure: 3.4.77. Silver by aqua regia-ICPMS and MMI^{SM} along Traverse D.

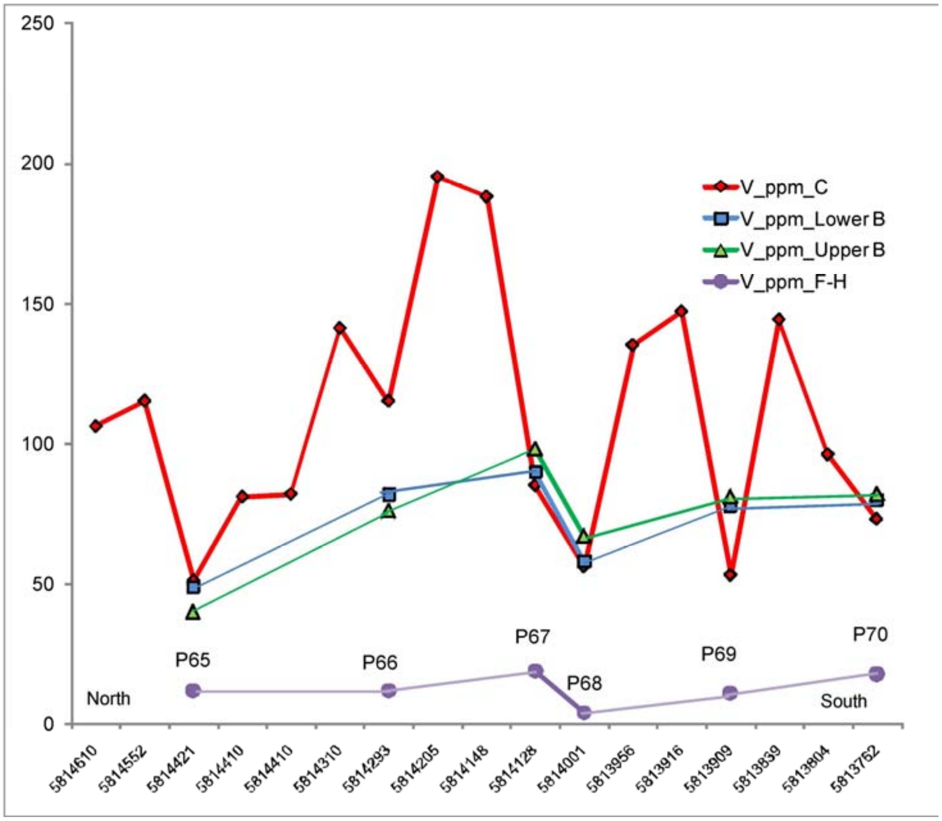

Figure: 3.4.78. Vanadium by aqua regia-ICPMS along Traverse D.

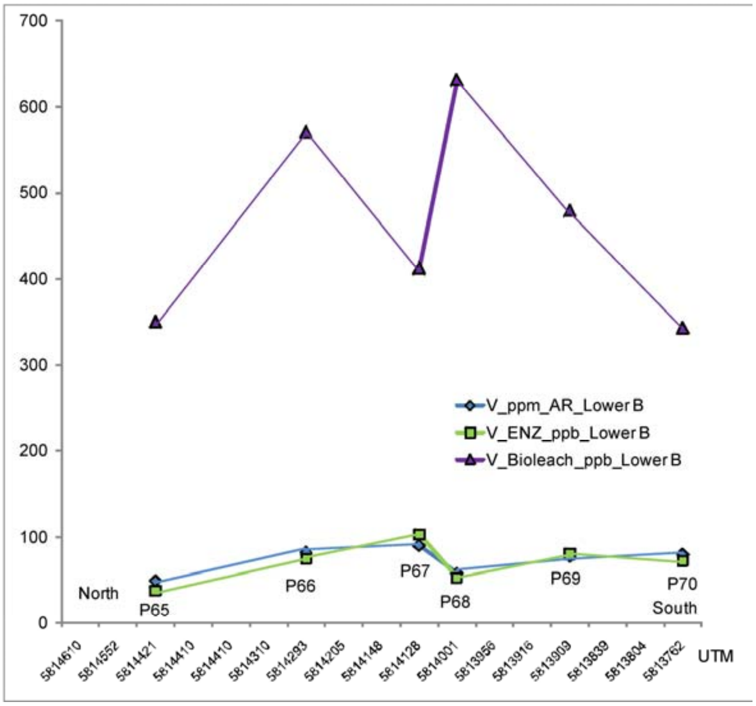

Figure: 3.4.79. Vanadium by aqua regia-ICPMS and partial leaches along Traverse D.

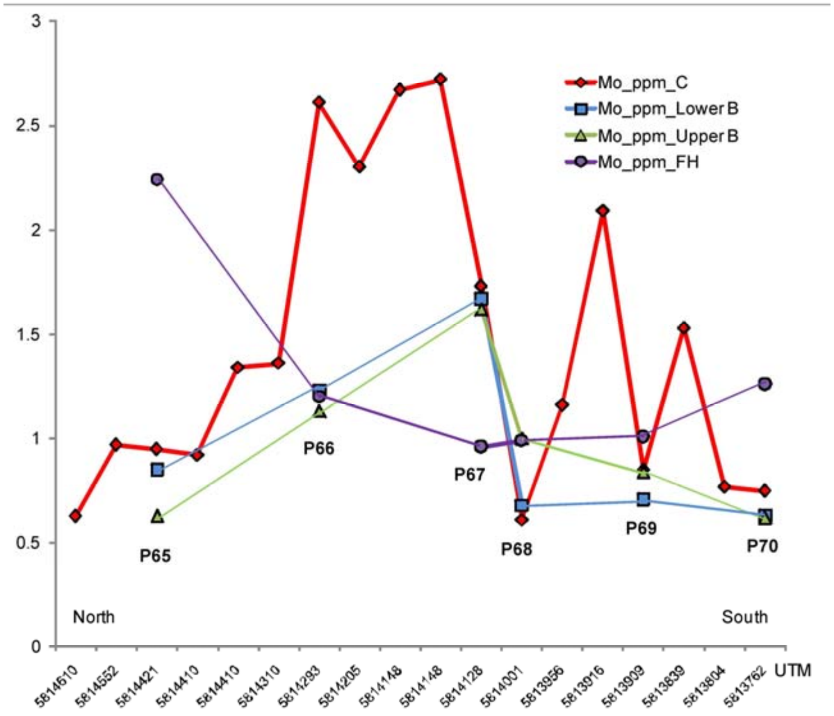

Figure: 3.4.80. Molybdenum by aqua regia-ICPMS along the Traverse D.

Element variations along Traverse D could reflect glacial mineralized bedrock in till, changes in soil organic matter, pH variation through soil-forming processes and pH/redox patterns induced redox cells over deeper weathering sulphides. The characteristic down-ice asymmetric shape of the C-horizon Cu anomaly, the abundance of pristine Au grains in the heavy mineral concentrate, Br and I patterns, and mobile metal ion Au contrast suggest a nearby Au-Cu mineral source to the anomaly peak. Although, regionally, ice flowed from south east to north west the local ice flow could have been deflected by the ridge between the North and Quarry zones so that till may have been deposited by a more north to south ice-flow. The source of mineralized rock detected by the geochemistry could therefore be close to the contact between intrusive and the volcaniclastics rock (i.e. near P68 and P69). A nearby diamond drill hole (SH91-18) intersected fine grained, moderately hornfelsed siltstone with up to 5 percent disseminated pyrite. The drill log records an overburden thickness of 4.6 metres (Petsel, 2006). Figure 3.4.81 shows variation of upper B soil horizon LOI values with BioLeach^{SM} Br and I. A similarity between the three variables suggests that soil organic matter is, in part, responsible for BioLeach^{SM} Br and V patterns.

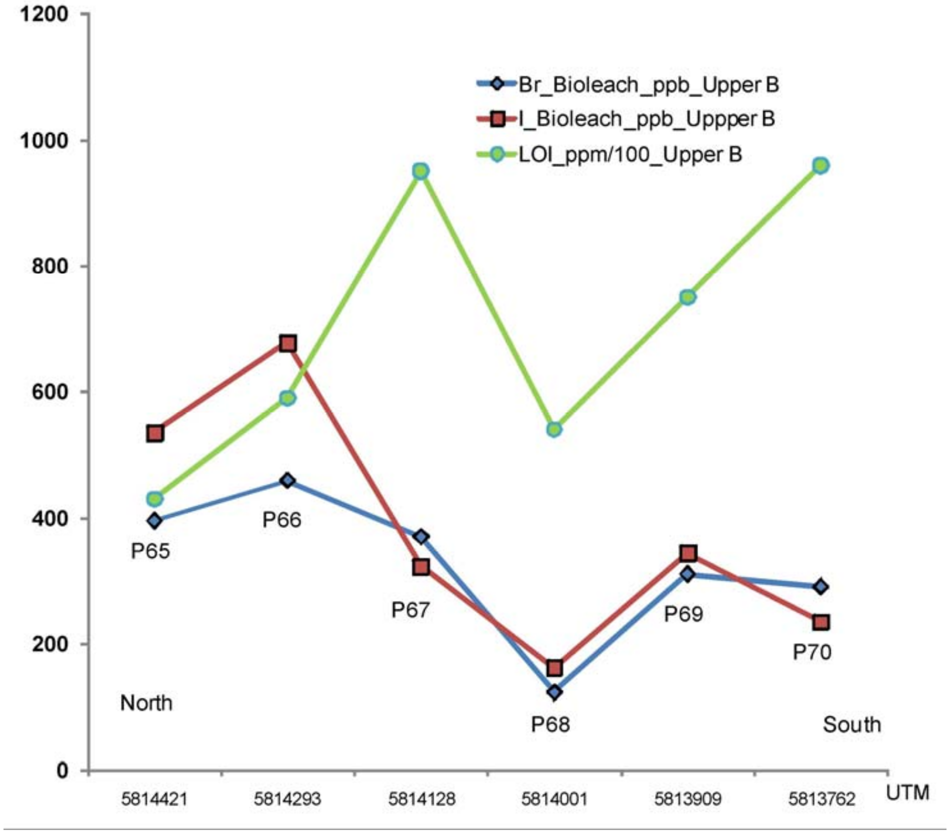

Figure: 3.4.81. Loss on ignition (LOI), BioLeach^{SM} Br and I in the Upper B horizon.

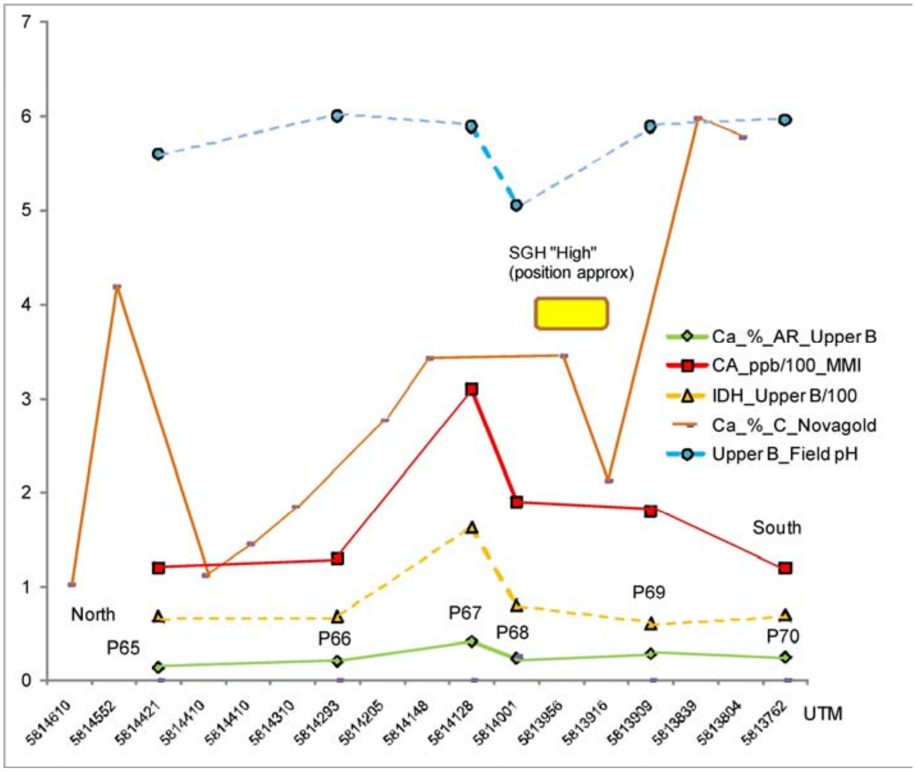

Figure: 3.4.82. Inverse difference pH (IDH), field pH, MMI^{SM} Ca, aqua regia Ca.

Field measured soil pH and IDH values calculated from laboratory measured soil pH are compared with soil Ca variation in Figure 3.4.82. There is an asymmetric IDH and field measured pH peak at between Profiles 67 and 68 reflected in higher MMI^{TM} Ca values and, to a lesser extent, the lower aqua regia-ICPMS upper B horizon Ca values. A noticeable difference between B and C soil horizon Ca patterns can be explained by different acid concentration used in the sample digestion for the Ca analysis. Sutherland and Hoffman, (2008), interpret an apical SGH^{SM} anomaly roughly 500 metres east of the north mineralized zone. They also identify a small SGH^{SM} peak, flanked by "lows" in contoured SGH^{SM} data between Profiles 68 and 69. This is roughly coincident with a decrease in upper B horizon field soil pH and an increase in IDH values.

Traverse E: Soil profiles along Traverse E, shown in Figure 3.4.69, are designed to test the expression of a Pb-Zn mineralized zone peripheral to the Skiko Lake stock. Bedrock under Traverse E is basalt covered by sandy till. Up to 105 ppm Cu is detected in the C horizon at profile 74 and there are similar Cu pattern in the B and F-H horizons, but the values are lower (Figure 3.4.83). In Figure 3.4.84 there are similar MMI^{TM} and BioLeach^{SM} Cu patterns in the Lower B horizon along the Traverse with a corresponding Cu peak by both methods at Profile 77. However, the MMI^{TM} and BioLeach^{SM} Cu patterns are not reflected by variation of Cu values in Lower B horizon soil samples. In figure 3.4.85 there is an isolated INAA Au peak in the C soil horizon peak at Profile 74 with a value of 27 ppm and a smaller, single sample, Au peak in the Upper B horizon at Profile 72. Only single Au grains have been isolated from most of heavy mineral concentrates of C horizon samples along the Traverse and grains from Profiles 73 and 74 samples have been described as “pristine” suggesting a local source for the Au. The elevated INAA Au (27 ppb) in the C soil horizon sample from Profile 74 is reflected by aqua regia-ICPMS value of 17 ppb Au and a smaller MMI^{TM} Au peak in the Lower B soil horizon (Figure 3.4.86). There are also coincident, but smaller, aqua regia-ICPMS C horizon Au, aqua regia-ICPMS lower B horizon Au and MMI^{SM} Au peaks at Profile P 77.

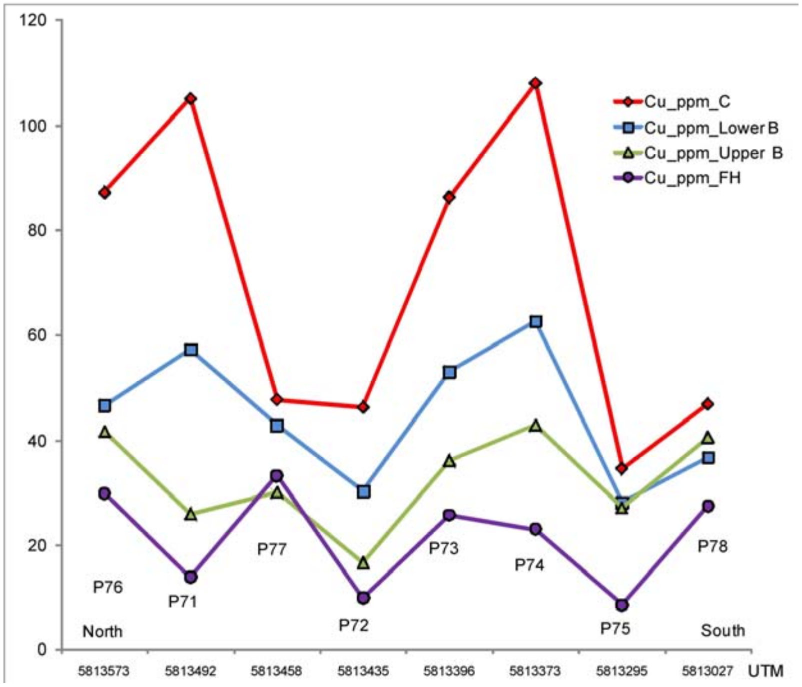

Figure: 3.4.83. Copper by aqua regia along Traverse E.

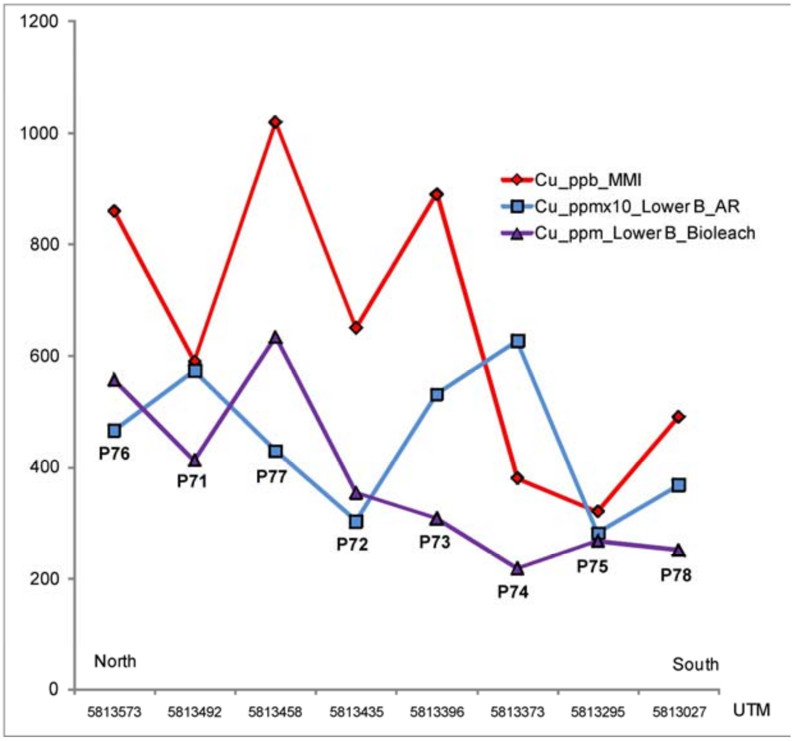

Figure: 3.4.84. Copper by aqua regia-ICPMS and partial leach analysis along Traverse E.

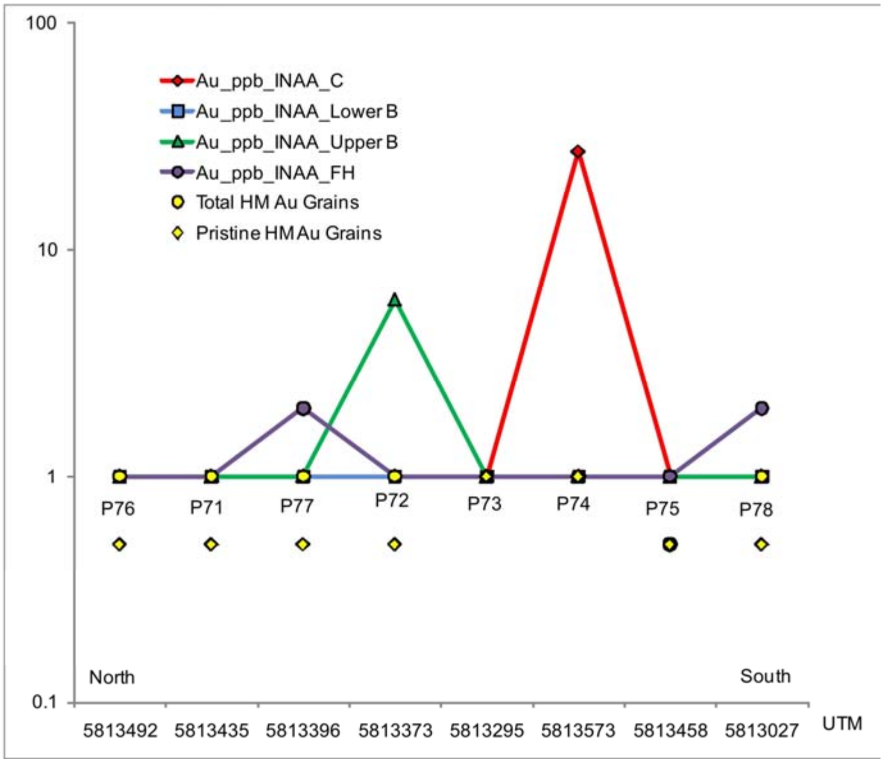

Figure: 3.4.85. Gold by INAA and Au grains in HMS along Traverse E.

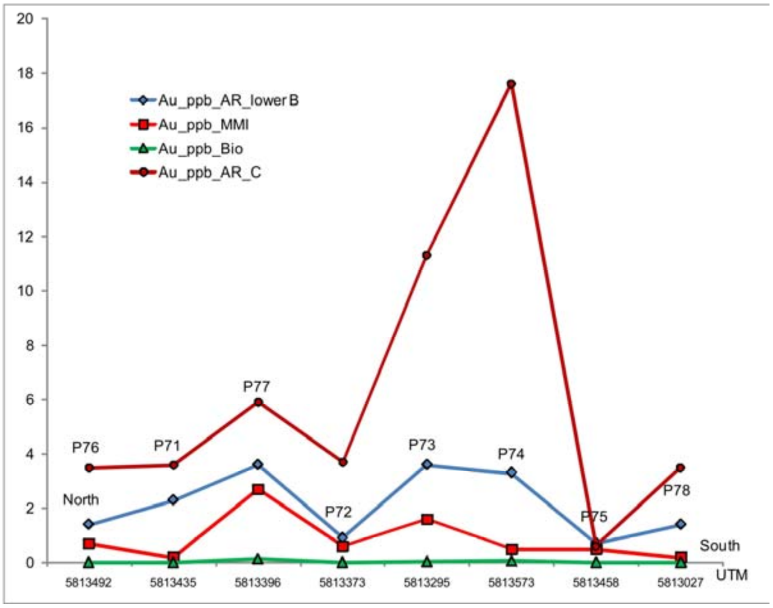

Figure: 3.4.86. Gold by aqua regia-ICPMS and partial leach analysis along Traverse E.

Silver in Figure 3.4.87 is higher in F-H horizon samples compared levels in B and C horizon samples along Traverse E and the there is a sharp, single sample, F-H horizon peak with up to 900 ppb Ag at Profile 55. There are only detectable MMI^{TM} Ag values for Lower B soil horizon samples and Figure 3.4.88 shows that there is a very similar MMI^{TM} Ag pattern to the Lower B soil horizon aqua regia-ICPMS Ag pattern. Molybdenum variation in the soil along Traverse E, shown in Figure 3.4.89 is similar of Ag are there are generally higher Mo values in F-H horizon samples compared to samples from B and C horizons. There is also noticeable correlation of F-H Mo values to C horizon Mo values at Profile 74. Vanadium in soil along Traverse E, shown in Figure 3.4.90, displays a “saw tooth” pattern in all horizons, especially in F-H horizon samples and there the highest values are in the C soil horizon sample from Profile 77.

Vanadium and Co have similar variation along Traverse E especially in the F-H and in the C horizons at Profile 71. BioLeach^{SM} Co in Figure 3.4.91 shows that this leach gives the largest Co Lower B soil anomaly contrast compared aqua regia-ICPMS, MMI^{TM} and Enzyme Leach ^{SM} analysis. Manganese in Figure 3.4.92 is clearly higher in the F-H soil horizon compared to levels in the B and C mineral horizons and there is a significant Mn peak between Profiles 73 and 74. There is also a subdued Mn peak in the C soil horizon at Profile 71 that corresponds to the elevated V and Co. In Figures 3.4.93 and 3.4.94, Pb and Zn have different levels in the soil horizons. Zinc increase to a peak in the F-H soil at Profile 71, but there are lower values in the C horizon. However, Pb is much higher in the C soil horizon at Profile 71 compared to the F-H horizon and there are two distinct Pb peaks at Profile 71 and 74. Figure 3.4.95 shows similar LOI, BioLeach^{SM} Br and BioLeach^{SM} I patterns in Upper B horizon soil samples with values increasing to a “high” at Profile 77 and then falling to a “low” at Profile 73. Aqua regia-ICPMS Ca and MMITM Ca vary together along Traverse E and fall from higher values at the north to Profile 72, the midpoint of the traverse and then increasing to south at Profile 78. Upper B soil pH, expressed as IDH, decrease to a ‘low” at Profile 77.

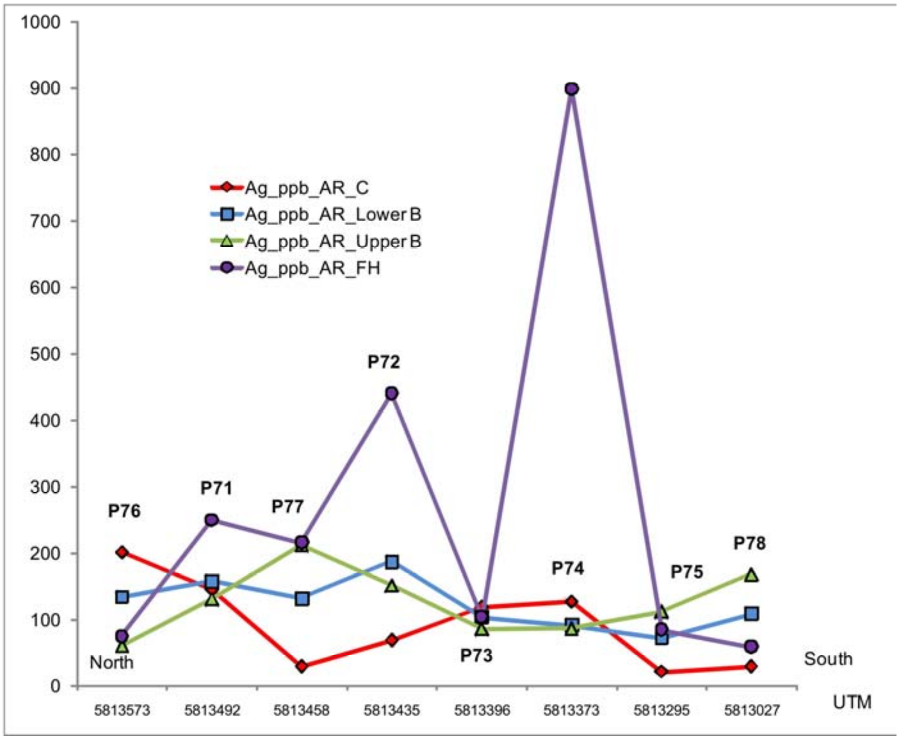

Figure: 3.4.87. Silver by aqua regia-ICPMS along Traverse E.

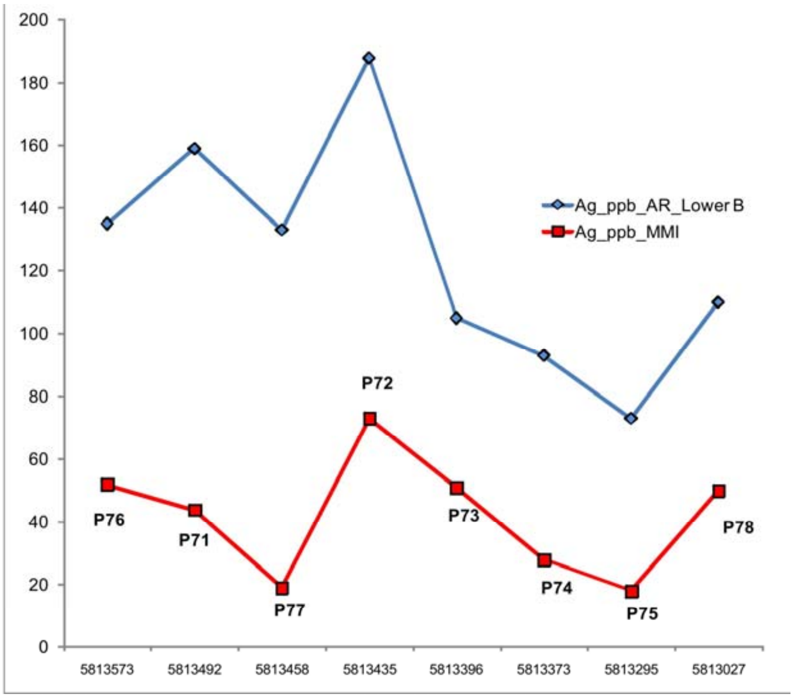

Figure: 3.4.88. Silver by aqua regia-ICPMS and MMI^{TM} analysis along Traverse E.

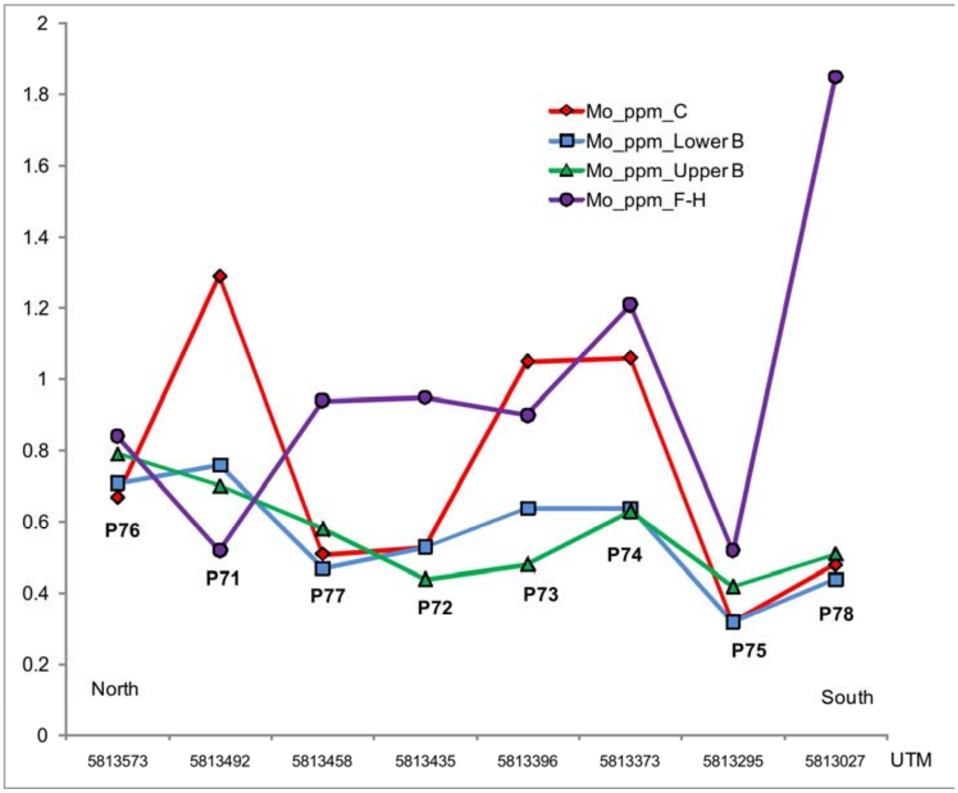

Figure: 3.4.89. Molybdenum by aqua regia-ICPMS along Traverse E.

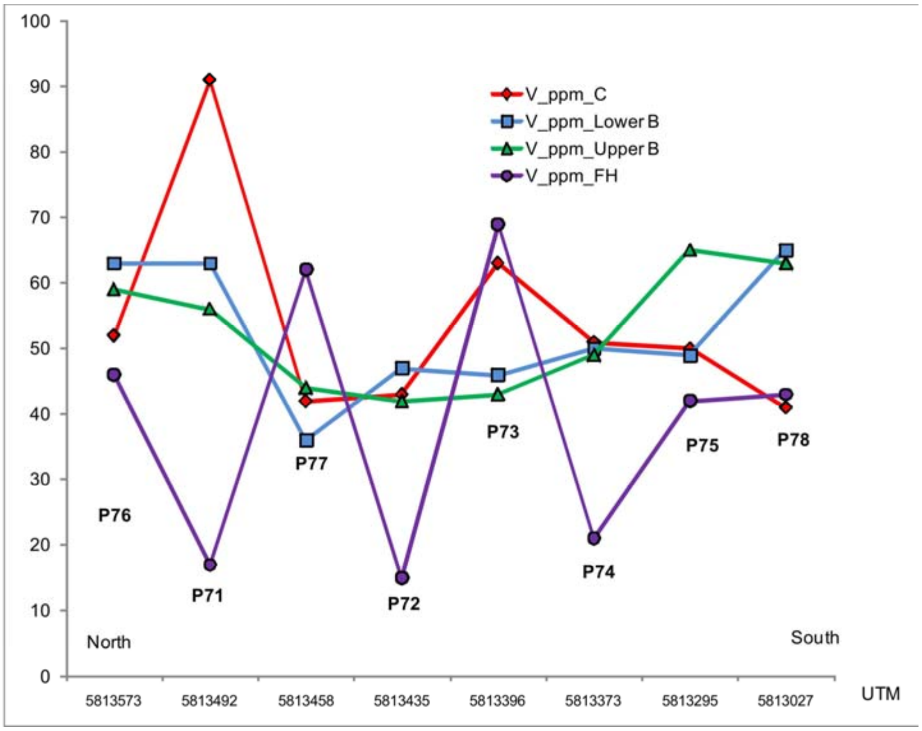

Figure: 3.4.90. Vanadium by aqua regia-ICPMS along Traverse E.

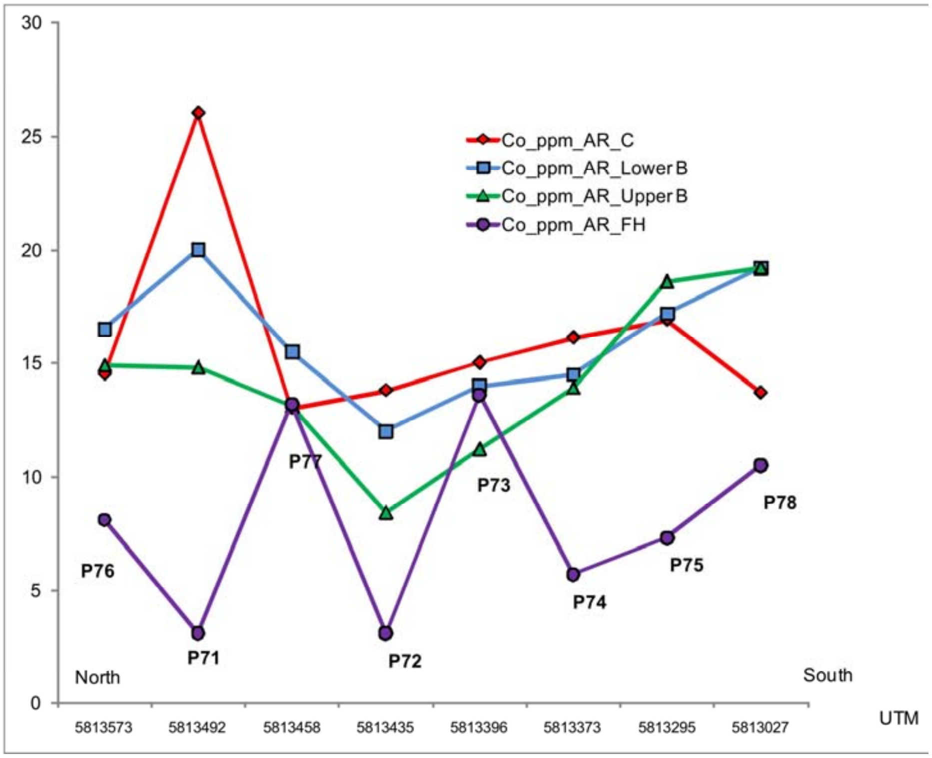

Figure: 3.4.91. Cobalt by aqua regia-ICPMS along Traverse E.

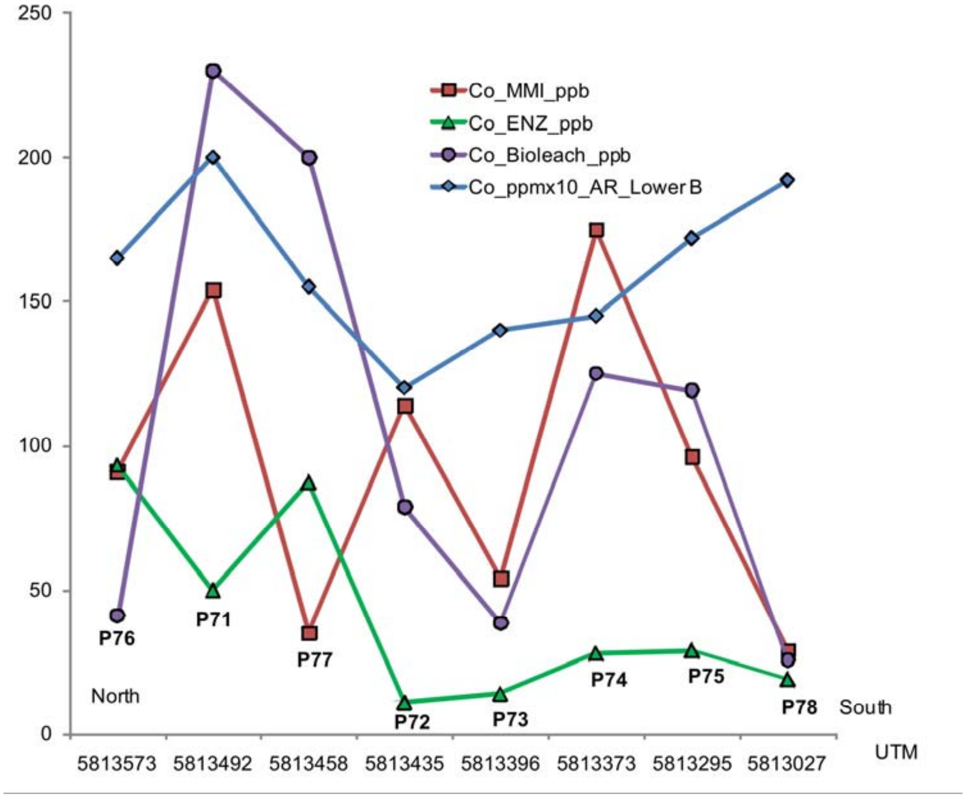

Figure: 3.4.92. Cobalt by aqua regia-ICPMS and partial leach analysis along Traverse E.

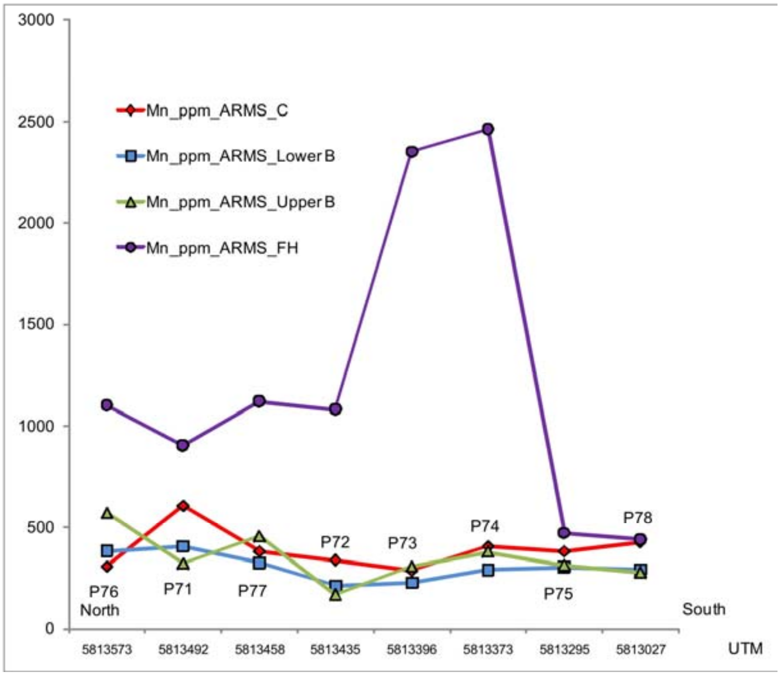

Figure: 3.4.93. Manganese by aqua regia-ICPMS along Traverse D.

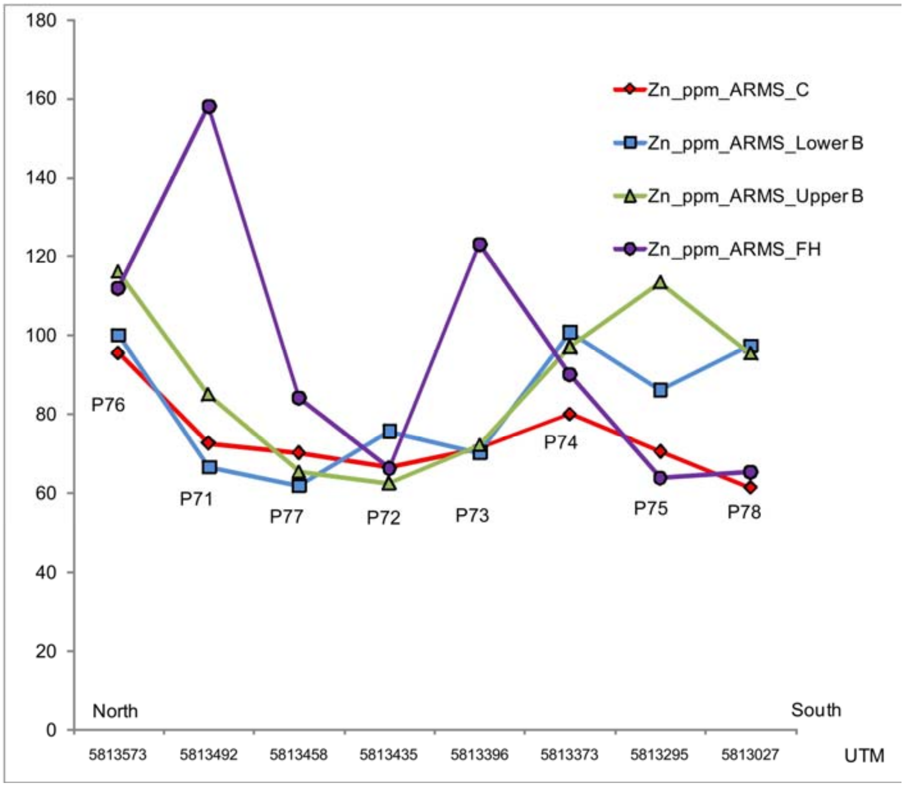

Figure: 3.4.94. Zinc by aqua regia-ICPMS along Traverse E.

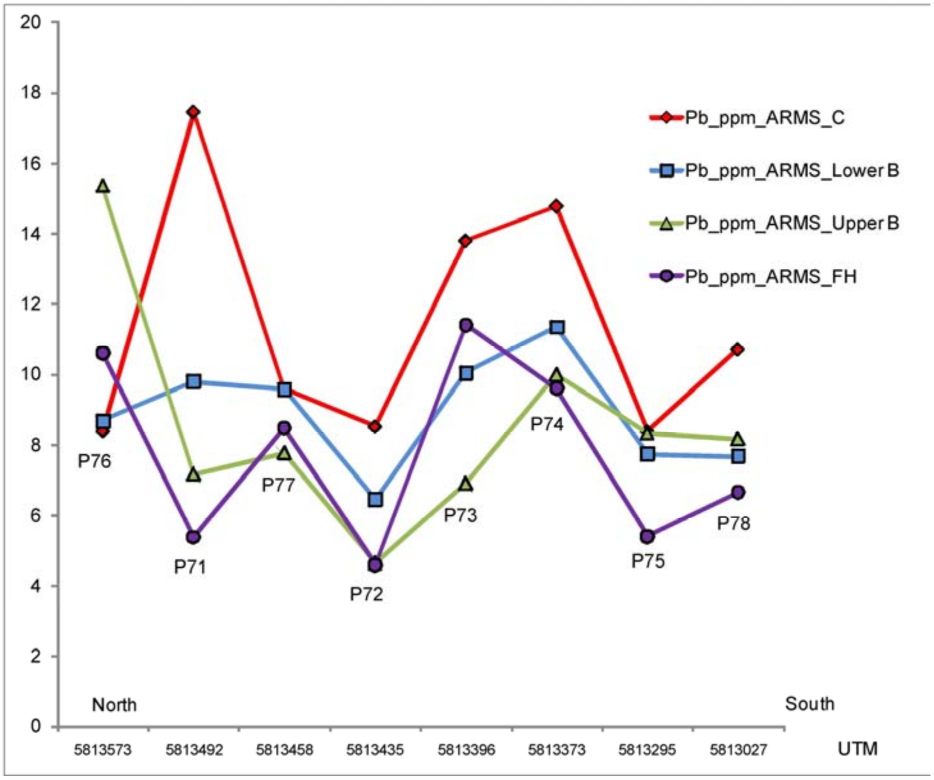

Figure: 3.4.95. Lead by aqua regia-ICPMS along Traverse E.

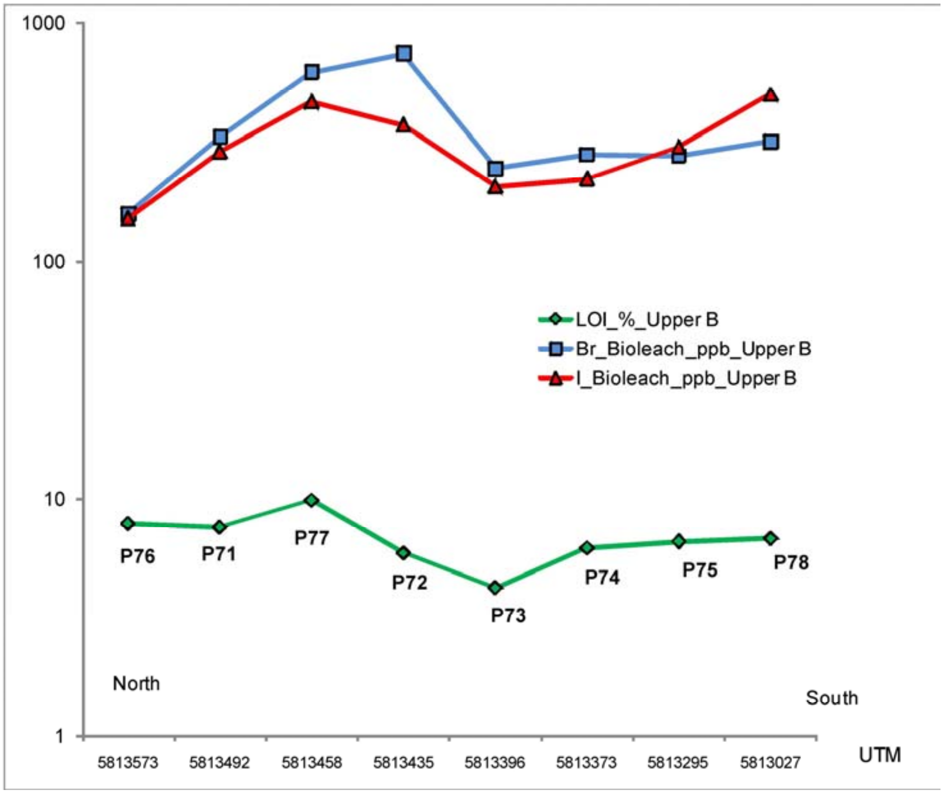

Figure: 3.4.96 Loss on ignition (LOI), Bioleach Br and BioLeach^{SM} I along Traverse E.

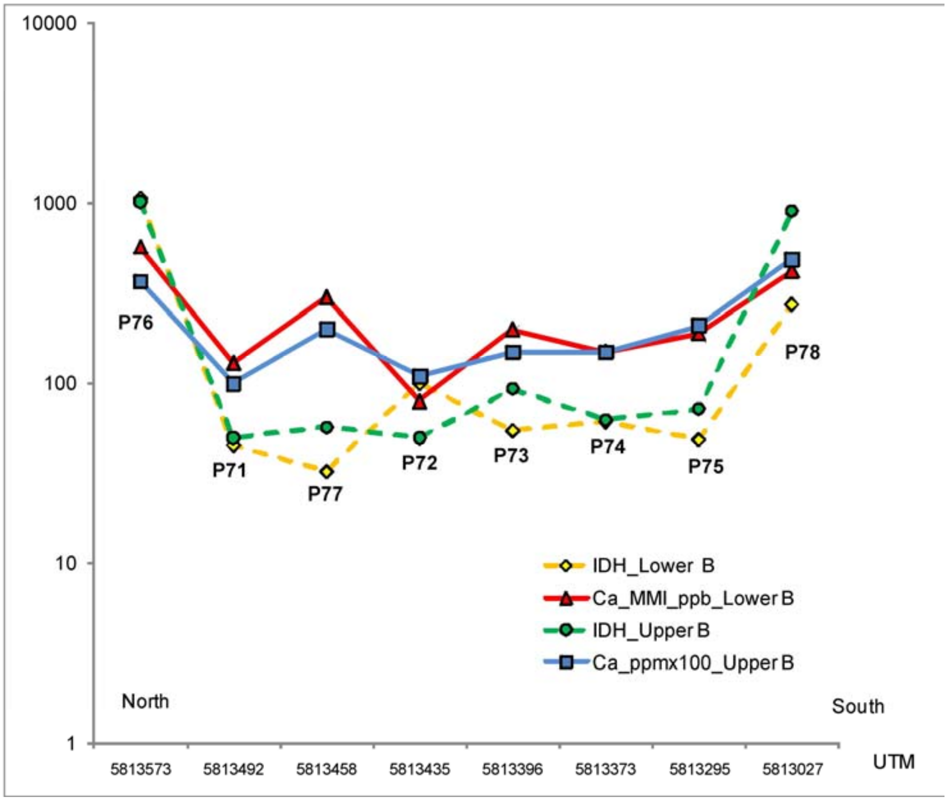

Figure: 3.4.97 Calcium by aqua regia-ICPMS, and MMI^{TM} and IDH along Traverse E.

Anomaly Definition

Element	Range (min-max)	Peak Value	Background (median)	Threshold (3rd quartile)	Contrast
Au_AR_FH	0.2 – 143 ppb	72.1 ppb	0.2 ppb	0.2 ppb	288
Au_AR_UB	0.2 – 138.7 ppb	93.5 ppb	2.9 ppb	9.6 ppb	9.7
Au_AR_LB	0.2 – 239 ppb	192.8 ppb	3.6 ppb	15 ppb	12.9
Au_AR_C	0.2 – 283.5 ppb	264.2 ppb	5.9 ppb	27.6 ppb	9.6
Au_INA_FH	0.5 – 90 ppb	62 ppb	1 ppb	2 ppb	30.8
Au_INA_UB	1 – 113 ppb	87 ppb	1 ppb	17 ppb	5.0
Au_INA_LB	1 – 137 ppb	101 ppb	6 ppb	36 ppb	2.8
Au_INA_C	1 - 298 ppb	282 ppb	3 ppb	44 ppb	6.4
Au_MMI_UB	0.05 – 3.4 ppb	3.05 ppb	0.5 ppb	1.3 ppb	2.3
Au_MMI_LB	0.05 – 20.1 ppb	11.7 ppb	0.7 ppb	1.7 ppb	7.2
Au_BioLeach_UB	0.05 – 0.26 ppb	0.22 ppb	0.03 ppb	0.04 ppb	8.8
Au_BioLeach_LB	0.05 – 0.27 ppb	0.24 ppb	0.05 ppb	0.14 ppb	1.7
Ag_AR_FH	41 – 1200 ppb	1050 ppb	205 ppb	429 ppb	2.4
Ag_AR_UB	60 – 390 ppb	388 ppb	137 ppb	163 ppb	2.4
Ag_AR_LB	57 – 580 ppb	448 ppb	123 ppb	184 ppb	2.4
Ag_AR_C	22 – 614 ppb	461 ppb	95 ppb	132 ppb	3.5
Ag_MMI_UB	2 - 58 ppb	48 ppb	11 ppb	20 ppb	2.4
Ag_MMI_LB	8 - 74 ppb	74 ppb	31 ppb	46 ppb	1.6
As_AR_FH	0.7 – 6.3 ppm	5.85 ppm	1.5 ppm	2.8 ppm	2.1
As_AR_UB	1.3 – 13.2 ppm	11.35 ppm	5.2 ppm	6.80 ppm	1.7
As_AR_LB	2.7 – 13.2 ppm	12.40 ppm	6.0 ppm	7.3 ppm	1.7
As_AR_C	3.5 – 27.2 ppm	22.1 ppm	8.0 ppm	10.8 ppm	2.0
As_MMI_UB	5 – 10 ppb	10 ppb	5 ppb	10 ppb	1.0
As_MMI_LB	5 – 50 ppb	45 ppb	5 ppb	13 ppb	1.3
As_Enz_UB	1 – 8 ppb	8 ppb	4.0 ppb	6.0 ppb	2.6
As_Enz_LB	0.5 – 10 ppb	8.5 ppb	3.0 ppb	5.0 ppb	1.7
As_BioLeach_UB	46.3 – 159 ppb	156 ppm	90.2 ppb	127 ppb	1.2
As_BioLeach_LB	51.3 – 189 ppb	186.5 ppm	94.8 ppb	117 ppb	1.6
Cu_AR_FH	7.0 – 212.0 ppm	204.5 ppm	13.9 ppm	25.8 ppm	7.9
Cu_AR_UB	15.87 – 255.9 ppm	222 ppm	46.5 ppm	103 ppm	2.2
Cu _AR_LB	19.9 – 483 ppm	385 ppm	57.3 ppm	136.5 ppm	2.8
Cu_AR_C	24.4 – 1096.4 ppm	904.1 ppm	84.8 ppm	156 ppm	5.8
Cu_MMI_UB	230– 2750 ppb	2585 ppb	1150 ppb	1960 ppb	1.3
Cu_MMI_LB	220 – 6070 ppb	4575 ppb	660 ppb	1333 ppb	3.4
Cu_BioLeach_UB	177 – 1380 ppb	1177 ppb	426 ppb	749 ppb	1.6
Cu_BioLeach_LB	145 – 2830 ppb	2710 ppb	524 ppb	904 ppb	3.0
Cu_EnzLeach_UB	4 – 156 ppb	119 ppb	28 ppb	44 ppb	2.7
Cu_EnzLeach_LB	1 – 305 ppb	193 ppb	25 ppb	63 ppb	3.1
Co_AR_FH	0.8 – 13.8 ppm	13.7 ppm	4.1 ppm	9.3 ppm	1.5
Co_AR_UB	8.4 – 27.1 ppm	25 ppm	15.0 ppm	18.5 ppm	1.3
Co_AR_LB	10.9 – 33.1ppm	32.3 ppm	17.3 ppm	19.2 ppm	1.7
Co_AR_C	10.9 – 63.5 ppm	49.1 ppm	15.8 ppm	19.3 ppm	2.6
Co_MMI_UB	28 – 322 ppb	294 ppb	88 ppb	193 ppb	1.5

Co_MMI_LB	19 – 1750ppb	165 ppb	50 ppb	111 ppb	1.5
Co_Enz_UB	12 – 68 ppb	68 ppb	27 ppb	41 ppb	1.7
Co_Enz_LB	11 – 93 ppb	90 ppb	30 ppb	45 ppb	2.0
Co_BioLeach_UB	21 – 291 ppb	239 ppm	59 ppb	93 ppb	2.6
Co_BioLeach_LB	22 – 245 ppb	238 ppm	61 ppb	74 ppb	3.2
Pb_AR_FH	4.59 – 22 ppm	19.05 ppm	10.1 ppm	11.9 ppm	1.6
Pb_AR_UB	3.61 – 15.35 ppm	13.04 ppm	6.00 ppm	7.80 ppm	1.7
Pb_AR_LB	4.22 – 11.34 ppm	10.7 ppm	6.6 ppm	7.74 ppm	1.4
Pb_AR_C	4.44 – 17.46 ppm	16.12 ppm	7.79 ppm	8.83 ppm	1.8
Pb_MMI_UB	40 – 830 ppb	620 ppb	195 ppb	230 ppb	2.7
Pb_MMI_LB	5 – 680 ppb	660 ppb	145 ppb	265 ppb	2.5
Pb_Enz_UB	0.5 – 13 ppb	9.5 ppb	3.0 ppb	4.0 ppb	2.4
Pb_Enz_LB	0.5 – 12 ppb	9.0 ppb	2.0 ppb	3.0 ppb	3.1
Pb_BioLeach_UB	16 – 286 ppb	278 ppm	54 ppb	88 ppb	3.2
Pb_BioLeach_LB	11 – 349 ppb	308 ppm	45 ppb	72 ppb	4.2
Mn_AR_FH	76 – 10000 ppm	9775 ppm	1190 ppm	2460 ppm	4.0
Mn_AR_UB	140 – 825 ppm	698 ppm	307 ppm	368 ppm	1.9
Mn_AR_LB	171 – 659 ppm	537 ppm	303 ppm	368 ppm	1.5
Mn_AR_C	210 – 665 ppm	636 ppm	360 ppm	405 ppm	1.6
Mn_Enz_UB	205 – 11900 ppb	9735 ppb	1800 ppb	3230 ppb	3.0
Mn_Enz_LB	443 – 5200 ppb	5160 ppb	1130 ppb	1740 ppb	3.0
Mn_BioLeach_UB	493 – 16900 ppb	16650 ppm	4050 ppb	6700 ppb	2.5
Mn_BioLeach_LB	784 – 16000 ppb	15150 ppm	2910 ppb	4980 ppb	3.0
Mo_AR_FH	0.52 – 6.95 ppm	5.62 ppm	1.01 ppm	1.63 ppm	3.4
Mo_AR_UB	0.42 – 4.30 ppm	3.2 ppm	0.72 ppm	1.2 ppm	2.7
Mo_AR_LB	0.32 – 6.09 ppm	4.60 ppm	0.71 ppm	1.18 ppm	3.9
Mo_AR_C	0.32 – 18.92 ppm	12.01 ppm	0.71 ppm	1.29 ppm	9.3
Mo_MMI_UB	3 – 36 ppb	24 ppb	4 ppb	6 ppb	3.8
Mo_MMI_LB	3 – 55 ppb	34 ppb	3 ppb	7 ppb	4.6
Mo_Enz_UB	0.5 – 151 ppb	84 ppb	4 ppb	6 ppb	13.9
Mo_Enz_LB	0.5 – 142 ppb	78 ppb	3 ppb	5 ppb	15.6
Mo_BioLeach_UB	11 – 181 ppb	117 ppm	17 ppb	24 ppb	4.9
Mo_BioLeach_LB	11 – 183 ppb	114 ppm	17 ppb	29 ppb	3.9
Ni_AR_FH	2.5 – 41.7 ppm	39.05 ppm	11.5 ppm	22.8 ppm	1.7
Ni_AR_UB	14.2 – 101.1 ppm	86.7 ppm	36.7 ppm	49.6 ppm	1.7
Ni_AR_LB	25.4 – 121.5 ppm	97.3 ppm	43.8 ppm	53.3 ppm	1.8
Ni_AR_C	24.4 – 139.6 ppm	113.55 ppm	37.4 ppm	57.9 ppm	2.0
Ni_MMI_UB	32 – 286 ppb	272 ppb	150 ppb	216 ppb	1.3
Ni_MMI_LB	24 – 321 ppb	253 ppb	76 ppb	146 ppb	1.7
Ni_Enz_UB	4 – 44 ppb	40 ppb	16 ppb	20 ppb	2.0
Ni_Enz_LB	4 – 26 ppb	26 ppb	9 ppb	15 ppb	1.7
Ni_BioLeach_UB	38 – 281 ppb	261 ppm	111 ppb	179 ppb	1.5
Ni_BioLeach_LB	27 – 292 ppb	272 ppm	105 ppb	133 ppb	2.0
V_AR_FH	4 – 92 ppm	88 ppm	19 ppm	41 ppm	2.1
V_AR_UB	39 – 155 ppm	139 ppm	70 ppb	80 ppm	1.7
V _AR_LB	36 – 134 ppm	131 ppm	71 ppb	84 ppm	1.6
V_AR_C	36 – 248 ppm	221 ppm	63 ppb	87 ppm	2.5
V_Enz_UB	34 – 171 ppb	169 ppb	64 ppb	85 ppb	2.0
V_Enz_LB	28 – 316 ppb	242 ppb	76 ppb	102 ppb	2.4

V_BioLeach_UB	288 – 941 ppb	930 ppb	520 ppb	608 ppb	1.5
V_BioLeach_LB	301 – 731 ppb	722 ppb	489 ppb	541 ppb	1.3
Zn_AR_FH	24.4 – 213 ppm	210.5 ppm	65.3 ppm	112 ppm	1.9
Zn_AR_UB	50.7 – 158.9 ppm	145.1 ppm	86.6 ppb	98.6 ppm	1.5
Zn_AR_LB	44.4 – 145.9 ppm	131.1 ppm	71.3 ppb	99.5 ppm	1.4
Zn_AR_C	37.4 – 111.7 ppm	103.6 ppm	64.6 ppb	72.3 ppm	1.4
Zn_Enz_UB	5 – 330 ppb	285 ppb	60 ppb	10 ppb	2.9
Zn_Enz_LB	5 – 130 ppb	120 ppb	30 ppb	40 ppb	3.0
Zn_BioLeach_UB	51 – 1370 ppb	1340 ppb	368 ppb	580 ppb	2.3
Zn_BioLeach_LB	34 – 1340 ppb	892 ppb	162 ppb	300 ppb	3.0
Zn_MMI_UB	8 – 2710 ppb	2530 ppb	530 ppb	2028 ppb	1.2
Zn_MMI_LB	10 – 1660 ppb	1395 ppb	180 ppb	665 ppb	2.1
LOI – Upper B	3.7 – 18.7%	15.1 %	7.65 %	8.6 %	1.8
LOI – Lower B	3.5 – 9.5 %	9.4 %	6.3 %	8.5 %	1.1
Br_BioLeach_UB	124 – 750 ppb	696 ppb	319 ppb	393 ppb	1.8
Br_BioLeach_LB	114 – 787 ppb	724 ppb	392 ppb	505 ppb	1.4
I_BioLeach_UB	151 – 678 ppb	631 ppb	374 ppb	475 ppb	1.3
I_BioLeach_LB	156 – 842 ppb	837 ppb	459 ppb	603 ppb	1.4

Table 3.6: Anomaly characteristics for ore indicator and pathfinder elements in F-H, Upper B, Lower B and C soil horizon samples calculated from the Shiko Lake soils data. The peak value is calculated from the average of the two highest values and values below detection limit are set and 0.5 detection limit.

4. Interpretation of Survey Data

Open File 2010-09 examines the soil and drainage sediment geochemical expression of porphyry Cu-Au-Mo mineralization in areas where the bedrock is partly or completed covered by glacial sediments and plateau basalt. Four case histories in the Open File range from Shiko Lake where there is a relatively clear link between the surficial geochemistry and the sulphide mineralized bedrock, to Mouse Mountain where the mineral source-surface geochemistry relationship is less obvious to Soda Creek with there are no documented mineral occurrences, but where results of past geochemical surveys suggest that mineralization might be present. The case histories represent a range of surficial environments, glacial sediment types, soils and landforms typical of those encountered during a routine soil geochemical surveys in central BC. For example, at Shiko Lake and Mouse Mountain a till veneer and colluvium covers a rugged topography whereas thicker till mantles plateau surface at Soda Creek and Alexandria. Figure 4.1 illustrates the principal landforms, surficial sediments and soil types common to the four areas. Also shown are concentric trace element patterns in the bedrock around a Cu-Au mineralized porphyry. The zonation reflects a geochemical model developed by Hoffman, (1990), to explain results of multi-element soil and lithogeochemical surveys on the Cat Mountain Ag-Cu porphyry deposit. Hoffman proposed concentric lithogeochemical zones radiating outwards from a W-Ag-Mo core through a predominantly Au mineralized zone, a Cu-Co-Fe-V-enriched zone and finally into a peripheral zone where there is elevated As, Al and Mn. Not all of the zones may exist or may be truncated in other deposits (e.g. Shiko Lake, Mouse Mountain) where the style of mineralization, geology, structure and erosion level are different from that at the Cat Cu-Au mineralized porphyry.

Figure 4.1 shows the relationship between mineralized bedrock and common glacial sediments in the Quesnel - Soda Creek – Williams Lake area. Sediment types range from lodgement till, melt-out till, fluvial glacial deposits, alluvium and colluvium. A thin diamicton (lodgement or melt-out till) and colluvium covers much of the bedrock at Mouse Mountain and Shiko Lake whereas at Soda Creek the plateau Chilcotin basalt is concealed beneath thicker basal till. Gravel and sand interbedded with a diamicton at Mouse Mountain could have been deposited by fluvial processes active along a proglacial lake shore that extended between Prince George and Quesnel along the Fraser River valley. Geochemistry of this fluvio glacial sediment will have tenuous reflection of the bedrock source material because of partitioning of minerals during sedimentation. Basal till geochemistry, on the other hand, can be more clearly linked to the source bedrock because entrained mineralized rock clasts in a till dispersal train commonly display a fan shape distribution and has an asymmetric longitudinal profile. Copper and Au geochemical patterns in the C horizon along of several the traverses sampled in profiles at Shiko Lake are characteristic of a dispersal train profile. A more direct relationship between a surficial deposit and bedrock is demonstrated by colluvium geochemistry where the sediment transport is local and by a gravity process.

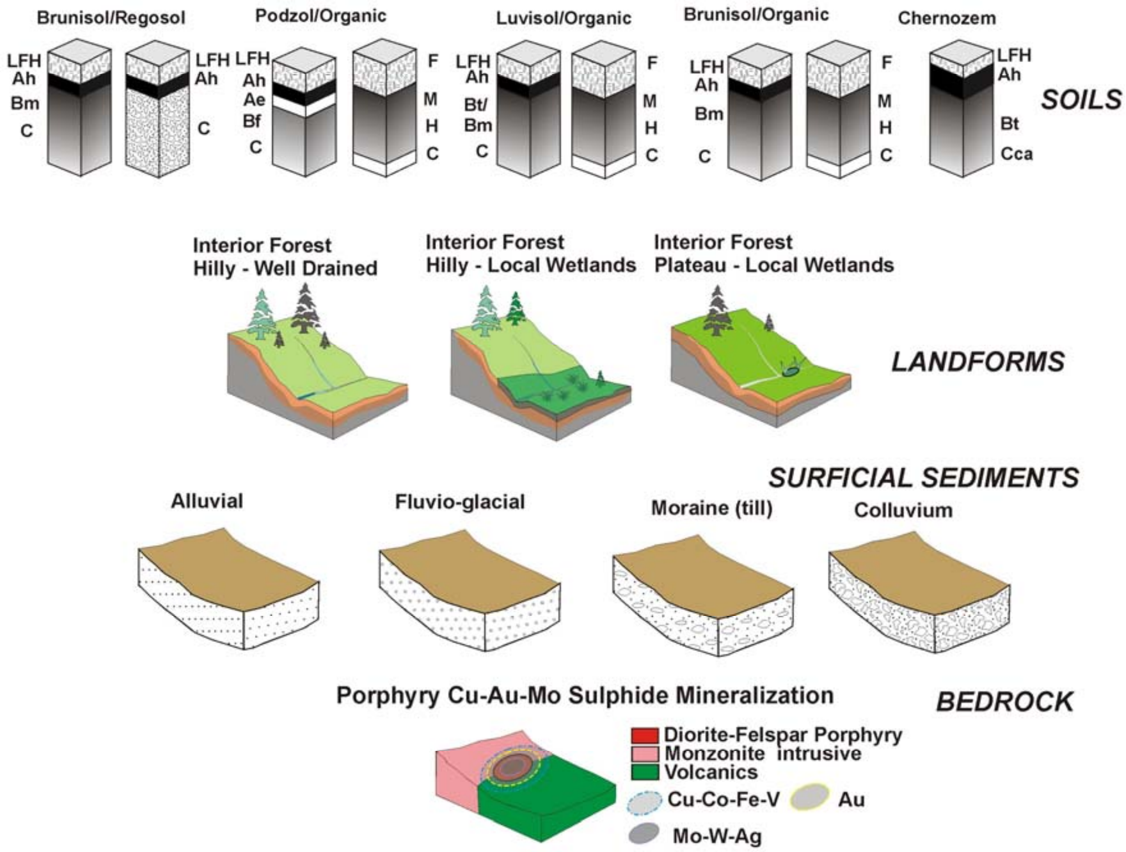

Table 4.1: Landscape components common to Quesnel – Soda Creek – Williams Lake area.

Irrespective of the relationship that exists between surficial sediment and bedrock sediment geochemistry will be modified by soil forming processes. Among factors influencing soil development are climate, drainage, landform and the parent material. Figure 4.1 summarizes the principal soil types developed in the Quesnel - Soda Creek – Williams Lake area and the landforms most characteristic of the region. The most soil common is a Brunisol where the principal horizons are present, but generally immature. Less common are clay-rich luviosols, iron-rich podsols, chernozem that are essentially grassland soil in a semi-arid environment with accumulation of calcium carbonate (Cca). Organic soil (> 30% LOI) and gleysolic soil are developed in poorly drained areas such as seepage zones and wetland margins. Superimposed on the natural soil geochemistry will be an exogenic geochemical signature from the bedrock Cu-Au-Mo mineralization. The signature might reflect a result of a predominately physical process such as dispersal of mineralized bedrock in till or gravity transport forming colluvium and /or a physico-chemical effect such as the mobilization and redistribution of elements along pH and redox gradients. These gradients can induced in soil above weathering, buried suphides as proposed in an electro chemical model developed by Smee, (1998), Hamilton, (2007), Govett, (1976) and Cameron, *et al*, (2004) to explain the relationship between soil geochemical patterns and deeply buried massive sulphide bodies. A reduced chimney in the overburden, a low pH zone in the soil where the chimney meets the active soil zone and a peripheral halo of secondary carbonate surrounding the foot print of the halo are key features of this model.

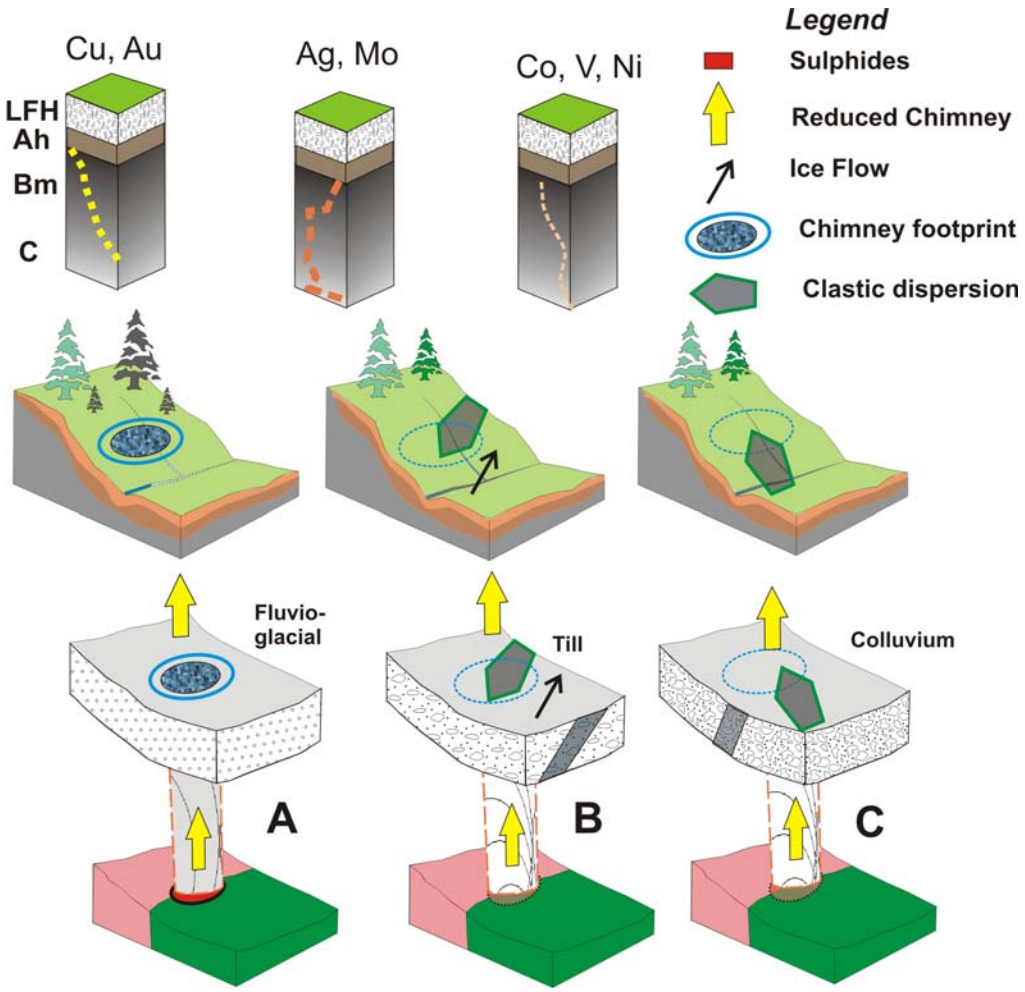

Table 4.2: Summery of different processes that are likely to form soil geochemical anomalies above porphyry style disseminated sulphide mineralization. Broken lines (e.g ▬ ▬) for Cu, Au; Ag, Mo and Co, V, Ni on profiles are intended to show the typical geochemical variation of these elements with depth in the soil.

Three different processes that could explain the geochemical patterns found in the Quesnel-Soda Creek-Williams Lake area are illustrated in Figure 4.2. Model A shows a reducing chimney above a significant sulphide concentration in bedrock beneath glacio-fluvial sediment. Lower pH might be expected where the reduced column enters the soil active zone with a secondary carbonate halo forming. Depletion of more mobile elements might be expected within the acid soil with their secondary accumulation away from the center core as pH increases. Higher inverse difference hydrogen (IDH) values define the secondary carbonate halo and higher SHG values could reflect greater microbial activity associated with weathering sulphides. Soil geochemical patterns that Heberlein, (2009), report over the Kwanika Cu-Au porphyry deposit may be consistent type of dispersion. A redox column extending from bedrock is also displayed in Model B, but is shown to be less intense because of a smaller, more disseminated, concentration of bedrock sulphides. Model B model also shows the physical transport of mineralized bedrock debris as till down-ice from the bedrock-till contact. Model C shows a redox column, but now the physical transport is by gravity to form a colluvial parent to the soil. Figure 4.2 also illustrates typical geochemical patterns down soil profiles with Cu and Au increasing from the upper B horizon into till and elements such as Ag and Mo accumulating in the F-H horizon. Table 3.6 summarises the geochemistry of the four survey areas.

Area	Shiko Lake	Mouse Mt.	Soda Cr.	Alexandria
Drainage sediment & water Geochemistry	Cu & Hg anomalous in RGS samples from streams draining area.	Au & As anomalous in RGS type sediment samples from streams draining area. Cu, As, Mo, Ni, Pb levels are < 2 ppb in water; Zn < 3 ppb. Alkaline water (pH > 7.4) limits dispersion.	Cu & Ni Au & As anomalous in RGS samples from streams draining area.	Au anomalous in RGS samples from streams draining area.
F-H Horizon	Ag & Mn higher in F-H samples compared to levels in B horizon samples. Mo & Pb F-H horizon peaks often do not correspond to Mo B -horizon peaks. High Au contrast (>200) & Cu contrast (>8) reflects isolated F-H Au-Cu anomalies.	Ag, Mn & Mo higher in F-H samples compared to levels in B horizon samples. Single point Au anomaly in aqua regia F-H horizon not confirmed by INAA.	Mn & Zn higher F-H samples compared to levels in B horizon samples.	Cu, Zn, Pb higher F-H samples compared to levels in B horizon samples.
B soil horizon (upper & lower)	Au, Cu, Zn, Mo, Co V typical increase from Upper B into Lower B and C horizons. Au, Cu, Mo most reflect Cu-Au mineralization Cu and Au anomaly contrast not appreciable greater by partial leaches compared to aqua regia. Soil pH, Ca and SGH may indicate one half of dual peak anomaly close to redox “chimney” near area of high Cu in bedrock. Bioleach Br & I corresponds to LOI variations suggesting an association between halogen and organic matter. Very high Cu, Co, and Mo by aqua regia and partial leaches in lower B soil from one Profile (52) reflect metal concentration in organic soil.	Cu, Mo, Ni, V, As & Hg patterns in B horizon subdued compared to contrast shown by metals in C horizon. Levels higher in lower B horizon and patterns generally reflect C horizon variation. Most Au values below detection limit in B soils. High contrast MMITM Cu along midpoint of Rainbow traverse near SGH redox “chimney”.	Cu, Ni, V higher in Lower B horizon compared to upper B horizon and patterns show very little correlation. No correlation between element patterns and a weak predicted redox chimney for SGH data interpretation.	All elements show single sample peak at mind point along traverse. Peak corresponds to increased LOI, Bioleach Br and I and weak redox “chimney”. Distinct change in soil texture and colour in anomalous profile.
C – Horizon	Asymmetric Cu and Au material in C horizon	Marked C soil, Cu, V, As, Hg anomaly at east	Cu, Ni, V patterns similar in C horizon	Cu, Ni, Cr, V & Fe all show single Profile

	with abundant Au grains indicate till dispersal of mineralized bedrock as one source for soil geochemical anomalies. Displacement may be in order on 300-500 m based on average till thickness and pattern shape.	end of Rainbow traverse with increased number of HM Au grains reflect till dispersal from south. Pattern shape may reflect englacial > basal till source.	can be explained by till geochemistry. Scattered Au values < 20 ppb not an indication of mineralization. Broad pH patterns along traverses most likely reflection of till composition.	peak in C horizon. May be reflection of glacial sediment or possibly anthropogenic related to power line construction.
Lithogeochemistry	Au, Te, Cu, Pb, Bi, Ag, Re, Hg, Cd, Cs, Mo, Sb elevated in Novagold samples.	Cu, Au, V, Pd elevated in GSB collected samples.	No data available.	No data available.

Table 3.6: Anomalous pathfinder elements in the Shiko Lake, Mouse Mountain, Soda Creek and Alexandria areas. Bracketed elements (e.g. Mo) are often elevated in a horizon, but not consistently anomalous.

5. Conclusions

The geochemistry has shown:

1. The principal source for geochemically anomalous Cu, Au, Ag, Pb, Zn, Mo, As and Hg in the soil at Shiko Lake and Mouse Mountain is glacially transported bedrock in either englacial or basal till. Lower B and C horizon samples are the preferred medium for detecting evidence for till geochemical dispersal patterns. The C soil horizon anomaly contrast is likely improved using the 0.063 mm fraction of the sample for analysis rather than the – 80 mesh fraction and C horizon data can be directly compared to the results of regional till geochemical surveys. Identification of Au and other mineral grains in C soil horizon heavy mineral concentrates is useful because the number and shape of Au grains can confirm the geochemical patterns and relate the anomaly to the source of the Au. Cobalt, Ni and V are elevated in the C and B horizon samples in all four survey areas including Soda Creek and Alexandria suggesting that the distribution of these elements is is a geochemical expression of till derived for no-mineralized bedrock.

2. The C horizon Cu and Au anomalies are generally reflected by similar, but more subdued patterns in the lower and upper B soil horizons, but Ag, Mn and Mo are typically higher in the F-H horizon. There are also scattered F-H horizon Au anomalies, but these should be treated with caution because they are isolated and single sample. In some cases at Shiko Lake and Mouse Mountain there is a spatial link between the F-H Ag, Mo and Mn patterns and the corresponding B and C horizon patterns, in others these elements in the F-H and mineral horizons are unrelated. At Soda Creek and Alexandria where there is no known Cu-Au mineralization in the bedrock Ag and Mo values are lower in the F-H horizon compared to the B and C horizons. The F-H horizon Ag geochemistry appears to be pathfinder for Cu-Au mineralization and has an advantage of relatively faster sample collection compared to collecting deeper B and C soil. A disadvantage is that not all the key indication elements (e.g. Cu) are enhanced in the F-H horizon. However, Heberlein,

(2009), has clearly shown that the Ah horizon at the base of the F-H horizon accumulates a wide range of pathfinder elements over concealed Cu-Au porphyry mineralization and, in addition, enhances anomaly contrast. While not examined as a specific geochemical sample medium in this study, the Ah horizon should certainly be considered as a viable option for a soil survey. Accumulation of metals by soil organic matter only occurs in the B horizon at one Shiko Lake profile. However, very high aqua regia digestion, MMI^{TM}, BioLeach^{SM} and Enzyme^{SM} Leach determined Cu, Co, Mn, Hg, Mo and Ni values in organic soil (> 30% LOI) caution that this effect must be carefully recognised when interpreting soil survey data.

3. Size and contrast of B horizon soil anomalies of selected elements determined by MMI^{TM}, BioLeach^{SM} and Enzyme Leach ^{SM} is generally similar anomaly characteristics by the more rigorous aqua regia-ICPMS digestion, but the different partial leaches display a preference for enhancing certain metals. For example MMI^{TM} increases Au anomaly contrast rather than Cu whereas BioLeach^{SM} enhances Co and Cu contrast compared to Au. The size of anomaly contrast by a partial leach also reflects the horizon sampled. For example, MMI^{TM}, BioLeach^{SM} and Enzyme Leach^{SM} contrast for Cu, Mo, Pb, Ni and Zn is smaller in Upper B horizon samples compared to that in lower B horizon samples emphasising the need for consistency when sampling a soil from the same horizon.

4. Existence of soil geochemical patterns developed in response to redox and pH gradients that are induced by the oxidation of buried, mineral sulphides is less obvious compared to the soil anomalies developed from glacially transported material. At Shiko Lake a Soil Gas Hydrocarbon (SGH^{SM}) anomaly, rated as being indicative of Cu-Au porphyry mineralization has possible soil Ca and pH variations that suggest one half of a double peak anomaly might the present, but the density of sampling is a limitation of confirming that this process is operating. One probable cause for the confused patterns could be the relatively shallow burial of the sulphides and their disseminated distribution.

6. Acknowledgements:

Peter Bernier, Richfield Ventures Corp generously allowed the author and his assistant, Zoe Sandwith, to collect samples over the Mouse Mountain property and Shelia Jonnes kindly gave a guided of the property before the sampling began. Permission from Rudi Durfeld, Durfeld Geological Management Ltd to collect samples over the Shiko Lake property is much appreciated by the author. Rudi kindly explained the property geology willingly helped sample several of the profiles on the property. Zoe Sandwith very ably assisted with fieldwork, helping in preparation of samples for analysis and coauthoring a fieldwork paper that reported preliminary results of the project. Her patience and constant good humour is greatly appreciated by the author. A visit from Dr. David Lefebure, Chief Geologist, BC Geological Survey, to Mouse Mountain at the start of the sampling program was most welcome. Alain Plouff, Quaternary Geologist, Geological Survey of Canada generously provided funding for sample analysis and very willingly advised on questions from the author about surficial geology. Discussions with David Heberlein, Consultant Geochemist, greatly helped with an interpretation of the soil geochemical data. Finally, Dr. Stephen Rowin, Director of the Cordilleran Geology

Section, BC Geological Survey is especially thanked for a very careful and constructive review of preliminary draft of the Open File.

7. References

Bailey, D.G. (1988a): Geology of the Central Quesnel Belt, Hydraulic, south-central British Columbia (93A/12); *British Columbia Ministry of Energy, Mines and Petroleum Resources*, Geological Fieldwork, 1987, Paper 1988-1, pages147-153.

Bailey, D.G. (1988b): Geology of the Hydraulic map area, NTS 93A/12; *British Columbia Ministry of Energy, Mines and Petroleum Resources*, Preliminary Map 67, scale 1:50 000.

Bailey, D.G. (1990): Geology of the Central Quesnel Belt, British Columbia *British Columbia Ministry of Energy, Mines and Petroleum Resources*, Open File 1990-31, 1:100 000 scale map with accompanying notes.

BC Geological Survey (2010): MINFILE mineral invenstory; *BC Ministry of Energy and Mines*, MapPlace website. URL <http://www.MINFILE.ca.

BC Geological Survey (2010): MapPlace GIS internet mapping system; *BC Ministry of Energy and Mines*, MapPlace website. URL <http://www.MapPlace.ca.[July 2010]

Canada. Soil Classification Working Group (1998): The Canadian system of soil classification, *3rd Edition*, *National Research Press*, Ottawa, 1998, 187 pages.

Clark, J.R. (1999): Concepts and Models for interpretation of enzyme leach data for mineral and petroleum exploration: in 19th International Geochemical Exploration Symposium, Short Course on Geoanalysis, April 10th, 1999.

Cameron, E.M., Hamilton, S.M., Leybourne, M.I., Hall, G.E.M. and McClenaghan, M.B. (2004). Finding deeply buried deposits using geochemistry, *Geochemistry, Exploration, Environment, Analysis*, Volume 4, pages 7-32.

Cameron, E.M., Hamilton, S.M., Leybourne, M.I., Reich, M. and Palacois, C. (2010): Surface geochemical anomalies in northern Chile: A product of the extended metallogenesis of buried copper deposits; in Proceedings of the 24th International Applied Geochemistry Symposium Abstract Volume 1, Editors Lentz, D.R., Thorne, K.G., and Beal, K.B. page 15.

Davis, J.C. (1973): Statistics and data analysis in geology, *John Wiley and Sons*, 550 pages.

Friske, P.W.B. and Hornbrook, E.H.W. (1991) Canada's National Geochemical Reconnaissance program; *Transactions of the Institution of Mining and Metallurgy*, Section B; Volume 100, pages. 47-56.

Govett, G.J.S (1976): Detection of deeply buried and blind sulphide sulphide deposits by measurement of H+ and conductivity of closely spaced surface samples; *Journal of Geochemical Exploration*, Volume 6, Number 3, pages 359-382.

Hall, G.E.M. (1998): Analytical perspective on trace element species on interest in exploration. *Journal of Geochemical Exploration, Special Issue on Selective Extractions*, Hall, G.E.M and Bonham-Carter, G.F., Editors, Volume 61, pages 1 to 9.

Hamilton, S.M (2007): Major advances in soil geochemical exploration methods for areas of thick glacial drift cover; in Proceeding of Exploration 07: Fifth Decennial International Conference on Mineral Exploration, Editor, B.Milkereit, pages 263-280.

Heberlein, D.R. and Samson, H. (2010): An Assessment of Soil Geochemical Methods for Detecting Copper-Gold Porphyry Mineralization through Quaternary Glaciofluvial Sediments at the Kwanika Central Zone, North-Central British Columbia; *Geoscience BC Report 2010-3.*

Heberlein, D.R. (2010): An Assessment of Soil Geochemical Methods for Detecting Copper-Gold Porphyry Mineralization through Quaternary Glaciofluvial Sediments at the WBX-MBX and 66 Zones, Mt. Milligan, North-Central British Columbia (NTS 93N); *Geoscience BC Report 2010-8.*

Hoffman, S.J. and Perkins, D. (1990): Report on the Cat and Betty Mineral Claims Geology, Geochemistry, Geophysics and Drill Exploration; *British Columbia Department of Mines and Petroleum Resources* Assessment Report 19956, 383 pages.

Holland, S.S. (1964): Landforms of British Columbia – A Physiographic outline; *British Columbia Department of Mines and Petroleum Resources*, Bulletin 48, 138 pages.

Jackaman, W. (1999): British Columbia Regional Geochemical Survey - Quesnel Lake (NTS 93A), *British Columbia Ministry of Energy, Mines and Petroleum Resources*, RGS 50.

Jackaman, W. (2001): British Columbia regional geochemical survey, NTS 93B – Quesnel; *British Columbia Ministry of Energy and Mines,* RGS 54, 138 pages.

Jackaman, W. (2008): QUEST project sample re-analysis (NTS 93A, 93B, 93H, 93G, 93N) *Geoscience BC Report 2008-3.*

Jackaman, W. (2008): Regional Lake Sediment and Water Geochemical Data, Northern Fraser Basin, Central BC (parts of NTS 93G, H, J, K, N & O); *Geoscience BC Report 2008-5.*

Jonnes, S. and Logan, J.M. (2007): Bedrock geology and mineral potential of Mouse Mountain, Central BC, *British Columbia Ministry of Energy, Mines and Petroleum Resources* Fieldwork Paper 2007-1, pages 55-66.

Klassen, R.A. (2001): A Quaternary geological perspective on geochemical exploration in glaciated terrain, in Drift Exploration in Glaciated Terrain, Editors McClenaghan, M.B., Bobrowsky, P.T., Hall. G.E.M, S. J. Cook, *Geological Society Special Publication*, Number 185, pages 1 -18.

Levson, V.M. and Giles, T.R. (1993): Geology of Tertiary and Quaternary Gold bearing placers in the Cariboo region, British Columbia (93A, B, G and H). *British Columbia Ministry of Energy, Mines and Petroleum Resources,* Bulletin 89, 201 pages.

Logan, J.M, Schiarizza, P., Struik, L.C., Barnett, C. Nelson, J.L., Kowalczyk, P., Ferri,. Mihalynuk, M.G., Thomas, M.D., Gammon, P., Lett, R., Jackaman W. and Ferbey, T. (2010): Bedrock geology of the QUEST map area, central British Columbia*, Geoscience BC Report 2010-5 / Geoscience Map 2010-01/GSC Open File 6476.*

Logan, J.M. and Bath, A.B. (2006): Geochemistry of Nicola Group basalt from the central Quesnel Trough at the latitude of Mount Polley (NTS 093A/5, 6, 11, 12), central British Columbia; *British Columbia Ministry of Energy, Mines and Petroleum Resources,* Geological Fieldwork, 2005, Paper 2006-1, pages 83-98.

Logan, J.M. and Mihalynuk, M.G. (2005): Regional geology and setting of the Cariboo, Bell, Springer and Northeast porphyry Cu-Au zones at Mount Polley South-central British Columbia; *British Columbia Ministry of Energy, Mines and Petroleum Resources,* Geological Fieldwork, 2004, Paper 2005-1, pages 249-269.

Logan, J.M., Mihalynuk, M.G. Ullrich, T and Friedman, R.M. (2007): U-Pb ages of intrusive rocks and ^{40}Ar/^{39}Ar plateau ages of copper-gold-silver mineralization associated with alkaline intrusive centers at Mount Polley and the Iron Mask Batholiths, southern and central British Columbia; *British Columbia Ministry of Energy, Mines and Petroleum Resources,* Geological Fieldwork, 2006, Paper 2007-1, pages 93 - 116.

Logan, J. (2008): Geology and mineral occurrences of the Quesnel Terrane, Cottonwood Map Sheet, Central British Columbia, (NTS 093G/01); *British Columbia Ministry of Energy, Mines and Petroleum Resources,* Geological Fieldwork, 2007, Paper 2008-1, pages 69 - 86.

Lord, T.M. (1984): Soils of the Horsefly area, British Columbia, *Agriculture Canada, British Columbia Soil Survey* Report Number 32, 108 pages.

Massey, N.W.D., MacIntyre, D.G., Desjardins, P.J. and Cooney, R.T. (2005): Digital geology map of British Columbia. *BC Ministry of Energy, Mines and Petroleum Resources*, Geofile 2005_1.

Mann, A.W. (1983): Gold – Nuggets and Solutions; *CSIRO Research Review*, Ewers, W.E. Editor, pages 99 -102.

Mann, A.W., Birrell, R.D., Mann, A.T., Humphreys, D.B. and Perdix, T. (1998) Application of mobile metal ion technique to routine geochemical exploration, in Journal of Geochemical Exploration Special Issue on Selective Extractions, Editors Hall, G.E.M and Bonham-Carter, G.F., Editors, *Journal of Geochemical Exploration*, Vol. 61, pages 87 to 102.

Mihalynuk, M.G.(2007): Neogene and Quaternary Chilcotin Ground cover rocks in the Interior Plateau, South Central British Columbia: A preliminary 3-D thickness model, *British Columbia Ministry of Energy, Mines and Petroleum Resources,* Geological Fieldwork, 2006, Paper 2007-1, pages143-147.

Panteleyev, A. (1987): Quesnel gold Belt – alkalic volcanic rocks between Horsefly and Quesnel lakes (93A/12); *British Columbia Ministry of Energy, Mines and Petroleum Resources,* Geological Fieldwork, 1986, Paper 1987-1, pages 125-133.

Panteleyev, A. (1988): Quesnel Mineral Belt – the central volcanic axis between Horsefly and Quesnel lakes (93A/12); *British Columbia Ministry of Energy, Mines and Petroleum Resources,* Geological Fieldwork, 1987, Paper 1988-1, pages 131-137.

Panteleyev, A., Bailey, D.G., Bloodgood, M.A. and Hancock, K.D. (1996): Geology and mineral deposits of the Quesnel River – Horsefly map area, central Quesnel Trough, British Columbia (93A/5, 6, 7, 11, 12, 13; 93B/9, 16; 93G/1; 93H/4); *British Columbia Ministry of Energy, Mines and Petroleum Resources,* Bulletin 97, 156 pages.

Panteleyev, A. and Hancock, K.D. (1989): Quesnel mineral belt: summary of the geology of the Beaver Creek - Horsefly River map area; *British Columbia Ministry of Energy, Mines and Petroleum Resources*, Geological Fieldwork, 1988, Paper 1989-1, pages 159-166.

Petsel, S. A. (2006): Rock and soil sampling survey assessment report on the Shiko Lake property; *BC Ministry of Energy, Mines and Petroleum Resources Assessment Report 2866, 182 pages.*

Rouse, G.E. and Mathews, W.H. (1979): Tertiary Geology and Palynology of the Quesnel area, British Columbia; *Canadian Petroleum Geology,* Bulletin, Volumn 27, pages 418-445.

Smee, B.W. (1998): A new theory to explain the formation of soil geochemical response over deeply covered gold mineralization in arid environments; *Journal of Geochemical Exploration,* Volume 61 pages 149-172.

Smee, B.W. (2003): Theory behind the use of soil pH measurements as an inexpensive guide to buried mineralization, with examples; Explore, January 2003, Number 118, pages 1 – 18.

Smee, B.W. (2010): Soil micro-layer, airborne particles, and pH: the Govett connection; in Proceedings of the 24th International Applied Geochemistry Symposium Abstract Volume 1, Editors, Lentz, D.R., Thorne, K.G., and Beal, K.B. page 91.

Stanley, C.R. and Lawie, D. (2008): Thompson-Howarth error analysis: unbiased alternatives to the large sample method for assessing non-normally distributed measurement in geochemical samples; *Geochemistry, Exploration, Environment and Analysis,* Volume 8, Part 2, pages 173-182.

Stanley, C.R. and Nobel, R.R.P. (2008): Quantitative assessment of the success of geochemical exploration using minimum probability methods; *Geochemistry, Exploration, Environment and Analysis,* Volume 8, Part 2, pages 115-128.

Sutherland, D and Hoffman, E. (2008): SGH – Soil Gas Predictive Geochemistry; *Activation Laboratories* internal report for BC Ministry of Energy, Mines and Petroleum Resources, 28 pages.

Sutherland, D (2007): Cutting edge geochemistry detects organic signatures in surficial samples originating from bacterial-mineral interactions to locate and identify buried exploration targets; in Proceeding of Exploration 07*:* Fifth Decennial International Conference on Mineral Exploration, Editor, B.Milkereit, pages 989-992.

Thompson, M and Howarth, R.J. (1978): Anew approach to the estimation of analytical precision; *Journal of Geochemical Exploration,* Volume 9, pages 23-30.

Tipper, H.W. (1971): Glacial geomorphology and Pleistocene history of central British *Columbia. Geological Survey of Canada*, Bulletin 196, 89 pages.

Yeager, J.R., Clarke, J.R., Mitchell, W and Renshaw, R. (1998): Enzyme leach anomalies associated with deep Mississippi Valley-type zinc ore bodies in the Elmwood Mine, Tennessee. in Journal of Geochemical Exploration Special Issue on Selective Extractions, Editors, Hall, G.E.M and Bonham-Carter, G.F., *Journal of Geochemical Exploration,* Volume 61, pages 103 to 112.

8. Appendix: All sample location, sample description, geochemical analyses and heavy mineral concentrate data for each survey area described in Open File 2010-9 are collected in a MICROSOFT ^{TM} Access database. In addition, the following MICROSOFT ^{TM} Excel file has been created from the Access database. The worksheets in the Excel file are:

Location_Field_pH: Sample location, sample description and field measured soil pH results.
INAA_ICPMS: Instrumental neutron activation and aqua regia digestion -inductively coupled plasma, loss on ignition results.
HM_Au: Heavy mineral concentrate gold results.
CLAY: Clay fraction (< 0.002 mm) of ten till samples prepared by the Geological Survey of Canada and analysed by aqua regia digestion-inductively coupled plasma. These data are not described in the Open File.
MMI_ENZ_BIO: Mobile Metal Ion (MMI)^{TM} , Enzyme Leach^{SM} and BioLeach^{SM} results.